CENTRAL RESEARCH LIBRARY
DOCUMENT COLLECTION

[redacted]

AEC RESEARCH AND DEVELOPMENT REPORT

ORNL-2096
Progress

cy. 8

MARTIN MARIETTA ENERGY SYSTEMS LIBRARIES
3 4456 0049747 9

CENTRAL RESEARCH LIBRARY
DOCUMENT COLLECTION
LIBRARY LOAN COPY
DO NOT TRANSFER TO ANOTHER PERSON
If you wish someone else to see this document, send in name with document and the library will arrange a loan.

HOMOGENEOUS REACTOR PROJECT

QUARTERLY PROGRESS REPORT

FOR PERIOD ENDING APRIL 30, 1956

This document contains Confidential Restricted Data relating to Civilian Applications of Atomic Energy.

OAK RIDGE NATIONAL LABORATORY
OPERATED BY
UNION CARBIDE NUCLEAR COMPANY
A Division of Union Carbide and Carbon Corporation
UCC
POST OFFICE BOX P · OAK RIDGE, TENNESSEE

[redacted]

Printed in USA. Charge 1.10 cents. Available from the U. S. Atomic Energy Commission, Technical Information Extension, P. O. Box 1001, Oak Ridge, Tennessee. Please direct to the same address inquires covering the procurement of other classified AEC reports.

LEGAL NOTICE

This report was prepared as an account of Government sponsored work. Neither the United States, nor the Commission, nor any person acting on behalf of the Commission:

A. Makes any warranty or representation, express or implied, with respect to the accuracy, completeness, or usefulness of the information contained in this report, or that the use of any information, apparatus, method, or process disclosed in this report may not infringe privately owned rights; or

B. Assumes any liabilities with respect to the use of, or for damages resulting from the use of any information, apparatus, method, or process disclosed in this report.

As used in the above, "person acting on behalf of the Commission" includes any employee or contractor of the Commission to the extent that such employee or contractor prepares, handles or distributes, or provides access to, any information pursuant to his employment or contract with the Commission.

[redacted]

DECLASSIFIED
CLASSIFICATION CHANGED TO: ____
BY AUTHORITY OF: TID-1148
BY: R. Merriman 7/25/58

ORNL-2096

8

Contract No. W-7405-eng-26

HOMOGENEOUS REACTOR PROJECT

QUARTERLY PROGRESS REPORT

For Period Ending April 30, 1956

Project Director – R. B. Briggs
Associate Director – C. E. Winters

Homogeneous Reactor Test – S. E. Beall
Reactor Design and Analysis – J. A. Lane
Engineering Development – J. A. Lane
Corrosion and Materials – E. G. Bohlmann
Chemical Engineering Development – F. R. Bruce
Supporting Chemical Research – E. H. Taylor

Compiled by

H. F. McDuffie
W. D. Reel

DATE RECEIVED BY INFORMATION AND REPORTS DIVISION
(MAY 10, 1956)

DATE ISSUED

JUL 6 1956

OAK RIDGE NATIONAL LABORATORY
Operated by
UNION CARBIDE NUCLEAR COMPANY
A Division of Union Carbide and Carbon Corporation
Post Office Box P
Oak Ridge, Tennessee

MARTIN MARIETTA ENERGY SYSTEMS LIBRARIES
3 4456 0049747 9

[redacted]

[redacted]

[redacted]

[redacted]

[redacted]

INTERNAL DISTRIBUTION

1. C. E. Center
2. iology Library
3. lth Physics Library
4. Me llurgy Library
5-6. Re or Experimental Eng eering Library
7-9. Centr esearch Library
10-18. Laborat Records Dept.
19. Laborator Records, ORNL R.C.
20. G. M. Ada n
21. R. E. Aven
22. S. E. Beall
23. D. S. Billington
24. E. P. Blizard
25. E. G. Bohlmann
26. C. J. Borkowski
27. G. E. Boyd
28. F. R. Bruce
29. A. D. Callihan
30. D. W. Cardwell
31. W. L. Carter
32. G. H. Cartledge
33. R. A. Charpie
34. W. E. Clark
35. G. H. Clewett
36. T. E. Cole
37. E. L. Compere
38. D. D. Cowen
39. S. Cromer
40. F. L. Culler
41. J. S. Culver
42. J. S. Drury
43. W. K. Eister
44. L. B. Emlet (K-25)
45. D. E. Ferguson
46. J. H. Frye, Jr.
47. J. L. Gabbard
48. W. R. Gall
49. H. E. Goeller
50. C. B. Graham
51. J. C. Griess
52. P. N. Haubenreich
53. J. W. Hill
54. C. J. Hochanadel
55. A. Hollaender
56. A. S. Householder
57. G. H. Jenks
58. W. H. Jordan
59. P. R. Kasten
60. C. P. Keim
61. M. T. Kelley
62. R. B. Korsmeyer
63. A. S. Kitzes
64. K. A. Kraus
65. J. A. Lane
66. R. E. Leuze
67. S. C. Lind
68. R. B. Lindauer
69. R. S. Livingston
70. M. I. Lundin
71. R. N. Lyon
72. J. L. Marsh (C&CCC, South Charleston)
73. W. L. Marshall
74. H. F. McDuffie
75. J. P. McBride
76. R. A. McNees
77. J. R. McWherter
78. O. Menis
79. E. C. Miller
80. K. Z. Morgan
81. E. J. Murphy
82. M. L. Nelson
83. E. O. Nurmi
84. J. P. Murray (Y-12)
85. L. F. Parsly
86. H. F. Poppendiek
87. L. R. Quarles
88. W. D. Reel
89. P. M. Reyling
90. A. M. Rom
91. W. L. Ross
92. d. C. Savage
93. H. Secoy
94. . Segaser
95. E. Shipley
96. M. J kinner
97. R. W. ughton
98. A. H. S l
99. I. Spiewa
100. C. D. Susa
101. J. A. Swartou
102. E. H. Taylor
103. D. G. Thomas
104. P. F. Thomason

[redacted]

[redacted]

105. M. Tobias
106. D. S. Toomb
107. W. E. Unger
108. Van Winkle
109. Weaver
110. A. Weinberg
111. T. Welton
112. E. P. ner (consultant)
113. G. C. W ams
114. J. C. Wils
115. C. E. Winters
116. F. C. Zapp
117. J. E. Baker
118. H. O. Day
119. W. J. Leonard
120. M. L. Picklesimer
121. ORNL – Y-12 Technical Library, Document Reference Section
122. HRP Director's Office, Y-12

EXTERNAL DISTRIBUTION

123. AF nt Representative, Burbank
124. AF t Representative, Marietta
125-126. AF Pl Representative, Seattle
127. AF Plan epresentative, Wood-Ridge
128. Aircraft oratory Design Branch (WADC)
129. ANP Proje Office, Fort Worth
130-141. Argonne Na al Laboratory
142. Armed Forces ecial Weapons Project, Sandia
143. Armed Forces cial Weapons Project, Washington
144. Army Chemical ter
145-148. Atomic Energy C nission, Washington
149. Battelle Memorial titute
150-155. Bettis Plant (WAPD
156-158. Brookhaven National boratory
159. Bureau of Ships
160. Chicago Operations Offi
161. Chicago Patent Group
162. Chief of Naval Research
163. Department of the Navy – Op 62
164-167. duPont Company, Aiken
168. duPont Company, Wilmington
169-170. General Electric Company (ANPD
171-178. General Electric Company, Richla
179. Hanford Operations Office
180. Headquarters, Air Force Special Weap s Center
181. Iowa State College
182-185. Knolls Atomic Power Laboratory
186-189. Los Alamos Scientific Laboratory
190. Massachusetts Institute of Technology (Ben dict)
191. Materials Laboratory (WADC)
192. Materials Laboratory Plans Office (WADC)
193. Mound Laboratory
194. National Advisory Committee for Aeronautics, Cle land
195. National Advisory Committee for Aeronautics, Washington
196-197. Naval Research Laboratory
198-199. New York Operations Office

[redacted]

[redacted]

200. North American Aviation, Inc.
201. Office of the Quartermaster General
202. Patent Branch, Washington
203-209. Phillips Petroleum Company (NRTS)
210. Powerplant Laboratory (WADC)
211. San Francisco Operations Office
212. USAF Project RAND
213. U. S. Naval Postgraduate School
214. University of California Radiation Laboratory, Berkeley
215. University of California Radiation Laboratory, Livermore
216. Vitro Laboratories
217. Division of Research and Development, AEC, ORO
218-532. Technical Information Extension, Oak Ridge

[redacted]

[redacted]

Reports previously issued in this series are as follows:

ORNL-527	Date Issued, December 28, 1949
ORNL-630	Period Ending February 28, 1950
ORNL-730	Feasibility Report – Date Issued, July 6, 1950
ORNL-826	Period Ending August 31, 1950
ORNL-925	Period Ending November 30, 1950
ORNL-990	Period Ending February 28, 1951
ORNL-1057	Period Ending May 15, 1951
ORNL-1121	Period Ending August 15, 1951
ORNL-1221	Period Ending November 15, 1951
ORNL-1280	Period Ending March 15, 1952
ORNL-1318	Period Ending July 1, 1952
ORNL-1424	Period Ending October 1, 1952
ORNL-1478	Period Ending January 1, 1953
ORNL-1554	Period Ending March 31, 1953
ORNL-1605	Period Ending July 31, 1953
ORNL-1658	Period Ending October 31, 1953
ORNL-1678	Period Ending January 31, 1954
ORNL-1753	Period Ending April 30, 1954
ORNL-1772	Period Ending July 31, 1954
ORNL-1813	Period Ending October 31, 1954
ORNL-1853	Period Ending January 31, 1955
ORNL-1895	Period Ending April 30, 1955
ORNL-1943	Period Ending July 31, 1955
ORNL-2004	Period Ending October 31, 1955
ORNL-2057	Period Ending January 31, 1956

[redacted]

[redacted]

HRP QUARTERLY PROGRESS REPORT

SUMMARY

PART I. HOMOGENEOUS REACTOR TEST

1. HRT Operations

The construction phase of the HRT was completed in April. Several photographs are presented to show equipment within the reactor tank and the control-room area.

The operating group started working on a three-shift basis to complete the cleaning and pretreatment of the process piping in preparation for a series of engineering tests. The nonnuclear experiments are scheduled over a five-month period, to be followed by the loading of enriched fuel solution. Reports covering the detailed procedures for 12 experiments were issued during the quarter.

2. HRT Design

Designs were completed of the pressurizer and outer-dump-tank liquid-level controllers, the fission- and ion-chamber positioners, the temporary and permanent freeze jackets, and the pressurizer heaters. The diaphragm-pump suction check valves were redesigned to overcome failures encountered in the mockup, and an improved rupture-disk holder was developed which overcomes the complexities of the original units in the pressure-balancing system and facilitates replacement in the event of failure. Aluminum foil was determined to be acceptable for insulating the pressurizers. The preliminary studies of a gas pressurization system for the HRT were completed. A study was also completed of the copper concentrations required for internal recombination of radiolytic gases in the HRT.

3. Reactor Component Development

A seal-welded stainless steel thermal barrier with titanium-inserted wear ring and labyrinth operated satisfactorily for 250 hr in the 400A-1 pump.

The 300A-1 pump (in the mockup) has operated 1627 hr without incident since seal-welding.

The thermal-barrier gasket of the reactor fuel pump failed after 550 hr of operation in a test loop.

The HRT heat exchangers were cleaned with hot oxygenated water and calibrated for flow vs pressure drop.

Specifications were completed for a spare heat exchanger for the HRT.

Further improvement of feed pumps is required, especially since two diaphragms have failed in the mockup after approximately 3000 hr of operation.

Uniform samples were obtained with the HRT sampler, but drops of sample deposited on top of the flask. The sampler is now connected to the mockup system.

Satisfactory freeze jackets were developed for the HRT.

The HRT mockup completed a 1122-hr fuel-solution run, which indicated a corrosion rate of 2 mpy. The pressurizer performed satisfactorily, but feed-pump failures were experienced. Some special tests were run to study the performance of the letdown system.

4. HRT Reactor Analysis

The power-time relation for the HRT after shutdown was obtained for several situations. With the steam valve from the core heat exchanger closed, the reactor would become subcritical in approximately 2 min if the 400A pump continued to operate, and might remain critical indefinitely if the 400A pump were turned off. In the latter case the rate of energy release would be less than 60 kw for times greater than several seconds following stoppage of the pump. If the heat exchanger were operated in a normal fashion, natural convective flow would keep the reactor power at approximately 700 kw.

The insertion of corrosion specimens within the HRT core region will effectively add poisons to the reactor and increase the fuel concentration required for criticality. The maximum poisoning associated with these specimens was calculated to be less than 11%. This maximum poisoning would increase the core critical concentration from approximately 7.1 to approximately 8.7 g of U^{235} per kilogram of D_2O at 280°C.

[redacted]

If two-phase separation occurred in the HRT core with the 400A pump off, large amounts of reactivity could be injected into the reactor upon pump startup. This situation can be eliminated by requiring that the reactor be critical before restarting the pump.

5. HRT Controls and Instrumentation

All major reactor-system components have been received, calibrated, and installed. A total of $197,000 has been spent for materials, including valves.

The checkout of the instrumentation and control system was finished, and the system was approved for use by the Operations Group.

Fabrication of the level indicators at ORNL was completed. Operation of the prototypes was satisfactory, although zero shifts with temperature changes were not eliminated completely.

Low-pressure-system valves were received and appear to be satisfactory. The core-system dump valve was returned to the vendor for plug redesign after poor performance during tests. The letdown valve has given excellent service in 1100 hr of mockup operation to date.

6. HRT Fuel Processing Plant

Previously it was planned that weekly batches of solids centrifugally removed by the hydroclone would be collected in a shielded carrier located outside the processing cell. Now a heavily shielded carrier having a one-week capacity will be substituted for one of the two carrier-evaporators in the processing cell. The heavily shielded carrier will be removed for dissolution, sampling, and analysis of its contents to confirm the representativeness of the underflow-receiver sampler.

The integrally flanged hydroclone developed for the HRT-CP has been tested to confirm that its efficiency and characteristics are not substantially different from those of hydroclones of the standard design used heretofore. The underflow-receiver heat-transfer coefficient has been experimentally determined to ensure that the rate of cooling is adequate to reduce the underflow-pot pressure before sufficient radiolytic decomposition can occur to constitute an explosion hazard.

The construction is very nearly on schedule, with shop and field work 90 and 30% complete, respectively, compared with the scheduled 100 and 35%. The two low-pressure units, consisting of an entrainment separator, superheater, recombiner, condenser, and associated valves and piping, are assembled and installed in the processing cell, and services have been connected.

The principal items not yet received are the canned-rotor pump (delivery expected May 30) and the roof shielding plugs (delivery expected June 15).

PART II. REACTOR DESIGN AND ANALYSIS

7. Reactor Analysis

Fuel costs for U^{235} burners using highly enriched feed were calculated for H_2O- and D_2O-moderated reactors between 2 and 10 ft in diameter. The fuel cost was approximately 4 mills/kwhr independent of size, power level, or moderator, if the fuel was processed on a batch basis after operating times longer than 2000 days. With the D_2O reactors, chemical processing could be economically eliminated if the spent fuel were disposed of cheaply at the reactor site. Such a procedure with the H_2O reactors would increase the fuel costs by 1 to 2 mills/kwhr because of the large uranium inventory.

Nuclear and economic calculations were made for some cylindrical, two-region, thorium breeder reactors. Low power density at the core-tank wall (and low average power density) can be achieved with core tanks of small diameter by making them long. Minimum fuel costs were associated with high core power densities; increasing the reactor length and reducing the power density increased the inventory charge until that charge controlled the fuel cost. Where corrosion attack is related to power density, the costs related to corrosion must be balanced against fuel costs.

Two-group studies were made of 10- and 12-ft-dia spherical reactors with different blanket materials and containing 200 g of thorium per liter in the core region. For these reactors, the breeding ratio increased when a reflecting blanket was replaced by one containing ThO_2; no significant increase in breeding ratio was obtained for thorium blanket concentrations greater than 2 kg of thorium per liter; the breeding ratio and power density at the core wall increased with decreasing core diameter for a fixed over-all reactor diameter.

Fermi ages and diffusion constants for two-group calculations were evaluated for thorium oxide slurries, UO_2SO_4 solutions, and equimolar UO_2SO_4-Li_2SO_4 solutions over a range of concentrations and temperatures. Various mixtures of light and heavy water were considered.

[redacted]

PART III. ENGINEERING DEVELOPMENT

8. Development of Fuel-System Components

Three leaks developed in the high-pressure recombiner loop. Two appear to have been caused by stress corrosion, even though the chloride content was very low.

A test in the natural circulation recombiner at 100 psia indicates that the explosion limit is above 10.5 mole % stoichiometric gas mixture.

Inhomogeneity in the vapor phase led to the low values of explosion limits reported previously.

Increased stator life with some decrease in pumping head has resulted from a change from parallel to series connection of windings in 5-gpm pumps. One series-wound pump has circulated water at room temperature without difficulty.

Fabrication of titanium-lined pipe and of a small titanium-lined heat exchanger will start at the Crane Co. and The Pfaudler Co. as soon as purchased material is delivered.

Specimens for testing a titanium-cladding method were prepared at Armour Research Foundation, and tests are planned.

Thermal cycling tests with 4-in.-dia ring-joint flanges are in progress.

9. Development of Blanket-System Components

The Westinghouse 200A slurry pump has been operated for more than 1000 hr in the present run. Power fluctuations were encountered initially when the loop temperature was raised above 175°C. Successive additions of sulfuric acid to the slurry raised the temperature at which the fluctuations occurred to above 300°C, and the loop has been running normally since then.

Analysis of the hard cake which formed in the 200A loop during the third run was completed. The preliminary report, that no large concentration of impurities was present, was confirmed. X-ray measurements and particle-size analysis failed to reveal any reason for the cake formation. Since aluminum and silica were found, by analysis, slurries prepared with these impurities were circulated in the small loops in an effort to obtain hard cakes; the effort was not successful. The cause of the hard cake in loop 200A is still unknown.

A porous aluminum oxide coating sprayed in place was tested for use as a pump-bearing material. Although no dimensional changes could be measured, the contact area of the shoes appeared to be glazed, and there was some pitting of the thrust runner. The results were not impressive.

High-density, sintered aluminum oxide was tested for attack by circulating thorium oxide slurries by installation of an aluminum oxide orifice plate in a pump loop. The plate was severely attacked on its face, although the orifice maintained a sharp edge. Evidently the attack was not the result of high shear forces, which are characteristically present in bearings. Additional tests are required to determine the feasibility of testing bearings of this material in pumps as large as the 200A one.

Slurries specially prepared by the Chemical Technology Division were circulated in the 5-gpm loops to compare the effect of pumping on their properties with the effect on the properties of the standard slurry prepared from thorium oxide calcined at 800°C. The results have been reported.

The race-track and cone-type dump tanks were operated successfully with numerous startups and shutdowns. At no time were cakes formed which could not be redispersed on startup.

The piping of the slurry blanket system was cleaned chemically, and in-place calibration of flow instruments was completed. The system has been run on water at operating pressure and temperature (2000 psi at 300°C) for over 300 hr. The water runs will be continued until all components have been proved to operate satisfactorily and base heat transfer data have been obtained. The stainless steel core for the dummy reactor was received and installed.

10. Instrument and Valve Development

A flow transmitter of the variable-area type, suitable for metering reactor feed- and purge-pump flows, is being evaluated in a test loop. A float-type liquid-level control designed for use as an alarm unit in reactor low-pressure systems will be delivered in June. Three sealing bellows similar to those used in HRT valves averaged 45,000 cycles in uranyl sulfate at 300°C and 2000 psi before failure. A flush-diaphragm pressure transmitter desirable for slurry service was used in a component test loop.

PART IV. CORROSION AND MATERIALS

11. Solution Corrosion

The all-titanium loop, loop G, was modified to allow a greater latitude in operation. The small, 1½-in.-dia pipe which served as a pressurizer was

[redacted]

replaced with a 3½-in.-dia pressurizer, and a bypass line was added to the loop. The former change makes the liquid volume of solution in the loop less critical, and the latter allows corrosion specimens to be exposed at two different flow rates.

A new stainless steel loop is being constructed to circulate uranyl sulfate solutions containing beryllium sulfate. Because of the toxicity of beryllium, the shield will be of leaktight construction with a filtered exhaust system.

Further testing with uranyl sulfate–lithium sulfate solutions was completed. It was shown that at 200°C a protective coating does not form on stainless steel and that corrosion proceeds at a rate dependent on the uranium concentration; however, the rate is substantially lower than is found when a comparable solution is used without lithium sulfate. Recent tests at higher temperatures confirmed previous results which demonstrated the beneficial action of including essentially an equimolal concentration of lithium sulfate in uranyl sulfate solutions. However, in the concentration range of 40 to 200 g of uranium per liter, no change in critical velocity was observed on the addition of lithium sulfate to uranyl sulfate solutions at 250°C.

Additional testing at 250°C in a solution containing 0.03 *m* UO_3 in 0.17 *m* Li_2CO_3 with oxygen and carbon dioxide overpressures was completed. The results show that carbon steel and the austenitic stainless steels corroded at a rate of less than 1 mpy after a protective film was formed. The critical velocity on stainless steel was about 45 fps.

The 4000-gpm loop was used to make two runs at 250°C with a solution similar to that proposed for use in the HRT. In both runs the oxygen concentration was maintained at 50 to 100 ppm, and average corrosion rates for the high-temperature system were 0.3 to 0.5 mpy. No signs of solution instability were noted.

Four 100A loops were descaled with a descaling solution developed by the Chemical Technology Division. Only in one case was the loop completely descaled, but in the other loops substantial quantities of oxide scale were dissolved.

The susceptibility of type 347 stainless steel to stress corrosion cracking was demonstrated by spraying tap water on bent pipes through which 153°C steam was being passed. After approximately 10,000 hr, all pipes showed many transgranular cracks, some of which very nearly penetrated the pipe wall. Presumably the low concentration of chloride ions in the tap water was the cause of the cracking.

Elgiloy, which had shown good corrosion resistance to uranyl sulfate solutions at 300°C, has shown on continued testing a marked tendency toward stress corrosion cracking both in the solution and in the gas phases. Analysis of the solution showed less than 2 ppm of chloride.

A number of high-strength titanium alloys were tested in a variety of uranyl sulfate solutions both in the stressed and annealed condition. No evidence of cracking was observed, and in all cases the attack on the metal was nearly negligible.

12. Slurry Corrosion

Dynamic slurry corrosion studies in which thorium oxide slurry is circulated in the 100A pump loop were facilitated by the addition to the loop of an improved condensate system to provide more purge water to the 100A pump rotor cavity and by the incorporation of a device for adding slurry to the loop while operating. One slurry run was completed with slurry prepared from a more nearly pure lot of thorium oxide which was produced at ORNL by calcination of thorium oxalate at 800°C. In the 312-hr run at 300°C, the circulating slurry concentration was raised from 444 to 1008 g of thorium per kilogram of water while operating. Operating characteristics, along with loop- and pin-corrosion data, are presented.

13. Radiation Corrosion

13.1 In-Pile Loops. – Construction of in-pile loop assemblies for operation in beam holes HB-2 and HB-4 at the LITR is continuing. In-pile loop L-4-13 was completed and tested during the past quarter and is now ready for installation in beam hole HB-4 at the LITR.

Fabrication was completed of the all-titanium in-pile loop L-2-14 designed for installation in beam hole HB-2 of the LITR. The all-titanium loop assembly is now being installed in the mockup facility at Y-12 for operational testing at design temperatures and pressures.

Exposure of in-pile loop L-4-12 in the LITR was completed, but disassembly and examination have not yet begun. The loop for this experiment was equipped with a titanium core. Otherwise, the experimental conditions were similar to those

[redacted]

of previous loop experiments. The in-pile operation period was 2020 hr, and the energy output of the LITR during the operation was 4386 Mwhr.

Exposure of in-pile loop experiment L-4-11 in the LITR was completed. Disassembly and examination of the loop and loop specimens are in progress. The in-pile operation period with enriched solution was 1109 hr. The energy output of the LITR during this time was 2175 Mwhr.

Conceptual design studies of an in-pile corrosion loop facility for the ORR were initiated. The loop under consideration is similar to the loops in use at the LITR and is being designed for operation at an average fission power density of 33 w/ml in a core volume of 300 ml.

13.2 In-Pile Autoclave Tests. – The bomb from an early Zircaloy-2 experiment, for which the solution was about 0.5 *m* in excess H_2SO_4, was opened. Specimen data indicate that the high concentration of excess acid markedly reduced the radiation corrosion of the Zircaloy-2.

A Zircaloy-2 experiment for which the solution employed was free of copper was completed. There is no evidence from this experiment that the radiation corrosion is affected by the presence or absence of copper in the solution.

The results of one Zircaloy-2 experiment and one stainless steel experiment indicate that the addition of $KTcO_4$ to the uranyl sulfate solution had no effect on the radiation-induced corrosion.

The results of a stainless steel experiment with a solution which contained no added acid confirmed the results of early bomb experiments; the rate increased markedly after several days of irradiation. These consistent results are regarded as evidence that the added H_2SO_4 is responsible for the improved corrosion behavior observed in the more recent series of steel experiments.

14. Metallurgy

A satisfactory metallographic procedure was developed for the identification and examination of hydrides in zirconium and Zircaloy-2. The prior conclusions that the hydrides in Zircaloy-2 occur in the grain boundaries and in the grains in crystal-bar zirconium were confirmed by the micrographs shown. Crystal-bar zirconium specimens containing hydrogen were quenched from 900°C in oil and in mercury. Considerable amounts of hydrogen can be retained in supersaturated solution by a fast quenching rate.

Binary and ternary combinations of alloys of crystal-bar zirconium and high-purity Nb, Ta, Mo, and Fe were arc cast, rolled to strip, and heat treated to determine the amount of beta phase retained by quenching and the decomposition products of the retained beta phase. No alloy has shown complete retention of beta phase, with the possible exception of the 10 wt % Mo alloy. Specimens were submitted for glancing-electron-diffraction analyses to determine the nature of the precipitate in the niobium alloys.

Cathodic etching of Zircaloy-2 specimens confirmed the prior conclusion that the stringers observed in the as-fabricated material are intermetallics and not voids.

Air-cooled and water-quenched beta structures of Zircaloy-2 specimens, annealed after cold-working 10, 15, and 20%, were examined to determine the amount of cold-working required to produce a fine-grained equiaxed alpha grain structure. Cold-working 20% is required for both air-cooled and water-quenched material. Air-cooling gave coarser grains than water-quenching in all cases.

Results of impact tests on specimens of Zircaloy-2, aged at 250°C for 0, 500, 1085, and 1585 hr prior to testing, are presented. No effect of aging on properties was noted.

The preplaced consumable-insert welding method was modified and used to make satisfactory welds in titanium.

If it is not necessary to have a complete bond, it may be possible to butt-weld titanium-lined steel pipes by using many layers of carbon steel ribbon as the transition region. An attempt to use vanadium weld metal as the transition layer resulted in severe cracking wherever it contacted the steel.

Nitrogen of suitable purity is shown to be an acceptable backup gas for inert-gas shielded-arc welding of type 347 stainless steel.

Several methods for detecting flaws in pipe and tubing were studied. The method thought most likely to yield the precision required is the immersed pulse-echo ultrasonic method.

The cast pulsator housings for the reactor injection pumps were inspected and found to be faulty. The use of forgings was recommended.

A considerable decrease in impact energy values was found for irradiated 8½% nickel steels.

[redacted]

[redacted]

PART V. CHEMICAL ENGINEERING DEVELOPMENT

15. Thorium Oxide Slurry Development

Slurries of thorium oxide containing 0.5 mole % of 93% enriched uranium have been irradiated at 300°C in the LITR. At a thorium concentration of 1000 g per kilogram of H_2O the slurries were too concentrated to be pumped for longer than a few hours in the dash-pot irradiation bomb. With 500 g of thorium per kilogram of H_2O no difficulty was experienced in stirring slurries both in- and out-of-pile. X-ray photographs of slurries in the dash-pot irradiation bomb showed them to be homogeneously suspended by the action of the stirrer at temperatures of 100 to 300°C. When stirring was stopped at above 200°C, structural characteristics were evident in the settled slurry; these became more pronounced with increasing temperature to 300°C.

The effect of MoO_3 catalyst concentration on the combination rate of stoichiometric hydrogen and oxygen mixtures in thorium oxide slurries was studied. With slurries containing 1000 g of thorium per kilogram of H_2O and catalyst concentrations of 0.05 to 0.20 *m*, the combination rates were more than sufficient at 300°C to maintain steady-state gas pressures at less than 2000 psi under TBR conditions.

Relative viscosities of slurries of 900°C calcined thorium oxide measured in the dash-pot irradiation bomb increased from 3.6 centistokes at a thorium concentration of 250 g per kilogram of H_2O to 5.0 and 8.5 centistokes, respectively, at a concentration of 750 and 1000 g per kilogram of H_2O. A similar slurry which had been pumped showed viscosities of 4, 11, and 20 centistokes for the same slurry concentrations. No significant changes in slurry viscosities were observed over the temperature range 50 to 300°C.

An apparatus to study the settling characteristics of slurries in stainless steel at elevated temperatures and pressures by continuous x-ray photography was constructed and demonstrated. In initial settling studies, pumped thorium oxide slurries were found to be in compaction at concentrations of 500 to 700 g of thorium per kilogram of H_2O. At a slurry concentration of 250 g of thorium per kilogram of H_2O, the initial settling rates increased with increasing slurry temperature from less than 0.2 cm/sec at 110°C to 0.66 cm/sec at 265°C. Analysis of the rate data indicated that the increase in settling rate with temperature resulted primarily from the decrease in the viscosity of water with temperature rather than from a change in the flocculation characteristics of the slurry.

The addition of 1 mole % calcium to thorium oxide by the coprecipitation of the oxalates and subsequent calcination apparently resulted in a densification of the oxide particles.

Sols with ThO_2/NO_3^- mole ratios as high as 6.3/1 have been obtained by the dialysis of thorium nitrate solutions adjusted to pH 3.6 with ammonium hydroxide. After drying at 300°C the solids were readily redispersed in water to re-form the sol.

16. Fuel Reprocessing

The chemistry of iodine was studied further to determine the behavior of iodine under reactor conditions. At 250°C with an atmosphere of oxygen, the free/combined iodine ratio in the liquid phase was 9/1. The presence of ruthenium reduced the ratio to 0.1/1 with oxygen present. The presence of hydrogen or of stainless steel partially offset this effect of ruthenium. No other fission product yet examined has the same effect as ruthenium on iodine valence distribution. Transfer of iodine from the liquid phase to silver in the vapor phase was also inhibited by ruthenium in the liquid. Data were obtained which indicate that the transfer of iodine from vapor to silver is a significantly reversible reaction at 250 to 300°C.

At Vitro Laboratories a 1000-psi ejector loop was constructed and is now undergoing preliminary testing prior to its being used for studies on removing iodine from circulating uranyl sulfate solutions at 250 to 300°C. Bench studies showed that water was an efficient (98%) scrubber for removing iodine from a circulating gas stream as long as the iodine concentration in the scrubber solution did not exceed 0.007 g/liter. Dilute Ag_2SO_4 and NaOH solutions were 100% efficient.

Additional work on the equilibrium distribution coefficient of elemental iodine between vapor and uranyl sulfate solutions at 260 to 330°C consistently gave values ranging from 6 to 12. With water the coefficient ranged from 0.2 to 0.5.

Based on visual observations in quartz tubes, selenium is soluble to the extent of 50 to 250 mg per kilogram of H_2O at 300°C, Se(IV) being apparently somewhat less soluble than Se(VI). Filter bomb experiments, using Sb^{124} tracer,

[redacted]

[redacted]

indicate antimony solubility at 275°C of 20 mg per kilogram of H_2O in 0.02 *m* UO_2SO_4–0.005 *m* H_2SO_4. Hydrous niobium oxide suspended in UO_2SO_4 solution changed from an amorphous to a crystalline state above 200°C. Upon cooling, the solid phase lost its crystalline form rapidly. Indications of a very low solubility (<<10 mg per kilogram of H_2O at 250 to 300°C) were obtained.

Technetium(VII) was reduced by hydrogen in uranyl sulfate solutions at 275°C and precipitated as TcO_2, with 12 mg of technetium per kilogram of H_2O remaining in solution. The uranium was also reduced and precipitated. When TcO_2 was suspended in 0.02 *m* UO_2SO_4–0.005 *m* H_2SO_4 and heated to 250°C under an atmosphere of air, it remained as TcO_2 at 250°C but with pure oxygen present it rapidly dissolved to give a solution containing at least 10 g of technetium per kilogram of H_2O.

In further tests, 10.8 *M* H_2SO_4 at 165°C continued to be a satisfactory solvent for synthetic reactor solids varying widely in composition, pretreatment, and age. Therefore it is recommended that solids removed by the HRT Chemical Plant be treated with three successive batches of 10.8 *M* H_2SO_4. Each batch should be 1 liter of acid per 100 g of solids.

17. Plutonium-Producer Blanket Processing

Plutonium adsorption on titanium and Zircaloy-2 from 1.4 *m* UO_2SO_4 at 250°C under 90-psi oxygen and 180-psi hydrogen is presented approximately by the equations

$$A(\mathrm{Ti}) = 0.01\ C^{2/3} t^{1/2} ,$$

$$A(\mathrm{Zr\text{-}2}) = 0.03\ C^{2/3} t^{1/2} ,$$

where A is the adsorption in $\mu g/cm^2$, C is the plutonium concentration in mg/kg of H_2O, and t is the exposure time in hours. The equations were devised to fit data for plutonium concentrations up to 3 mg per kilogram of H_2O (no PuO_2 precipitation) and exposure times up to 160 hr, and for untreated machined surfaces. However, experimental results deviated from calculated results by a factor of 4 for 15% of the titanium data and for 25% of the Zircaloy-2 data. The deviation is believed to be a result of a variation of the amount and nature of oxide film on the metal surfaces. Preliminary data for plutonium adsorption on type 347 stainless steel indicated that the amount of plutonium adsorbed is directly proportional to exposure time.

A plutonium solubility of 520 mg per kilogram of H_2O was obtained when 4.0 *m* UO_2SO_4–4.0 *m* Li_2SO_4 containing 0.1 *m* Cr and 0.1 *m* H_2SO_4 was heated at 250°C under 200-psi oxygen. This value is too low to permit use of such a solution as a fuel in a plutonium-burner power reactor.

In 700 hr of operation under reactor conditions (1.4 *m* UO_2SO_4–0.3 *m* H_2SO_4, > 250°C), a titanium hydroclone showed no sign of attack by the simulated fuel.

18. Equipment Decontamination

Type 347 stainless steel contaminated under homogeneous reactor (uranyl sulfate fuel, 250°C) conditions was satisfactorily descaled and decontaminated by 0.4 *M* $CrSO_4$–0.5 *M* H_2SO_4. An inert atmosphere was used to prevent oxidation. At 85°C, 2 hr was required to decontaminate test coupons from 800 to 35 mr/hr or a length of pipe from an in-pile test loop from 25 to 0.9 r/hr. In the former case the remaining activity appeared to have been replated from the reagent; in the latter case the remaining activity was essentially neutron-induced activity in the stainless steel. Corrosion rates were several hundred mils per year when the reagent was circulated in the equipment being descaled, but this is not serious in the short contact time required. At H_2SO_4 concentrations below 0.2 *M* the descaling rate was very slow; at concentrations above 0.5 *M* the corrosion rate increased.

Titanium and Zircaloy-2 coupons contaminated at 250°C with plutonium and mixed fission products from a 1.7 *m* UO_2SO_4 solution were decontaminated in 2 hr from 130 to 3 mr/hr. The reagent was 0.4 *M* $CrSO_4$–1.0 *M* H_2SO_4 at 87°C.

PART VI. SUPPORTING CHEMICAL RESEARCH

19. Aqueous Systems at Elevated Temperatures

The vapor pressures of several concentrated salt solutions were measured over the temperature range 200 to 400°C. Solutions of either $LiNO_3$ or $Ca(NO_3)_2$ show some promise for application as primary heat transfer media for solid-fuel-element reactors as well as fuel-bearing material for homogeneous reactors.

A survey study of the temperatures at which phase separation occurs in dilute solutions in the

[redacted]

[redacted]

system UO_2SO_4-$CuSO_4$-$NiSO_4$-H_2SO_4-H_2O disclosed the approximate temperature limits of homogeneity as a function of the composition of the solution. The data indicate that operation of the HRT at the design temperature will result in partial or complete precipitation of the uranium.

20. Radiation Studies of Thorium Nitrate Solutions

Autoclave experiments have shown that there was no back reaction between nitrogen and other decomposition gases in the temperature range 140 to 240°C with gas pressures over 2000 psi. The vapor pressure of 7 *m* $Th(NO_3)_4 \cdot 2HNO_3$ solutions can be represented by the equation

$$\log P_{Th} = 1.049 \log P_{H_2O} + 0.071 ,$$

where P_{Th} is the vapor pressure of the solution and P_{H_2O} is the vapor pressure of pure water at the same temperature.

21. Capture Cross Section of U^{236}

The effective capture cross section of U^{236} in highly irradiated MTR fuel elements was measured, and data are presented. The average value obtained for $\sigma(U^{236})_{eff}$ for these irradiations is 34 ± 6 barns.

22. Protactinium Chemistry

The extraction of tracer protactinium by kerosene solutions of di(2-ethylhexyl)phosphoric acid was studied. When 2% (wt/vol %) 2-ethylhexanol was added to 0.1 *M* di(2-ethylhexyl)phosphoric acid in kerosene, the distribution coefficient of tracer protactinium between this solvent and 0.1 *M* HNO_3 was observed to increase from 32 to 154. It is probable that observed distribution coefficients and differences between them in HNO_3 systems are only apparent.

Since thorium also extracts into 0.1 *M* D2EHP–kerosene–2% 2EH, an attempt was made to find conditions that would reduce its extractability. The extraction of yttrium was also studied.

[redacted]

[redacted]

CONTENTS

SUMMARY vii

PART I. HOMOGENEOUS REACTOR TEST

1. HRT OPERATIONS 3
   - 1.1 Construction 3
     - 1.1.1 Reactor Area 3
     - 1.1.2 Control Room Area 3
   - 1.2 Operations 12

2. HRT DESIGN 16
   - 2.1 General Status of Design 16
   - 2.2 Feed- and Purge-Pump Check Valves 16
   - 2.3 Fuel and Blanket Pressurizer Hangers 17
   - 2.4 Fuel and Blanket Pressurizer Insulation 17
   - 2.5 Refrigeration System and Freeze Jackets 17
   - 2.6 Sampling Stations 19
   - 2.7 Rupture-Disk Holder for Pressure-Balancing System 19
   - 2.8 Gas Pressurization 20
   - 2.9 Copper as a Homogeneous Catalyst 21
   - 2.10 Composition of the Gas Phase During Dump 21

3. HRT COMPONENT DEVELOPMENT 22
   - 3.1 Pump Development 22
     - 3.1.1 400A-1 Pump and Loop 22
     - 3.1.2 300A-1 Pump 22
   - 3.2 Reactor Fuel and Blanket Pumps 22
     - 3.2.1 Spare Reactor Fuel Pump and 400A-2 Test Loop 22
     - 3.2.2 Spare Reactor Blanket Pump and 230A Test Loop 22
   - 3.3 HRT Heat Exchangers 23
     - 3.3.1 HRT Fuel Heat Exchanger 23
     - 3.3.2 HRT Spare Heat Exchanger 23
   - 3.4 HRT Feed Pumps 23
   - 3.5 HRT Dump Test 23
   - 3.6 HRT Sampler 26
   - 3.7 HRT Mockup 26
     - 3.7.1 Present Mockup System 26
     - 3.7.2 Operation 26
     - 3.7.3 Pressurizer Inspection 26
     - 3.7.4 Loop Corrosion 27
     - 3.7.5 Behavior of Loop Components 27
     - 3.7.6 Special Tests 28

4. HRT REACTOR ANALYSIS 29
   - 4.1 Reactor Power After Shutdown 29
     - 4.1.1 Shutdown with Forced Circulation 29
     - 4.1.2 Shutdown with Natural Circulation 30
     - 4.1.3 Effect of Heat Loss 30
     - 4.1.4 Steady Power Removal with Natural Circulation 30

[redacted]

[redacted]

4.2 Fuel Concentration as a Function of Poison Level 30
4.3 Reactivity Effects Associated with Two-Phase Separation 31

5. HRT CONTROLS AND INSTRUMENTATION 32

5.1 Procurement 32
5.2 Construction 32
5.3 Liquid-Level Indicators 32
5.4 Pressure and Differential-Pressure Indicators 32
5.5 Valves and Operators 32
5.5.1 HRT Low-Pressure-System Valves 32
5.5.2 HRT High-Pressure-System Valves 32

6. HRT FUEL PROCESSING PLANT 37

6.1 Process Flowsheet 37
6.2 Instrumentation 37
6.2.1 Pressure 37
6.2.2 Level 37
6.2.3 Temperature 41
6.2.4 Flow 42
6.2.5 Electrical and Instrument Connections 42
6.2.6 Transducers 42
6.2.7 Control-Panel Board 42
6.3 Remote Tools 42
6.4 Equipment Testing 45
6.4.1 Flange Leakage Tests 45
6.4.2 Underflow Pot Test 45
6.4.3 Hydroclone 45
6.5 Construction Status 47

PART II. REACTOR DESIGN AND ANALYSIS

7. REACTOR ANALYSIS 57

7.1 Fuel Costs for U^{235} Burners 57
7.2 Cylindrical Reactor Studies 57
7.3 Two-Group Studies of Large Spherical Reactors 60
7.4 Calculation of Two-Group Constants 62

PART III. ENGINEERING DEVELOPMENT

8. DEVELOPMENT OF FUEL-SYSTEM COMPONENTS 65

8.1 Recombiner Development 65
8.1.1 High-Pressure Recombiner Loop 65
8.1.2 Natural Circulating Recombiner 65
8.1.3 Battelle and Syracuse Subcontracts 65
8.2 Small Reactor Components 65
8.2.1 20-cfm Canned-Rotor Blower 65
8.2.2 Small Circulating Pumps 65
8.3 4000-gpm Loop 66
8.4 Titanium-Lined Equipment 66
8.5 High-Pressure Flange Test 66

[redacted]

[redacted]

9. DEVELOPMENT OF BLANKET-SYSTEM COMPONENTS 67
9.1 Study of Cake Formation in 200A Loop 67
9.2 Slurry Component Development and Loop Operation 67
9.2.1 Westinghouse Slurry Pump 200A 67
9.2.2 Aluminum Oxide Abrasion Test 69
9.2.3 Evaluation of Special Thorium Oxides 70
9.2.4 Dump-Tank Evaporator Tests 70
9.3 Slurry Blanket System Test 70
9.4 Heat-Transfer and Fluid-Flow Studies 70

10. INSTRUMENT AND VALVE DEVELOPMENT 75
10.1 Fuel System Components 75
10.1.1 Flow Transmitter 75
10.1.2 Liquid-Level Controller 75
10.1.3 Experimental Valve Program 75
10.2 Blanket-System Components 77
10.2.1 Flush Diaphragm Pressure Transmitter 77

PART IV. CORROSION AND MATERIALS

11. SOLUTION CORROSION 81
11.1 Pump Loops 81
11.1.1 Loop Engineering 81
11.1.2 Loop Test Results 82
11.2 Laboratory Tests 85

12. SLURRY CORROSION 87
12.1 Pump Loops 87
12.1.1 In-Pile Slurry Loop 89
12.2 Toroids 89

13. RADIATION CORROSION 90
13.1 In-Pile Loops 90
13.1.1 Development and Construction 90
13.1.2 In-Pile Loop Experiment L-4-11 91
13.1.3 In-Pile Loop Experiment L-4-12 92
13.2 In-Pile Autoclave Tests 92
13.2.1 LITR Tests 92
13.2.2 MTR Tests 95

14. METALLURGY 96
14.1 Physical Metallurgy 96
14.1.1 Effect of Hydrogen on Zirconium and Its Alloys 96
14.1.2 Zirconium Alloy Development 97
14.1.3 Structures of Zircaloy-2 98
14.2 Mechanical Metallurgy of Zirconium Alloys 99
14.2.1 Zircaloy-2 99
14.3 Welding Development 99
14.3.1 Titanium Welding Development 99
14.3.2 Welding of Titanium-Lined Steel Pipes 100
14.3.3 Inert-Gas-Shielded Arc Welding of Type 347 Stainless Steel 101

[redacted]

[redacted]

14.4 Nondestructive Testing 102
14.4.1 Inspection of Pipe and Tubing 102
14.4.2 Inspection of Reactor Components 103
14.5 Effects of Radiation on Structural Metals and Alloys 104
14.5.1 Equipment and Facilities 104
14.5.2 Nickel Steels 104

PART V. CHEMICAL ENGINEERING DEVELOPMENT

15. THORIUM OXIDE SLURRY DEVELOPMENT 107
15.1 Irradiation Studies 107
15.1.1 Postirradiation Examination of Slurries 107
15.1.2 Radiographic Studies with the Dash-Pot Bomb 107
15.2 Gas Recombination Studies 109
15.3 Slurry Viscosity Measurements 109
15.3.1 Slurry Viscosity Measurements in the Dash-Pot-Stirred Bomb 109
15.3.2 Slurry Viscosity Measurements with the Ultraviscoson 110
15.4 Slurry Characterization and Preparation Studies 112
15.4.1 Settling Properties of Thorium Oxide Slurries 112
15.4.2 Effect of Calcium Addition on Thorium Oxide 113
15.5 Sol Stability Studies 115
15.6 ThO_2 Dissolution 116

16. FUEL PROCESSING 117
16.1 Fission-Product Chemistry 117
16.1.1 Iodine Chemistry 117
16.1.2 Iodine-Removal Development Studies 117
16.1.3 Selenium 118
16.1.4 Antimony 118
16.1.5 Niobium 118
16.1.6 Technetium 118
16.1.7 Rhenium 118
16.2 Reactor Solids Dissolution 118

17. PLUTONIUM-PRODUCER BLANKET PROCESSING 120
17.1 Adsorption of Plutonium on Metals 120
17.2 Solubility of Plutonium in Uranyl Sulfate–Lithium Sulfate Solutions 121
17.3 In-Pile Chemistry of Plutonium and Neptunium 121
17.4 Process Testing Loops 121
17.4.1 Equipment Tests 121
17.4.2 Plutonium-Producer Blanket Processing Loop Facility 123

18. EQUIPMENT DECONTAMINATION 124
18.1 Oxide Scale Removal 124
18.2 Decontamination 124

PART VI. SUPPORTING CHEMICAL RESEARCH

19. AQUEOUS SYSTEMS AT ELEVATED TEMPERATURES 129
19.1 Concentrated Salt Solutions for Reactor Fuel Media or Heat Exchanger Fluids 129
19.2 A Study of Dilute Solutions in the System UO_2SO_4-$CuSO_4$-$NiSO_4$-H_2SO_4-H_2O 130

[redacted]

[redacted]

20. RADIATION STUDIES OF THORIUM NITRATE SOLUTIONS 136

21. CAPTURE CROSS SECTION OF U^{236} 138

22. PROTACTINIUM CHEMISTRY 140

22.1 Extraction of Protactinium 140
22.2 Extraction of Thorium and Rare Earths 140
22.3 Behavior of Protactinium toward Hydroxylamine 140
22.4 Carrier Precipitation of Protactinium 141

[redacted]

Part I

HOMOGENEOUS REACTOR TEST

S. E. Beall

1. HRT OPERATIONS

S. E. Beall

R. E. Brooksbank
W. D. Burch
C. C. Cardwell[1]
J. S. Culver
N. W. Curtis[2]
J. R. Engel
K. E. Estes
J. D. Flynn
J. L. Gory
J. J. Hairston
B. H. Hamling[3]
P. N. Haubenreich
J. W. Hill, Jr.
D. M. Johnson[4]
R. W. Jurgensen[5]
S. I. Kaplan
J. O. Kolb
J. D. Perret, Jr.
H. K. Search[2]
R. Van Winkle
H. E. Williamson

1.1 CONSTRUCTION

1.1.1 Reactor Area

At the beginning of this quarter the installation of high-pressure piping between the major high-pressure-system components (pressure vessel, heat exchangers, and circulating pumps) had just begun. By the end of the quarter, all construction work within the reactor tank was completed, and process lines were flushed out so that a program of engineering tests could begin (see Sec. 1.2). Several phases of the construction work are pictured on the following pages.

Figure 1.1 is an over-all view of the reactor tank from above the west end. In the foreground (to the right) can be seen the top of the blanket low-pressure assembly and (to the left) the blanket heat exchanger. Underneath the center bay can be seen a portion of the thermal shield surrounding the reactor pressure vessel. In the background is the fuel-system equipment.

Figure 1.2 is a closeup of the fuel side of the tank with the fuel low-pressure system in the foreground and the reactor thermal shield in the center background. Several valve-operator assemblies are visible at various locations near the top of the cell. Figure 1.3 is a view of the reactor compartment and shows the fuel and blanket pressurizers, as well as the outlet piping from the core and the pressure vessel. Figure 1.4 is a closeup of the blanket side of the reactor tank, with temporary access stairs in the right foreground.

Figure 1.5 shows the off-gas-system charcoal-bed assembly and its valve pit. The large concrete pit contains four separate charcoal beds, each filled with activated coconut charcoal for the purpose of adsorbing fission gases which are released from the reactor system. The beds will be immersed in water for cooling purposes and will be shielded by 10 ft of earth.

1.1.2 Control-Room Area

Construction work in the control-room area was completed in April, and a checkout was made of all electrical and control circuits. Figure 1.6 is a photograph of the completed main control panel. The graphic arrangement of the process instruments with silhouette symbols of equipment pieces is well illustrated by this panel. Nuclear and power control recorders are located in the center of the board, with all blanket instrumentation to the right and all fuel instrumentation to the left. Figure 1.7 shows a portion of the instrument conduit piping which penetrates the shielding wall between the control area and the reactor tank. Air-line bundles to the remotely operated valves are shown in the foreground. At the top of these lines are the air-operated stop valves which close to seal the process air lines if activity is released inside the reactor tank. Near the center of the photograph are large conduits, which carry thermocouple and electrical lines through the shielding wall. Attached to the pull boxes near the bottom of the conduit lines are air lines, which are used to pressurize the conduit to prevent the inleakage of water when the reactor tank is flooded. The conduit is also blocked with a sealing compound at this point. In the right background of this photograph are lines leading into the west (fuel) instrument cubicle. This cubicle, shown in Fig. 1.8, is a portion of a cylindrical tank, welded onto the north wall of the reactor-to-control-room shield. In this shielded cubicle are located the primary sensing elements

[1]On loan from Babcock & Wilcox Co.

[2]On loan from Pennsylvania Power and Light Company.

[3]On loan from Union Carbide Nuclear Company, New York Office.

[4]On loan from The Glenn L. Martin Co.

[5]On loan from American Gas and Electric Company.

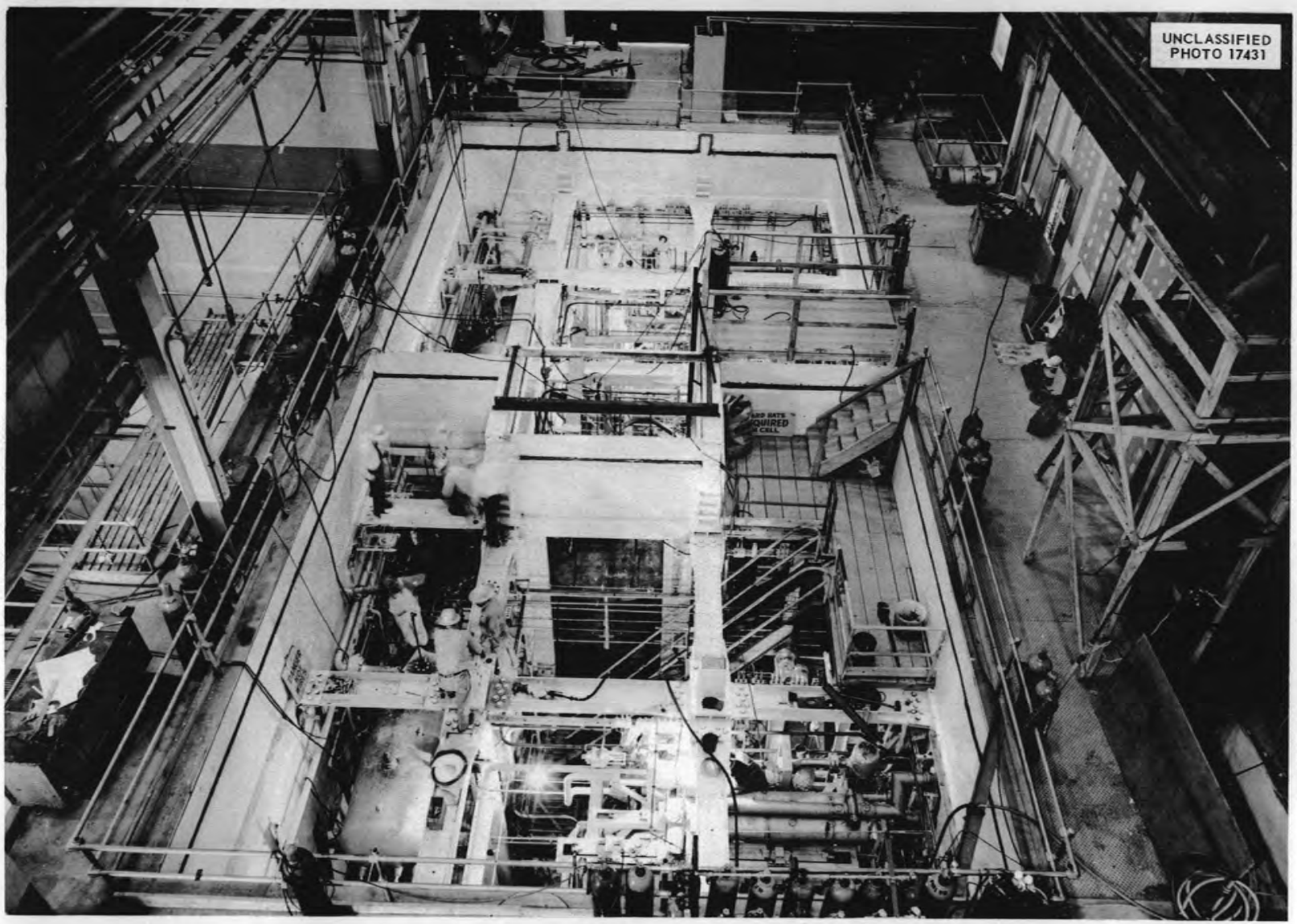

Fig. 1.1. Over-all View of the Reactor Tank Looking from Above the West End.

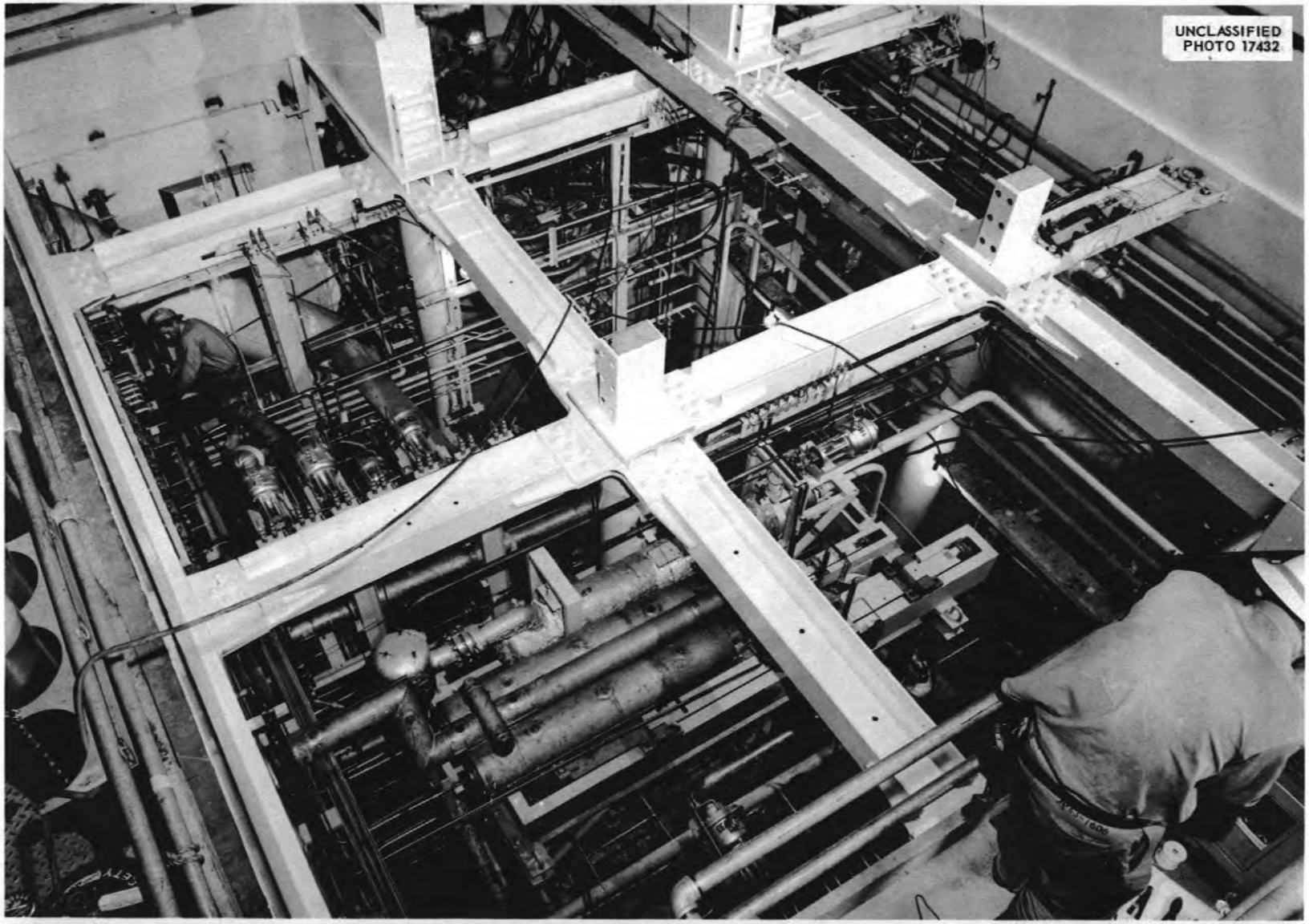

Fig. 1.2. Closeup of the Fuel Side of the Tank with the Fuel Low-Pressure System in the Foreground and the Reactor Thermal Shield in the Center Background.

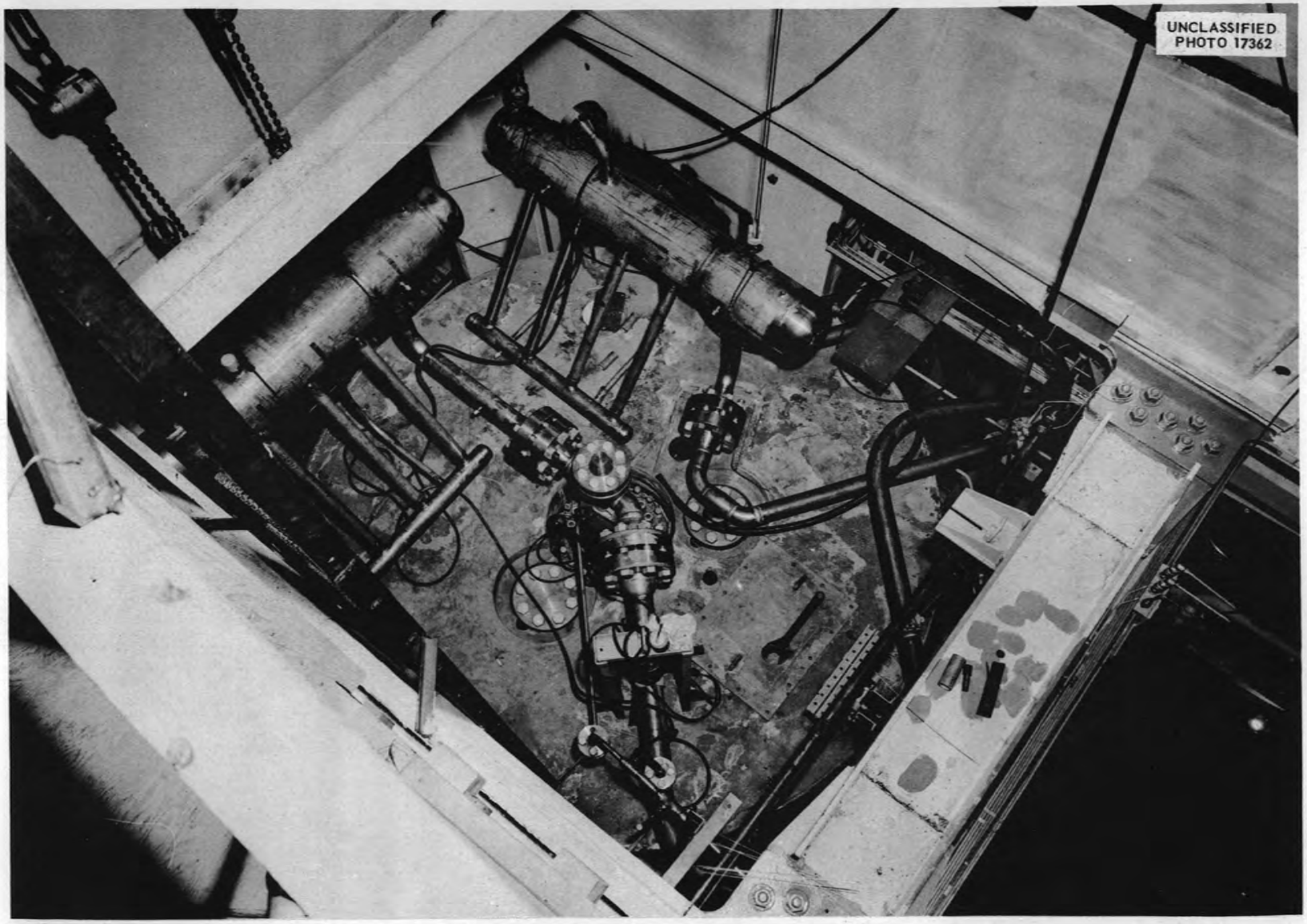

Fig. 1.3. View of the Reactor Compartment.

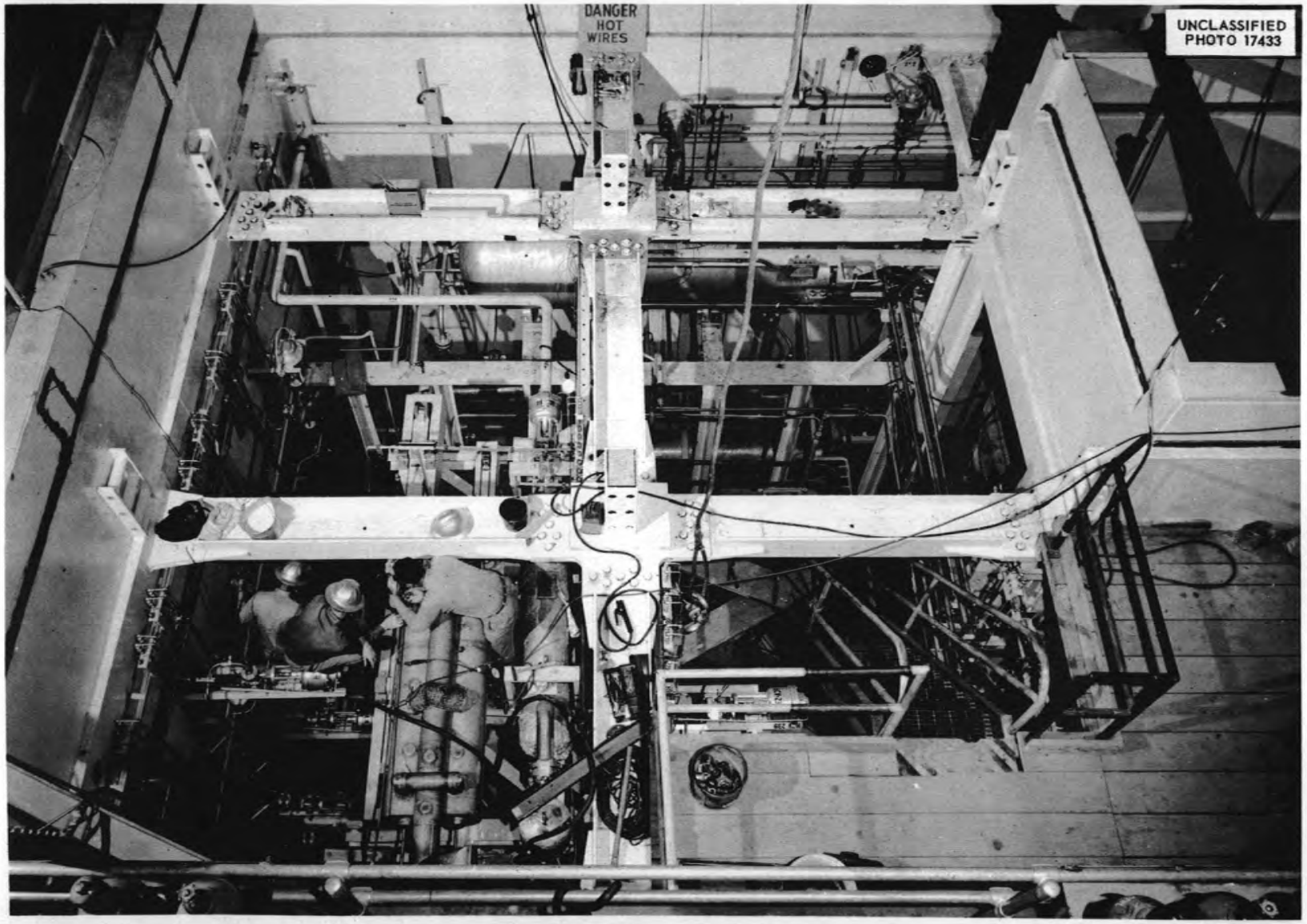

Fig. 1.4. Closeup of the Blanket Side of the Reactor Tank.

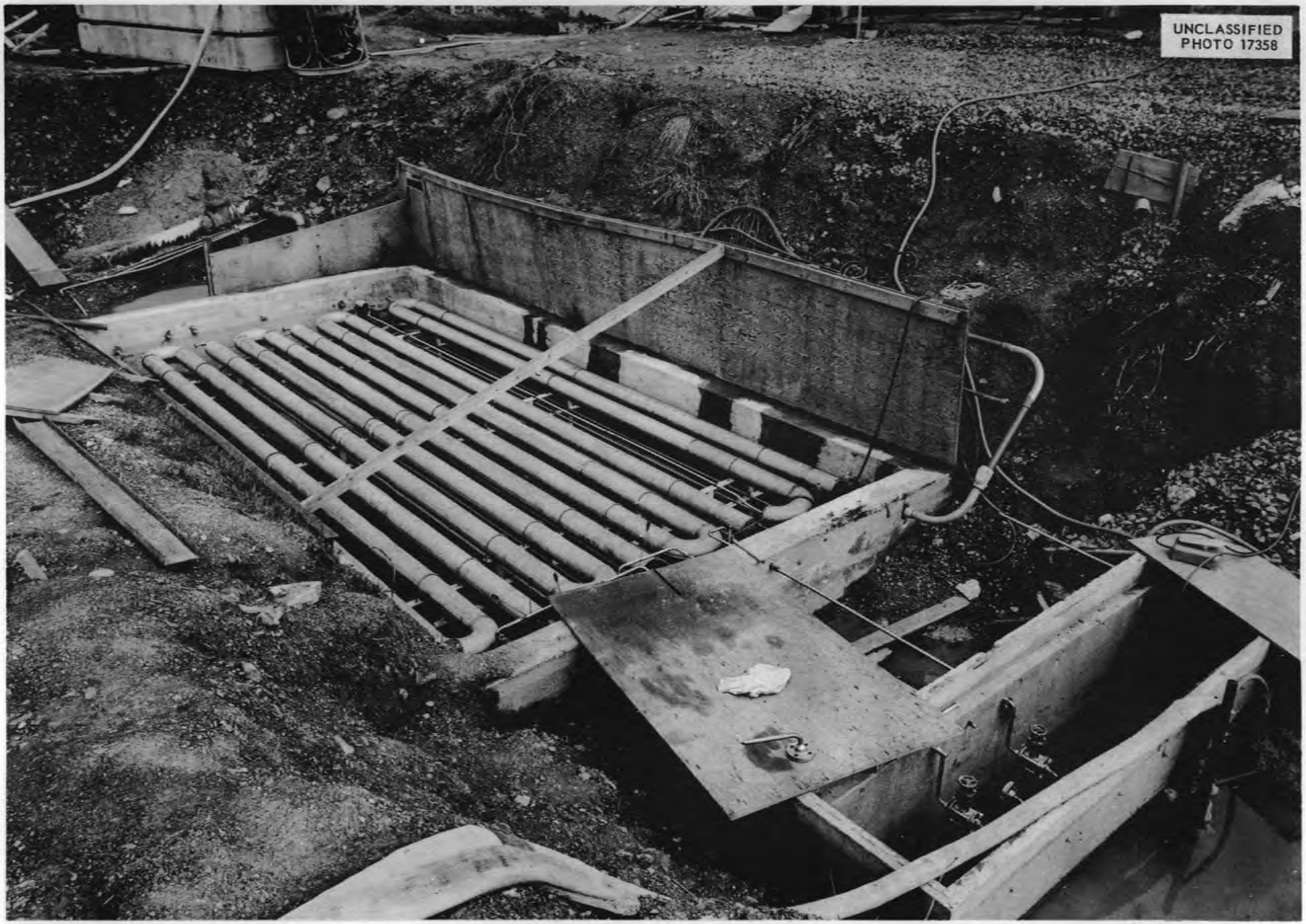

Fig. 1.5. Off-Gas-System Charcoal-Bed Assembly and Its Valve Pit.

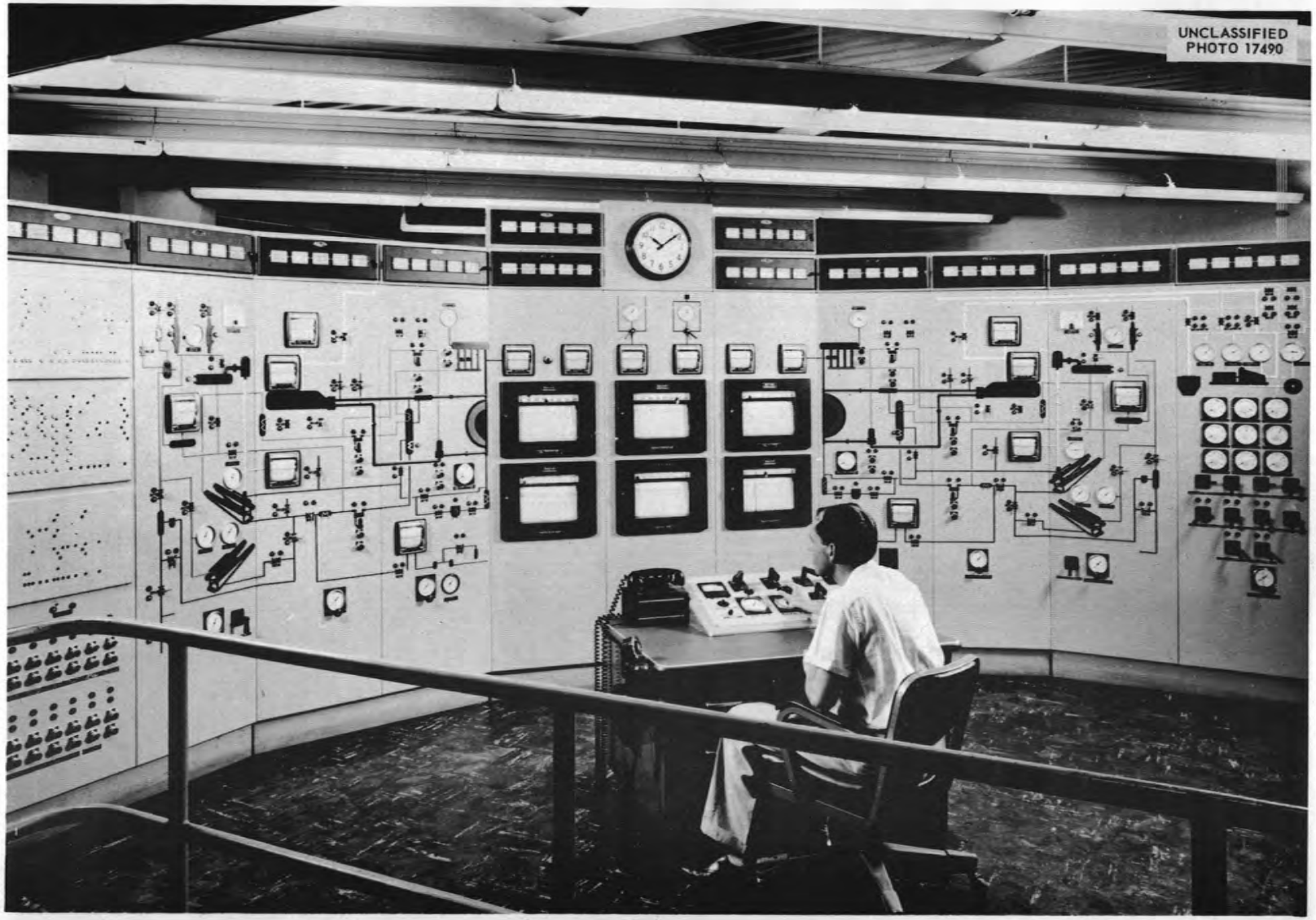

Fig. 1.6. Completed Main Control Panel.

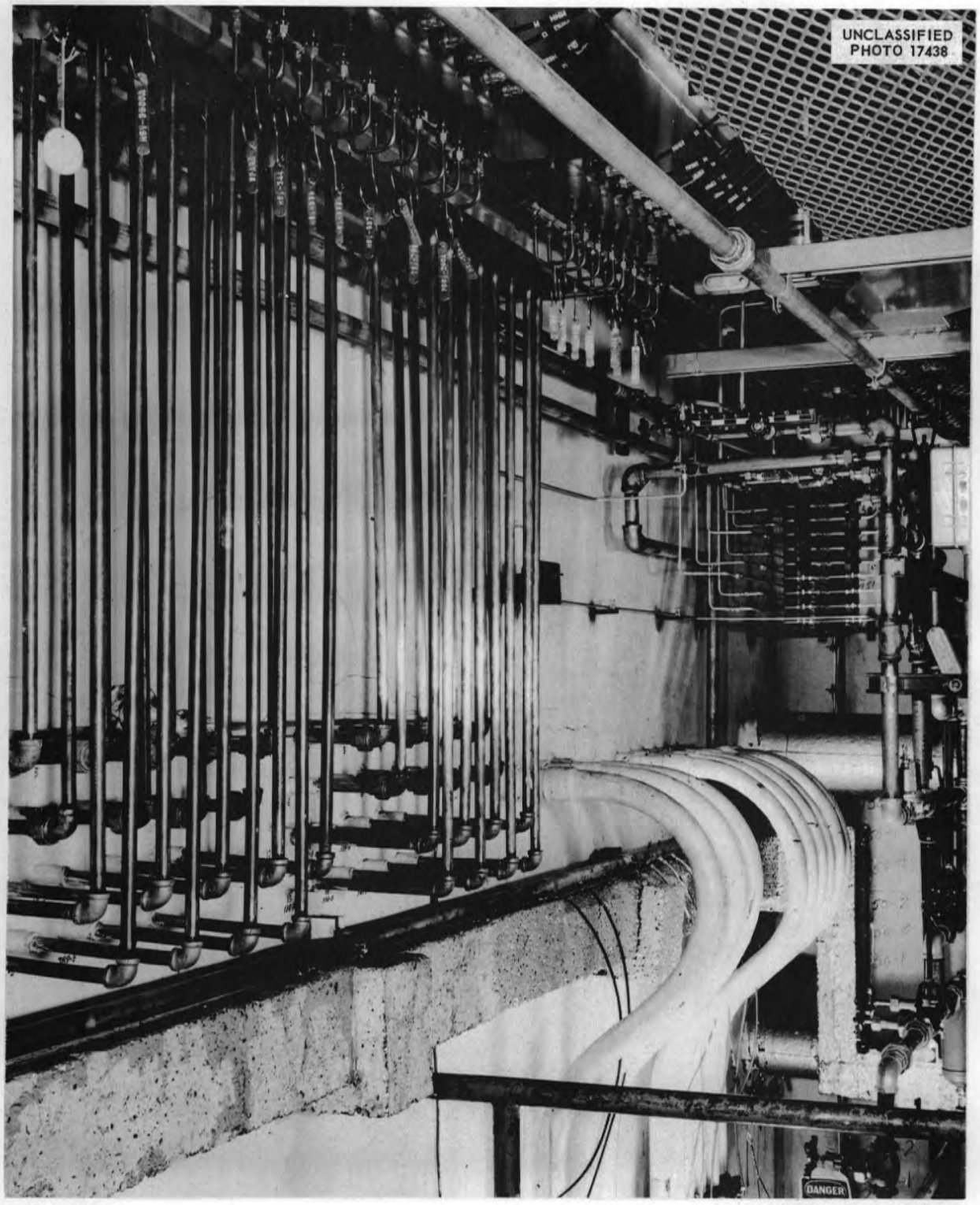

Fig. 1.7. Portion of the Instrument Conduit Piping Which Penetrates the Shielding Wall Between the Control Area and the Reactor Tank.

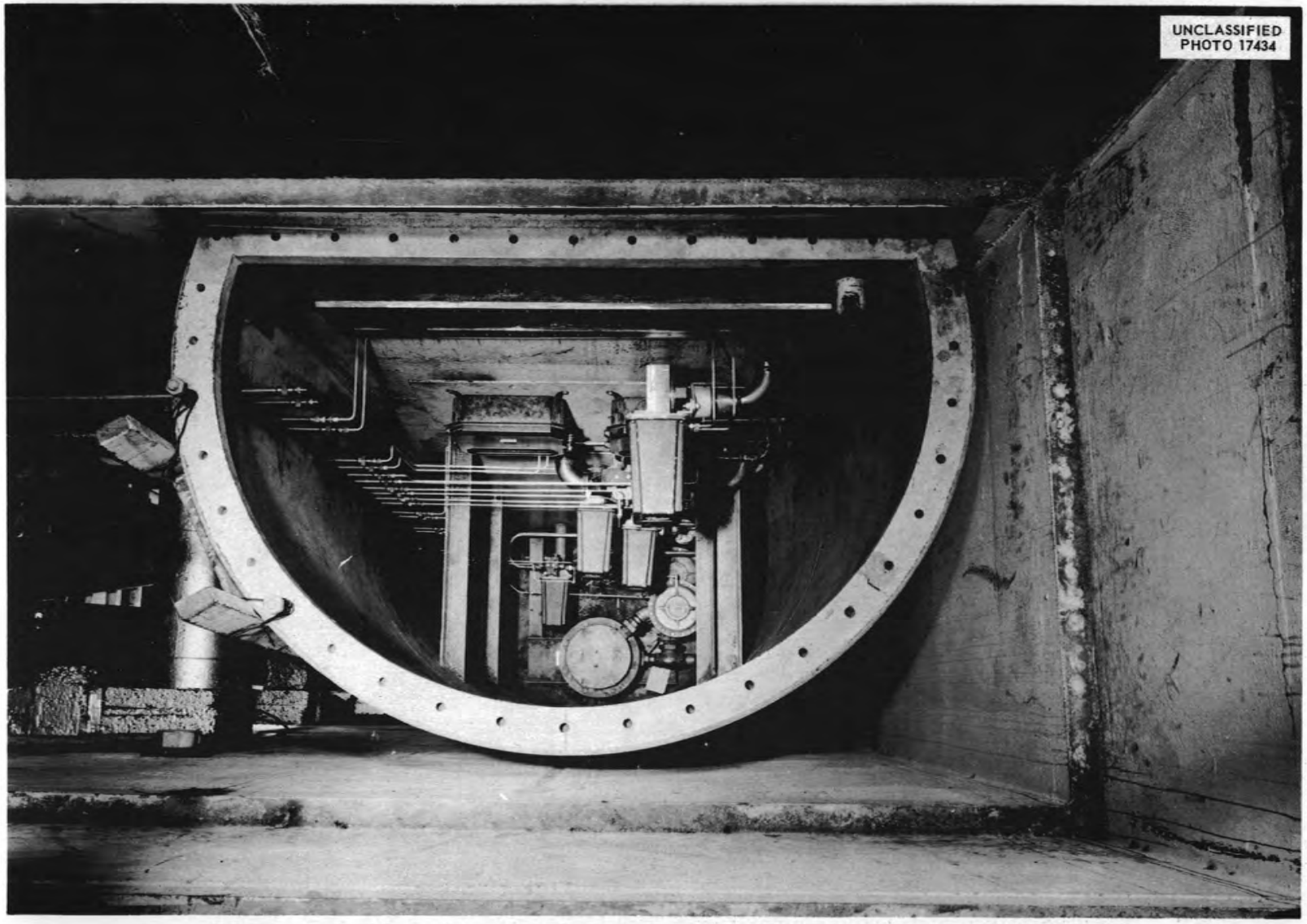

Fig. 1.8. Portion of a Cylindrical Tank, Welded onto the North Wall of the Reactor-to-Control-Room Shield.

such as pressure cells and *D/P* cells. Since these instruments are connected directly to the reactor piping, the cubicle is normally sealed closed; however, a quick-opening entrance on the top closure (not shown) will permit entrance into the cubicle during periods of reactor shutdown.

Figure 1.9 shows the thermocouple "patch panel," in which some 400 thermocouples are terminated. The plug-in type of board permits easy rearrangement of the thermocouple signals for experimental purposes. Figure 1.10 is a view of one half of the leak-detector installation located on the bottom floor of the control area. A leak-detector line is attached to each ring-joint flange in the reactor cell. The leak-detector lines penetrate the shielding wall and are manifolded through valves as shown in this photograph. In normal operation a hydrostatic pressure, always greater than the reactor operating pressure, is applied to all the leak-detector lines, and the pressure is monitored continuously. Leakage is indicated by a reduction in header pressure. The leak is found by first isolating banks of lines and then by closing off individual lines in a single bank.

The refrigeration system, which supplies cold Freon-11 to freezer stations and cold traps within the reactor cell, is shown in Fig. 1.11. This installation is also located on the bottom floor of the control gallery. The compressor, rated at 3 tons at –40°F, is pictured in the foreground, with the circulating pump for cold Freon to the left of the compressor and the storage tank for cold Freon in the background. Not visible is the circulating equipment for warm Freon, which is used to defrost cold traps, or the control panel, which houses the instrumentation for automatic defrosting and refreezing of cold traps on a chosen cycle.

1.2 OPERATIONS

An operating crew of approximately 30 engineers and technicians, in addition to four industrial loanees, completed the HRT operations training course and was assigned on a three-shift basis beginning April 23. The initial work of the Operations Group will be devoted to cleaning and preconditioning of the process piping, calibration of vessels, and preparation of auxiliary equipment for operation. This will be followed by the program of engineering tests outlined by Hill.[6] These tests are scheduled for the period from May through September and are to be followed by the first critical experiment.

During the quarter, memoranda were issued describing the procedures and methods for testing the following equipment:

HRT Test No.	Title	ORNL CF No.
II-A, 10a, b, c, d	Fission Product Adsorbers	56-4-102
II-A, 49a, b; 39	Blanket Storage Tanks and Reflux Condenser	56-4-65
IV-A, 7c, b	Blanket Entrainment Separator Performance	56-3-143
IV-34a, b, c; 37	Calibration of Blanket Dump Tanks and Condensate Tanks	56-4-115
V-A, 1a, b	Turbine Generator	56-4-28
V-A, 2a, b, c	Turbine Condenser	56-4-140
V-A, 3a, b	Feed Water Pumps	56-2-159
V-A, 4a, b	High-Pressure Warmup Boiler	56-3-123
V-A, 5a, b	Air-Cooled Condenser	56-4-98
V-A, 8a	Core and Blanket Steam Drums	56-3-144
VI-A, 2, 3, 4, 5	Cooling Water System	56-4-134
VII-A	Refrigeration System and Cold Traps	56-4-99
	Hydrostatic Test on HRT Fuel and Blanket Systems	56-4-167

[6] J. W. Hill, *HRT Engineering Tests*, ORNL CF-55-5-143 (May 20, 1955).

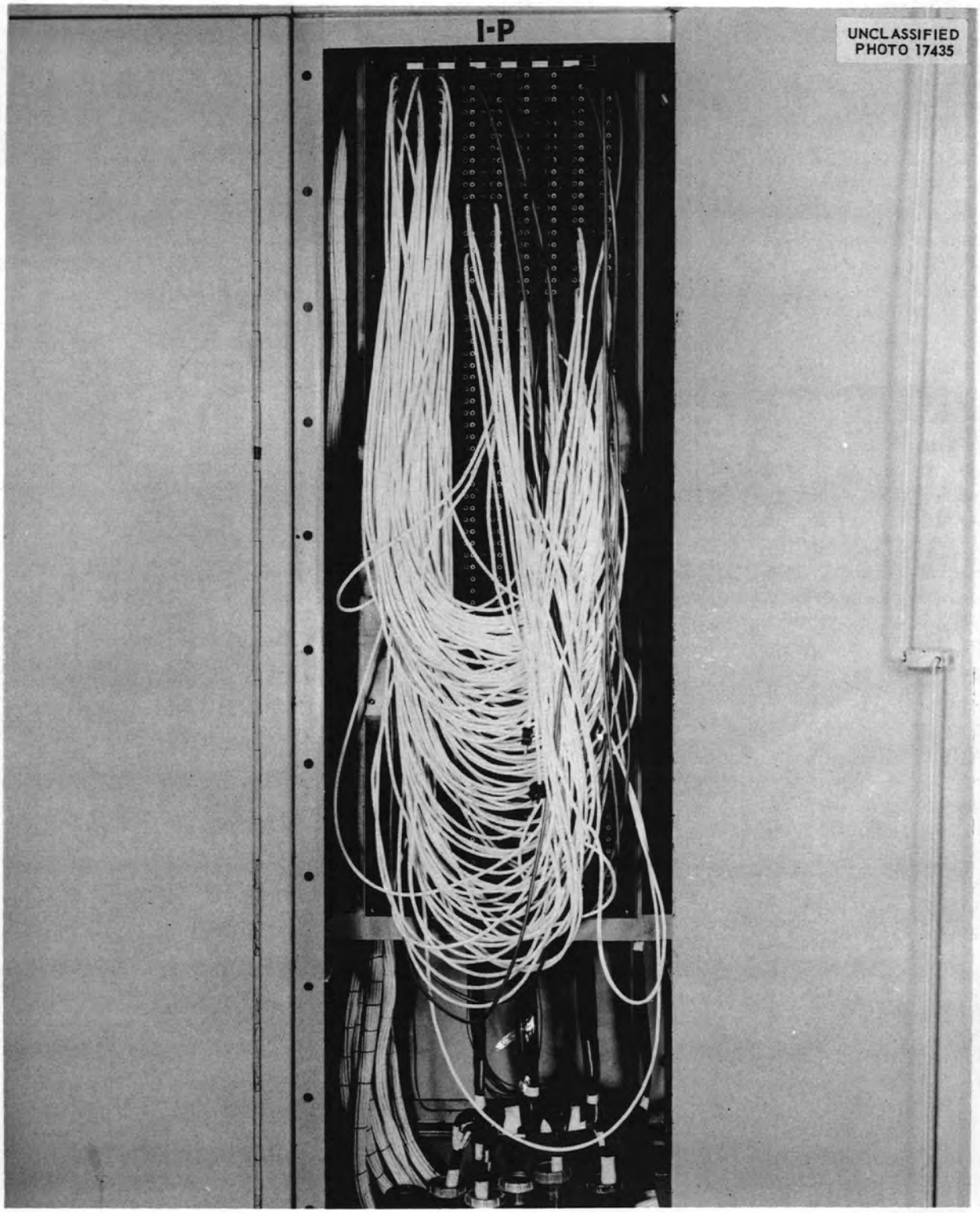

Fig. 1.9. Thermocouple "Patch Panel" in Which Some 400 Thermocouples Are Terminated.

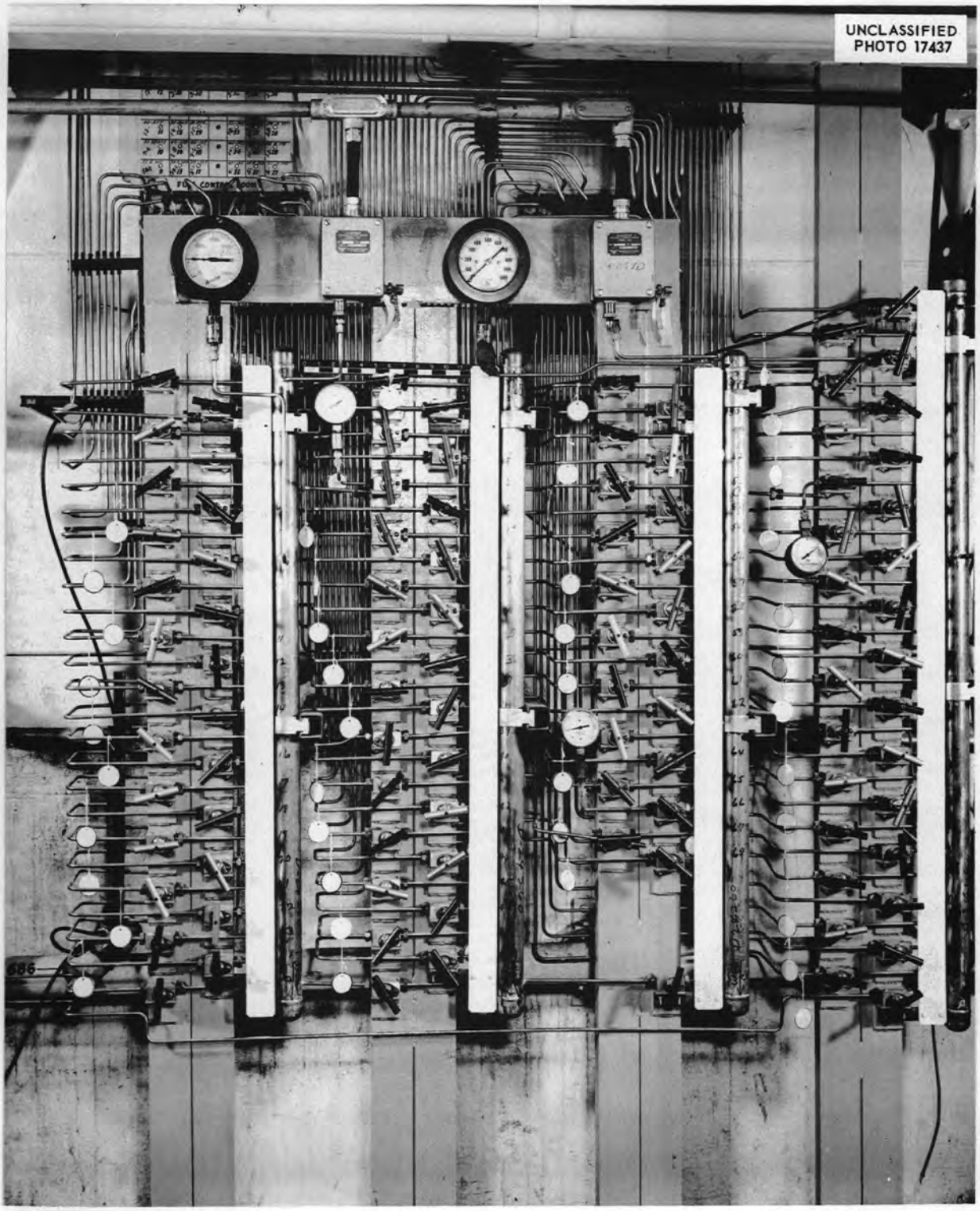

Fig. 1.10. View of One Half of the Leak-Detector Installation Located on the Bottom Floor of the Control Area.

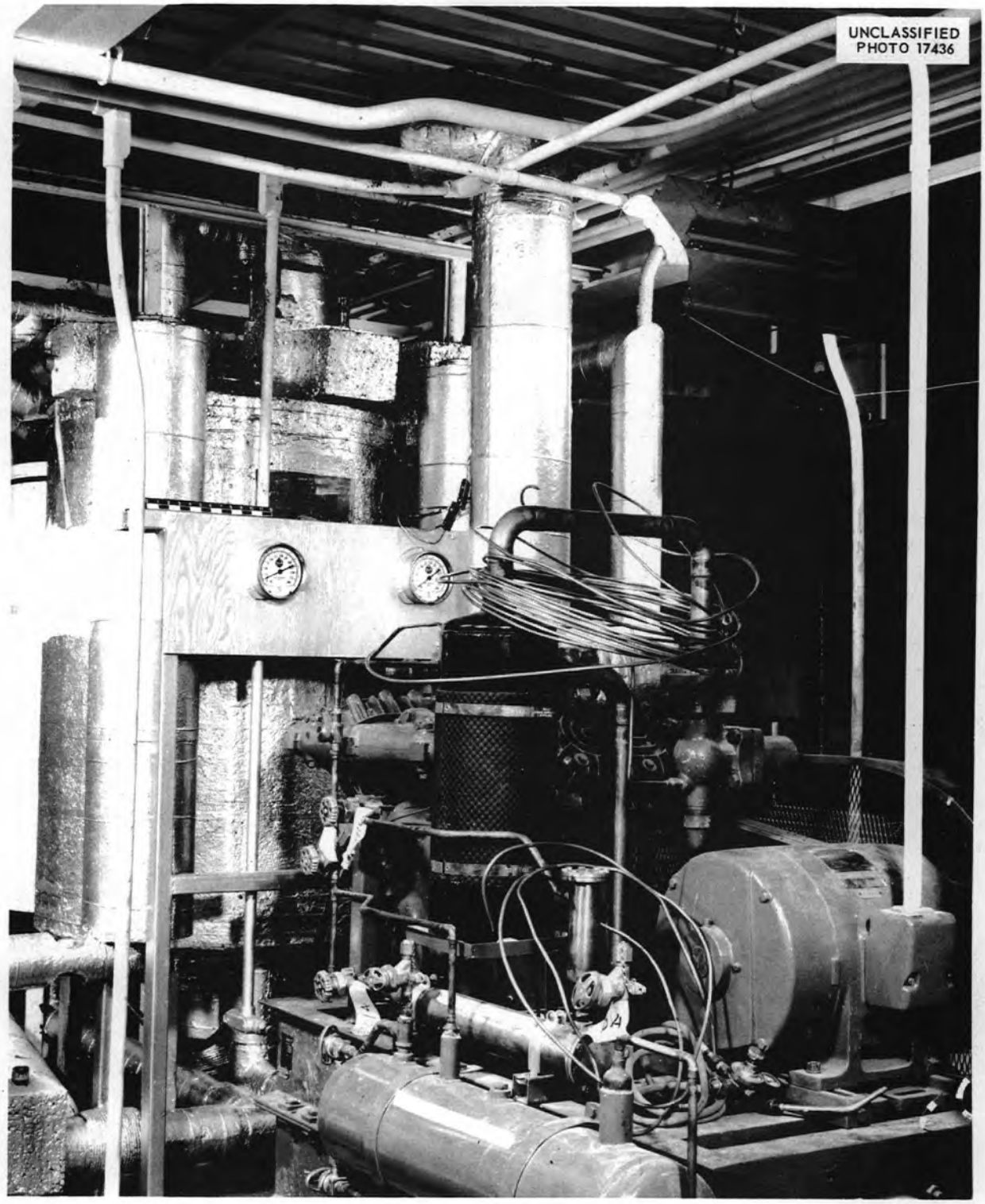

Fig. 1.11. Refrigeration System, Which Supplies Cold Freon-11 to Freezer Stations and Cold Traps Within the Reactor Cell.

2. HRT DESIGN

W. R. Gall R. B. Korsmeyer

R. E. Aven
C. A. Bruchsted
R. H. Chapman
C. J. Claffey
H. N. Culver[1]
R. F. Hughes[2]
R. W. Jurgensen[3]
J. E. Kuster[4]
M. C. Lawrence[5]
H. A. McLain
M. I. Lundin
C. Michelson[1]
R. C. Moren[6]
R. C. Robertson
J. N. Robinson
C. L. Segaser
W. F. Taylor[7]
W. Terry
T. H. Thomas
F. C. Zapp

2.1 GENERAL STATUS OF DESIGN

The preparation of working drawings for the HRT is approximately 98% complete. During the quarter the following general items of design were completed:

Pressurizer location, piping, and supports
Pressurizer liquid-level indicators and heaters
Outer-dump-tank liquid-level controllers
Sampler details and assembly
Fuel feed- and purge-pump check-valve redesign
Underground waste and vent system piping and layout
Rupture-disk holder for pressure-balancing system
Space cooler supports and location
Temporary-freeze-jacket details
Fission- and ion-chamber positioners, design and layout
Electrical and thermocouple disconnects in cell

Minor design changes were made as required during construction, and a survey of piping installed within the cell was completed to determine conformance with, and necessary revisions to, approved drawings and to locate possible areas of conflict between erected piping and maintenance requirements.[8]

2.2 FEED- AND PURGE-PUMP CHECK VALVES

The suction check valves of the feed and purge pumps were redesigned as a result of the failures which occurred during mockup-loop operations. Examination of the valves that failed revealed small notches in closure welds; these notches served as stress raisers for the fatigue cracks, which culminated in failure of the valve bodies. The closure weld was relocated in the new design in order to relieve shrinkage stresses due to welding and to improve the stress distribution in the highly stressed cap region. Relief from radial shrinkage due to welding was provided about the upper cage. The protrusion on the inside of the cap shown in Fig. 2.1 serves to reduce the volume of liquid

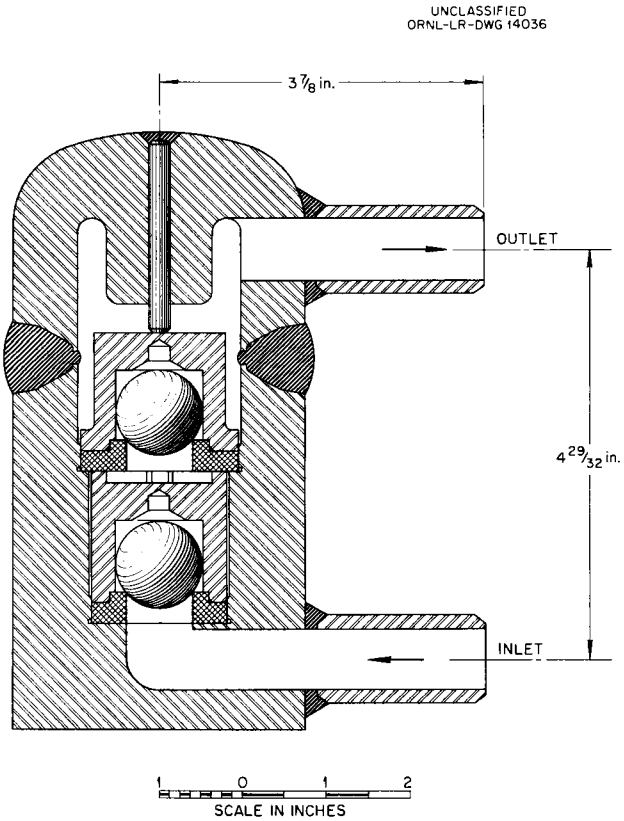

Fig. 2.1. Suction Check Valve for Diaphragm Pumps.

[1]On loan from TVA.

[2]On loan from Kaighin & Hughes, Inc.

[3]On loan from American Gas and Electric Company.

[4]On loan from Maxon Construction Co.

[5]On loan from General Dynamics Corp.

[6]On loan from Westinghouse Electric Corporation.

[7]On loan from Pioneer Service & Engineering Co.

[8]H. N. Culver, *Piping Installation*, interoffice memorandum, (April 9, 1956).

within the valve; the pin through the cap retains the upper cage in position.

The suction check valves of the feed and purge pumps operate on a pressure cycle alternating between subatmospheric and 2500 psia, at 78 to 120 cpm. The severe stresses produced by such loading are conducive to fatigue failures such as have been encountered. No failures have occurred in the discharge check valves, which operate on a pressure cycle from 2000 to 2500 psia.

2.3 FUEL AND BLANKET PRESSURIZER HANGERS

Pipe hangers of the "constant support" type were specified for support of the fuel and blanket pressurizers in order to avoid excessive stresses in the nozzles of the reactor core vessel. The pressurizers are expected to rise approximately ½ in., relative to the top of the thermal shield, when brought to operating temperature. The hangers, two for each pressurizer, are suspended from above to permit their removal in the event that the pressurizers must be removed for maintenance.

The liquid-level controllers associated with the blanket pressurizer are supported from a structural-steel frame extending from the end of the pressurizer drum. One of the controllers associated with the fuel pressurizer is mounted on a bracket welded to the pressurizer inlet line, and the other is mounted on a pedestal welded to the top of the thermal shield.

2.4 FUEL AND BLANKET PRESSURIZER INSULATION

Both crinkled aluminum foil and preformed sheet aluminum were found to provide adequate thermal insulation for the pressurizers. Design factors considered in the investigation of these materials for this purpose included heating capability of the pressurizer heaters, the fixed heating loads present, and the allowable surface losses.

The heating capacity of each pressurizer is limited to 13.5 kw of the 32-kw capability of the heaters by contact resistance between the heaters and the pressurizer piping and by the 850°F maximum permitted operating temperature. Fixed load, which includes feedwater preheating and surface losses from the liquid-level indicators, totals about 6.2 kw. Parts of the indicators must be cooled and might be left uninsulated.

A minimum insulation efficiency of 82%, based on bare-surface losses, was specified to limit the loss of heat from 55 ft^2 of pressurizer and piping surface to 7.3 kw.

Aluminum foil, although not so reliable an insulating medium as the preformed aluminum sheet, is favored because of the greater ease of application to the complex geometry of the pressurizers and because of its lower cost.

2.5 REFRIGERATION SYSTEM AND FREEZE JACKETS

The two-stage, 5-hp refrigeration compressor, originally installed in the primary Freon-12 refrigeration system, was replaced with a Brunner single-stage, 15-hp, air-cooled compressor having a capacity of 3 tons at –40°F evaporator temperature.[9] This unit will chill the coolant circulated to the cold traps and freeze jackets in the reactor cell.

Because severe radiation-induced corrosion effects might be encountered through the use of Freon-11 in the circulating system, tetralin ($C_{10}H_{12}$) is being considered as a substitute refrigerant.[10] The use of sulfur dioxide, which was considered earlier, has been discouraged because of its high toxicity.

Four designs for freeze jackets to be used for sealing off lines were completed following performance tests. Two types of jackets are permanently connected to the refrigeration system and can be operated while the reactor is in operation. Two temporarily connected types can be used only when the reactor cell is open.[11] The type-A permanent jacket is made of stainless steel tubing wound about and welded to the process line. It will be used on process lines in which temperatures exceed 300°F. The second type of permanent jacket, type B, consists of copper tubing wound about and soft-soldered to lines in which temperatures will not exceed 300°F. The general configuration of the permanent freeze jacket is illustrated in Fig. 2.2. The type-C temporary freeze jacket, shown in Fig. 2.3, is simply copper

[9] F. C. Zapp, *HRT Process Flowsheets (Rev. II)*, ORNL CF-55-5-156 (March 6, 1956).

[10] R. C. Robertson and J. E. Kuster, *Possible Substitutes for Freon-11 in HRT Cold Trap Refrigeration System*, ORNL CF-56-4-20 (April 5, 1956).

[11] R. C. Robertson, *Permanent Freeze Jackets for HRT Process Lines 1/2" and Smaller*, ORNL CF-56-2-137 (Feb. 23, 1956).

tubing wound tightly about the process line; it is installed at points which are inaccessible from the top of the cell. The type-D jacket is intended for remote installation as needed; it is operated remotely by a manually controlled operator as indicated in Fig. 2.4. Crinkled aluminum-foil insulation, similar to that used on process piping, has been specified for the jackets of types A, B, and C. The type-D jacket is covered by a split, waterproof, formed aluminum insulation. Freeze jackets have been specified for both sides of all major valves and at each of the pumps, in order to prevent the entry of light water into the system during the removal of those components.[12]

[12]R. C. Robertson, *HRT Freeze Jacket Locations*, interoffice memorandum (April 15, 1956).

UNCLASSIFIED
ORNL-LR-DWG 14037

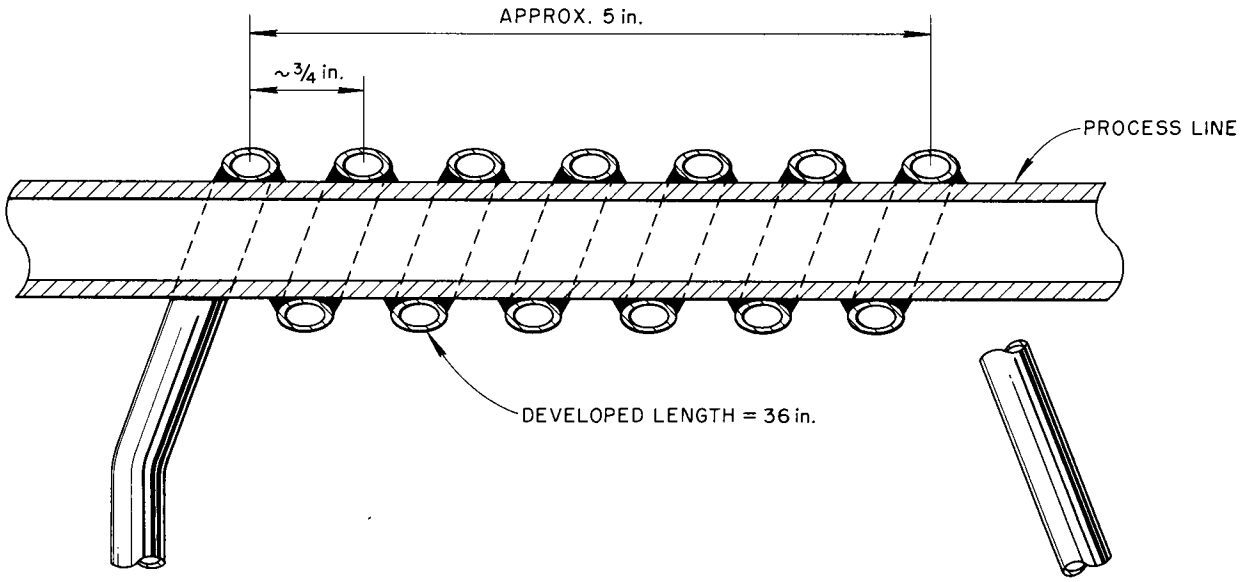

Fig. 2.2. Permanent Freeze Jacket.

UNCLASSIFIED
ORNL-LR-DWG 14038

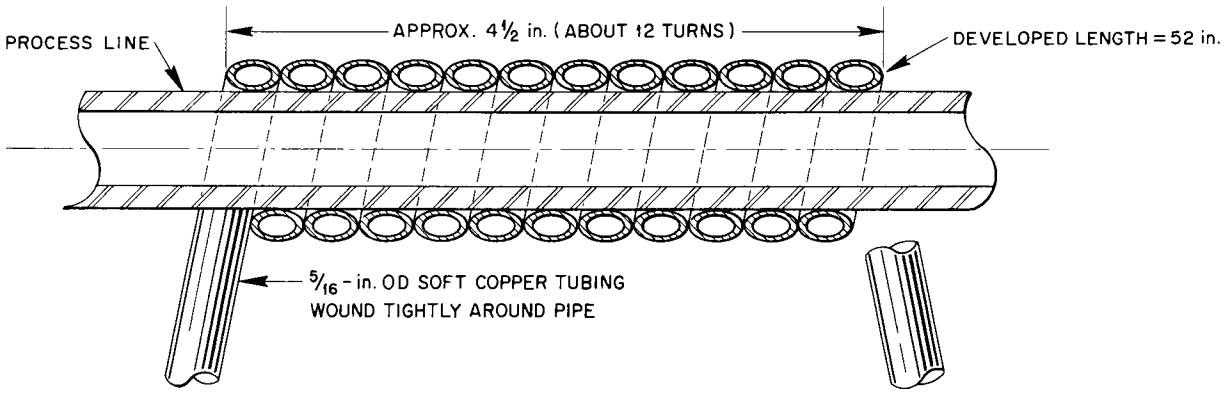

Fig. 2.3. Temporary Freeze Jacket Type C.

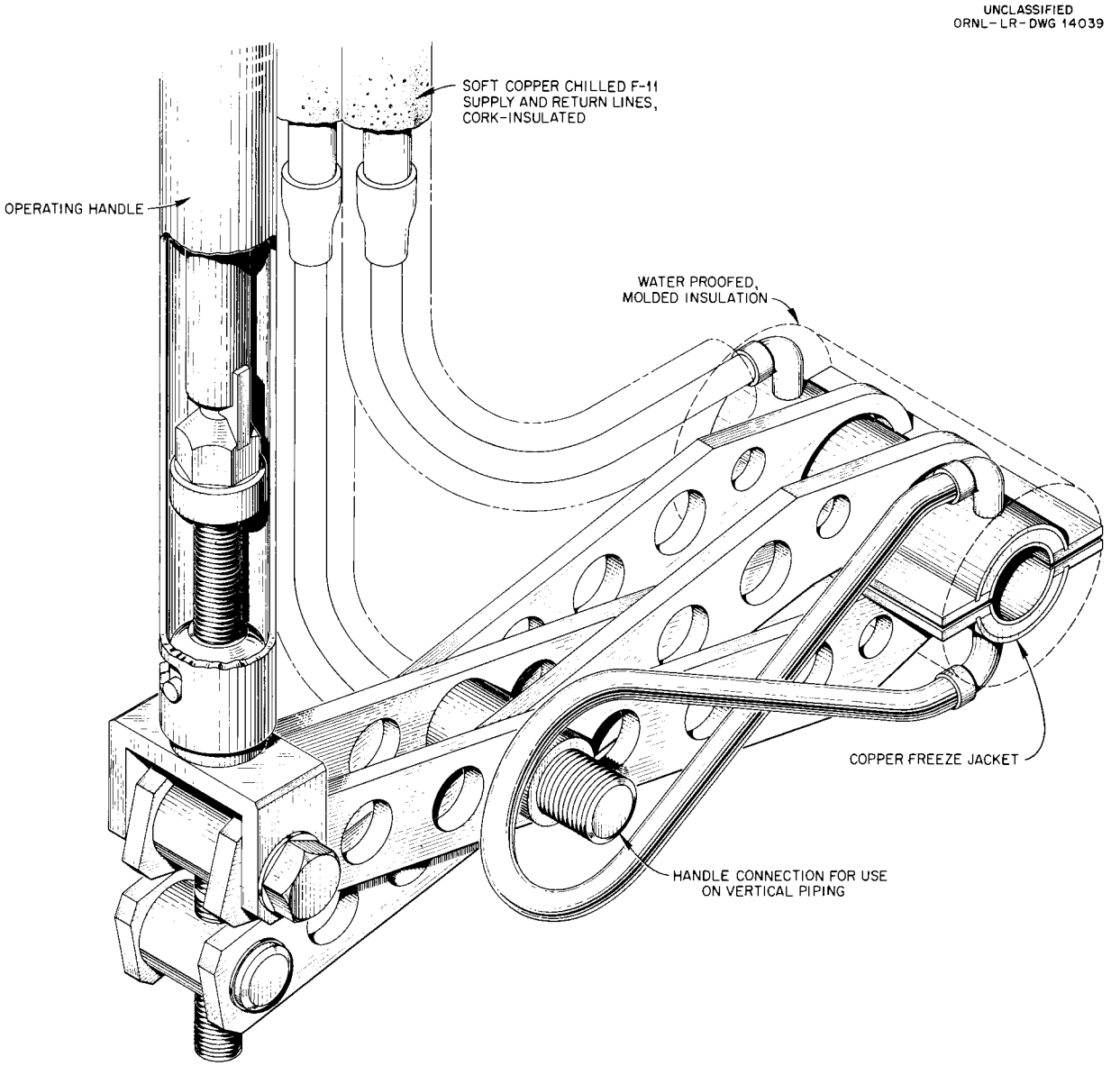

Fig. 2.4. Type D Remote-Operator and Clampon-Type Freeze Jacket.

2.6 SAMPLING STATIONS

Final design of the sampling stations was completed following operational tests of the prototype.[13] The diameter of the main indexing shaft was increased to improve operational integrity, and the differential pressure cells were raised to facilitate their drainage.

[13] W. R. Gall *et al.*, *HRP Quar. Prog. Rep. July 31, 1955*, ORNL-1943, p 13.

2.7 RUPTURE-DISK HOLDER FOR PRESSURE-BALANCING SYSTEM

A special rupture-disk holder was designed to replace the two standard holders originally specified[9] for the pressure-equalization line connecting the blanket and fuel pressurizers (line 146). The new design, Fig. 2.5, incorporates both rupture disks in a single vessel to which entry may be gained by the removal of a single blind flange.

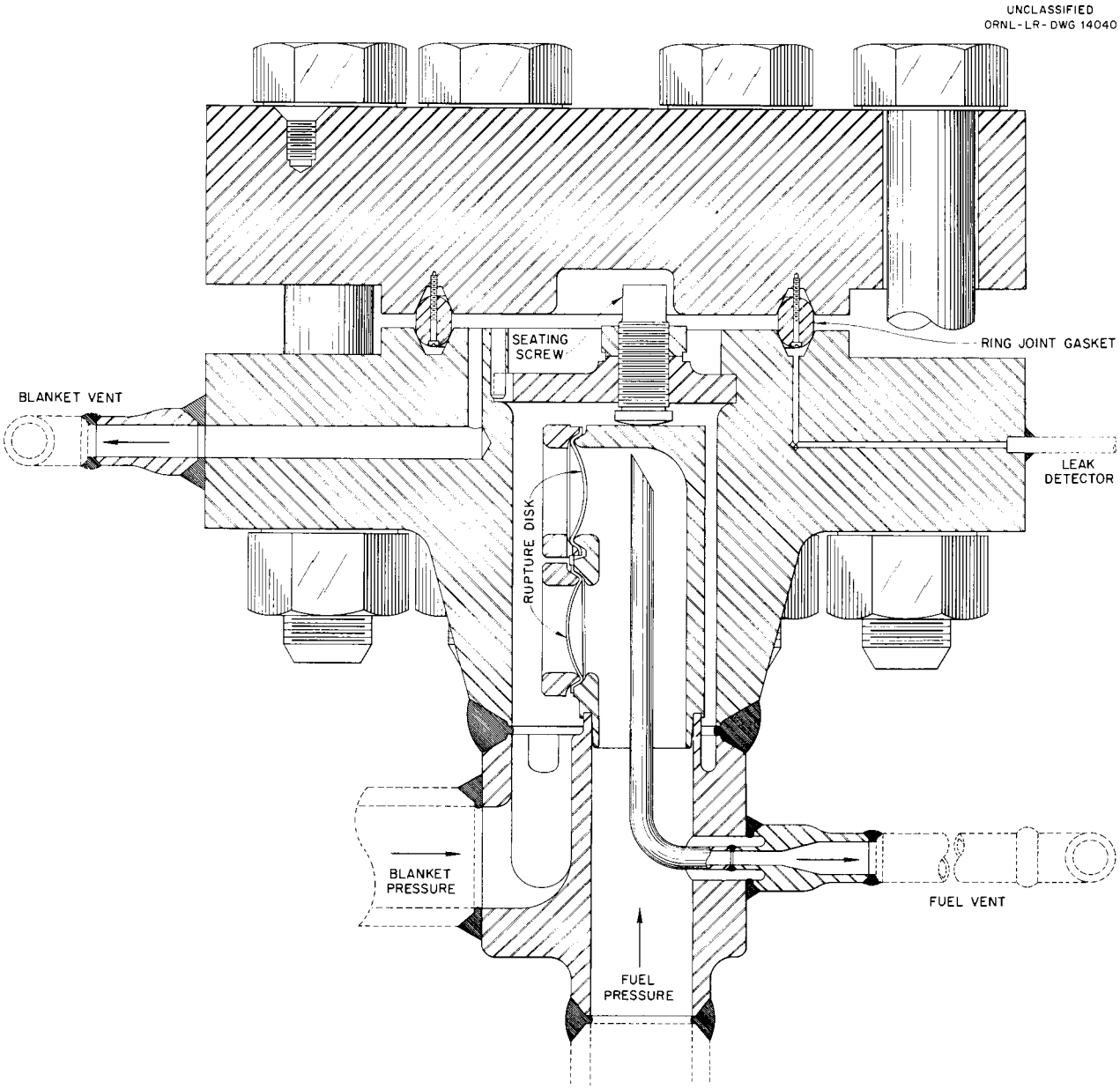

Fig. 2.5. Rupture-Disk Holder for Pressure-Balancing System.

2.8 GAS PRESSURIZATION

The studies of gas pressurization of the HRT[14-16] were completed and will serve as the basis for further investigations if steam pressurization should prove to be unsatisfactory. Oxygen was recommended to be the most suitable pressurizing gas. The final report of Arthur D. Little, Inc.,[17] contains engineering flowsheets and design data applicable to such a system.

[14] J. W. Hill, Jr., *HRT Power and Fuel Temperature After Fuel Circulation Stops*, ORNL CF-54-9-64 (Sept. 9, 1954).

[15] R. E. Aven, *Survey of Gas Pressurization for the HRT*, ORNL CF-56-3-17 (March 30, 1956).

[16] Contract between AEC and Arthur D. Little, Inc., AEC Activity 4103.1.

[17] Arthur D. Little, Inc., *Gas Pressurization of Homogeneous Reactor Test*, Memorandum C-60034 (Feb. 14, 1956).

2.9 COPPER AS A HOMOGENEOUS CATALYST

A study was completed concerning several aspects of internal recombination of radiolytic gases in HRT solutions, with dissolved copper being used as a catalyst.[18] The use of homogeneous catalysts results in a reduction in the amount of gas that is generated in the reactor and that must be recombined in the low-pressure system. Although sufficient copper could be introduced to recombine all the radiolytic gases, some gas letdown is desirable for use in stripping fission-product gases from the fuel solution. The concentrations listed in Table 2.1 are indicated for the HRT when it is operating at a power level of 5 Mw.

TABLE 2.1. HRT INTERNAL RECOMBINATION

Internal Recombination (%)	Copper Concentration (g-moles/liter)	
	At 2000 psia	At 1700 psia
80	0.0019	0.0032
90	0.0022	0.0037
100	0.0025	0.0042

Calculations based on experimental data indicate that gamma-induced recombination of D_2 and O_2 in the heavy-water blanket should be sufficient to prevent the appearance of radiolytic gases; therefore no copper catalyst is required in the blanket. However, the presence of ionic impurities tends to destroy the recombination process, necessitating the use of high-purity D_2O.

[18] R. E. Aven and M. C. Lawrence, *Calculation of Effects of Copper Catalyst in the HRT*, ORNL CF-56-4-4 (to be issued).

2.10 COMPOSITION OF THE GAS PHASE DURING DUMP

During operation of the reactor, fuel solutions will be at, or very close to, saturation with radiolytic deuterium; at design temperatures and pressure the concentration of deuterium will be sufficiently great (0.0025 to 0.0031 mole fraction) to cause concern regarding explosive concentrations in the high-pressure system following a sudden dump. Estimates of the concentrations present during the dumping were calculated for both gas- and steam-pressurized systems; explosive mixtures were indicated in both cases. A delay is therefore desirable between power shutdown and the start of a dump in order to permit the catalytic recombination of part of the deuterium. The delay times indicated and the resultant changes in concentration of deuterium at a power level of 5 Mw with 80% recombination are presented in Fig. 2.6.

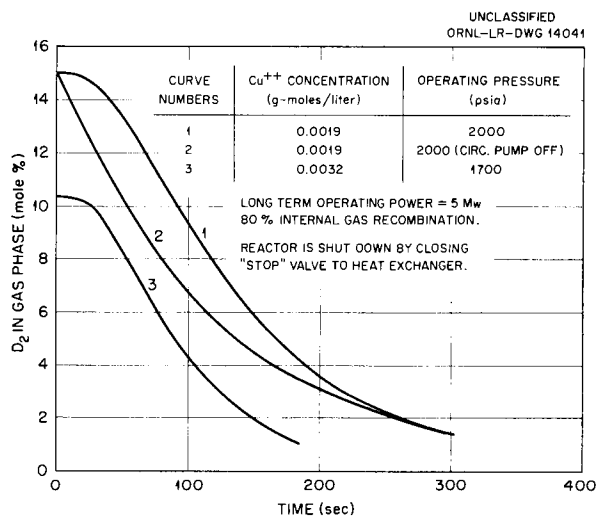

Fig. 2.6. Maximum Mole % D_2 Expected in the Gas Phase of the HRT During a Dump vs Delay Time for a Controlled Reactor Shutdown. Delay time includes time it takes for reactor to go subcritical (~2 min).

3. REACTOR COMPONENT DEVELOPMENT

C. B. Graham

L. J. Bell
R. Blumberg
B. D. Draper[1]
H. L. Falkenberry[1]
C. H. Gabbard
L. F. Goode
B. A. Hannaford
P. H. Harley
E. C. Hise
P. P. Holz
P. F. Pasqua[2]
W. L. Ross
I. Spiewak
D. S. Toomb
D. E. Willis
H. D. Wills

3.1 PUMP DEVELOPMENT

HRT-size pumps are being tested in the mockup and test loops to improve the reliability of thermal-barrier seals and to check the performance of titanium parts.

3.1.1 400A-1 Pump and Loop

The 400A-1 Westinghouse pump, with a new thermal barrier welded into the stator flange, was operated on 250°C water for 250 hr. The thermal barrier contains a titanium insert at the labyrinth wear ring and shaft seals, where corrosion was observed on all-stainless-steel thermal barriers. Close observation of a thermocouple well located near the Kingsbury thrust bearing and heat-balance checks on the cooling water indicated that no leakage occurred around the thermal barrier.

The loop is shut down for replacement of ¼-in. tubing and fittings with pipe and welded connections.

3.1.2 300A-1 Pump

Since the seal-welding of both the thermal barrier and the main flange, the 300A-1 pump has operated without incident in the HRT mockup for 1627 hr, including 1234 hr on uranyl sulfate solution at 300°C.

3.2 REACTOR FUEL AND BLANKET PUMPS

3.2.1 Spare Reactor Fuel Pump and 400A-2 Test Loop

The spare 400-gpm reactor fuel pump, which contains titanium parts, was installed in the 400A-2 loop for testing. One 550-hr run, in which a solution containing 0.04 *m* UO_2SO_4, 0.005 *m* $CuSO_4$, and 50 mole % excess H_2SO_4 was circulated at 250°C, was completed. The oxygen concentration was held at approximately 750 ppm. Chemical analyses indicated low corrosion rates during this run.

The loop was shut down because of a sudden increase in heat loss to the cooling water in the back of the pump, indicating a leak past the thermal barrier.

The pump was dismantled and found to be generally in good condition. However, there had been leakage through the thermal barrier O-ring seal and flaking of the gold plate from the O-ring. The seating surfaces bearing on the O-ring were in good condition, but there had been a slight corrosive attack on several places just outside the line of sealing. Except for oxide film formation, there were no evidences of corrosion on any of the titanium parts. There was no leakage across the solid, gold-plated, stainless steel gasket in the main flange of the pump.

3.2.2 Spare Reactor Blanket Pump and 230A Test Loop

The spare reactor blanket pump, containing titanium parts, was assembled into the 230A test loop. The system was given a 2000-psi hydrostatic test and operated on water for 30 hr prior to addition of UO_2SO_4 solution (290 g of uranium per kilogram of H_2O). Nine hours after the loop was restarted, a ¼-in. tube failed, with loss of the loop contents. At the time of failure, the system was at 250°C and 1050 psi with an oxygen concentration of about 750 ppm. Subsequent analysis showed that the tube was nickel instead of stainless steel.

A careful inspection after the incident showed no damage to either the pump or loop components. There were slight evidences of corrosion in both the titanium impeller and titanium thermal barrier in the wear-ring region.

All tubing in the loop is being replaced with ¼-in. seamless pipe, welded at the joints.

[1]On loan from TVA.
[2]Consultant.

3.3 HRT HEAT EXCHANGERS

3.3.1 HRT Fuel Heat Exchanger

The HRT fuel heat exchanger was received in late January. Several cleaning and test operations were carried out before the exchanger was installed at the reactor site:

1. The pressure drop was determined as a function of flow rate at room temperature and at 250°C. The test results are expressed empirically as[3]

$$\Delta P = 5.11 \times 10^{-4} F^{1.83} e^{-0.00276T} ,$$

where

ΔP = pressure drop, psi,

F = flow, gpm,

T = water temperature, °C.

2. Cleaning was conducted[4] with the exchanger attached to the modified 400A-2 loop: first, for 64 hr, with water at 250°C containing 1000 ppm oxygen and then, for 140 hr, with UO_2SO_4 solution containing 10 g of uranium per kilogram of H_2O and 50 mole % excess H_2SO_4. Analytical information obtained during the water run indicated that organic deposits in the exchanger were removed effectively. The chemical data for the solution part of the run are given in Figs. 3.1 and 3.2. The rapid initial rise in nickel concentration is normal for new stainless steel material.

3. The uranyl sulfate run also produced a probable verification of minute leakage observed during a helium leak test in the Foster Wheeler Corp. plant. Analysis of the condensate from the exchanger shell revealed traces of uranium in the first two of a total of 12 samples taken. Results of the helium leak test following the fuel run indicated a heat exchanger leak rate of 0.006 cc/day, with 1200 psi helium, on the primary side of the exchanger.

4. Evaluation of heat losses from the exchanger shell gave an over-all heat-transfer coefficient of 0.53 Btu/hr·ft^2·°F through the steam shell, aluminum-foil insulation, blast shield, and air film.

The fuel heat exchanger was delivered to the HRT site on February 17.

3.3.2 HRT Spare Heat Exchanger

Specifications were prepared and released for the procurement of a third 5-Mw heat exchanger. This exchanger will serve as a spare for both core and blanket units in the HRT.

Bids will be obtained on completely new designs to be recommended by the manufacturers. An additional bid will be requested from Foster Wheeler Corp. on a replica of the HRT heat exchanger.

3.4 HRT FEED PUMPS

The feed-pump test loop[5] was completed and operation was begun in March. The loop was shut down after 550 hr because of a suction-check-valve housing failure. Both suction check valves were replaced by a new girth-welded design, which has a much stronger housing (see Sec. 2.2).

Failures of feed-pump parts on the HRT mockup[6] demonstrated the need for improvements in feed-pump design. Extending pump life is therefore the primary objective of the injection-pump test loop. The most serious mockup failures were those of two diaphragms, after 3298 and 2702 hr of operation. These failures are believed to have resulted from a combination of the following conditions:

1. high stresses resulting from deflection of the diaphragm to the extreme face of the head,
2. high local stresses due to small dirt particles embedded in the diaphragm surface and causing stress concentrations,
3. general fatigue caused by the large number of cycles (approximately 10 million for failures mentioned above),
4. stress corrosion.

Several methods of increasing diaphragm life are being studied. One, the use of a titanium diaphragm, is now being tested on the mockup. Another consists in improving the method of adjusting the intermediate system to ensure minimum working of the diaphragm.

3.5 HRT DUMP TEST

The construction for phase II of the dump test, in which the contents of two concentric vessels

---

[3] J. R. Engel, *Pressure Drop Calibration of Fuel Heat Exchanger HRT Report No. A(4)a*, ORNL CF-56-3-14 (March 6, 1956).

[4] P. P. Holz, *HRT Heat Exchangers — Cleaning Runs Performed at Y-12*, ORNL CF-56-3-135 (March 20, 1956).

[5] C. B. Graham *et al.*, *HRP Quar. Prog. Rep. Jan. 31, 1956*, ORNL-2057, p 23.

[6] H. L. Falkenberry and I. Spiewak, *Pulsafeeder and Purge Pump Failures on the HRT Mockup*, ORNL CF-56-3-173 (March 1, 1956).

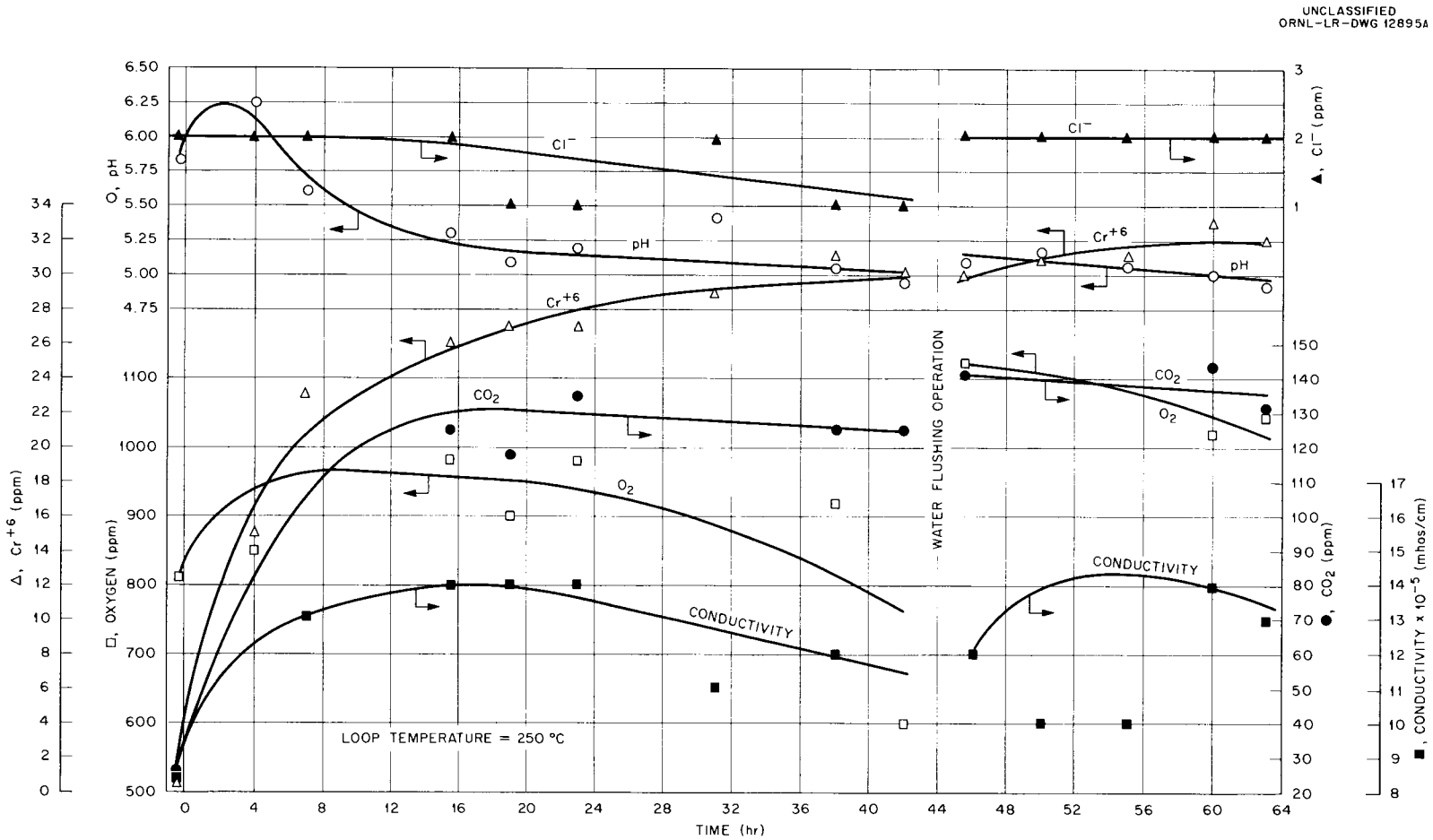

Fig. 3.1. Chemical Analysis Data for Water Flushing (2/3/56–2/6/56) of HRT Fuel Heat Exchanger.

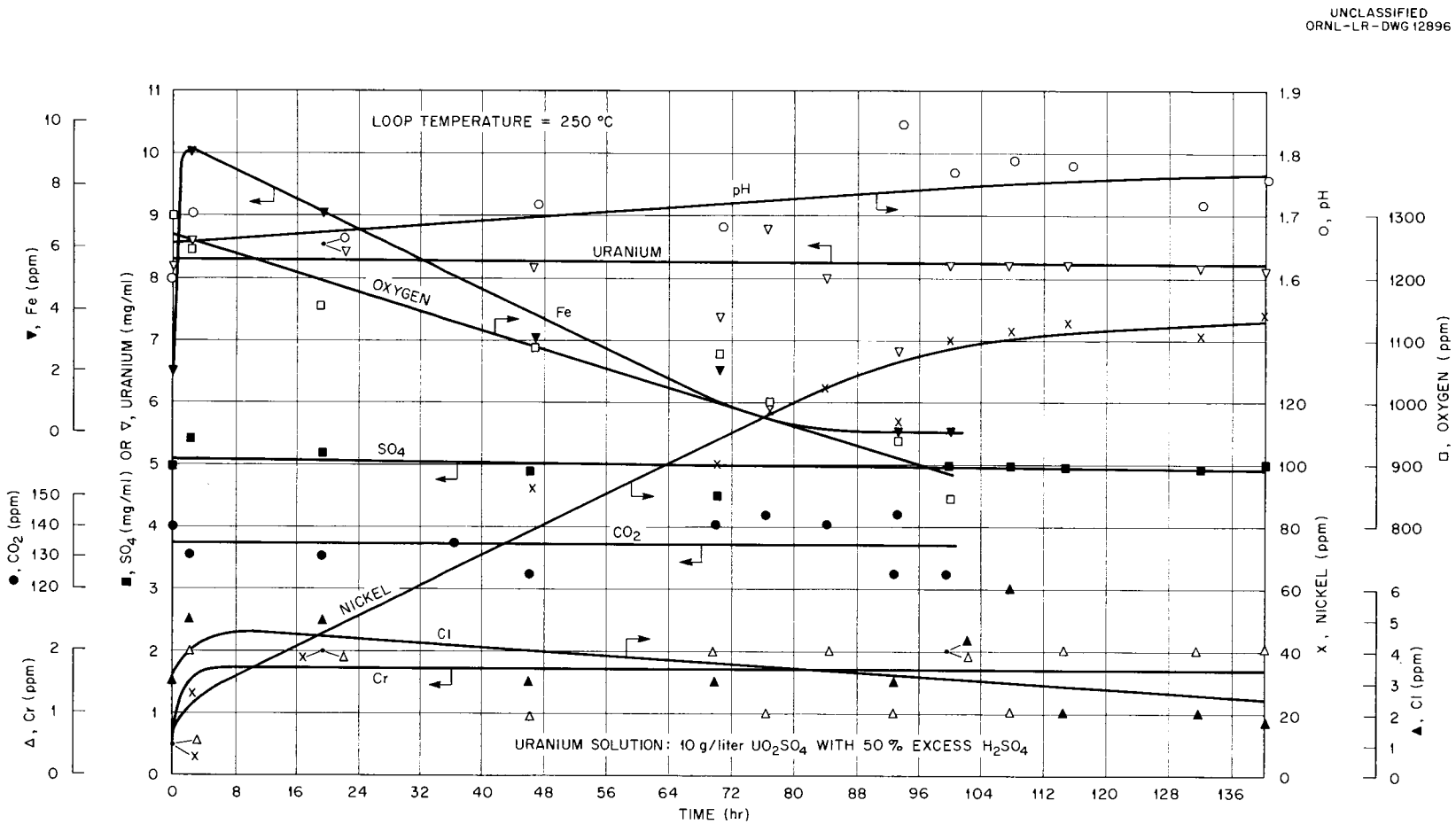

Fig. 3.2. Chemical Analysis Data for Uranium Flushing (2/6/56–2/12/56) of HRT Fuel Heat Exchanger.

will be dumped simultaneously, was completed. In preliminary tests, the pressurizer-vent block valves leaked excessively. These were replaced by reactor-grade valves, which have given excellent service. The tests also showed the need for additional instrumentation, which is being installed at the present time.

A prototype HRT pressurizer-vent metering valve was tested to determine its flow-vs-position characteristics. These were found to be satisfactory for controlling the pressure reduction during the start of a dump.

3.6 HRT SAMPLER[7]

Fabrication of the HRT sampler prototype was completed, and trials have begun. The sample size is reasonably consistent at 4 to 5 ml. Drops of sample are usually deposited on top of the flask; varying the needle size and sampling technique has not prevented the deposition.

Preliminary tests indicate that the tendency of the sampler to "remember" previous samples is slight.

In order to test the sampler under conditions closely simulating those of the reactor, the sampler was connected to the HRT mockup. The piping includes a prototype HRT sample cooler and throttling valve.

3.7 HRT MOCKUP

3.7.1 Present Mockup System

The HRT mockup contains a number of prototype HRT components operating under reactor conditions in an integrated system. The system described in the last quarterly report[8] was augmented by a prototype HRT magnetically damped level controller, the HRT oxygen converter (which permits high-pressure oxygen injection), the HRT sampler (see Sec. 3.6), and some additional sample points. Samples can now be taken from the high-pressure circulating loop, the pressurizer at two points, the back of the circulating pump, the letdown line, the injection- and purge-pump suction lines, and the dump-tank evaporator.

3.7.2 Operation

The mockup operated for 1627 hr during the quarter, with 1234 hr of operation at 300°C on a uranyl sulfate solution containing 10 g of uranium per liter.

One run of 1122 hr was performed (0.042 *m* UO_2SO_4, 0.0235 *m* H_2SO_4, 0.005 *m* $CuSO_4$, 120 ppm O_2) primarily to check the chemical behavior of the pressurizer in simulated reactor operation. The run was interrupted twice in order to replace feed-pump parts which had failed. Other failures, including two purge-pump check valves, occurred during this run, but repairs were made without requiring a shutdown.

Another run with uranyl sulfate solution containing 10 g of uranium per liter is now under way. In this run the effect of increased oxygen concentration on the corrosion rate will be investigated, sampling problems will be studied in a system similar to the HRT, and the pressurizer will continue to be observed.

3.7.3 Pressurizer Inspection

After the 1122-hr run, the pressurizer was cut open for inspection. The surfaces in contact with boiling water and steam were coated with a thin, slightly rusty film. There were no evidences of corrosive attack.

The connecting piping between pressurizer and circulating loop was also examined. The vertical pipe from the bottom of the steam drum had a smooth gray film. The horizontal portion of this line showed three distinct areas of film: (1) the entire lower half was black, (2) the uppermost portion was the same gray as the vertical section, and (3) between these two areas was a strip ½ in. wide containing little or no film covering the metal. Corrosion coupons in the vertical pipe showed weight losses corresponding to 0.07 to 0.28 mpy. There were no evidences of corrosive attack. However, an accumulation of black needle-like crystals and some amorphous brown silt was found at the bottom of the horizontal run from the pressurizer to the loop. According to chemical analysis, this material is principally an unidentified reduced uranium oxide with some trace contaminants. It does not dissolve in oxygenated HRT fuel solution. A total of approximately 50 g of uranium had precipitated.

In the present run, it is hoped that a higher oxygen concentration will depress the formation of these solids.

---

[7] C. B. Graham *et al.*, *HRP Quar. Prog. Rep. Oct. 31, 1955*, ORNL-2004, p 25..

[8] C. B. Graham *et al.*, *HRP Quar. Prog. Rep. Jan. 31, 1956*, ORNL-2057, p 25–26.

3.7.4 Loop Corrosion

The generalized corrosion rate experienced during the 1122-hr run was 2 mpy, according to nickel and manganese analyses of the solution. A corrosion coupon in the main circulating stream, but at very low velocity, showed a rate of 0.36 mpy. The concentration of major chemical constituents during the run is shown in Fig. 3.3.

The loop piping had a thin gray corrosion film which flaked off rather easily. Precipitation of small amounts of UO_2 was found in parts of the loop which were semistagnant.

3.7.5 Behavior of Loop Components

During the past quarter most of the loop components performed well, as evidenced by the number of operating hours. The 300A circulating pump, with welded flange and thermal-barrier seals, gave no trouble. The HRT prototype letdown valve showed no wear after about 1200 hr of service. The magnetically damped level controller was satisfactory.

However, there were a number of failures in the injection feed and purge pumps.[9] These

[9] H. L. Falkenberry and I. Spiewak, *Pulsafeeder and Purge Pump Failures on the HRT Mockup*, ORNL CF-56-3-173 (March 1, 1956).

UNCLASSIFIED
ORNL-LR-DWG 14042

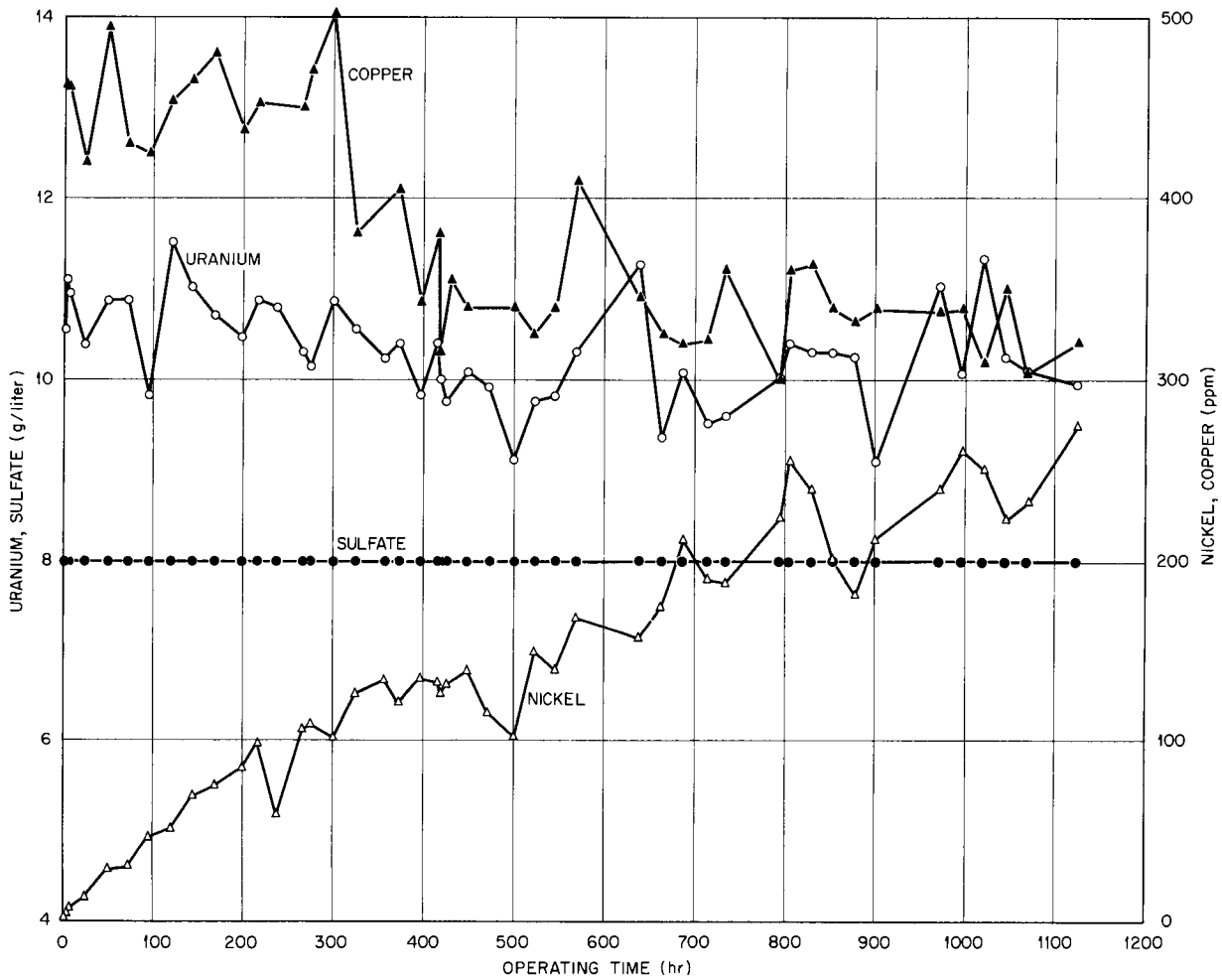

Fig. 3.3. Chemical Analyses of HRT Mockup Fuel During Steam Pressurization Run with Modified Pressurizer Design.

included three check-valve failures, two cracked diaphragms, and three pulsator-housing failures. Development is under way in the injection-pump test loop (see Sec. 3.4) and the mockup in order to extend the pump life. The check valves were redesigned; no failures have been experienced with new valves to date. A bolted head, containing a titanium diaphragm, is being tested on the mockup. Forged pulsator housings, to replace the present castings, are on order.

3.7.6 Special Tests

A number of experiments were carried out with distilled water in the system to determine some of the characteristics of the level controllers, gas separator, letdown heat exchanger and valve, and the pressurizer.

With the system operating at 200 and 300°C, air was injected into the high-pressure loop to simulate reactor off-gas. The rate of air injection varied from 13.1 scfm continuously to 120 scfm for short periods. The gas separator removed the gas smoothly, and control of level during gas injection was good. It was also learned that stable gas removal could be obtained with the feed pump off and only the purge pump supplying the necessary makeup for letdown steam and entrainment (0.2 gpm).

The pressurizer was subjected to compressions in order to get information on the pressure rise to be expected in such an event in the reactor. The pressure rose at 75% of the theoretical adiabatic rate for a compression of 2% $\Delta V/V$ per second, and 35% of the theoretical for 0.2% $\Delta V/V$ per second. The rate of pressure loss in the event that the letdown valve should stay open was found to be 5.3 to 7.5 psi/sec when no gas was injected into the high-pressure loop and 2.2 psi/sec with 13.1-scfm air injection.

The letdown-heat-exchanger cooling-water requirements were found to be 1.25 gpm under normal conditions but estimated to be 12 gpm when the valve is wide open, to keep the valve from vapor-binding during abnormal conditions.

The letdown valve was found to have a capacity of about 3.8 gpm when wide open. The valve was not quite large enough to handle 1.7 gpm of liquid plus 13 scfm of gas at 2000 psi.

In a special test to check chemical behavior during a simulated HRT power startup, the fuel concentration was increased gradually at 200°C with frequent sampling. There was no loss of uranium or copper from solution.

4. HRT REACTOR ANALYSIS

P. R. Kasten

C. W. Nestor, Jr. M. W. Rosenthal

4.1 REACTOR POWER AFTER SHUTDOWN

M. W. Rosenthal

Shutdown of the HRT can be accomplished by closing the stop valve (No. 537) in the steam line leading from the core heat exchanger. This action would cause cessation of energy removal from the shell side of the heat exchanger. However, the heat storage capacity of the steam-water system in the shell, plus the metal of the heat exchanger, would permit energy removal from the fuel solution for several minutes.

The power-time relationships in the HRT following closure of the stop valve were computed[1] for two situations, namely:

1. the circulating pump continues to operate;
2. the circulating pump is stopped simultaneously with closure of the stop valve, and fuel flow continues by natural circulation.

4.1.1 Shutdown with Forced Circulation

The estimated power-time behavior of the reactor following long-term operation at 5 Mw is plotted in Fig. 4.1. Total reactor power, P_T, is the sum of the rates of energy released instantaneously by fission and by fission-product decay. For a steady or slowly changing condition, the total power of the reactor, when critical, would equal the heat-removal rate. If the total power decreased, the fission power would change so as to equal the difference between the heat-removal rate and the rate of energy release by accumulated fission fragments. The fraction of total power represented by decay energy would therefore increase with time. The boiler-water temperature would rise with increasing time, and at some point the heat-removal-rate capacity would be no greater than the rate of energy release by fission-product decay. For times beyond this point, the reactor would become subcritical. Under these conditions, the HRT would become subcritical in about 2 min.

[1] R. E. Aven and M. W. Rosenthal, *Delay Time Required to Reduce D_2 Explosion Hazard During the HRT Dump*, ORNL CF-56-5-40 (May 21, 1956).

The total power in Fig. 4.1 was obtained from simultaneous solution of heat-transfer and energy-storage equations describing the system. The fission-product energy curve was obtained by approximating the effect that a gradual reduction in fission power would have on the curves computed by Hill,[2] who assumed complete flow stoppage. The instantaneous fission energy in Fig. 4.1 is the difference between total power and fission-product decay energy. The fission-recoil energy was taken as 85% of the instantaneous fission energy.

[2] J. W. Hill, Jr., *HRT Power and Fuel Temperature After Fuel Circulation Stops*, ORNL CF-54-9-64 (Sept. 9, 1954).

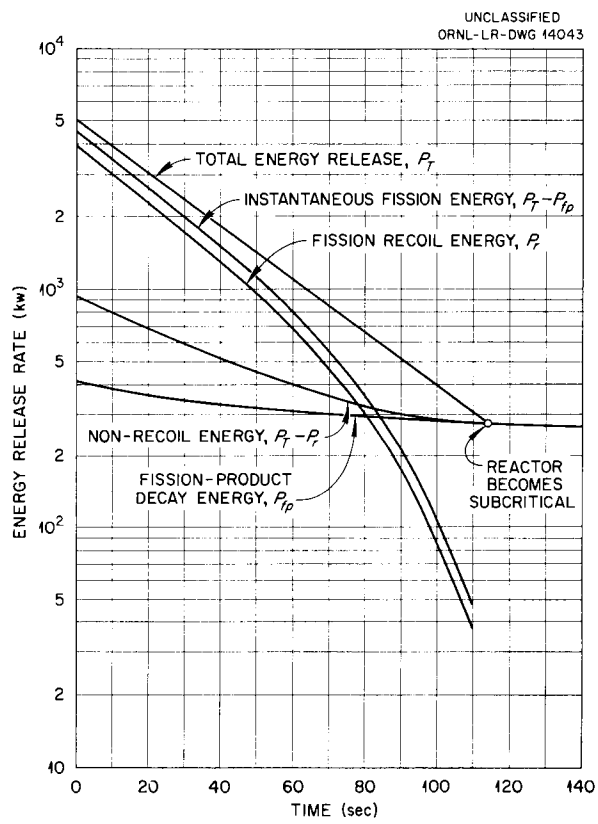

Fig. 4.1. HRT Power Following Closure of Stop Valve. After long-term operation at 5 Mw.

4.1.2 Shutdown with Natural Circulation

If the circulating pump were stopped simultaneously with closing of the stop valve, the fuel solution would slow down over a period of 3 to 5 sec until the natural circulation rate is reached. The reactor would become subcritical momentarily during this period, and the power would fall rapidly; however, criticality would be established after this transient. The circulation rate would then be determined by the temperature difference between the hot and cold legs of the system.

The calculated reactor behavior following simultaneous pump stoppage and stop-valve closure is shown in Fig. 4.2. The initial reduction in flow rate would cause the power to decrease quite rapidly. After this rapid transient the power would be lower than if the pump continued to operate, and the heat-exchanger temperature would rise relatively slowly with time. Thus the slope of the P_T-time curve would be much less for this case, as illustrated in Figs. 4.1 and 4.2. With natural circulation, about 7 min would be required for the heat-removal rate to decrease to the point where the reactor is subcritical.

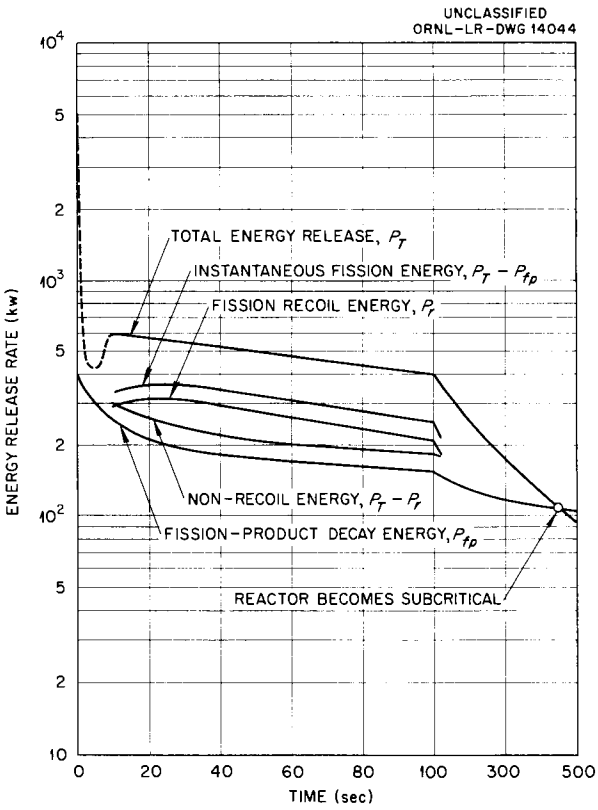

Fig. 4.2. HRT Power Following Simultaneous Closure of Stop Valve and Stoppage of Circulating Pump. After long-term operation at 5 Mw.

4.1.3 Effect of Heat Loss

Loss of heat from the system to the surroundings was not considered in obtaining the curves of Figs. 4.1 and 4.2. The rate of heat loss from the core high-pressure system to the reactor cell was estimated[3] to lie between 20 and 60 kw and is dependent upon the extent of pipe-flange insulation. A heat loss of 60 kw would delay the time at which subcriticality is attained by about 15 sec in the forced-circulation case. The time delay would be appreciably extended for the natural-circulation case; possibly, the rate of fission-product energy release would fall below 60 kw before the heat-exchanger temperature reached 280°C (the critical temperature), under which circumstance the core would remain critical indefinitely.

4.1.4 Steady Power Removal with Natural Circulation

If the circulating pump were stopped but steam withdrawal from the heat exchanger continued, the reactor would exhibit a transient behavior, such as shown for the first 10 sec in Fig. 4.2, followed by steady operation under natural-circulation conditions. The natural-circulation power for a shell-side pressure of 520 psia would be about 700 kw with a circulation rate of about 40 gpm.

4.2 FUEL CONCENTRATION AS A FUNCTION OF POISON LEVEL

C. W. Nestor, Jr. P. R. Kasten

Placing corrosion specimens within the HRT core region will increase the fuel concentration required for criticality, owing to the neutron-poisoning effect of the specimens and their holder. Calculations[4] based upon a preliminary coupon-holder design indicate that the poisoning effect would be less than 11% poisons. This result was obtained by calculating the poisoning effect, on

[3] F. C. Zapp, *HRT Space Cooler Heat Load*, ORNL CF-55-10-17 (Oct. 5, 1955).

[4] C. W. Nestor, Jr., and P. R. Kasten, *HRT Fuel Concentration as a Function of Poison Level*, ORNL CF-56-4-66 (April 11, 1956).

the assumption that the corrosion specimens and their holder were titanium metal uniformly distributed throughout the core region, and then weighting the result with the neutron importance function according to the actual position of the metal. If the metal were all stainless steel, the equivalent uniform poison fraction would be approximately 6.8%; use of some Zircaloy-2 would further reduce the poisoning effect.

The effect of poison level upon critical concentration is given in Fig. 4.3 (the poison fraction was based upon the fission cross section). In obtaining these results, two-group calculations were performed; this appeared to be an adequate treatment, based upon some multigroup results.[5]

To take into account resonance phenomena, it was estimated that approximately 25% of the fissions could be caused by epithermal neutrons (based on some multigroup results). This would result in a critical concentration approximately 6.5% higher than that obtained by two-group calculations. The effect is indicated in Fig. 4.3. Even with the above correction, the critical concentration would not exceed 10 g of U^{235} per kilogram of D_2O, with 11% poisons present.

[5]C. W. Nestor, Jr., *HRP Quar. Prog. Rep. Jan. 31, 1956*, ORNL-2057, p 66–68.

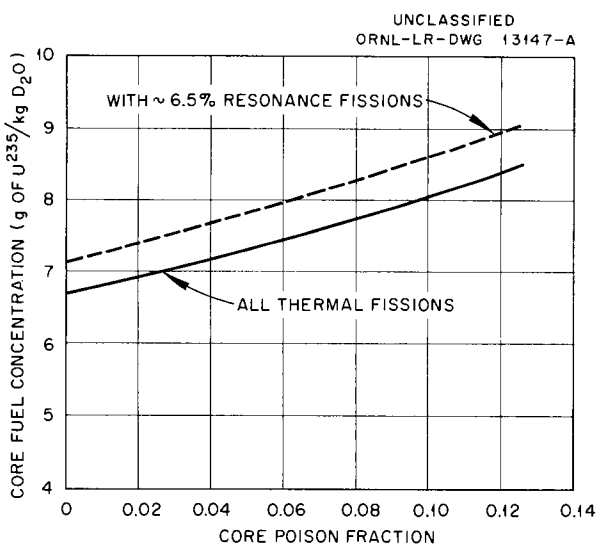

Fig. 4.3. Critical Concentration Required in HRT as a Function of Core Poison Level.

4.3 REACTIVITY EFFECTS ASSOCIATED WITH TWO-PHASE SEPARATION

P. R. Kasten

Based on experimental work at LASL,[6] the HRT would be extremely subcritical if two-phase separation occurred and the heavy phase were not dispersed. Also, if the heavy phase were dispersed under steady-state conditions, no reactivity problem would exist. Under certain non-steady-state conditions, however, some reactivity problems would be encountered. The most serious one is associated with the following situation: Consider that two-phase separation has occurred, that the 400A pump is off, and that all the fuel has accumulated at the bottom of the core vessel (as a result of natural convective fluid flow). Although the reactor would be extremely subcritical under these conditions, startup of the 400A pump at this time could disperse the heavy phase throughout the core volume, with an accompanying rate of reactivity addition of approximately 10% Δk_e/sec. This reactivity addition could result in pressure-vessel rupture. If the dispersion does not occur until after full pump speed is attained, the rate of reactivity addition could be approximately three times greater than the above figure.

To eliminate the above situation, the 400A pump should not be started when the reactor is subcritical (this presupposes previous operation and the possibility of two-phase separation). Following previous operation, the reactor should attain a power level of approximately 700 kw by natural convective flow within a minute following pump failure, if two-phase separation has not occurred. If criticality were not attained, the safest procedure would be to dump the reactor.

A much less serious reactivity problem would be associated with two-phase separation under conditions of normal pump operation. If two-phase separation occurred at 280°C and all the fuel accumulated within the core in accordance with the fluid flow rate, the associated rate of reactivity addition would not cause rupture of the pressure vessel, or of the core tank if the initial reactor power were approximately 5 Mw. The two-phase separation temperature would have to be less than 200°C before danger of rupturing the pressure vessel would exist for this case.

[6]R. N. Olcott, *Homogeneous Heavy Water Moderated Critical Assemblies, Part I, Experimental* (to be submitted to *Nuclear Science and Engineering*).

5. HRT CONTROLS AND INSTRUMENTATION

D. S. Toomb

A. M. Billings J. C. Gundlach R. E. Toucey
J. R. Brown R. L. Moore W. P. Walker[1]
C. H. Gabbard L. R. Quarles[1] K. W. West

5.1 PROCUREMENT

All valves, valve operators, and instrument transmitters and associated receivers for the reactor system have been received. Total expenditures for instrument and control material to date, including valves, are $197,000. Fourteen thousand dollars is presently outstanding, approximately half of which is for remote area radiation monitors scheduled for shipment in early May. A prototype of the monitor was approved at the vendor's[2] plant. The remaining outstanding orders are for reactor-system valves and instruments and miscellaneous auxiliary-systems equipment.

5.2 CONSTRUCTION

The checkout of the process instrumentation and control system was completed. The nuclear system will be checked after the process equipment has been placed in operation.

5.3 LIQUID-LEVEL INDICATORS

The designs for the liquid-level indicators[3] for the pressurizers and the outer storage tanks were completed, and construction at ORNL was also completed. The operation of the prototypes[4] indicates that zero shifts with temperature have not been completely eliminated and that the sensing-coil temperature should be below 200°C to obtain reliable operation.

The design of the pressurizer level indicator is shown in Fig. 5.1. The float is damped by the action of permanent magnets on a one-turn copper coil attached to the float stem. The range of the indicator is 5 in. of water.

The level indicator for the outer storage tanks is shown in Fig. 5.2. Float vibration in this design is hydraulically damped by the interaction of the disks attached to the float stem and the fixed baffle attached to the housing. The range of this device is 47 in. of water.

5.4 PRESSURE AND DIFFERENTIAL-PRESSURE INDICATORS

The pressure and differential-pressure indicators were calibrated and found to meet the design specifications. Construction specifications were met except for the welds joining pressure-tap-pipe extensions to the housings. These welds are being repaired at ORNL. Future specifications will require that an ORNL inspector be present at the vendor's plant when welding operations are being performed.

5.5 VALVES AND OPERATORS

5.5.1 HRT Low-Pressure-System Valves

Delivery, testing, and installation of the HRT low-pressure-system valves are complete. All valves for the low-pressure system were satisfactory as received from the vendor.

5.5.2 HRT High-Pressure-System Valves

All high-pressure-system valves needed for HRT construction have been received. Seventy-five per cent of the spare units are also now on hand.

The fuel-system dump valve and spares were rejected after initial tests and returned to the vendor for redesign of the plug. The 25-deg angle in the original design caused the plug to wedge in the seat and resulted in sticking. The redesigned valve has a 60-deg plug angle.

The letdown valve, which throttles a mixture of reactor fluids and gases from the high-pressure system to the low-pressure dump tanks, is shown in Figs. 5.3 and 5.4. No evidence of trim erosion in this valve was visible upon inspection after a 1100-hr test with uranyl sulfate in the HRT mock-up loop. This valve was reinstalled in the mockup for further testing.

---

[1]Consultant from University of Virginia.

[2]Victoreen Instrument Co., Cleveland 3, Ohio.

[3]D. S. Toomb *et al.*, *HRP Quar. Prog. Rep. Jan. 31, 1956*, ORNL-2057, p 35.

[4]R. L. Moore, *HRT Level Controller Development Status Report*, ORNL CF-56-4-61 (April 24, 1956).

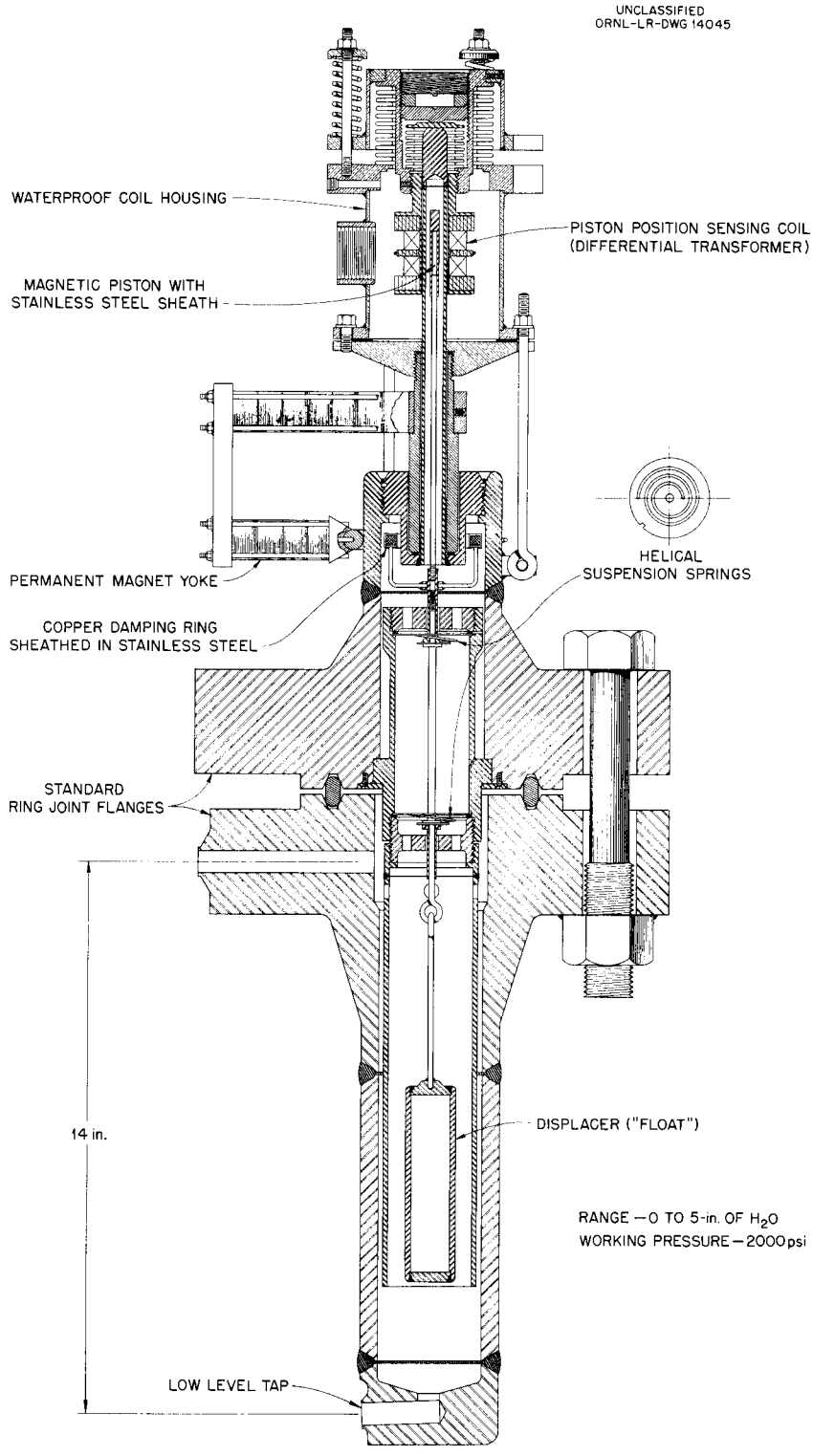

Fig. 5.1. HRT Pressurizer Level Indicator. Working pressure, 2000 psi.

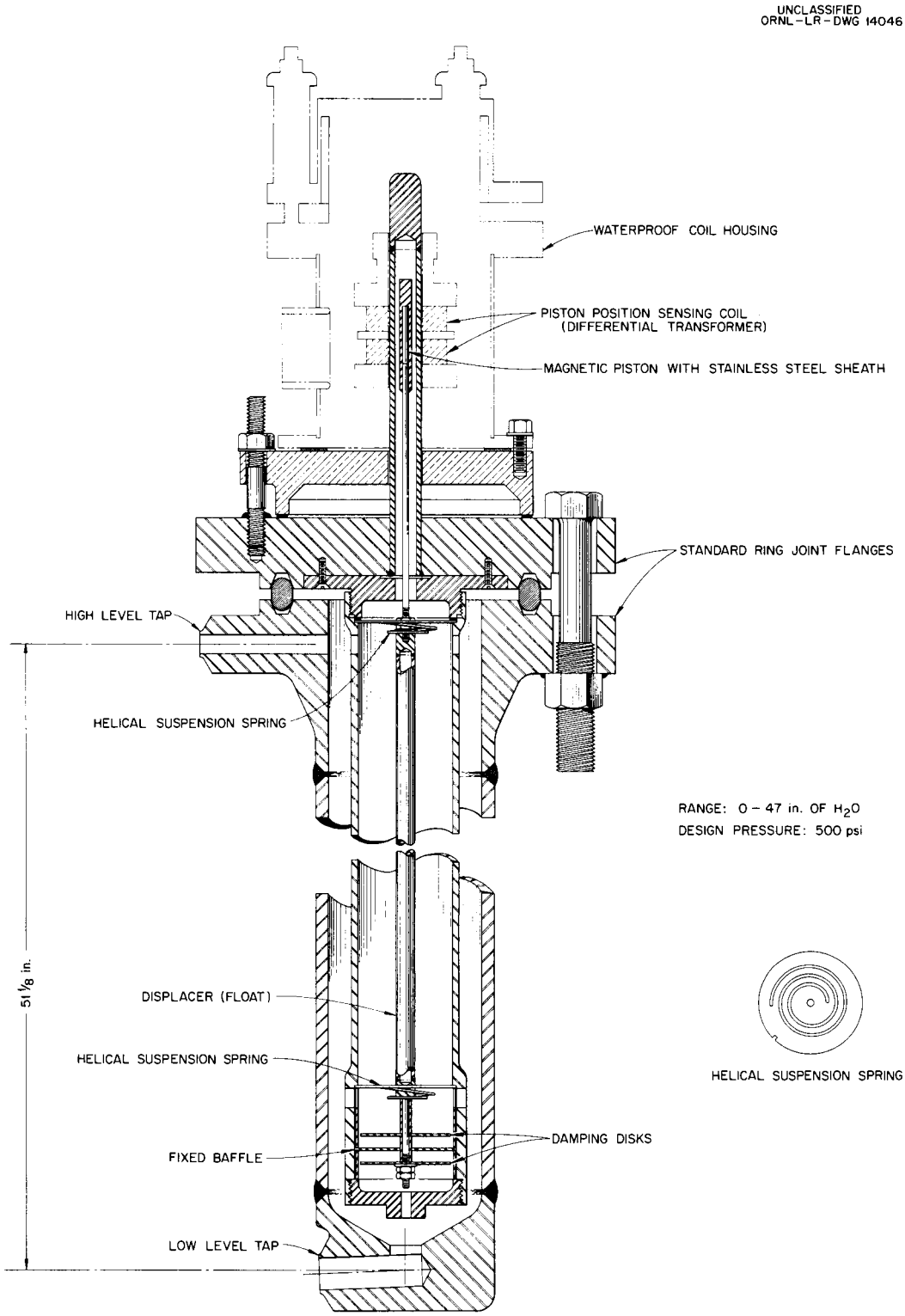

Fig. 5.2. HRT Storage-Tank Level Indicator. Design pressure, 500 psi.

UNCLASSIFIED
PHOTO 25843

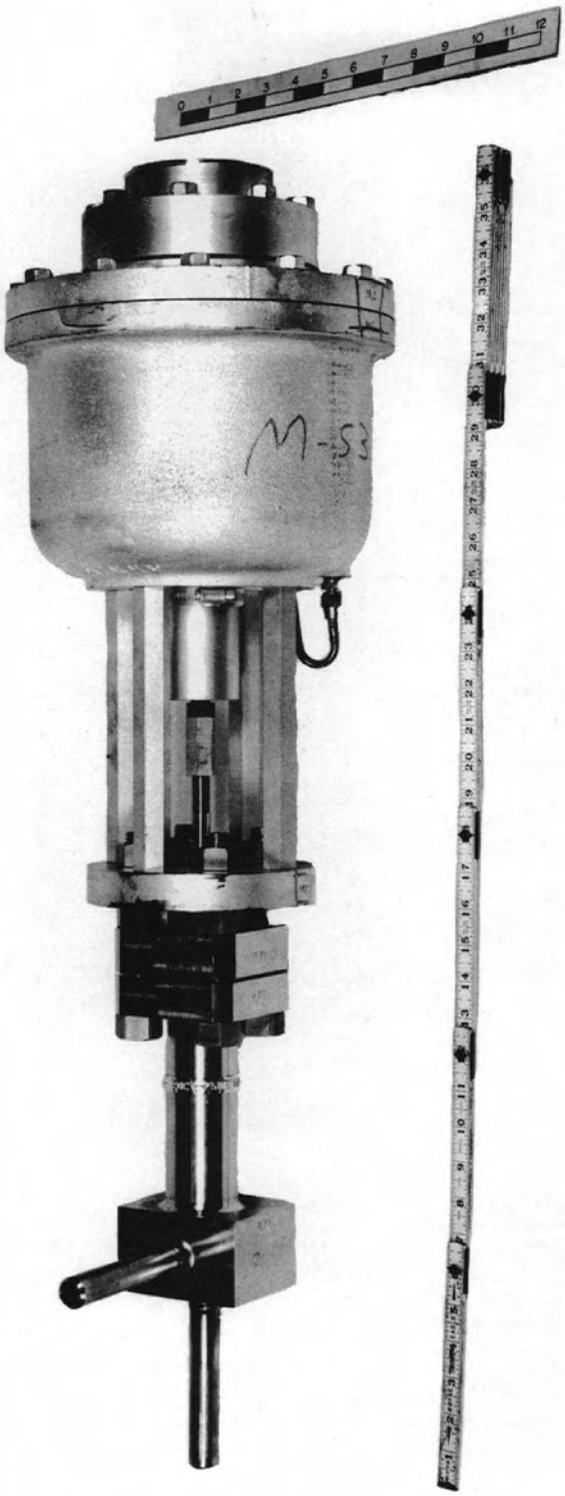

Fig. 5.3. HRT Letdown Valve.

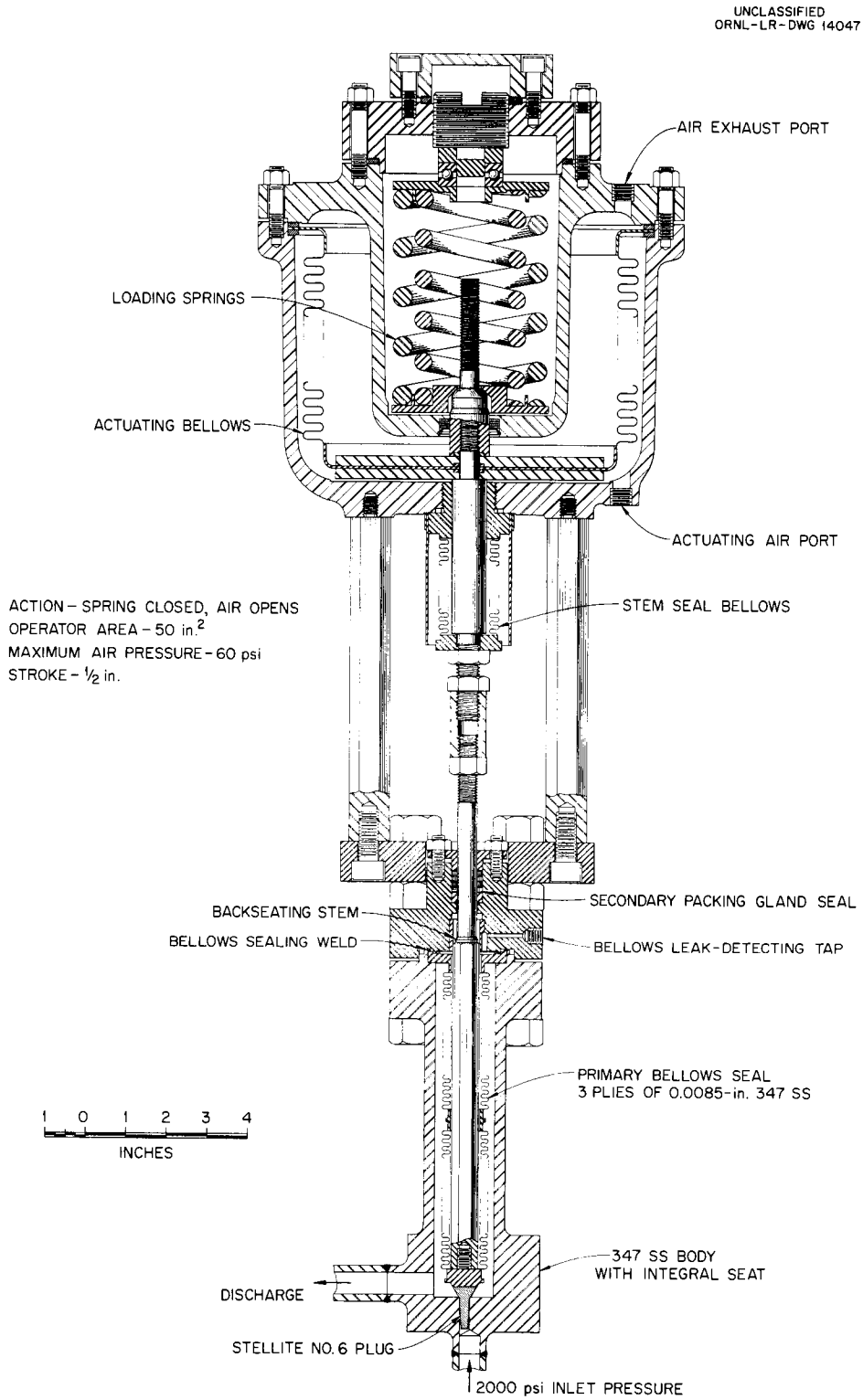

Fig. 5.4. HRT Letdown Valve and Operator Assembly.

6. HRT FUEL PROCESSING PLANT

W. E. Unger

T. A. Arehart
N. A. Brown
W. L. Carter
G. W. Gray
P. A. Haas
C. C. Haws
R. W. Horton
R. B. Lindauer
F. C. McCullough
E. O. Nurmi
A. M. Rom
W. F. Schaffer
H. O. Weeren
R. H. Winget

6.1 PROCESS FLOWSHEET

One of the principal problems anticipated in the operation of the HRT Chemical Processing Plant[1] is that of determining whether the equipment is performing properly – that is, whether solids are being removed by the hydroclone. Since it is not certain that a representative sample can be taken from the solid-liquid mixture in the hydroclone underflow receiver, it is necessary that the entire contents of the receiver be removed and dissolved. A facility for removing a "one batch" receiver had been designed for location in the cell A operating area so that it would not be necessary to enter the process cell (C) frequently during the early stages of experimentation. This cell A carrier facility would have been separate from the two multibatch carriers already planned in cell C.

However, it was found that both design and operation of the cell A facility were complicated by the intense radioactivity of the underflow-receiver contents and the pressure design required to afford hazards protection consistent with the reactor cell design. Therefore, the one-batch carrier will be substituted for one of the two carrier-evaporators in cell C. The one-batch carrier will be removed through the roof plugs of cell C after each of as many runs as are found necessary to confirm the representativeness of the underflow sampler.

The revised design therefore provides a sample carrier of approximately 3-gal capacity to be interchangeable with either of carriers C-1 and C-2 shown on Fig. 6.1, which is a schematic flow diagram of the HRT Chemical Processing Plant.

6.2 INSTRUMENTATION

The instrumentation for the core processing facility of the HRT is different from that encountered in the normal radiochemical processing plant in that it must perform at much higher operating temperatures, pressures, and radioactivity levels.

The lack of accessibility to the primary elements warrants the use of electrical rather than pneumatic primary elements on the basis of maintenance probability. The electrical signals are converted to pneumatic by transducers. Thus the receiving instruments are pneumatically operated. A graphic panelboard is being installed so that the operator will have an exact over-all view of the process.

6.2.1 Pressure

Each of the primary pressure elements will be located in a lead-shielded watertight cubicle attached near the top of the process cell. A length of $\frac{1}{4}$-in. pipe filled with D_2O will be provided to prevent process solutions from contacting the primary elements. Diffusion and mixing, even during process pressure letdowns, are not expected to cause radioactive process solutions to enter the primary elements.

The process pressure in the hydroclone circulation loop will be measured by a 0–2500 psi Baldwin-Lima-Hamilton Corp. type SR-4 strain-gage element.

The differential pressure drop across the hydroclone separator will be measured by a 0–50 psi inductance-type differential-pressure transmitter being fabricated by The Foxboro Company.

The pressure in the vapor lines between the carrier and the recombiner-condensers will be measured by a 0–50 psia Baldwin-Lima-Hamilton Corp. type SR-4 strain-gage element.

6.2.2 Level

Liquid-level measurement in radiochemical processing facilities is extremely difficult wherever the measurement involves small tanks. For this reason, development effort was applied to achieve a device suitable for this type of application which can be used to supplement a standard method of level measurement.

[1] F. R. Bruce *et al.*, *HRP Quar. Prog. Rep. Jan. 31, 1956*, ORNL-2057, p 41–59.

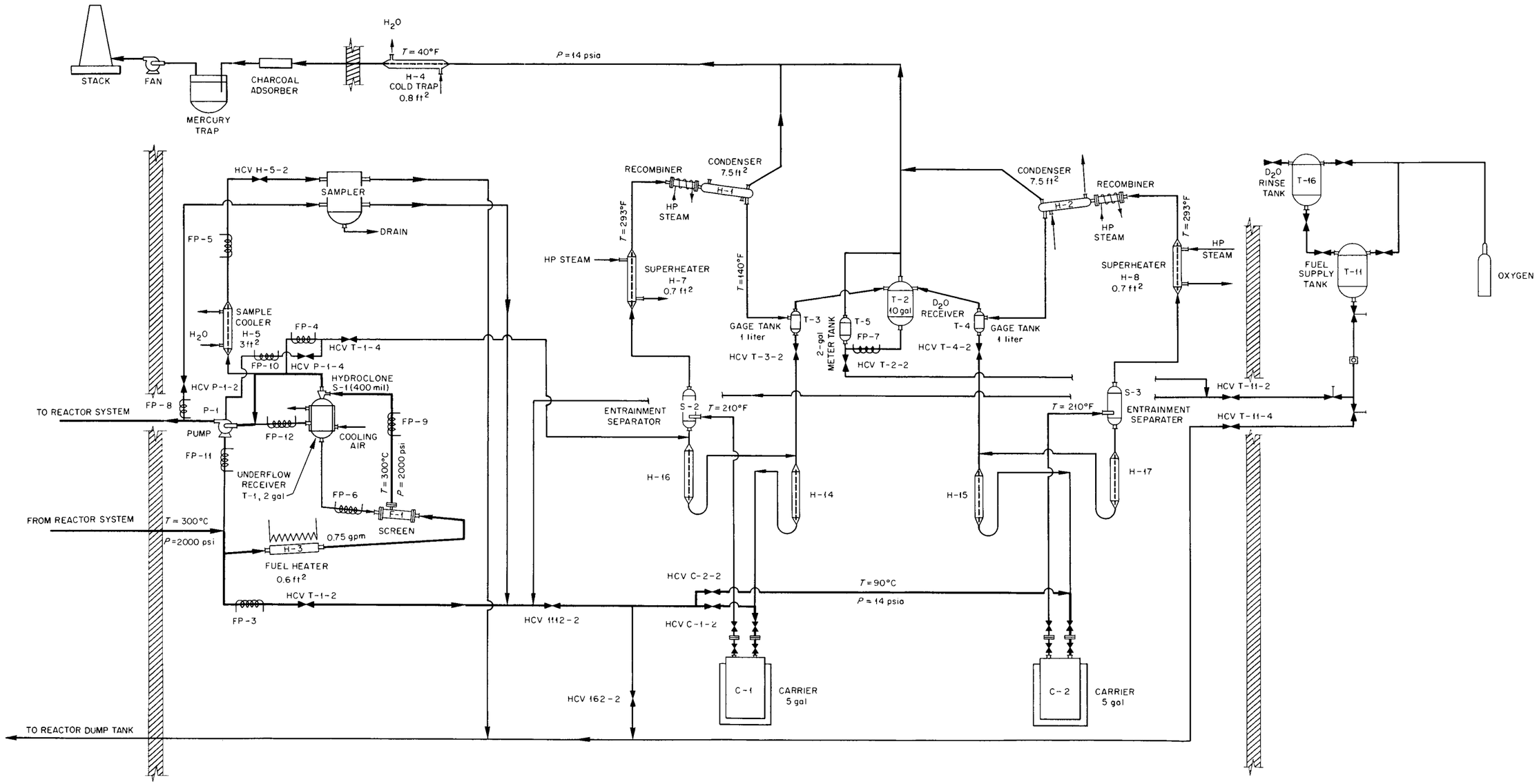

Fig. 6.1. Schematic Flow Diagram of the HRT Chemical Processing Plant.

The D_2O receiver inventory will be measured by a 0–200 lb Baldwin-Lima-Hamilton Corp. type SR-4 load cell. The tare weight of the tank (approximately 150 lb) will be electrically compensated for in the measuring instrumentation. The active weight of only 50 lb emphasizes the desirability of an additional measurement. This type of standard tank-weighing device is normally not used where the active weight is less than one-half the total weight.

The supplementary measurement of the D_2O receiver inventory will be made by a thermal-level probe developed by the Instrumentation and Controls Division and illustrated in Fig. 6.2. This probe consists of a heater surrounded by thermocouple junctions imbedded in a stainless steel housing. The thermocouple junctions are spaced in equal increments along the length of the probe. The electrical output from the thermocouples in the portion of the probe which is not immersed in the liquid will be greater than that from those submerged, because of the differences in heat-transfer coefficients of the probe-to-liquid and probe-to-vapor surfaces. The thermocouples are connected so as to produce an emf proportional to the liquid level. The bottom thermocouple junction, which is always immersed in the liquid, is used to compensate for variations in liquid temperature.

Alarms indicating high liquid levels in the cell C sump and in carriers C-1 and C-2 are important in warning of leaks onto the floor. Level alarm devices consisting of contact-making thermocouple galvanometers actuated from a signal derived from a spot-type thermal-level probe will be used. These thermal-level probes operate on the same principle as the level elements mentioned above, with the exception that the thermocouple junctions are not spaced to give continuous level measurement along the probe but are arranged to indicate absence or presence of liquid at a specific point.

6.2.3 Temperature

Temperature elements will be fabricated from thermocouple wire sheathed in $\frac{1}{8}$-in.-OD type 304 stainless steel tubing. The thermocouple junctions will be made by welding the wires and tubing into a closure of the end. The use of the stainless steel sheath allows the thermocouple installation to be made leaktight by the use of standard tubing

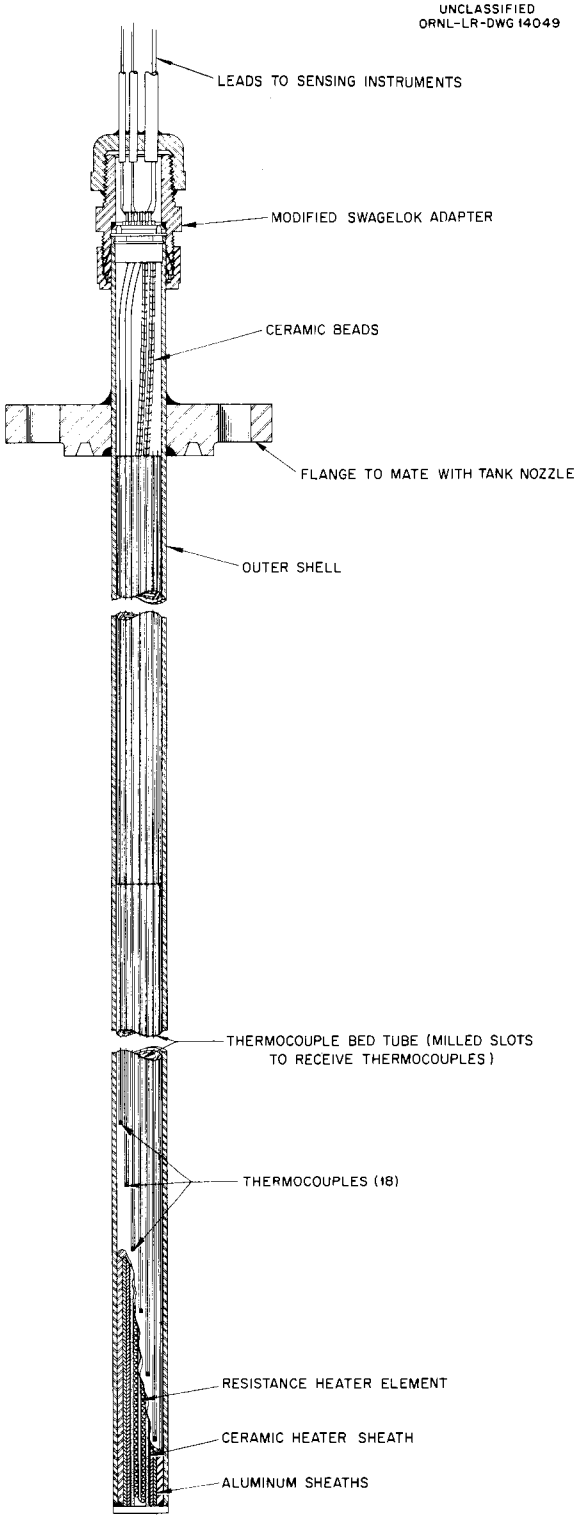

Fig. 6.2. Thermal-Level Probe.

fittings. Thermocouples will be welded to the high-pressure piping, carried parallel to the pipe for at least 6 in. to minimize heat loss from the junction, and then brought out through the piping insulation. Standard thermocouple wells will be inserted in the low-pressure piping. Each temperature-measuring point will have duplicate thermocouples which can be connected to the measuring or controlling instruments at a junction box near the operating panel board.

6.2.4 Flow

Vapor flow in the lines from the carrier to the recombiner-condensers will be measured by turbine-type flow elements fabricated by the Potter Aeronautical Co. The output signal from these elements will be electrical pulses whose frequency is proportional to the flow rate.

Auxiliaries to the process, such as cooling-water flow, steam pressure, etc., will be measured by standard rotameters and pressure gages, located in the control-room area.

6.2.5 Electrical and Instrument Connections

The stainless-steel-sheathed thermocouple lines will terminate in tubing fittings at a sealed junction box in the process cell C near the roof plugs. Wiring from these junction boxes will pass through sealing boxes in cell D filled with a sealing compound. The conduit between the sealing boxes and the junction boxes inside cell C will be pressurized with air.

Cell C electrical leads will pass through sealing boxes inside cell C and inside cell D. These conduits will be pressurized between the two sealing boxes.

6.2.6 Transducers

Transducers will convert the primary-element electrical output into pneumatic output; 1000-cps a-c transducers will be used wherever possible because of their ability to measure small signals accurately even when 60-cycle interference is present. The a-c transducer to be used in the core processing facility will be The Foxboro Company Dynalog indicator with 3 to 15 psi pneumatic output. One of these transducers will be used for each primary measurement – high static pressure, high-pressure differential, low static pressure, and D_2O level from the Baldwin load cell.

There are two primary signals which require the use of a d-c type of transducer – the D_2O-tank thermal-level probe and the controlling thermocouple from the underflow-pot temperature application. Fortunately, their relatively high electrical output signals will allow the use of d-c instrumentation. The d-c transducers will be The Swartwout Company emf transmitters, type T3C.

6.2.7 Control-Panel Board

The operating panel board consists of one 8-ft section of graphic process representation. It contains process-variable recorders, indicators, and valve and freeze-plug actuating switches, which are associated with individual process components and connecting lines. At each side of the graphic panel is a 2-ft section of panel in which instruments related to the entire process or instruments used to furnish auxiliary information are mounted (Fig. 6.3). Multipoint temperature recorders and indicators are mounted in these panels. In the lower portions of the side or wing panels are located the central control circuit and jumper panels. The patch and jumper panels display the control and interlock circuitry. When interlocks must be bypassed, this is readily and conveniently done at the panel board, and the bypassed interlocks are in full view of the operator.

6.3 REMOTE TOOLS

The underwater maintenance planned for the HRT core processing plant will require remote tools. Many of the tools designed for reactor maintenance will also be applicable to the processing plant with minor or no changes. Effort is being concentrated on the special tools that are required to remove the hydroclone retainer plug and the hydroclone.

The tool (finger type) for removing the hydroclone was designed, built, and tested. An alternate (collet type) design under test is expected to be more rugged (Fig. 6.4). The hydroclone was designed with four 45-deg mill cuts in the top surface to provide sockets for a twisting action from the special tool. This will assist in breaking the hydroclone loose from deposited corrosion products between the hydroclone itself and the flange wall.

The special tool for removing the hydroclone retainer plug is fabricated of $\frac{3}{4}$-in. sched-80 pipe (Fig. 6.5).

UNCLASSIFIED
ORNL-LR-DWG 14050

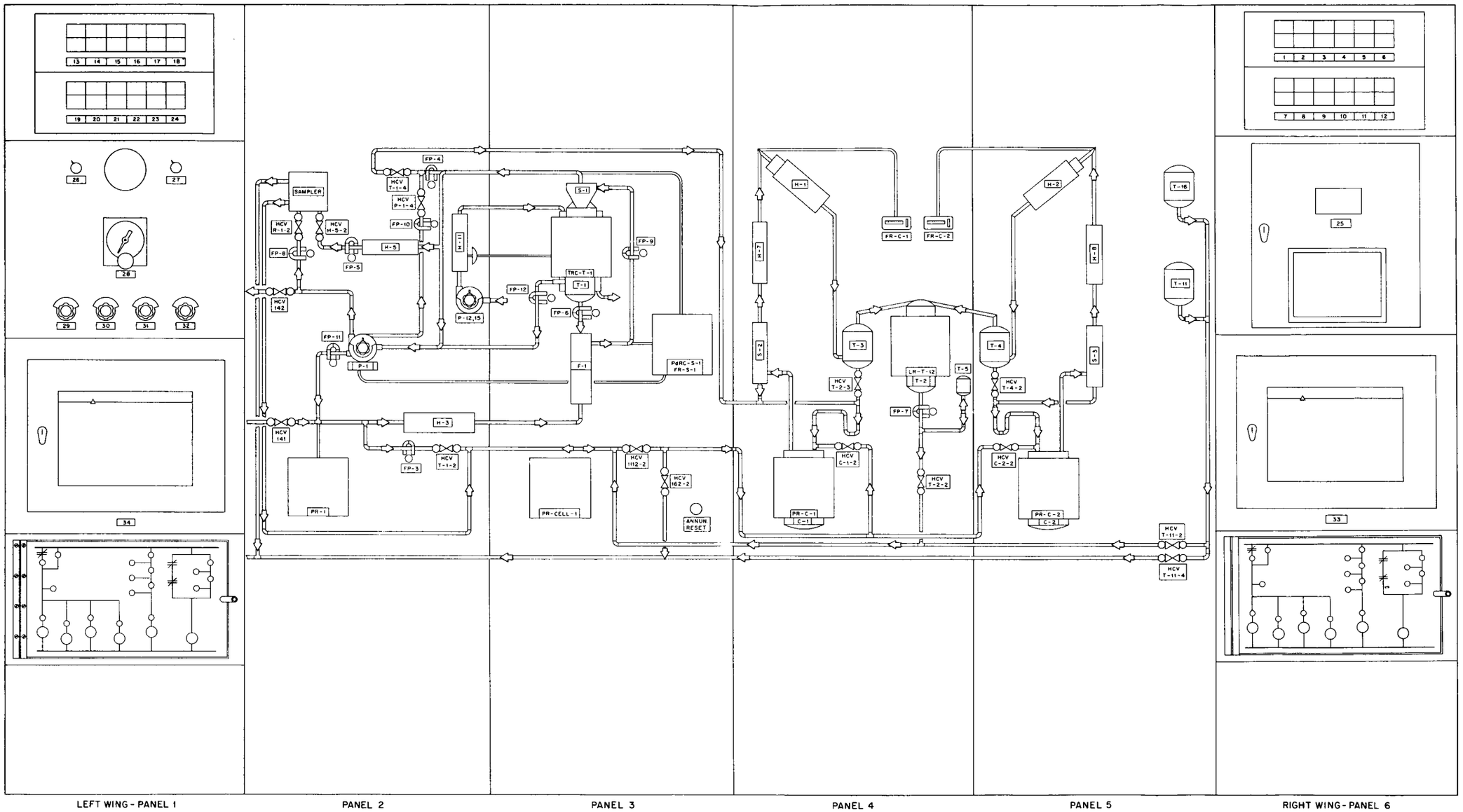

NAME PLATE SCHEDULE

1 RA-T-11; HIGH ACTIVITY, T-11
2 RA-CELL-1; HIGH ACTIVITY, CELL "C"
3 RA-1454; HIGH ACTIVITY, COLD WATER DRAIN
4 RA-T-12; HIGH ACTIVITY, T-12
5 RA-1458; HIGH ACTIVITY, SPACE COOL CWR.
6 RA-545; HIGH ACTIVITY, VACUUM PUMP SUCTION
7 RA-SAMPLER; HIGH ACTIVITY, SAMPLER
8 PA-T-14; PRESSURE LOSS, HIGH PRESSURE L.D.
9 PA-T-17; PRESSURE LOSS, LOW PRESSURE L.D.
10 SPARE
11 SPARE
12 SPARE
13 TA-H-11
14 TA-H-3
15 TA-T-13; LA-T-13; HIGH LEVEL, TEMPERATURE IN T-13
16 LA-CELL-1; HIGH LEVEL IN SUMP
17 LA-T-12; HIGH LEVEL IN T-12
18 FA-P-1; LOW WATER FLOW TO P-1
19 FA-H-11; LOW AIR FLOW TO H-11
20 PA-CELL-1; HIGH PRESSURE, CELL "C"
21 PA-1; LOW PRESSURE, HIGH PRESSURE FUEL
22 PA-1640; LOW DISCHARGE PRESSURE, FREON PUMP
23 PA-AIR; LOW PRESSURE, INSTRUMENT AIR
24 PdA-S-1; ABNORMAL DIFFERENTIAL, S-1
25 TI-3
26 NOISE PICKUP - STATION SELECTOR
27 NOISE PICKUP - VOLUME CONTROL
28 HIC-H-3
29 H-11
30 H-3
31 SPARE
32 SPARE
33 TR-1
34 TR-2

Fig. 6.3. Instrument Panel – HRT-CP.

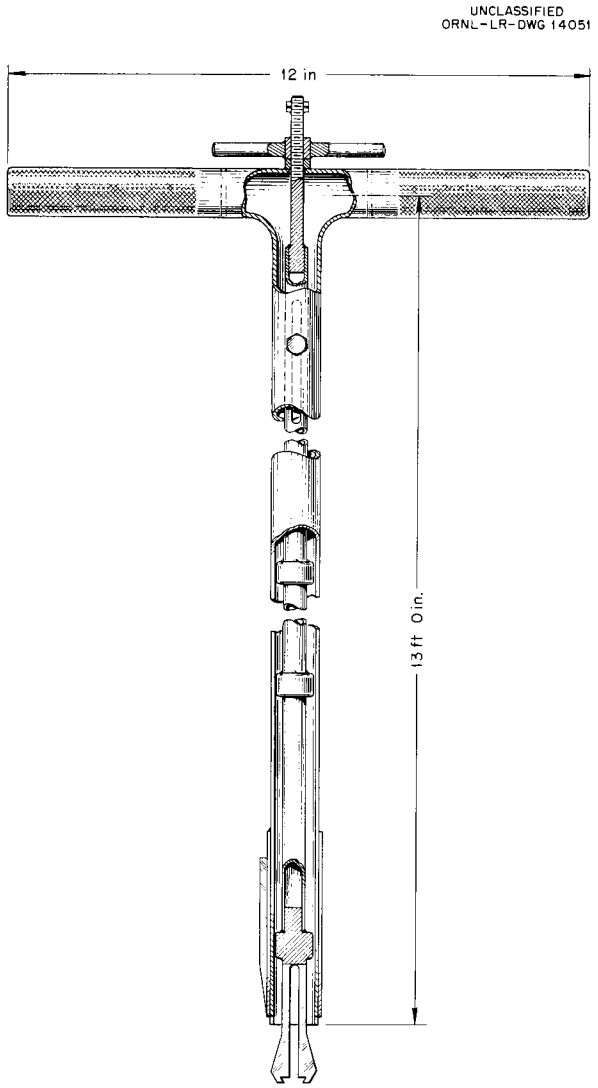

Fig. 6.4. Hydroclone Removal Tool.

Contamination of the system with light water will be minimized, during changing of the hydroclone, by a flanged shaft of $1\frac{1}{2}$-in. sched-5 pipe extending from the top of the bottom roof plug to the hydroclone flange (see Fig. 6.6). The top flange covering the hydroclone retainer plug will be removed to expose the retainer plug. The $1\frac{1}{2}$-in. pipe with flange will then be bolted over the retainer plug to exclude the shielding water. Air pressure will then be applied to force the light water from the shaft through a $\frac{1}{4}$-in. tube attached to the flange, running parallel to the shaft, terminating above the shielding water. In this manner the light water is excluded before the hydroclone retainer plug is removed.

The system can be filled with D_2O to reduce the differential static head pressure and reduce leakage past the retainer plug. The hydroclone retainer plug has been recessed into the top flange to reduce to about 10 cc the void space that would retain light water (Fig. 6.7).

The Reactor Experimental Engineering Division has designed a wrench for loosening the $\frac{5}{8}$-in. bolts on the low-pressure valves. Adapters for bolt sizes of $\frac{1}{2}$, $\frac{3}{4}$, and possibly $1\frac{1}{8}$ in. are being designed for use with this wrench. A right-angle drive is being designed for loosening horizontal bolts.

6.4 EQUIPMENT TESTING

6.4.1 Flange Leakage Tests

A ring-joint seal adapted for leak detection has not proved entirely successful on the small flanges to be used in the chemical plant. Commercial tolerances of flanges and ring seals were found to be excessive, and remachining of both elements was necessary. Use of studs threaded over their complete length (or turned to thread-root diameter where not threaded) appears to be superior to the use of standard bolts. Extension sleeves were also beneficial. Attempts to reseat oval rings in flanged joints subjected to excessive bolt loadings (15,000 lb per bolt) were unsuccessful, indicating that low bolt loadings must be used for any joint which is to be broken and resealed repeatedly.

6.4.2 Underflow Pot Test

The HRT-CP underflow pot was installed on the B loop. The underflow-pot heat-transfer coefficient was measured from steam inside the pot to the circulating air. This coefficient is 25 $Btu/hr \cdot ft^2 \cdot {}^\circ F$, which yields a coefficient of 19 when corrected to HRT-CP conditions. Design was based on a coefficient of 15, which is necessary to reduce the underflow-pot pressure by cooling before sufficient radiolytic decomposition occurs to constitute an explosion hazard.

6.4.3 Hydroclone

The integrally flanged hydroclone (Fig. 6.8) designed for the HRT-CP was tested to determine its efficiency and corrosion rate. At a normal

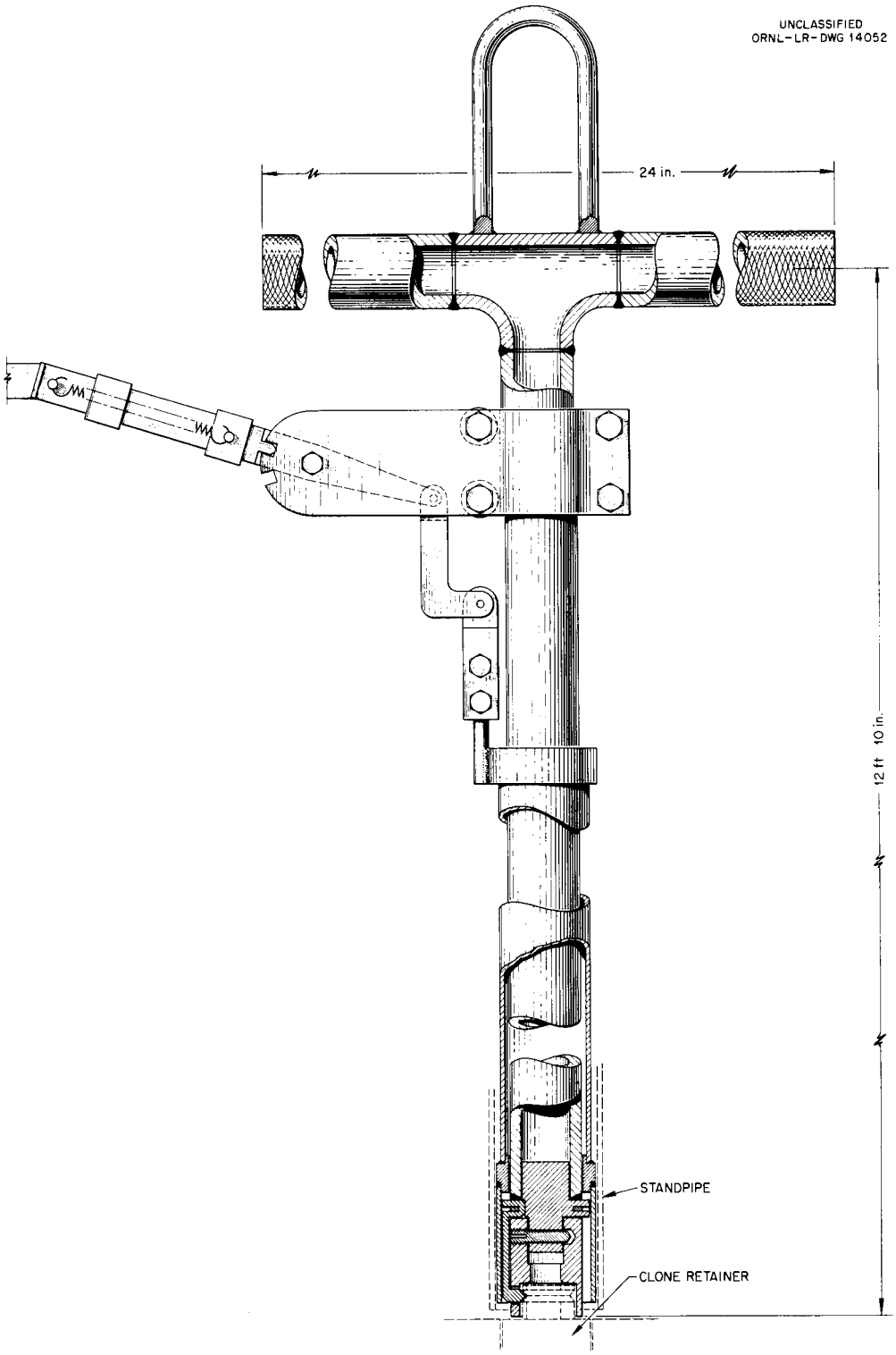

Fig. 6.5. Retainer-Plug Removal Tool.

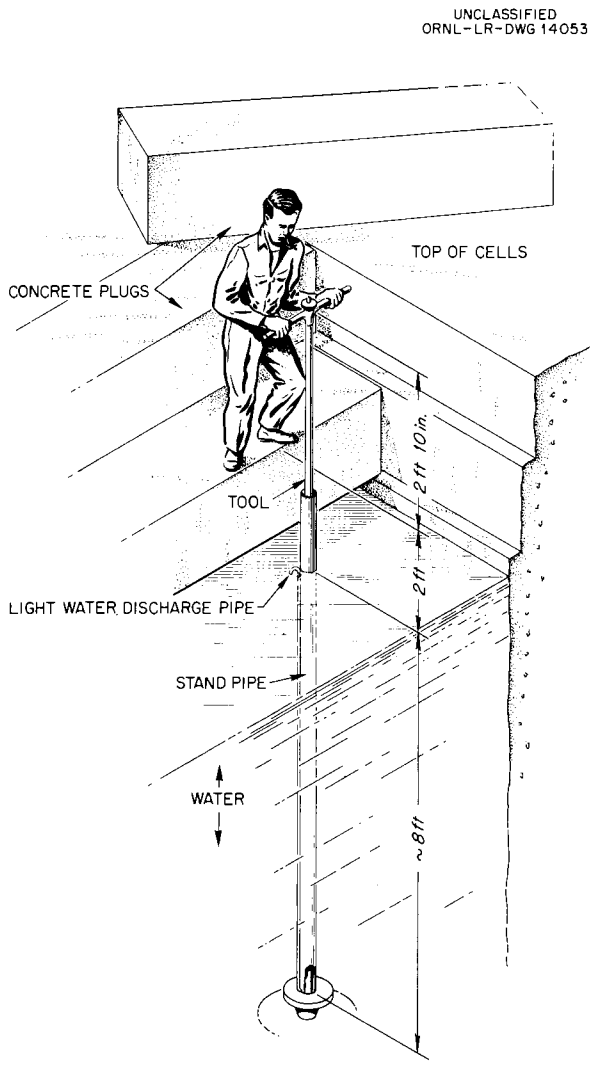

Fig. 6.6. Hydroclone Removal Operation.

flow rate the measured underflow ratio was 1.4 ± 0.3% (for HRT design an underflow rate not in excess of 2% is desired), and the centrifugal efficiency was found to be consistent with that obtained by standard hydroclones of the same dimensions used heretofore in experimental loops (see Table 6.1).

A 0.25 × 1.5 in. hydroclone operated for 2300 hr at 300°C, at the design flow rate of 0.25 gpm, displayed none of the changes in pressure drop vs flow which heretofore have been indicative of corrosion. The 2300-hr test on loop K in the Reactor Experimental Engineering Division was conducted at simulated HRT reactor conditions, except for the absence of the radiation corrosion products and the fission products that are expected to be in suspension in the HRT fuel solution.

6.5 CONSTRUCTION STATUS

The HRT Chemical Plant is scheduled for completion July 1, 1956. Shop work and field work are 90 and 30% complete, respectively, compared with a scheduled 100 and 35%. Work is slightly behind schedule, mainly because of the priority demand for craftsmen to complete reactor construction on schedule.

Material, equipment, and instruments in amounts totaling $130,000 were received from a total of $170,000 on requisition. The principal items not yet received and the expected delivery dates are: canned-rotor pumps, May 30; graphic instrument panel board, May 1; roof plugs, June 15.

TABLE 6.1. COMPARISON OF HYDROCLONE EFFICIENCIES

Material: TM-Y thorium oxide in water at room temperature, 80 wt % of thorium oxide between 0.6 and 3.0 μ

Hydroclone	Pressure Difference $P_F - P_0$ (psi)	Underflow Rate (%)	Hydroclone Efficiency (%)
Integrally flanged, 0.40-in. diameter, 2.40-in. length	44	10	38.8
	44	10	43.6
	44	10	42.3
Standard unit, 0.40-in. diameter, 3.14-in. length	44	9	36.5
	35	6	42.8
	35	6	34.2

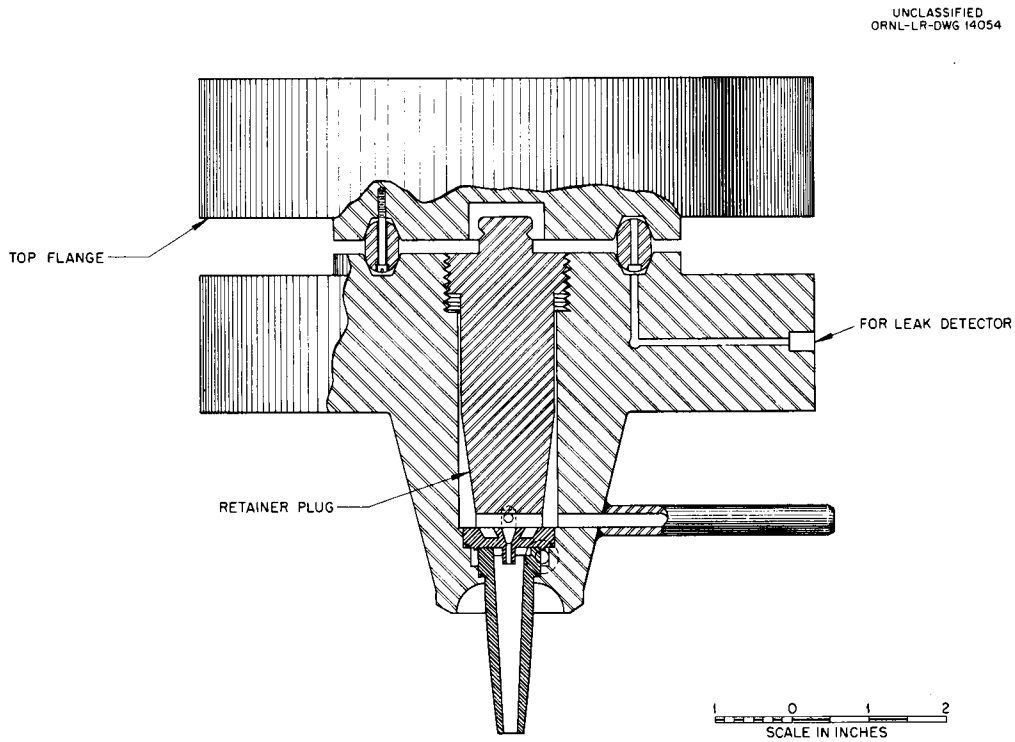

Fig. 6.7. Recessed Hydroclone Flange.

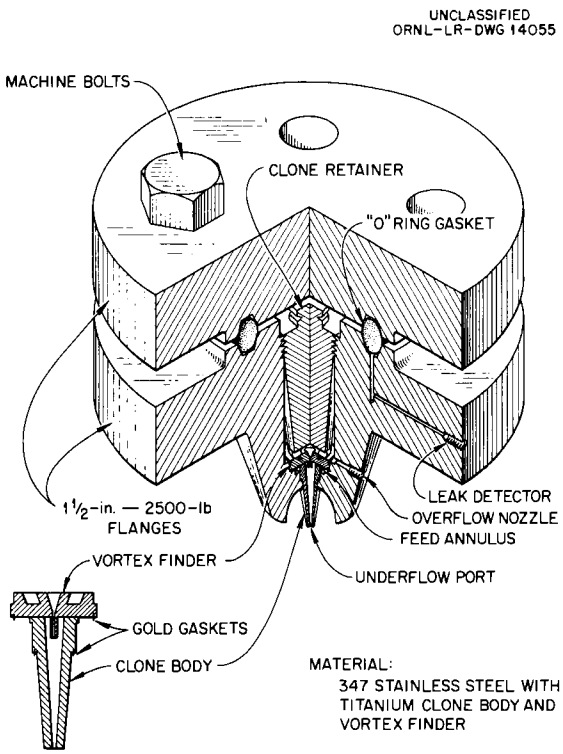

Fig. 6.8. Integrally Flanged Hydroclone.

Fabrication of all process components being constructed at ORNL is complete except the following.

1. Construction of the sampler has been held in abeyance pending completion of the sampler mockup tests being performed at Y-12. Construction of the modified isolation chamber and sampler needle for sampling liquids with high solids contents is complete and will be tested prior to installation.

2. Fabrication of the carriers will begin as soon as corrosion-rate investigations are completed.

The two low-pressure units, each consisting of an entrainment separator, superheater, recombiner, condenser, and associated valves and piping, are completed and installed in cell C. Cooling-water, steam, and leak-detector lines were connected to the units. The high-pressure unit is ready for assembly on completion of high-pressure tests now in progress.

Figure 6.9 shows both low-pressure units from the north end of cell C. Also shown are the space cooler, sampler housing, and suspended D_2O receiver. Figure 6.10 is a closer view of one of the low-pressure units from the east side of cell C.

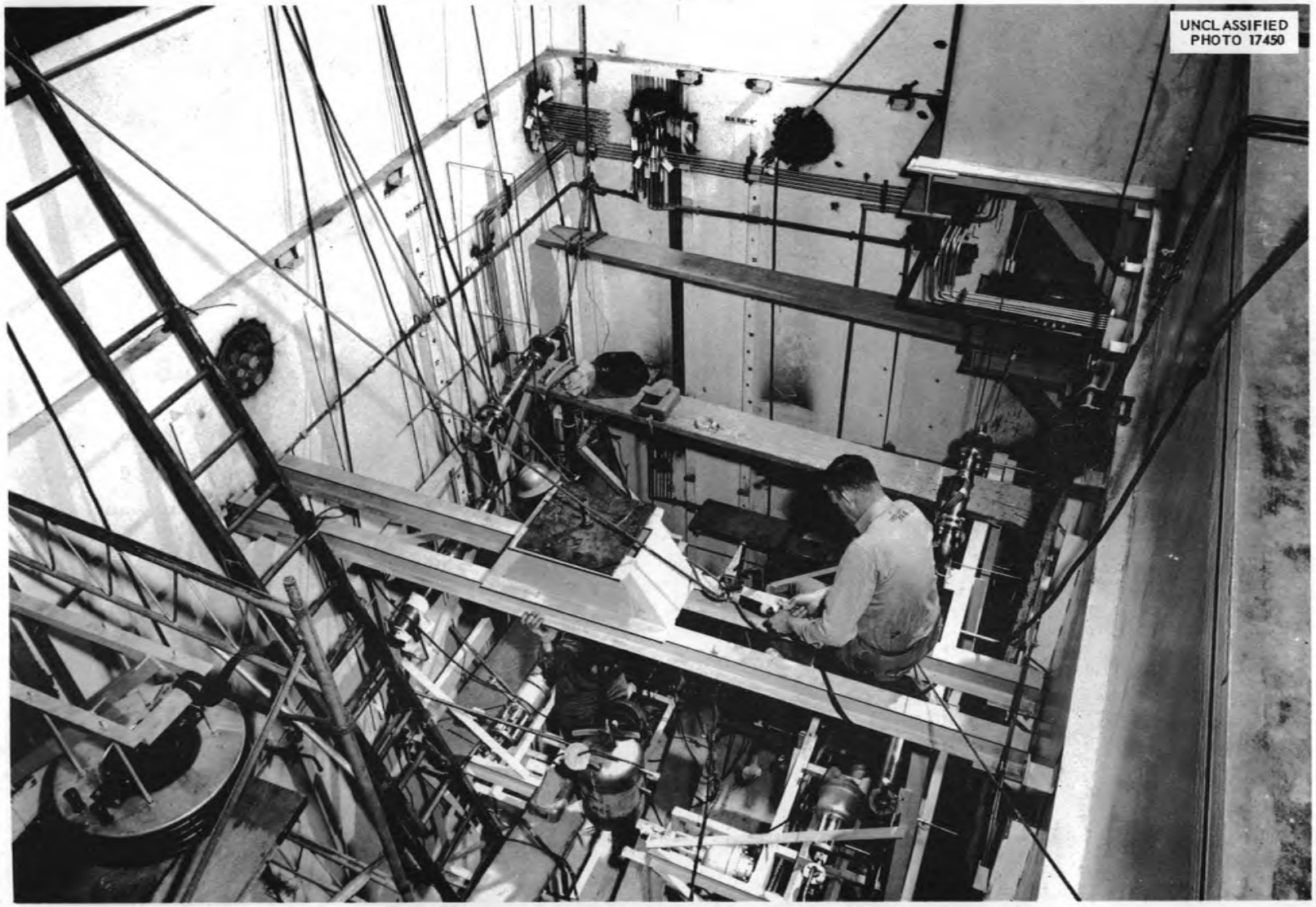

Fig. 6.9. Cell C from North.

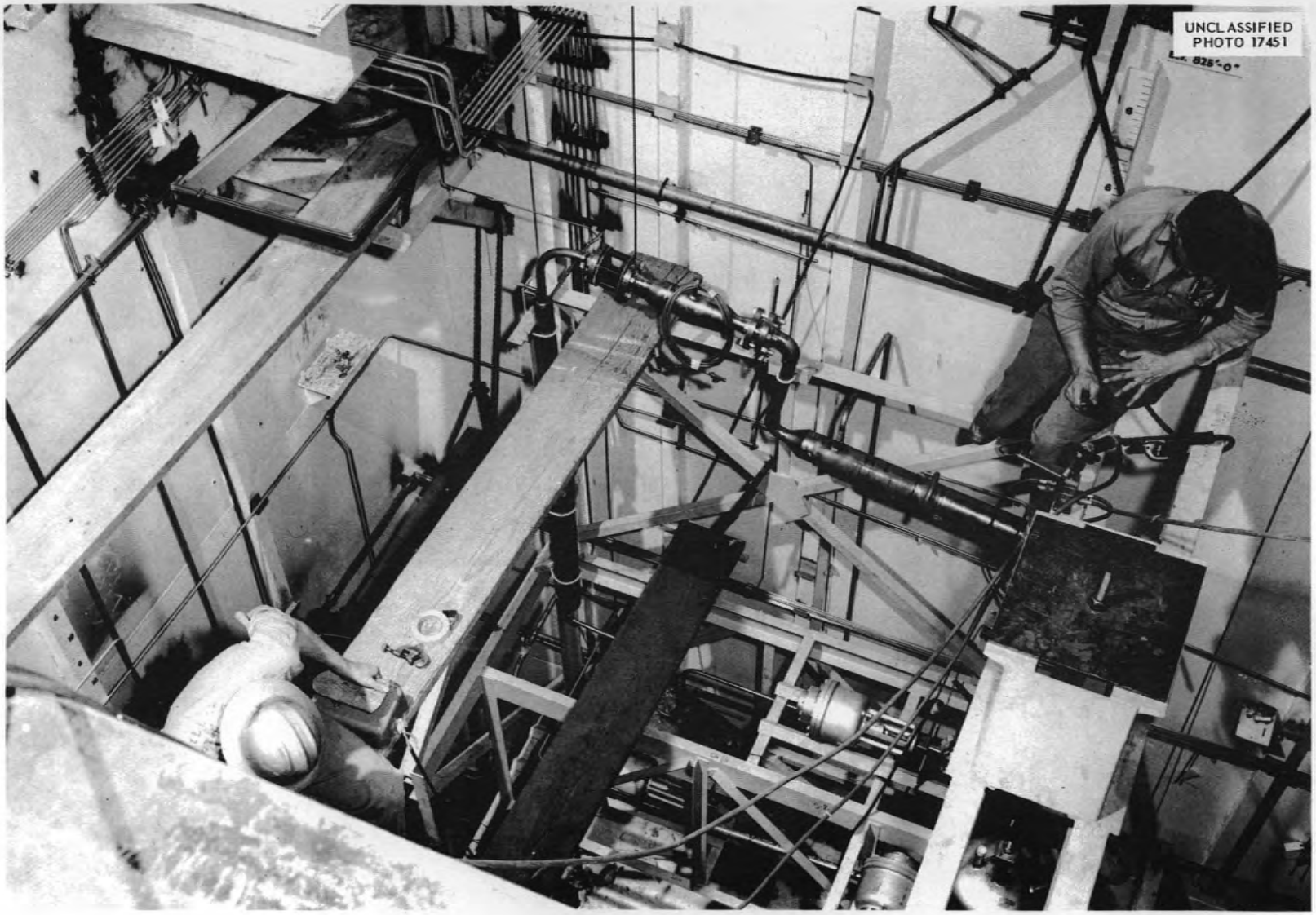

Fig. 6.10. Cell C from East.

Figure 6.11 shows the Chemical Plant refrigeration unit and the dewatering pump and valve manifold for removing shielding water from the reactor and chemical plant cells. Figure 6.12 is a view of the service valve rack for steam, water, and Freon. Figure 6.13 shows the valve manifolds for both the high- and low-pressure leak-detector systems.

Fig. 6.11. Dewatering Pump and Refrigeration Unit in Cell A.

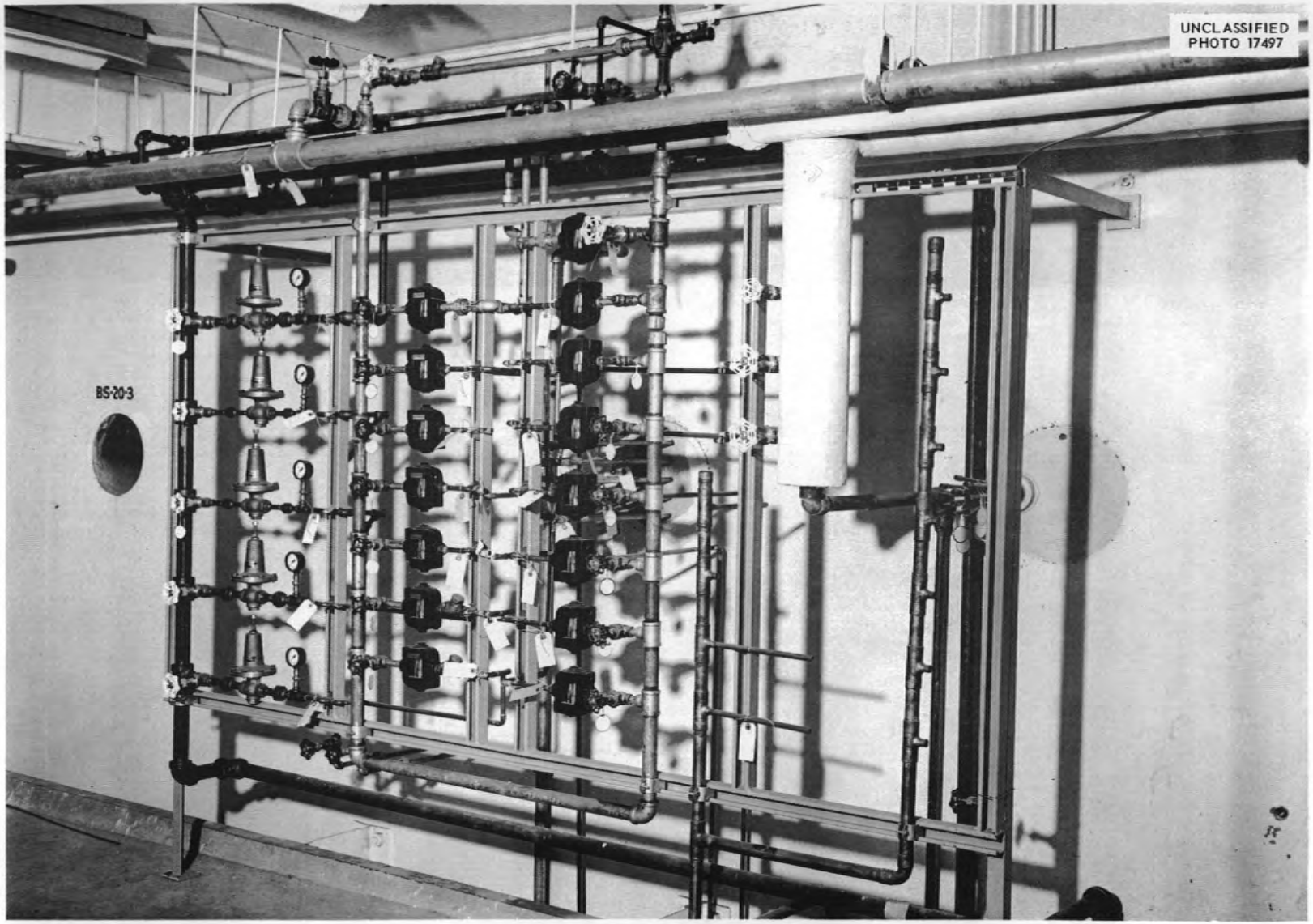

Fig. 6.12. Service-Valve Rack in Cell A.

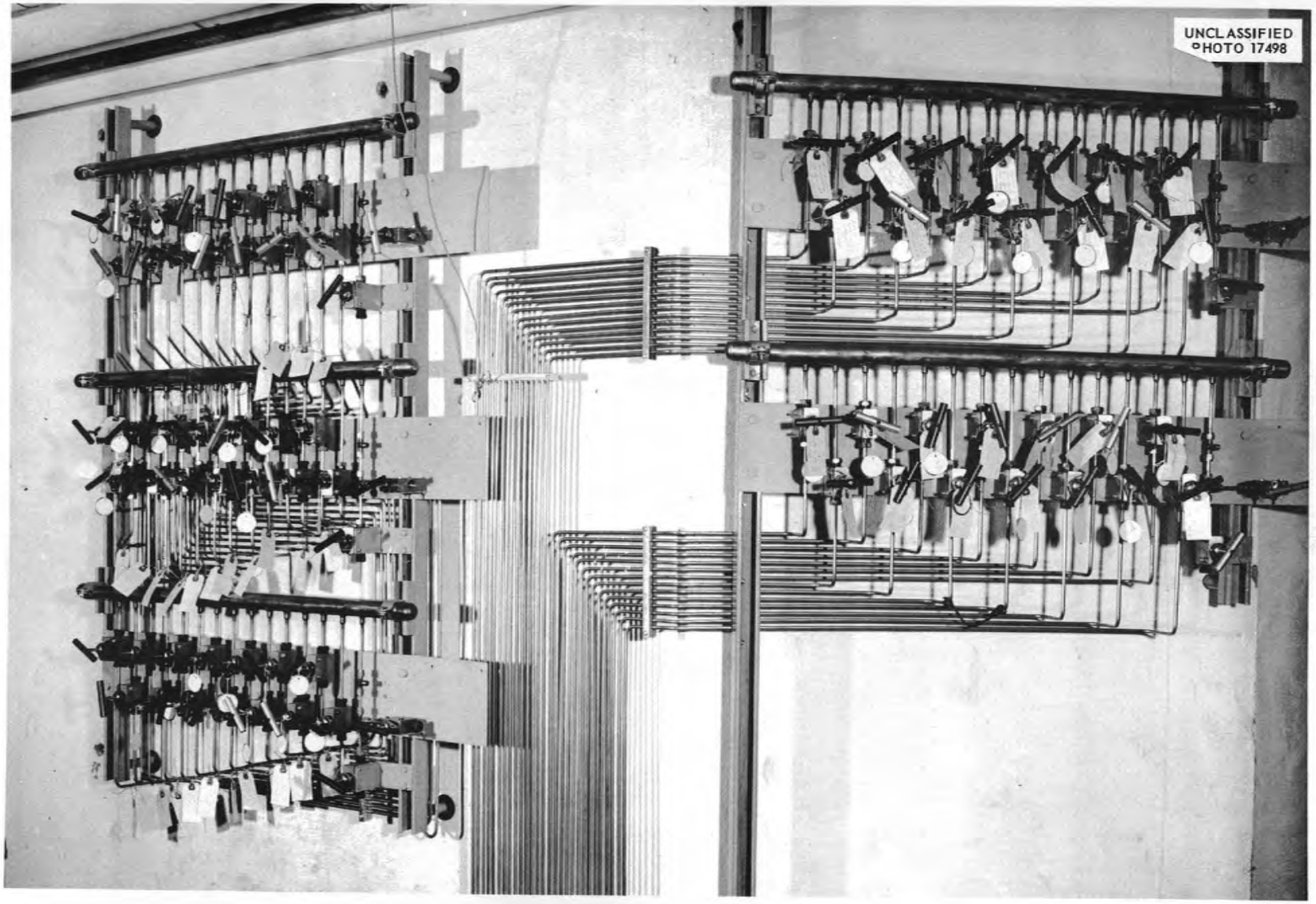

Fig. 6.13. Leak-Detector Manifolds in Cell A.

Part II

REACTOR DESIGN AND ANALYSIS

J. A. Lane

7. REACTOR ANALYSIS

P. R. Kasten

H. C. Claiborne
T. B. Fowler
D. C. Hamilton
M. K. Hullings
C. W. Nestor, Jr.
M. W. Rosenthal
M. Tobias

7.1 FUEL COSTS FOR U^{235} BURNERS

H. C. Claiborne T. B. Fowler

The production of competitive nuclear power implies low chemical processing costs; however, these costs can only be low when the processing plants serve a number of reactors generating a total of more than 300 Mw of electrical power. There is a market for power in the range of 5 to 10 Mw, usually in areas of relatively high fuel cost. At the present stage of development, nuclear power plants of these capacities cannot be serviced economically by their own processing plant. Consequently, chemical processing must be eliminated or the spent fuel shipped to some centrally located processing plant. This suggests that reactors capable of operating for long periods of time with no chemical processing are desirable. An investigation of fuel costs was made for reactors whose fuel is processed on a batch basis.

The reactors studied were spherical, one-region homogeneous reactors containing UO_2SO_4 in either D_2O or H_2O and using 93.5% U^{235} feed. In all cases the noble gases were assumed to be removed continuously. For some cases 75% of the poisons that precipitate in the fuel, along with any precipitated plutonium, were assumed to be removed by hydroclones. A cheap filtration or separation process capable of separating the fuel solution from the hydroclone underflow was also assumed. This would allow the fuel solution to be fed back to the reactor. To indicate the effect of power level, this study considered two power levels, 125 and 5 Mw.

A summary of some of the results is shown in Table 7.1. More detailed results for five reactors are reported in Table 7.2. The principal conclusion derived from Table 7.1 was that the fuel cost would be about 4 mills/kwhr regardless of the size, power, or moderator, if the spent fuel (at the end of operation) were shipped to a central processing plant. Also, the use of hydroclones for partial poison removal showed no economic advantage. The indicated operating times were not optimum. Actually, no minimum cost was reached; the cost continued to decrease up to the times shown. The cost decrease was small, however, after 2000 days. The results indicate that a reactor of this type can run economically for many years (engineering components and corrosion permitting) without chemical processing.

Table 7.1 indicates that there would be an insignificant penalty if the spent fuel from the higher power D_2O reactor were discarded without recovering the uranium. The costs for fuel recovery were based on the assumption of the existence of a large-capacity processing plant so that the fixed charges for the chemical plant could be considered negligible. Since this fixed charge would amount to about 0.1 mill/kwhr even for plants processing reactors of 2800 electrical Mw capability, it would be slightly cheaper to discard the uranium for the higher power D_2O reactors, provided that the spent fuel could be cheaply and safely disposed of at the site. The much higher uranium inventory in the H_2O-moderated reactors would lead to an appreciable penalty if the uranium were discarded, particularly for the low-power reactors.

7.2 CYLINDRICAL REACTOR STUDIES

D. C. Hamilton P. R. Kasten

Nuclear and economic calculations were made for a set of cylindrical, two-region, thorium breeder reactors by using two-group theory for the nuclear calculations and the method of ORNL-1810[1] for the economic calculations. The purposes of these studies were to determine the effect of geometry upon power density at the core wall, breeding ratio, and fuel costs.

The reactors had the characteristics reported in Table 7.3, and the results obtained are presented in Figs. 7.1 and 7.2. Figure 7.1 gives the variation of the maximum power density at the core-tank

[1] H. C. Claiborne and M. Tobias, *Some Economic Aspects of Thorium Breeder Reactors*, ORNL-1810 (Oct. 12, 1955).

TABLE 7.1. FUEL COSTS FOR ENRICHED BATCH OPERATED HOMOGENEOUS REACTORS[a]

Moderator	Diameter (ft)	Electrical Power (Mw)	Hydroclone Cycle (days)	Average Power Density (kw/liter)	Reactor Operating Time (days)	Uranium Concentration[b] (g/liter)	Poisons[c] (%)	Fuel Cost[b,d] (mills/kwhr)		Fuel Cost at 2000 Days (mills/kwhr)	
								Uranium Recovered	No Uranium Recovery	Uranium Recovered	No Uranium Recovery
D_2O	7	125	1	94	2000	9.2	18	3.93	3.99	3.93	3.99
	6	125	1	150	4200	18.6	23	3.90[c]	3.94	3.93	4.02
	5	125	1	260	2000	12.0	13	3.94	4.08	3.94	4.08
	6	125	∞	150	4400	22.8	53	3.90[c]	3.98	3.92	4.07
H_2O	7	125	1	94	2000	23.6	5	4.15	5.37	4.15	5.37
	6	125	1	150	2000	24.7	5	4.13[c]	5.31	4.13	5.31
	5	125	1	260	5600	44.7	8	4.04	4.45	4.13	5.31
	5	125	∞	260	3400	35.4	17	4.06	4.82	4.11	5.37
D_2O	3	5	∞	5	3400	21.4	23	4.10[c]	4.51	4.13	4.76
	3	5	1	5	3000	17.2	9	4.66	4.99	4.68	5.18
H_2O	3	5	∞	5	8200	55.6	21	4.20	4.72	4.34	6.34
	2	5	∞	16	5800	57.8	17	4.21[c]	4.95	4.33	6.33

[a]Average temperature, 280°C; fuel, UO_2SO_4; inventory charges for uranium and D_2O, 4%.

[b]At indicated operating time.

[c]Details in these cases are shown in Table 7.2.

[d]Assumes that the processing plants are servicing large enough reactor capacity to make the fixed charges for chemical processing negligible.

TABLE 7.2. ISOTOPE CONCENTRATIONS AND COST BREAKDOWN FOR SOME U^{235} BURNERS*

Electrical power, Mw	125	125	125	5	5
Diameter, ft	6	6	6	2	3
Moderator	H_2O	D_2O	D_2O	H_2O	D_2O
Hydroclone cycle, days	1	1			
Average power density, kw/liter	150	150	150	16	5
Operating time, days	2000	4200	4400	5800	3400
Initial U^{235} inventory, kg	353	34.3	34.3	21.8	5.7
System volume, liters	27,240	27,240	27,240	1080	1360
No. of shipping casks	50	84	90	6	3
Average U^{235} feed rate, kg/yr	239	233	237	9.8	9.8
Isotope concentrations,** g/liter					
U^{234}	0.98	0.30	0.52	2.4	0.83
U^{235}	13.64	1.99	3.82	26.8	7.73
U^{236}	7.19	12.00	13.70	20.8	9.50
U^{238}	2.90	4.27	4.74	7.8	3.37
Np^{239}	0.00007	0.007	0.0004	0.0001	0.0001
Pu^{239}	0.002	0.003	0.008	0.012	0.006
Pu^{240}	0.0006	0.0005	0.008	0.010	0.005
Pu^{241}	0.0001	0.00005	0.003	0.003	0.002
Estimated costs, mills/kwhr					
Uranium inventory	0.29	0.03	0.03	0.44	0.12
D_2O inventory and losses	0	0.19	0.19	0	0.24
Uranium feed	3.71	3.64	3.70	3.83	3.84
Chemical processing	0.08	0.03	0.03	0.06	0.05
Hydroclones	0.02	0.02	0	0	0
Shipping	0.02	0.02	0.02	0.02	0.02
Plutonium sale (credit)	0.0005	0.01	0.0003	0.0003	0.0003
Diffusion plant (credit)	0.002	0.02	0.08	0.14	0.18
Total (fuel cost)	4.13	3.91	3.90	4.21	4.10

*Average temperature, 280°C; inventory charges for uranium and D_2O, 4%.

**At indicated operating time.

wall (core side) as a function of reactor length, core radius, and blanket fuel concentration.

Figure 7.2 gives the fuel cost and breeding ratio as a function of the core-tank power density. Minimum fuel costs are associated with high power densities; highest breeding ratios are obtained with small core radii, thick blankets, and long reactors. Thus the reactors with the lowest fuel costs do not have the lowest core-wall power densities or the highest breeding ratios. If corrosion difficulties do not permit high power densities at the core wall, some compromise would be required. Increasing the reactor length increased the inventory charge until that charge controlled the fuel cost; the associated increase in breeding ratio was slight.

In these calculations, an effective extrapolation distance which was independent of region was used for the reactor ends. If a blanket were considered at the ends of the core region, the breeding ratio would increase, particularly for those reactors of relatively short length. Under these conditions the breeding-ratio curve in Fig. 7.2 would tend to become more horizontal and could possibly

TABLE 7.3. CYLINDRICAL REACTORS STUDIED

Feature	Unit
Reactor mean temperature	300°C
Total thermal power generated	450 Mw
Net electrical power generated	125 Mw
Fuel and inventory charge	12%
Core radius	2 and 3 ft
Zircaloy-2 core-tank thickness	½ and ¾ in.
Blanket radius	5 ft
Blanket thorium concentration	1000 g/liter
Blanket U^{233} concentration	1, 3, and 5 g/kg Th
Reactor length	10, 20, 30, and 40 ft

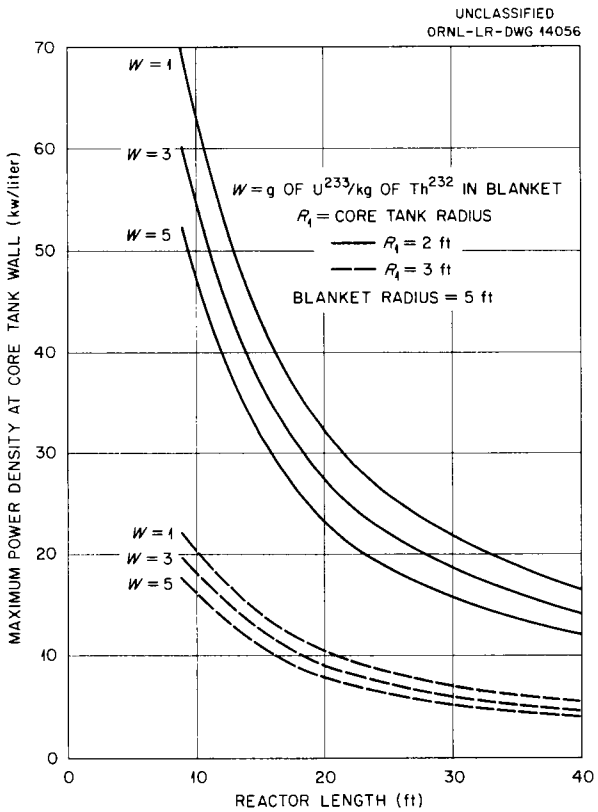

Fig. 7.1. Maximum Power Density at Core-Tank Wall for Two-Region Cylindrical Reactors.

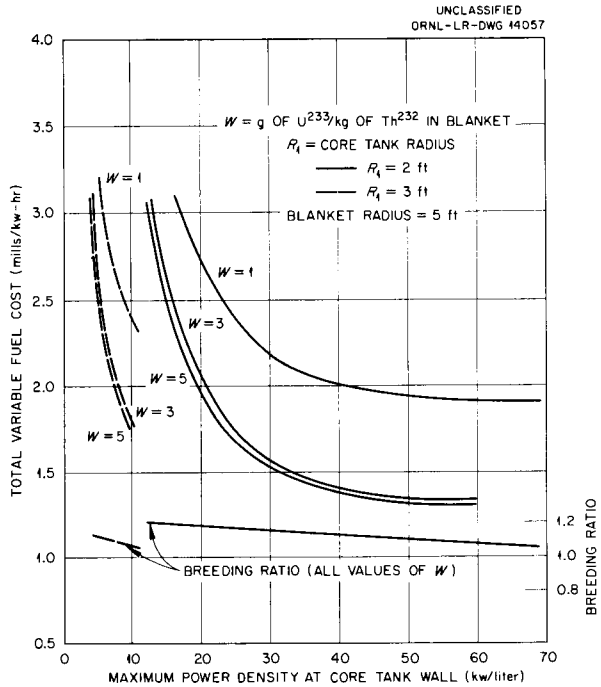

Fig. 7.2. Effect of Core-Tank Power Density on Breeding Ratio and Fuel Cost in Two-Region Cylindrical Reactors.

change to a positive slope as the power density increased. However, this effect is relatively unimportant insofar as fuel costs are concerned.

The nuclear results given here are based upon reactors which had only D_2O, U^{233}, and 6% poisons in the core region and D_2O, U^{233}, and Th^{232} in the blanket region. More refined calculations indicated that the breeding ratios given here were too large by approximately 0.002. In calculating the fuel costs, the blanket U^{233} chemical processing cost and inventory charge were multiplied by 1.4 to account for the Pa^{233} which would be present.

7.3 TWO-GROUP STUDIES OF LARGE SPHERICAL REACTORS

C. W. Nestor, Jr. M. W. Rosenthal

A two-group, two-region Oracle code[2] was used to compute the maximum power density, the power

[2] T. B. Fowler, *Oracle Code for a General Two-Region, Two-Group Spherical Homogeneous Reactor Calculation*, ORNL CF-55-9-133 (Sept. 22, 1955) and Supplement (Oct. 7, 1955).

density at the inside core wall, and the breeding gain for a number of reactors having 200 g of thorium per liter (as ThO_2) in the core region. Blanket materials considered were heavy water (99.75% D_2O), beryllium, and thoria–heavy-water slurries having thorium concentrations of from 1 to 5 kg/liter. The inside diameter of the pressure vessel was fixed at 10 ft for one set of calculations and 12 ft for a second set; core diameters ranged from 6 to 9 ft in the first set and from 6 to 11 ft in the second set. The average temperature of all systems was 280°C, and, for the purpose of calculating power densities at the core tank, total power was taken as 100 Mw. A ½-in.-thick zirconium core tank separated the core and blanket in all reactors. Neutron losses in this tank are taken into account by the code. No account has been taken of fission-product poison buildup in the core, protactinium losses, or fuel buildup in the blanket in these preliminary calculations.

The results are plotted in Figs. 7.3 and 7.4 and are summarized as follows:

1. The breeding ratio increased for any core diameter by replacing the D_2O blanket with one containing ThO_2.
2. No significant increase in breeding ratio was obtained by increasing the blanket thorium concentration above 2 kg of thorium per liter.

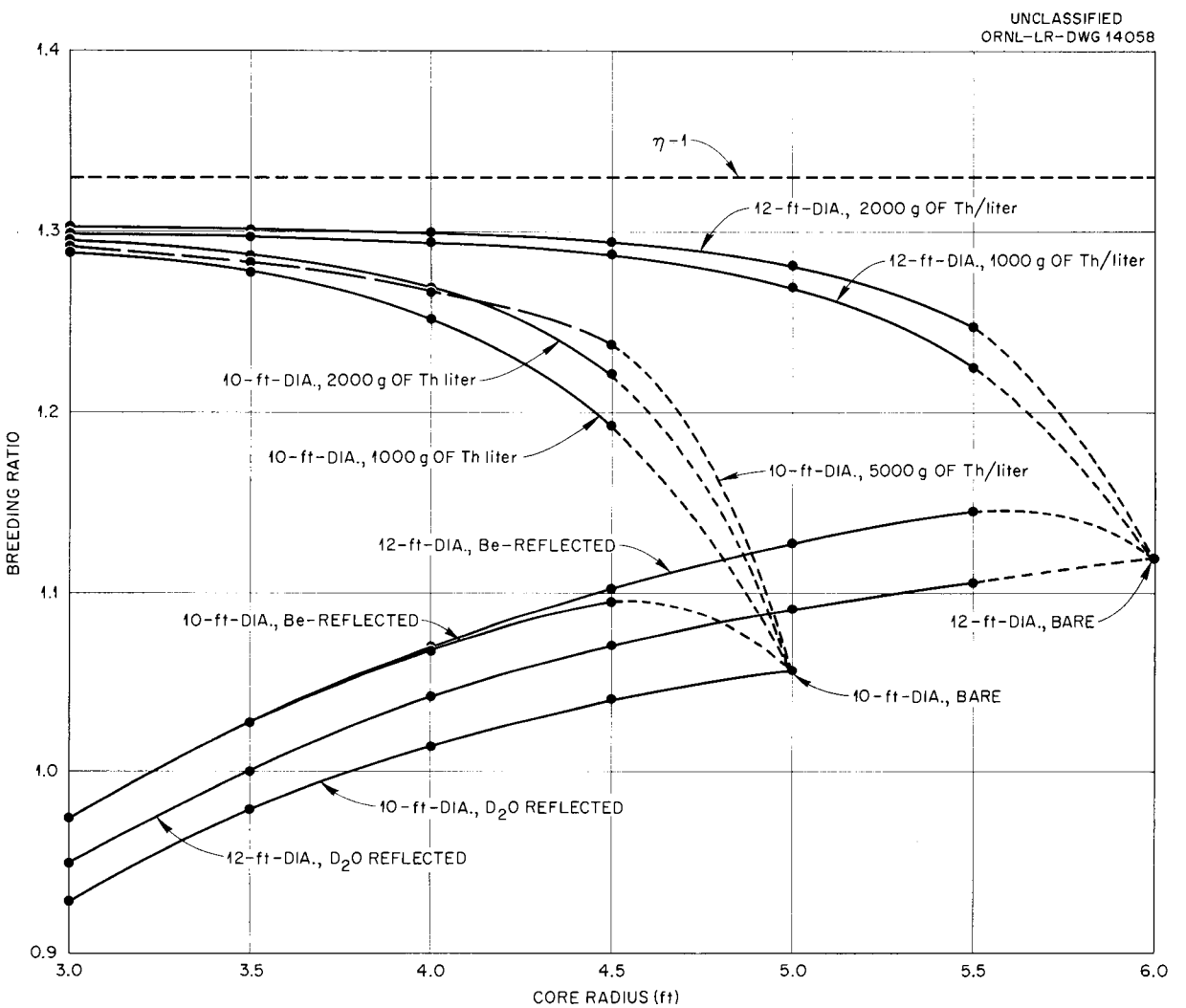

Fig. 7.3. Breeding Ratio and Power Density at Core Wall in Large Spherical Reactors.

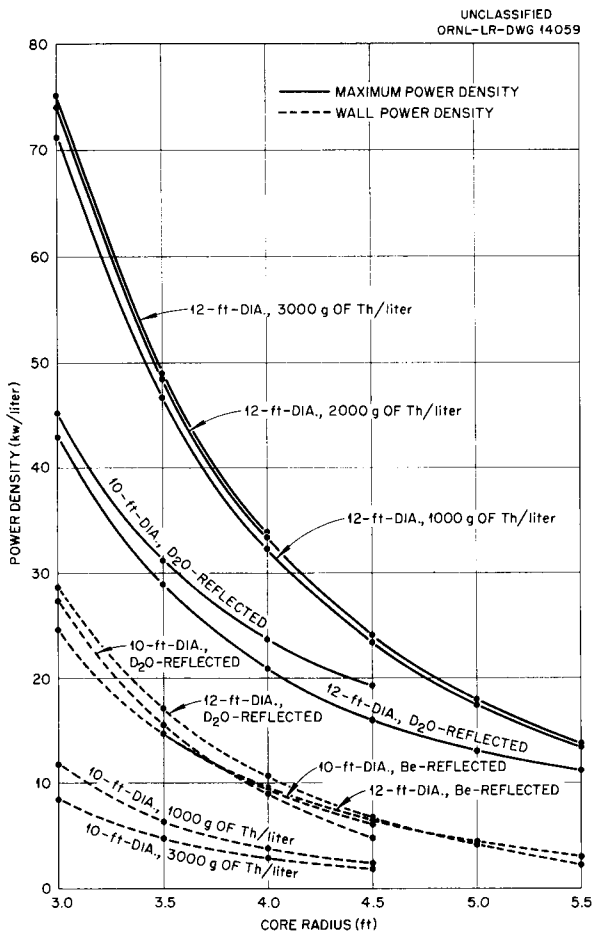

Fig. 7.4. Maximum and Wall Power Densities vs Core Radius for Several Two-Region Reactors.

3. For reactors with fertile material in the blanket, the breeding ratio increased with decreasing core diameter; however, the power density at the wall also increased.

4. The beryllium-reflected reactors had a higher breeding ratio than the D_2O-reflected reactor and very nearly the same wall power density.

7.4 CALCULATION OF TWO-GROUP CONSTANTS

M. Tobias M. K. Hullings

The Oracle code[3] for the calculation of ages and diffusion constants was employed for thorium oxide slurries and equimolar uranyl sulfate–lithium sulfate solutions in mixtures of light and heavy water. Some results were also obtained for uranyl sulfate solutions in heavy- and light-water solutions. Those calculations, which involved hydrogen, were carried out by use of empirical adjustments of the average logarithmic energy decrement and average cosine of the scattering angle. This procedure produced a value for the age-to-indium of light water which agreed with experimental data. Slow-diffusion constants were obtained with similar changes so as to give acceptable results at known points.

In the case of the thorium oxide slurries, the effect upon the two-group constants of concentrations of U^{233} between 0 and 5 g of U^{233} per kilogram of thorium was studied and found to be negligible for all concentrations of thorium.

Ages and diffusion constants are available for the media cited in Table 7.4. The results themselves will be reported at a later date.

[3] M. Tobias, *An Oracle Code for Calculation of Fermi Ages by Numerical Integration*, ORNL CF-56-4-53 (April 10, 1956).

TABLE 7.4. COMPOSITION OF REACTOR MEDIA

	Wt % Heavy Water in D_2O-H_2O Mixture	Concentration of U^{238} or Thorium (g per kg of water mixture)	Concentration of U^{233} (g per kg of thorium)	Temperature Range for Slow-Diffusion Constant (°C)
ThO_2 slurries	0–100	0–4000	0–5	200–320
Equimolar UO_2SO_4-Li_2SO_4 solutions	0–100	0–1000	0	200–320
UO_2SO_4 solutions	0 and 100	0–1500	0	320

Part III

ENGINEERING DEVELOPMENT

J. A. Lane

8. DEVELOPMENT OF FUEL-SYSTEM COMPONENTS

C. B. Graham

C. H. Gabbard
B. A. Hannaford
P. H. Harley
P. P. Holz
I. K. Namba
W. L. Ross
I. Spiewak
D. S. Toomb
H. D. Wills

8.1 RECOMBINER DEVELOPMENT

8.1.1 High-Pressure Recombiner Loop

The high-pressure recombiner loop, after being rebuilt,[1] operated intermittently for 400 hr at 500 psi and 400°C (recombiner temperature). During the first 300 hr 4% $Ba(OH)_2$, containing 3 ppm Cl^-, was used as an electrolyte. The loop was shut down as the result of a rupture-disk failure on one electrolytic cell. The line to the rupture disk had apparently been plugged with corrosion products, and sufficient gas pressure to break the disk had developed. There were no indications of an explosion on the loop pressure chart.

During the last 100 hr the electrolyte used was chloride-free KOH, which retained some traces of mercury from the process of chloride removal. During this period three piping leaks occurred downstream from the loop condenser. Although metallographic examination has not been completed, it appears that stress corrosion was involved in the failures.

Samples of titanium and zirconium alloys were placed in the loop for testing as containers for high-pressure homogeneous-reactor vapors.

8.1.2 Natural Circulating Recombiners

A mixture containing 10.5 mole % stoichiometric hydrogen and oxygen in steam reacted without flashbacks in a natural circulating recombiner system at 100 psi. This result indicates that the explosive limit is above 10.5 mole % at that pressure in a large pipe. Attempts to operate at higher concentrations were hampered by insufficient cooling capacity in the system.

8.1.3 Battelle and Syracuse Subcontracts

The work by Battelle on the solubility of gases in water and uranyl sulfate solutions is now complete, and a summary report[2] has been issued. Errors in the determination of explosive limits of H_2-O_2-steam mixtures in a 3-in. autoclave were discovered by vapor-phase chemical analysis. Apparently, inhomogeneity in the vapor phase led to errors in estimating the composition of the mixtures.

Syracuse University is continuing its investigation of detonation pressures, damping of explosion waves, transient loading, and vapor viscosity. Partial results on the pressure and viscosity work were reported. In particular, they confirmed the superheated-steam viscosity data at 2000 psi as reported by Timrot[3] and found that a 30% He–70% steam mixture has a slightly higher viscosity than pure steam.

8.2 SMALL REACTOR COMPONENTS

8.2.1 20-cfm Canned-Rotor Blower

Because of procurement and fabrication delays, Allis-Chalmers Mfg. Co. postponed their promised shipment of the 20-cfm gas circulator until early June. Meanwhile, most of the blower test loop piping was completed at ORNL, and instrumentation and electrical work is scheduled to start about May 1.

8.2.2 Small Circulating Pumps

Longer stator life appears to have resulted from a change from parallel connection to series connection of the windings of the commercial stators used in the 5-gpm pumps. The power input is lower, and there is some reduction in the head developed by the pump. The longest life experienced with parallel-connected windings was 6900 hr, but in some cases the windings failed within less than 1000 hr. With the windings in series,

[1] C. B. Graham *et al.*, *HRP Quar. Prog. Rep. Jan. 31, 1956*, ORNL-2057, p 73.

[2] E. F. Stephan *et al.*, *The Solubility of Gases in Water and in Aqueous Uranyl Salt Solutions at Elevated Temperatures and Pressures*, BMI-1067 (Jan. 23, 1956).

[3] D. L. Timroth, *J. Phys. U.S.S.R.* 2(6), 419–435 (1940).

no failures have been observed on three pumps operating under different conditions for 580, 865, and 8850 hr, respectively.

The first pump has accumulated 5750 hr of operation at 2000 psi and 300°C without difficulty other than stator failures. The second has accumulated 12,650 hr of operation at 1000 psi and 250°C without difficulty other than stator failure. The third pump, which has had series windings throughout its life, has given no difficulty during its entire 8850 hr of testing with room-temperature water. A recent examination of the moving parts of this pump showed them to be in excellent condition.

8.3 4000-gpm LOOP

The 4000-gpm loop,[4] containing a Byron-Jackson canned-rotor pump, was operated at 250°C to obtain corrosion information pertinent to an HRT startup. After a 100-hr water shakedown, UO_2SO_4 was added in gradually increasing concentration over a 421-hr period. At this time a shutdown was forced by a feed-pump pulsator failure.

8.4 TITANIUM-LINED EQUIPMENT

Material was ordered for a small titanium-lined heat exchanger to be made by The Pfaudler Co. and for the titanium-lined pipe that is to be fabricated by the Crane Co. The heat exchanger design was approved for construction. The pipe design is complete except for a solution to the problem of butt-welding the carbon steel outer pipe without the shrinkage crushing the liner.

The Armour Research Foundation prepared four test sandwiches with which they will attempt to hot-roll-clad titanium to carbon steel. After the rolling operation, the samples will be examined and then tested to determine the tensile strength and ductility of the bond. The contract, which was to expire at the end of April, is being extended for six months.

8.5 HIGH-PRESSURE FLANGE TEST[5]

The 4-in. 1500- and 2500-lb ring-joint flanges with gold-plated rings did not leak during a 3000-psi hydrostatic test with bolt stresses of 13,000 and 10,000 psi, respectively. However, during the first thermal cycle, when the temperature was raised at a rate of 125 to 150°F/hr, indication of leaks started at 300°F and 70 psi pressure. As temperature and pressure were increased to 600°F and 1750 psi, the leak rate went up correspondingly. The bolt stresses increased slightly during the heating cycle, according to strain-gage readings. When the flanges cooled, many of the bolts were only finger-tight.

The flanges were retightened with slightly higher bolt stresses and again cycled thermally, with similar results. They were then tightened to a bolt stress of about 16,000 psi, and leak-tested at atmospheric pressure with helium. The leak rates were 0.35 and 0.37 cc/day across the 1500- and 2500-lb flanges, respectively. At this point the 2500-lb gold-plated O-ring was examined visually and appeared to be undamaged.

In an attempt to reduce the leakage, an unplated O-ring was substituted in the 2500-lb flange, and it was tightened to 32,000-psi bolt load. The helium leak rate was measured at 0.07 cc/day. The 1500-lb flange will be tightened to approximately the same bolt stress before the next thermal cycle is attempted.

---

[4] C. B. Graham *et al.*, *HRP Quar. Prog. Rep. Jan. 31, 1956*, ORNL-2057, Sec. 8.3.1, p 74.

[5] *Ibid.*, Sec. 8.1.2, p 73.

9. DEVELOPMENT OF BLANKET-SYSTEM COMPONENTS

R. B. Korsmeyer R. N. Lyon

D. G. Davis C. G. Lawson M. Richardson
H. N. Fairchild L. E. McTaggart A. N. Smith
R. B. Gallaher I. M. Miller D. G. Thomas
W. Q. Hullings R. H. Nimmo R. P. Wichner
A. S. Kitzes L. F. Parsly

9.1 STUDY OF CAKE FORMATION IN LOOP 200A

D. G. Thomas R. B. Gallaher

Chemical, spectrographic, and particle-size analyses of the cake formed during test 200A-3 were completed.[1] The chemical and spectrographic analyses confirmed the preliminary report[2] that no large concentration of contaminants or impurities was present. However, the sulfate concentration was lower than in any other test in which $Th(SO_4)_2$ was added. X-ray crystallite measurements showed no difference between the pumped slurry and the cake. Sedimentation particle-size analysis indicated a broader particle-size distribution in the cake than in the slurry samples taken during the test, and the mean particle diameter of the cake removed from the pipe walls appeared to be smaller than in any of the samples taken from the circulating stream. X-ray-diffraction measurements on several different layers of cake showed no evidence of preferred orientation.

Figures 9.1 and 9.2 are photographs of a typical piece of cake removed from one of the stub-end flange sections. As can be seen from Fig. 9.1, the ThO_2 cake modeled the tool marks on the stub ends. Figure 9.2 is a photograph of the slurry side of the piece of cake shown in Fig. 9.1. The most distinctive features are the conchoidal fracture shown on the bottom edge of the right piece of cake and the texture of the surface of the cake next to the flowing stream.

Since aluminum and silica were found, by analysis, in the 200A slurry, an attempt was made to produce hard cakes by circulating slurries of high aluminum content and high aluminum and silica content in the 5-gpm loops. Two runs of about 100-hr duration were made in which a slurry of thorium oxide calcined above 1000°C and ball milled with aluminum oxide balls was circulated at 250°C. The slurry had a pH of 6.0 and contained about 10,000 ppm aluminum and 1,000 ppm sulfate. Soft cakes were found in the pressurizers, but no hard cakes developed.

Three other runs were made in which mullite ($3Al_2O_3 \cdot 2SiO_2$) was added to the slurry. In one run the slurry, containing 1000 g of thorium per kilogram of H_2O, 1500 ppm aluminum as mullite, and no sulfate, was circulated at 60°C. In the second and third runs a similar slurry was circulated at 250 and 60°C, respectively, before the mullite was added. No difficulty was encountered in circulating these slurries at lower temperatures, but the pump became noisy at 250°C. These noises disappeared when the temperature dropped to room temperature. When the loops were opened, soft cakes, and grainy material in some cases, were found, but there was no evidence of the hard cake found in the 200A loop. The cause of the hard cake in loop 200A is still unknown.

9.2 SLURRY COMPONENT DEVELOPMENT AND LOOP OPERATION

A. S. Kitzes

R. B. Gallaher M. Richardson
W. Q. Hullings A. N. Smith
R. P. Wichner

9.2.1 Westinghouse Slurry Pump 200A

W. Q. Hullings

In the 200A slurry pump, two modifications were made to improve the life of the Kingsbury bearing: the use of the lower bearing as a secondary seal and the reduction of thrust loads by increasing the diameter of the radial vanes on back of the impeller. The results of these modifications have been reported.[3]

[1] D. G. Thomas, *Further Information on the Cake Formed During Slurry Test 200A-3*, ORNL CF-56-4-120 (to be issued).

[2] W. Q. Hullings, *HRP Quar. Prog. Rep. Jan. 31, 1956*. ORNL-2057, p 80.

[3] W. Q. Hullings and A. S. Kitzes, *Improvements in the Operation of Westinghouse 200A Slurry Pump*, ORNL CF-56-2-33 (Feb. 3, 1956).

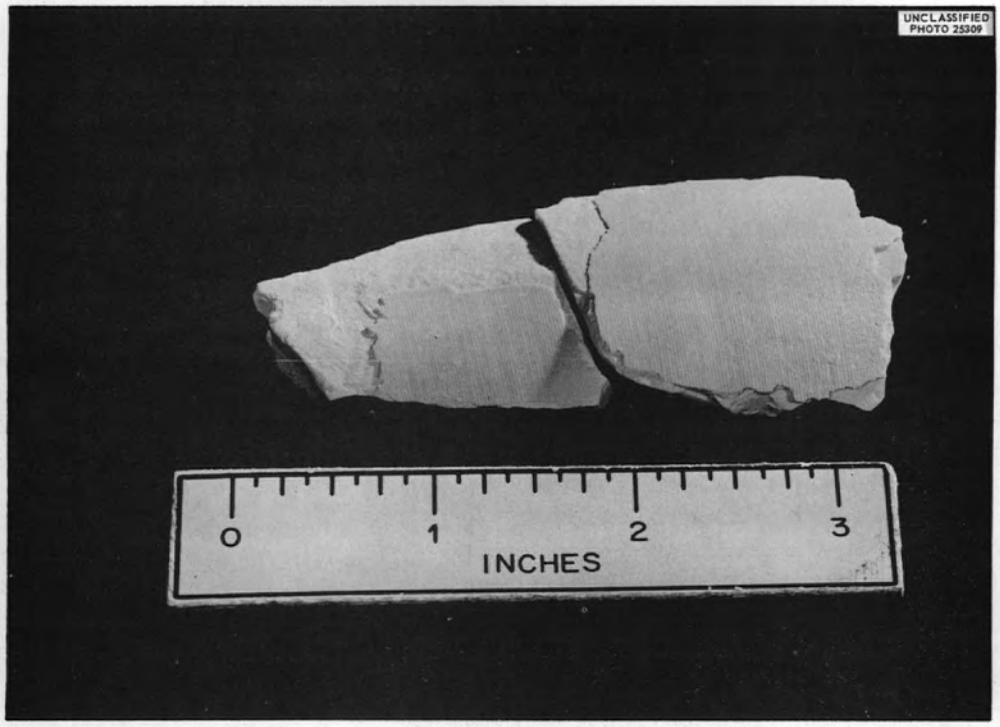

Fig. 9.1. Thorium Oxide Cake Formed During Test 200A-3.

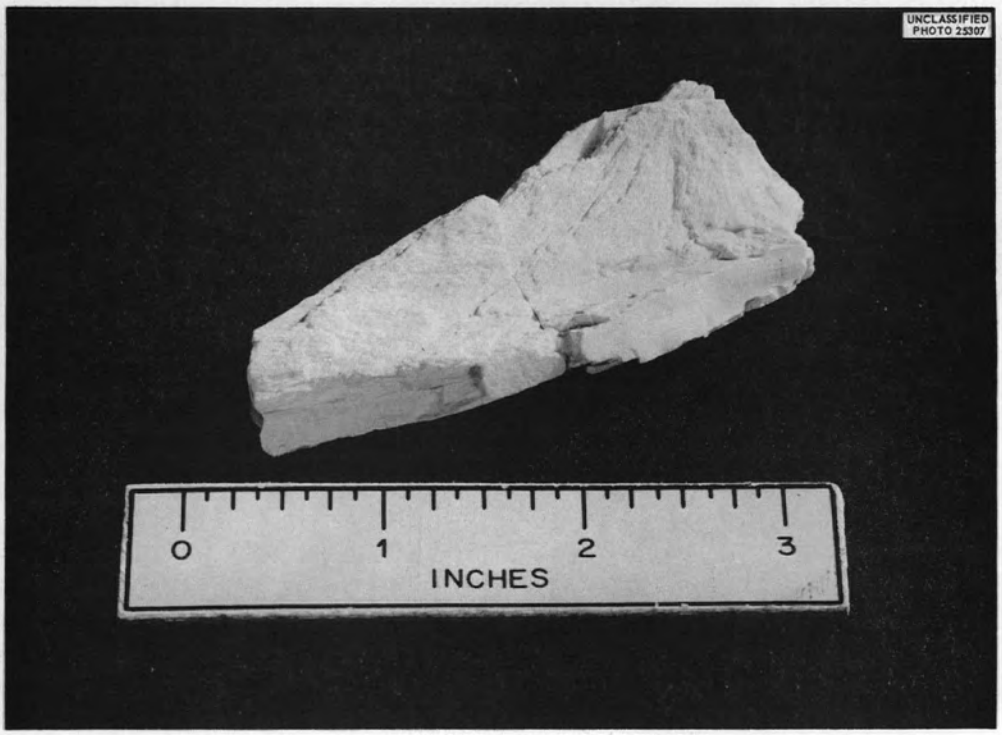

Fig. 9.2. Thorium Oxide Cake (Slurry Side) Formed During Test 200A-3.

Preliminary results of a test with the Westinghouse 200A slurry pump to determine the feasibility of substituting Al_2O_3 surfaces for Stellite-Graphitar bearings indicate that sprayed Al_2O_3 by the Rokite process may not be satisfactory for bearing use because of its high porosity (12%) and poor surface finish. For the test (run No. 200A-4) the Graphitar runner and the Stellite shoes of the Kingsbury assembly were replaced with Al_2O_3-coated prototypes. The condition of the shoes after 100 hr of operation at 300°C with water and 45 hr with slurry containing 500 g of thorium per kilogram of H_2O is shown in Fig. 9.3. Although no dimensional changes could be measured, the contact areas of the shoes (dark areas on photograph) appeared to be glazed. Examination of the thrust runner showed pitting in the corresponding area. During the slurry portion of the run one of the shoe coatings became loose. A black film, containing as major constituents Al_2O_3, ThO_2, and MoO_2, had formed at the metal-oxide interface.

Fig. 9.3. Al_2O_3-Coated Shoes for Kingsbury Thrust-Bearing Assembly After Circulation with Water and Slurry.

The Westinghouse 200A slurry pump has been operated for more than 1000 hr in the present slurry run (200A-5B). It is planned to continue the test for an accumulated running time of 2000 hr to check the operation of the pump and to demonstrate the feasibility of circulating concentrated slurries at 300°C for extended periods of time. For the run now in progress both the thermal barrier and the main pump flange were seal welded to eliminate the leakage that was experienced in other runs at 300°C and 2000 psi. The loop was loaded to give a circulating concentration of 1000 g of thorium per kilogram of H_2O containing 1500 ppm sulfate as $Th(SO_4)_2$.

During the startup of the run, pump power fluctuations of 1 kw, in 12.5 kw, were observed as the loop temperature rose above 175°C. These oscillations continued as the loop temperature rose to 300°C. After four additions of 1 *N* H_2SO_4 and with continued circulation at 300°C, the pump power oscillations stopped; no variations in pump power were observed during the last 120 hr of circulation. Each addition appeared to raise the temperature of inception of power fluctuations. Three of the acid additions were made to the circulating system and one to the pressurizer. The acid addition to the pressurizer lowered the pH of the liquid in the pressurizer from 6.1 to 1.6. As a result, the Fe/Th ratio, a measure of the attack on stainless steel by the slurry, showed a rapid increase from 0.2 to 0.9 mg/g but has since leveled off at a value of 1.0.

The chemical analysis of the sample drawn after 669 hr of circulation showed the following: (1) concentration, 1075 g of thorium per kilogram of H_2O; (2) iron content of slurry, 1100 ppm; (3) SO_4 content of slurry, 2400 ppm; (4) pH: slurry, 6.3; slurry filtrate, 5.7; pressurizer liquid, 4.1.

9.2.2 Aluminum Oxide Abrasion Test

R. B. Gallaher

The resistance of high-density sintered aluminum oxide to attack by ThO_2 slurries was investigated by inserting an aluminum oxide orifice plate in a 100A pump loop. For the test a slurry containing 800 g of thorium per kilogram of water and 2000 ppm sulfate as $Th(SO_4)_2$ was prepared (from ThO_2 which had been screened through 200 mesh) and was circulated at 300°C for 330 hr at a velocity of 70 fps through the orifice. After its removal from the loop the orifice was found to be fractured in two places, and severe attack was evident on the upstream and downstream faces; however, there was no pitting. The edges of the opening were still sharp, indicating that the attack was not the result of high shear forces, which are characteristically present in bearings. The pH of the slurry decreased from 7.3 to 4.2 during the course of the run; the fluoride and chloride content of the slurry averaged 50 ppm. Due to the high

rate of attack the results are inconclusive, and additional testing is required before a decision can be made as to whether sintered aluminum oxide is sufficiently attractive as a bearing material to warrant installation in large pumps.

9.2.3 Evaluation of Special Thorium Oxides

R. B. Gallaher

Slurries specially prepared in the Chemical Technology Division were circulated at 250°C for 100 hr in 5-gpm loops in order to compare the effect of pumping on the properties of these slurries with the effect on the properties of standard slurry prepared from 800°C calcined oxide. Some of the properties evaluated for the effect of pumping were particle degradation, corrosion-abrasion of stainless steel, and general handling characteristics.

Results of the study have been reported.[4] No difficulty was encountered in loading these slurries into the loops or in circulating them at elevated temperature. The resistance of stainless steel to attack was essentially the same for all the slurries evaluated. Only the oxide prepared from the oxalate precipitated at 10°C and then calcined at 900°C for 24 hr showed no particle degradation with pumping.

9.2.4 Dump-Tank Evaporator Tests

M. Richardson A. N. Smith

Two dump-tank systems for use in the HRT blanket are still being investigated in small steel or glass models.

(a) Combination Race Track–Vertical Gas Lift. – Results with the combination race track–vertical gas lift dump tank[5] continue to look promising. Slurries containing 900 to 925 g of thorium per kilogram of water were redispersed and circulated with no difficulty after shutdowns for varying lengths of time up to 30 days.

After the 30-day shutdown, with the bed in each riser leg approximately 18 in. deep, a steam pressure of 3 psig was required to set the bed in motion. Once in motion, 3-psig steam was needed to keep the solids suspended in 100 liters of slurry.

By supplying steam intermittently to the auxiliary heater, caking was less severe. In previous runs, regardless of concentration, a viscous sludge was always deposited between the auxiliary heater and the downcomer wall.

(b) Conical Dump Tank with Vertical Gas Lift. – An inverted-cone-shaped stainless-steel-lined tank, previously described,[5] has been operated successfully for a total of 50 hr with slurry containing 1000 g of thorium per liter. A steam pressure of 3.5 psig was required to move the settled bed. Once in motion, a steam lift rate of 1.25 lb/min of 3.5-psig steam was required to maintain homogeneity within ±50 g of thorium per liter.

The system was opened for inspection after 50 hr of operation. No evidence of caking was found (Figs. 9.4 and 9.5) except on those portions of the lift tubes located in the vapor phase. A "heel" of highly stable foam was found in the bottom of the cone; however, no difficulty with foaming was encountered during operation when sufficient vapor space was maintained.

9.3 SLURRY BLANKET SYSTEM TEST

L. F. Parsly I. M. Miller
L. E. McTaggart R. H. Nimmo

During the quarter the piping system was cleaned chemically, and in-place calibration of the flow elements was completed. The system was pressure tested, and a number of minor leaks were repaired. The system has been run on water at operating pressure and temperature for over 300 hr, and operation of part of the system has been checked. The water runs will be continued until all component parts of the system have been proved to operate in a satisfactory manner and base data on the performance of the heat exchanger have been obtained. The stainless steel core for the dummy reactor was received and installed.

9.4 HEAT-TRANSFER AND FLUID-FLOW STUDIES

C. G. Lawson

The mechanisms by which flowing thorium oxide slurries leave the laminar flow regime and develop turbulence are being investigated. At least two possible mechanisms can be postulated: (1) the yield stress will influence the flow as long as the wall shear stress is the same order of magnitude as the yield stress, or (2) the eddies formed

[4] R. B. Gallaher and A. S. Kitzes, *Comparison of Various Thorium Oxides*, ORNL CF-56-2-110 (Feb. 6, 1956).

[5] R. N. Lyon *et al.*, *HRP Quar. Prog. Rep. Oct. 31, 1955*, ORNL-2004, p 68–71.

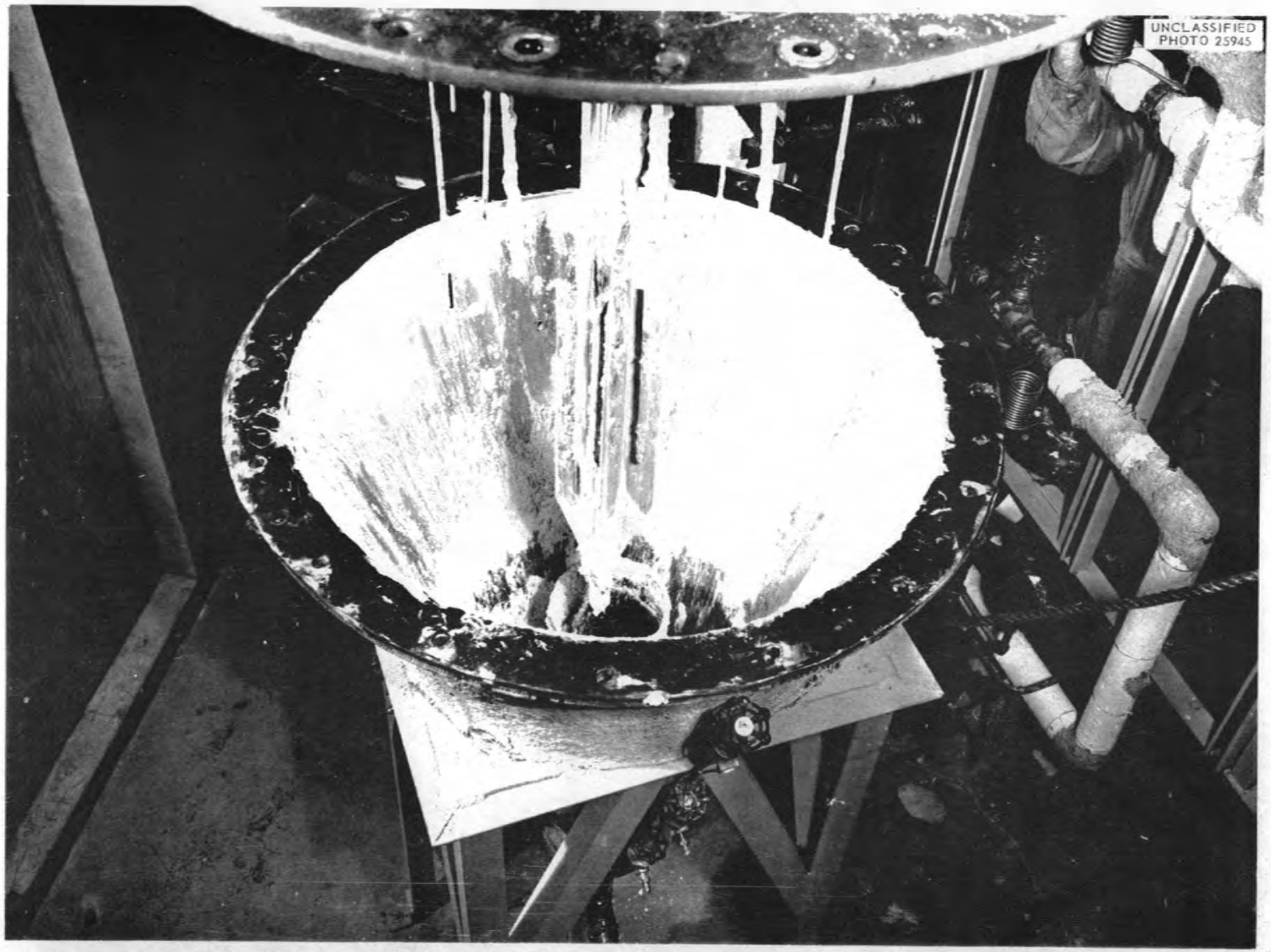

Fig. 9.4. Condition of Cone-Shaped Dump-Tank After 50-hr Operation with 1000-g/liter ThO_2 Slurry.

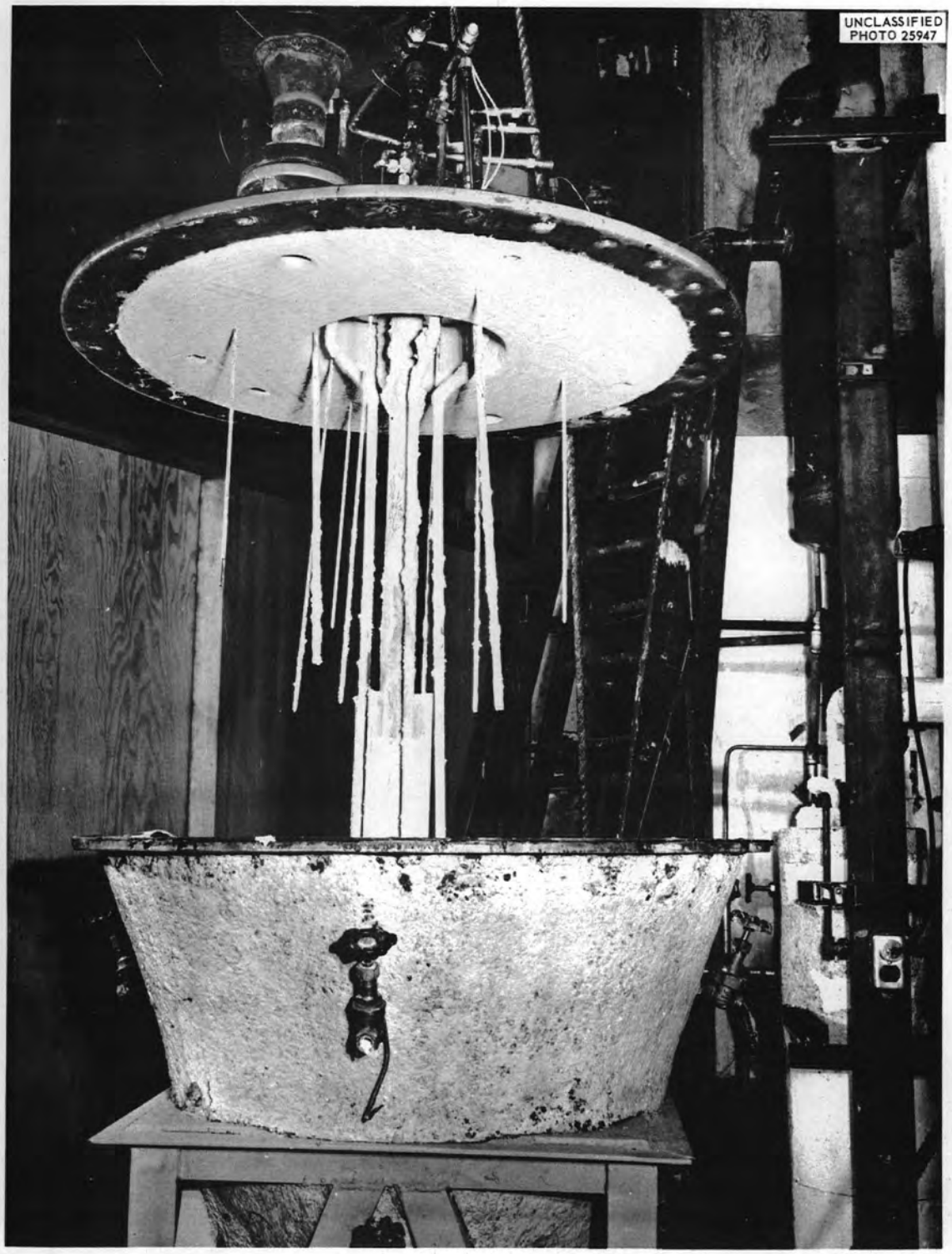

Fig. 9.5. Condition of Lift Tubes and Heaters After 50-hr Operation with 1000-g/liter ThO_2 Slurry.

as the fluid leaves the laminar flow regime rapidly destroy whatever structure causes the slurry to exhibit a yield stress. The transition region between the laminar and fully turbulent flow regimes is of particular interest; if the flow is described more nearly by the first mechanism, this region could very likely encompass the range of practical design velocities.

Pressure-drop data were taken in the temperature range 30 to 50°C in the laminar and nonlaminar flow regimes with slurry flowing in a 1-in. pipe 20 ft long. Two pressure taps are located 170 pipe diameters apart and 50 diameters downstream from the entrance to the pipe. The data are plotted in Fig. 9.6 in the form of a friction factor vs Reynolds number diagram in which the Hedstrom moduli are shown. The nomenclature in the figure is given in Table 9.1, and the data-point symbols refer to slurries and systems having the properties listed in Table 9.2.

A set of data taken with water to check the instrumentation is also plotted with the Von Kármán turbulent-flow friction factor vs Reynolds number for Newtonian fluids in smooth pipes. The figure shows that the slurry friction factors are higher than those for Newtonian fluids at the corresponding Reynolds numbers in the laminar flow regime and that the transition region is less clearly defined than is true for Newtonian fluids.

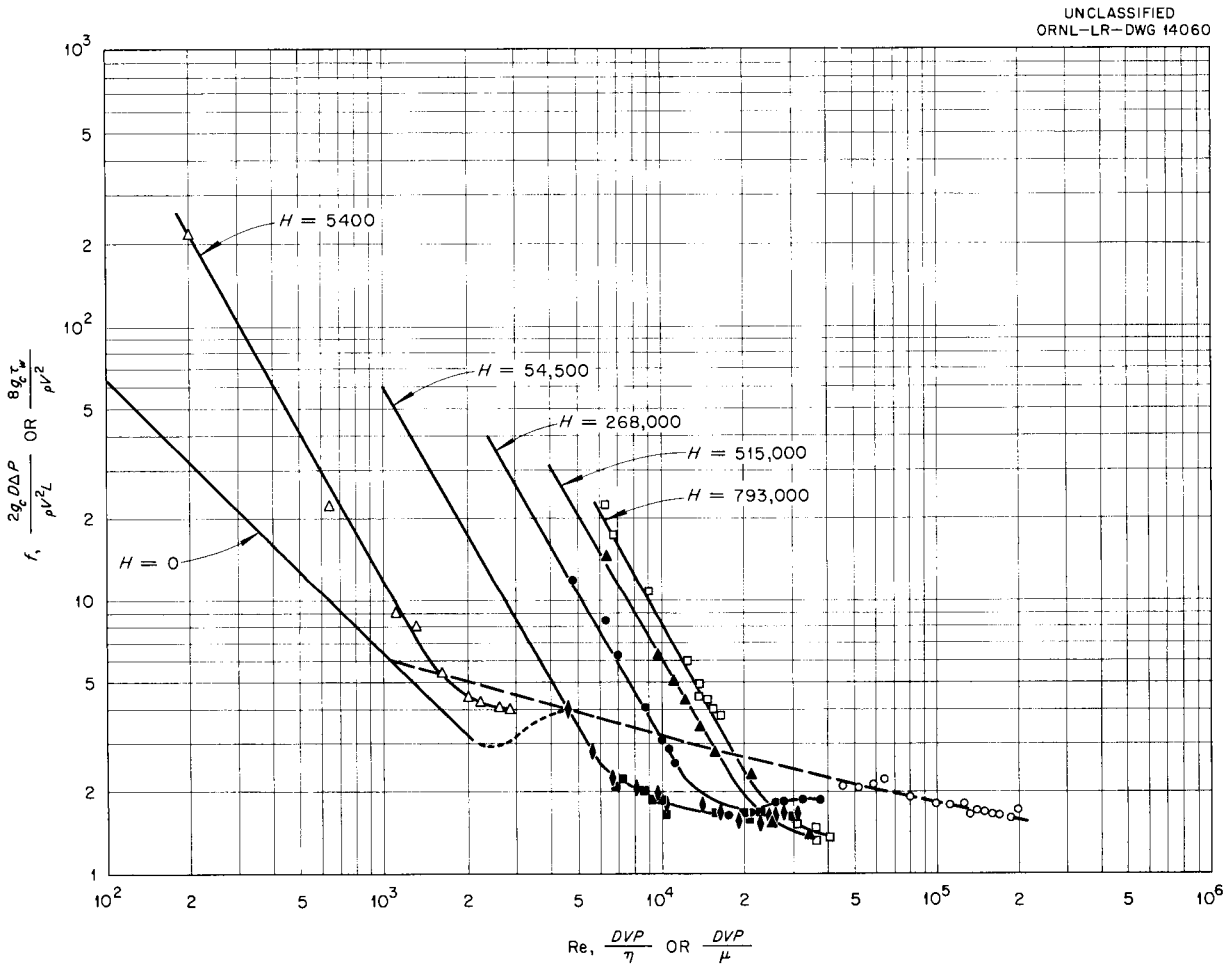

Fig. 9.6. Plot of Friction Factor vs Reynolds Number for ThO_2 Slurries (see also Tables 9.1 and 9.2).

TABLE 9.1. NOMENCLATURE FOR DATA PLOTTED IN Fig. 9.6

Symbol	Definition	Units
η or μ	Coefficient of rigidity of slurry (or viscosity of water)	$\frac{\text{lb-mass}}{\text{ft-sec}}$
τ_y	Yield stress of slurry	$\frac{\text{lb-force}}{\text{ft}^2}$
τ_w	Shear stress at pipe wall	$\frac{\text{lb-force}}{\text{ft}^2}$
ρ	Density of fluid	$\frac{\text{lb-mass}}{\text{ft}^3}$
H	Hedstrom modulus $\frac{g_c \tau_y D^2}{\eta^2}$	Dimensionless
L	Pipe length	ft
V	Bulk average fluid velocity	fps
f	Friction factor $\frac{8 g_c \tau_w}{\rho V^2}$	Dimensionless
ΔP	Pressure drop along length L	$\frac{\text{lb-force}}{\text{ft}^2}$
Re	Reynolds modulus $\frac{DV\rho}{\eta}$ or $\frac{DV\rho}{\mu}$	Dimensionless
g_c	Conversion constant	$\frac{\text{lb-mass}}{\text{lb-force}} \cdot \frac{\text{ft}}{\text{sec}^2}$

TABLE 9.2. PROPERTIES OF SLURRIES PLOTTED IN Fig. 9.6

Symbol	Slurry (g of ThO_2 per kg of H_2O)	Fluid Properties*				Temperature (°C)	Pipe Diameter (ft)
		τ_y	η	ρ	H		
♦	500	0.0785	0.0059	93	54,500	33	0.0874
■	500**	0.0785	0.0059	93	54,500	33	0.0874
▲	905	0.457	0.0050	114	515,000	30	0.0874
□	905	0.500	0.0042	114	793,000	47	0.0874
●	920	0.320	0.0058	115	268,000	48	0.0874
Δ	920	0.247	0.0045	115	5,400	47	0.012
O	Water	0	0.00071	62.4	0	18	0.0874

*See Table 9.1 for nomenclature.

**Second run.

10. INSTRUMENT AND VALVE DEVELOPMENT

D. S. Toomb

A. M. Billings D. G. Davis
H. D. Wills

10.1 FUEL SYSTEM COMPONENTS

10.1.1 Flow Transmitter

A variable-area type of flowmeter with an induction-coil pickup was installed on the feed-pump test loop and appears to be a solution to the difficult problem of measuring reactor feed- and purge-pump flows. Flowmeters for this service must be installed on the discharge side of the pumps to avoid pressure drops in the suction line. The flows pulse from the action of the diaphragm pumping heads; so a meter with linear output must be used for the damped record to be an accurate indication of the average flow. The flow transmitter[1] shown in Fig. 10.1 has been used to date.

10.1.2 Liquid-Level Controller

The weld-sealed liquid-level control, manufactured[2] to HRP specifications, which is to be delivered in June, is shown in Fig. 10.2. A spherical metal float actuates a mercury contact switch through the housing extension. The unit will be used as a high- and low-level alarm.

10.1.3 Experimental Valve Program

(a) Sealing Bellows. – Three Fulton-Sylphon type HR-2 bellows have been tested in uranyl sulfate at 2000 psi and 300°C, with an average life of 45,000 cycles for a $\frac{1}{8}$-in. stroke. The bellows testing stand which was used in these tests is shown in Fig. 10.3. The bellows actuator is mounted in an inverted position to permit the bellows to be surrounded with fluid while under test.

(b) Dump Valve Trim. – Of the approximately 30 valve trim materials proposed for investigation,[3] 9 have now been tested in the test loop (Fig. 10.4) and the two trim testing valves (Fig. 10.5) designed specifically for this program. Further tests on a type 347 stainless steel plug and seat reproduced

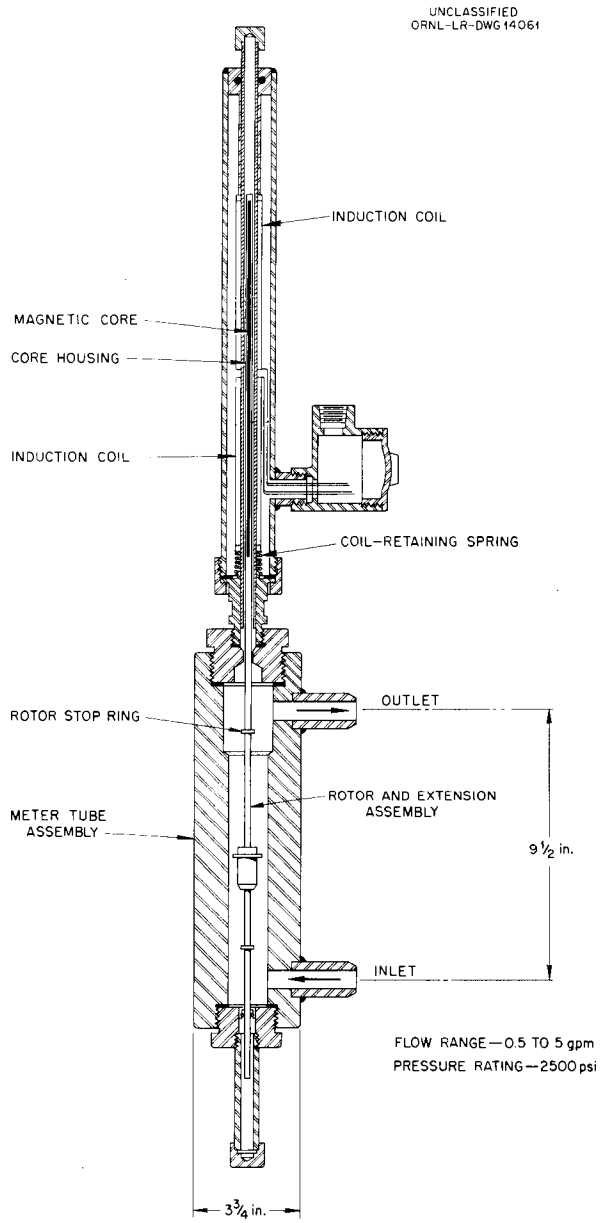

Fig. 10.1. Flow Transmitter.

[1] Schutte & Koerting Co., Cornwell Heights, Penn.

[2] Magnetrol Incorporated, Chicago 23, Ill.

[3] A. M. Billings, *HRP Experimental Valve Program*, ORNL CF-56-2-42 (Feb. 14, 1956).

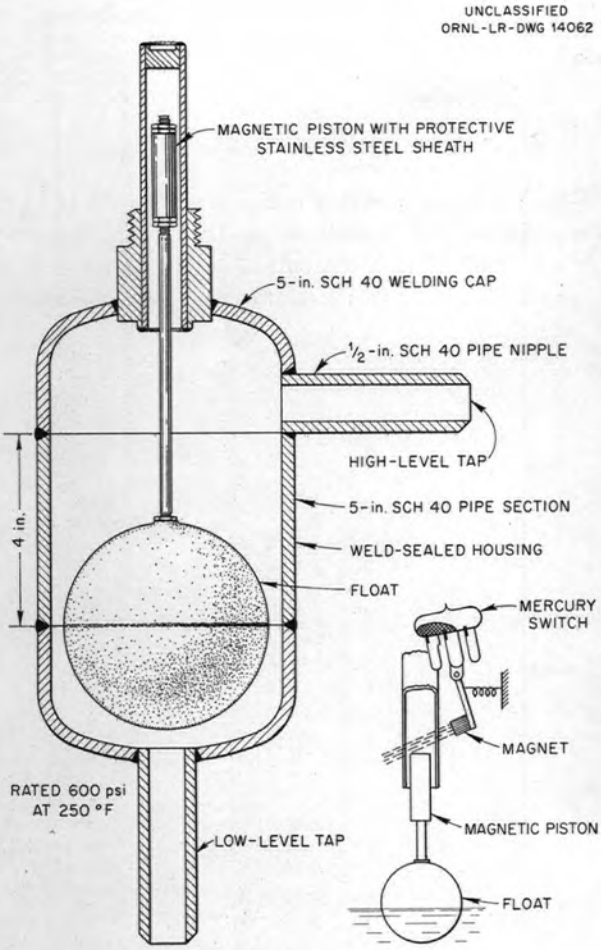

Fig. 10.2. Liquid-Level Controller.

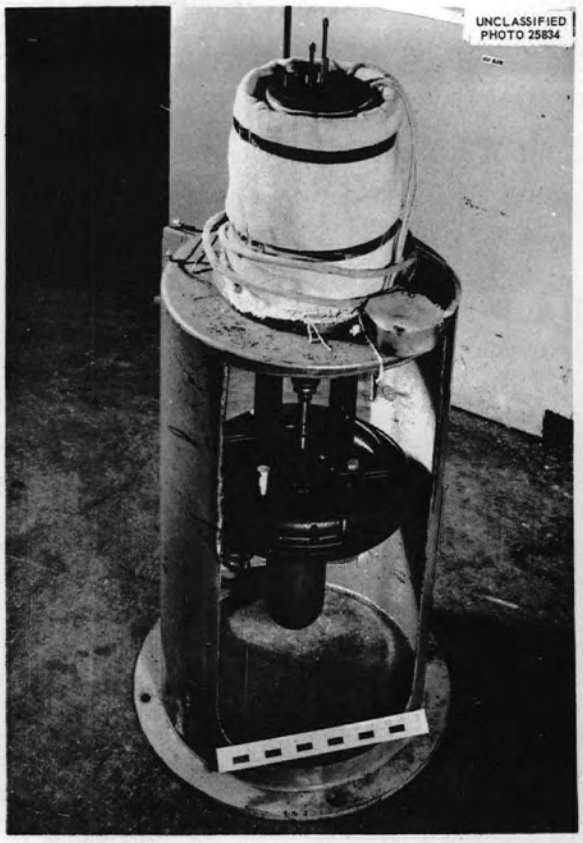

Fig. 10.3. Sealing Bellows Test Stand.

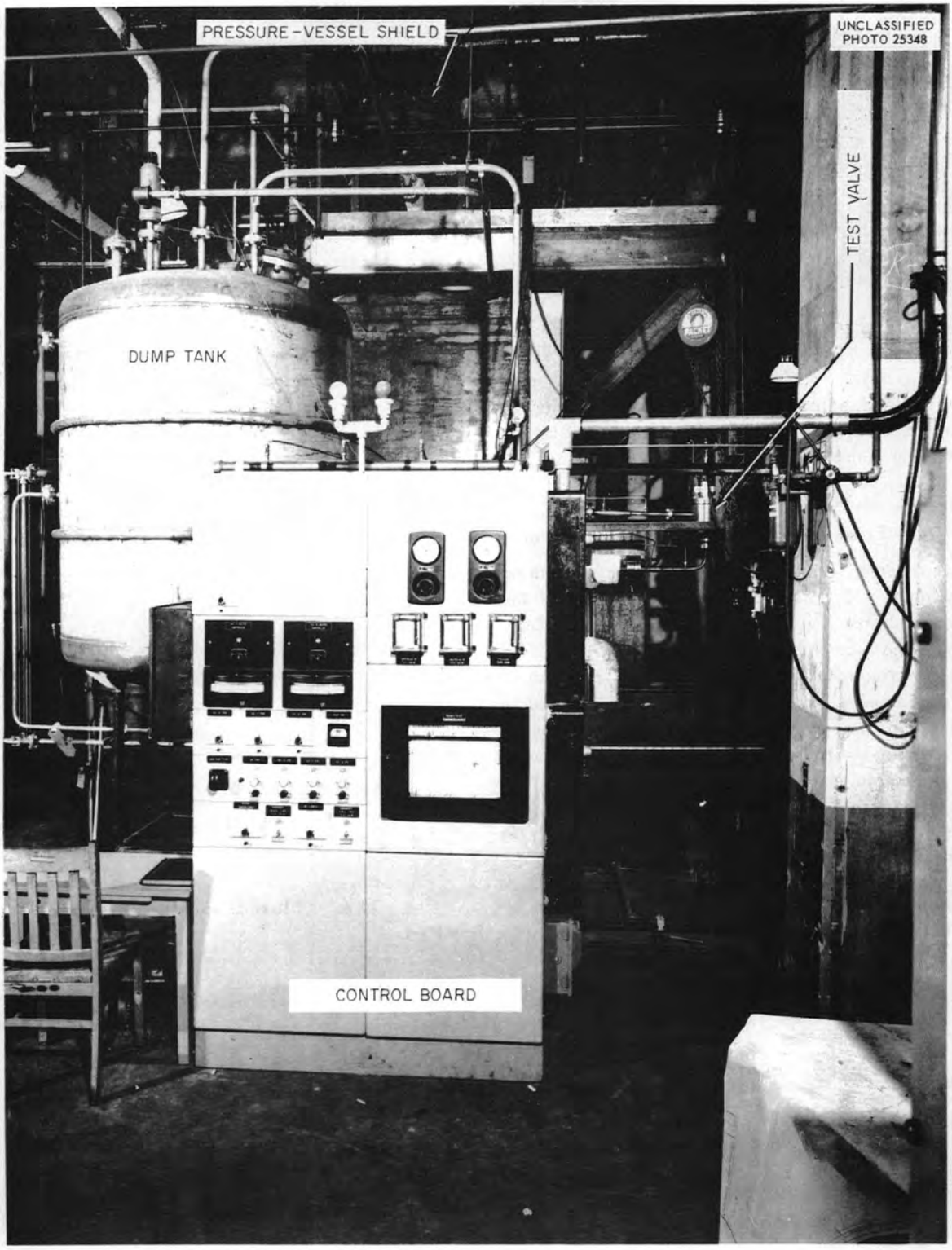

Fig. 10.4. Valve Test Loop.

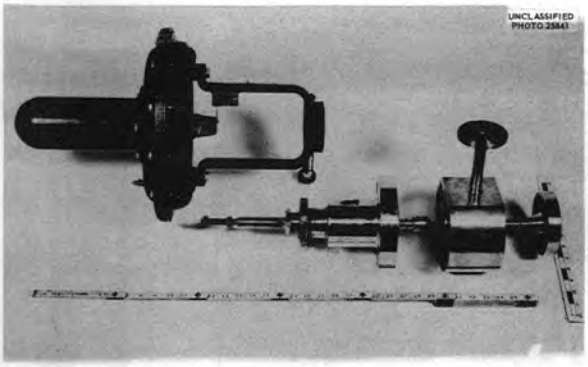

Fig. 10.5. Trim Testing Valve.

previous data. While type 347 trim showed good service, it does not appear to be as promising as titanium alloy 130AM, which was tested in the preceding quarter.

10.2 BLANKET-SYSTEM COMPONENTS

10.2.1 Flush-Diaphragm Pressure Transmitter

A pressure transmitter incorporating a sensing diaphragm which is flush with the inside of the process lines (Fig. 10.6) was used in a slurry circulating loop and performed satisfactorily except for a fatigue failure of the sensing diaphragm, which occurred because the unit was installed in a part of the system where there were severe pressure pulsations. These transmitters were developed for high-pressure polymer plants, but the vendor[4] indicated that their use would circumvent the plugging of pressure taps by slurry solids. Additional units are now on hand and will be placed in loops.

[4] The Swartwout Company, Cleveland 12, Ohio.

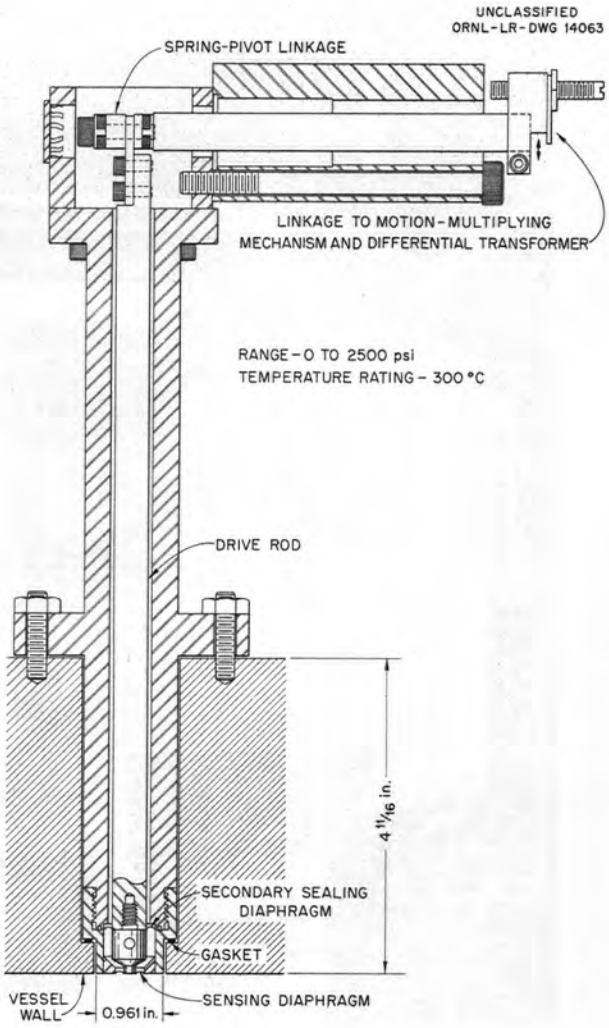

Fig. 10.6. Flush-Diaphragm Pressure Transmitter.

Part IV

CORROSION AND MATERIALS

E. G. Bohlmann

11. SOLUTION CORROSION[1]

J. C. Griess
S. R. Buxton
J. L. English
R. S. Greeley
H. C. Savage
R. M. Pierce[2]
J. A. Russell
R. M. Warner

11.1 PUMP LOOPS

J. C. Griess
S. R. Buxton
R. S. Greeley
H. C. Savage
R. M. Pierce
J. A. Russell
R. M. Warner

11.1.1 Loop Engineering

(a) Loop G – Titanium. – The all-titanium 100A dynamic-corrosion test loop has accumulated approximately 8500 hr of operating time at temperatures and pressures up to 300°C and 1800 psig. The excellent corrosion resistance of titanium to solutions of uranyl sulfate has made this loop extremely valuable in corrosion tests at the higher concentrations (up to 1.3 *m*) of uranyl sulfate solution.

As originally designed and built,[3] the titanium pressurizer was 1½-in.-OD by 1⅛-in.-ID pipe. Flexibility of operation of the loop was limited by the relatively small volume of the pressurizer. Very close control of the loop inventory was required to ensure that the solution level would be above the pressurizer heater section at all times and still allow for expansion of the solution in heating to 300°C.

One pressurizer failure[4] in this loop was attributed to low pressurizer solution level with resultant overheating of the titanium pipe wall. Thus sampling of the loop solution was limited, and temperature and pressure control was not entirely satisfactory.

With the availability of titanium pipe in larger sizes, along with improved welding techniques, a new titanium pressurizer was made for loop G from 3½-in.-OD by 2¾-in.-ID pipe with a volume of 6.0 liters as compared with a 1.7-liter volume of the original 1½-in.-OD pressurizer. A typical weld in the pressurizer is shown in Fig. 11.1. Figure 11.2 is a photograph of the completed pressurizer.

In addition to the larger pressurizer a new all-titanium bypass line with provisions for corrosion specimens was installed in loop G. Previously, only one corrosion specimen holder could be exposed in the circulating solution, and that in the main line. Thus pin-type specimens could be exposed to only one velocity in a given run. Variations in velocity, particularly at the lower velocities (under approximately 40 fps), were obtainable only by varying the circulating-pump

UNCLASSIFIED
PHOTO 25861

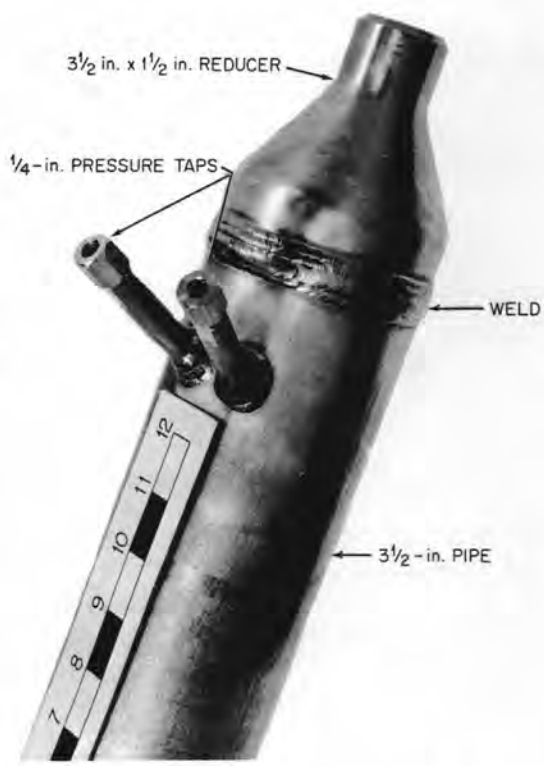

Fig. 11.1. Titanium-Pressurizer Weld.

[1] Reported in greater detail in ORNL CF-56-4-138 (to be issued).

[2] On loan from TVA.

[3] E. G. Bohlmann *et al.*, *HRP Quar. Prog. Rep. March 31, 1953*, ORNL-1554, p 47.

[4] E. G. Bohlmann *et al.*, *HRP Quar. Prog. Rep. April 30, 1954*, ORNL-1753, p 60 and Fig. 49.

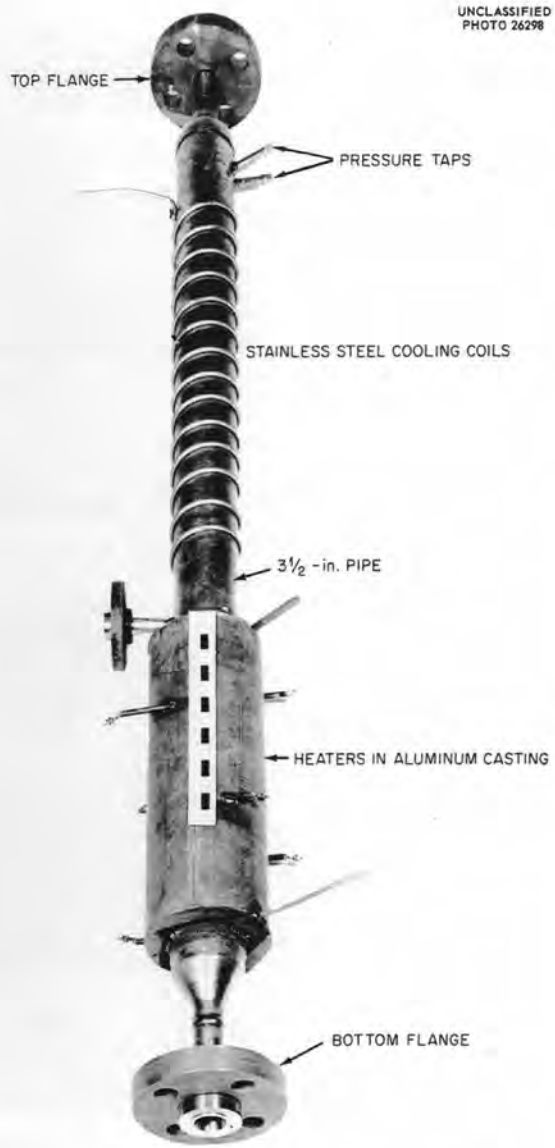

Fig. 11.2. Titanium Pressurizer.

speed. This was done by operating the pump with a variable-frequency motor-generator. With the new bypass line, pin-type corrosion specimens can be exposed to two different velocities in each run. After the modifications described were completed, satisfactory operation at temperatures up to 300°C was demonstrated.

(b) Loop O – Beryllium Solution Loop. – One new 100A dynamic-corrosion test loop, designated loop O, was designed and is now being fabricated. This loop, of type 347 stainless steel and similar to the dynamic-corrosion test loops described previously,[5] is to be used primarily to circulate uranyl sulfate solutions containing beryllium sulfate as an additive. Due to the toxicity of beryllium, the shielding facilities of the loop will be of leaktight construction with a filtered exhaust system. All auxiliary equipment necessary for loop operation, such as sampling equipment, injection-pump addition system, and fill and drain lines, will be incorporated inside the shield with provisions for remote operation. Instrumentation and control equipment is to be provided for operation up to 350°C.

11.1.2 Loop Test Results

In the last quarterly report[6] two runs were reported in which a solution containing 0.03 *m* UO_3 and 0.17 *m* Li_2CO_3 was circulated at 250°C with partial pressures of 600-psi CO_2 and 400-psi oxygen maintained in the pressurizer. One run was of 200-hr and the other of 537-hr duration. During the past quarter one additional run of 1175-hr duration was completed under the same conditions. The total pressure at the start of the run was 1600 psi at 250°C, composed of approximately 600-psi steam, 400-psi oxygen, and 600-psi CO_2. During the early stages of the run some gas was unexplainedly lost from the system, and, when the total pressure reached about 1350 psi, the uranium concentration decreased from an initial value of 6.7 to 4.5 g/liter. At this time, CO_2 was added to increase the total pressure to 1900 psi, and the uranium that had precipitated reappeared immediately in solution and remained soluble for the duration of the run.

The corrosion results were similar to those reported previously and showed that both the austenitic stainless steels and carbon steel exposed at a flow rate of 40 fps corroded at rates of less than 1 mpy after the first 200-hr period. The critical velocity observed on type 347 stainless steel coupons was about 45 fps. At flow rates greater than 45 fps, attack was not severe (3 mpy at 50 to 60 fps) and appeared to be localized at machining marks on the specimens.

---

[5] E. G. Bohlmann *et al.*, *HRP Quar. Prog. Rep. March 15, 1952*, ORNL-1280, p 40–44.

[6] J. C. Griess *et al.*, *HRP Quar. Prog. Rep. Jan. 31, 1956*, ORNL-2057, p 85.

Further corrosion testing was carried out in uranyl sulfate–lithium sulfate systems. One run was made with a solution containing initially 3.7 *m* UO_2SO_4 and 3.7 *m* Li_2SO_4. An attempt was made to operate at 360°C, but at this temperature the concentration of the salts became so high (~5.7 *m* UO_2SO_4) due to loss of water to the vapor that the solution actually crystallized in the cool rotor region of the pump. The system was cycled several times between 300 and 360°C, and as a result the corrosion of austenitic stainless steel was somewhat greater than was observed[6] in a similar run at 350°C. However, even with the thermal cycling, corrosion was slight at flow rates up to 60 fps.

Equimolal concentrations of uranium and lithium sulfates in solutions containing between 40 and 200 g of uranium per liter were circulated at 250 and 300°C. The corrosion results obtained on type 347 stainless steel specimens are given in Table 11.1, and the data are compared with those of similar runs in which the lithium sulfate was absent. Generally, the presence of lithium sulfate in the uranyl sulfate solutions did not change the critical velocity but did substantially decrease the corrosion rate at the higher flow velocities. At flow rates less than the critical velocity the amount of metal that dissolved during the formation of the protective film was less in the presence of lithium sulfate than in its absence, although the difference was not so striking as was the difference at high flow rates.

It should be noted that at high uranium concentrations (300 to 700 g/liter) the presence of lithium sulfate had a more pronounced effect in reducing corrosion than in the range of 40 to 200 g of uranium. The effect was particularly noticeable with regard to the critical velocity. At the higher concentrations at temperatures of 250°C and above, the critical velocity was increased on the addition of lithium sulfate, whereas no such increase was noted in the range of 40 to 200 g of uranium per liter at 250°C.

The corrosion of type 347 stainless steel by equimolal solutions of uranyl and lithium sulfates was studied at 200°C with uranium concentrations between 100 and 500 g of uranium per liter. The results can be summarized as follows:

1. There was no critical velocity; all specimens were corroded to the same extent regardless of flow rate.
2. The corrosion rate was essentially constant; a loose, black film formed at all flow rates but little protection was afforded by the film.
3. The corrosion rate was proportional to the uranium concentration; at 100 g of uranium per liter the corrosion rate was 8 mpy; at 300 g, 12 mpy; and at 500 g, 21 mpy.

The corrosion behavior of type 347 stainless steel at 300°C in solutions containing 300 g of uranium per liter and less than equimolal concentrations of lithium sulfate has been reported[7] previously. With the additional tests that were completed during the past quarter, corrosion data

[7] J. C. Griess *et al.*, *Quarterly Report of the Solution Corrosion Group for the Period Ending Jan. 31, 1956*, ORNL CF-56-1-167, p 7–8.

TABLE 11.1. CORROSION OF TYPE 347 STAINLESS STEEL IN UO_2SO_4 SOLUTIONS WITH AND WITHOUT EQUIMOLAL Li_2SO_4

Uranium Concentration (g/liter)	Temperature (°C)	Solutions with Li_2SO_4			Solutions Without Li_2SO_4		
		Critical Velocity (fps)	Weight Loss at 15 fps* (mg/cm^2)	Corrosion Rate at 70 fps (mpy)	Critical Velocity (fps)	Weight Loss at 15 fps* (mg/cm^2)	Corrosion Rate at 70 fps (mpy)
40	250	20–30	1–3	40	20–30	9	240
100	250	10–20	23	70	10–20	33	380
	300	30–40	4	230	**	**	**
200	250	10–20	27	130	10–20	70	660

*At this flow rate, after the initial weight loss, a protective film forms and the corrosion rate decreases to a very low value.

**No run made, since solution would form two liquid phases.

have now been obtained at 300°C in uranyl sulfate solutions containing 300 g of uranium per liter with the following concentrations of lithium sulfate: 0.4, 0.7, 1.4 (approximately equimolal), and 2.0 *m*. The results showed that with 0.4 and 0.7 *m* Li_2SO_4 the critical velocity was 10 to 15 fps, whereas with 1.4 and 2.0 *m* the critical velocity was 25 to 30 fps. Below the critical velocity a protective film formed, and corrosion was low after the formation of the film. Above the critical velocity the corrosion rate was high and varied inversely with the lithium sulfate concentration. At all concentrations of lithium sulfate the solution was phase-stable during the 200-hr test period.

Titanium, the high-strength titanium alloys, zirconium, and Zircaloy-2 showed no detectable difference in corrosion in solutions containing lithium sulfate and those under the same conditions without lithium sulfate. In all cases the corrosion resistance was excellent.

In a number of experiments it has been observed that the critical velocity is usually slightly lower on type 304L stainless steel than it is on type 347 stainless steel. The composition of the two alloys is the same except for the carbon content and the presence of niobium and/or tantalum in type 347. However, the grain size of the two alloys is greatly different; type 304L usually has an ASTM grain size of 2 to 5, whereas type 347 has a grain size of 7 to 8 or even smaller.

To determine whether grain size is an important variable in determining the critical velocity, corrosion specimens of the two alloys were prepared in a variety of grain sizes. The specimens were then exposed to 0.17 *m* UO_2SO_4 at 250°C in the critical velocity region (15 to 25 fps). The results clearly showed that with type 304L stainless steel the critical velocity varied inversely with the grain size. Although type 304L specimens of grain size 7 to 8 gave the same corrosion results as those obtained with standard as-received type 347 stainless steel, which was of similar grain size, there was no correlation between grain size and critical velocity for the specimens of type 347 stainless steel.

In order to produce large grain sizes, very high temperatures (as high as 2300°F) had to be used for long periods[8] of time, and it appeared that the carbides dissolved and, at least in some cases, reprecipitated as large particles. The results indicated that grain size and the distribution of carbides in the steel are important factors in determining the critical velocity under the conditions investigated.

It should be noted that the above effect of grain size is observable only in a narrow velocity range. At low flow rates all specimens develop protective films and practically stop corroding, and at high flow rates all specimens are free of a protective film and corrode at high rates.

The 4000-gpm pump loop[9] was used to make a series of runs at 250°C. In the preliminary operation a dilute solution of uranyl sulfate (less than 10 g of uranium per liter) with dilute sulfuric acid was circulated for short periods at 250°C. Then one run of 600-hr duration was made at 250°C, with the uranyl sulfate concentration gradually increased from 0 to 0.02 *m* and the copper sulfate and sulfuric acid concentrations from 0 to 0.005 and 0.006 *m*, respectively. The oxygen concentration was maintained at 50 to 100 ppm. The average corrosion rate of the high-temperature system based on nickel analyses was 0.5 mpy. A second, 506-hr run, similar except that the final concentrations were 0.04 *m* UO_2SO_4, 0.005 *m* $CuSO_4$, and 0.015 *m* H_2SO_4, was then made. The average corrosion rate was 0.3 mpy. The standard corrosion specimens showed corrosion rates comparable to those obtained in the 100A loops under similar conditions.

In order to demonstrate the feasibility of maintaining very low copper sulfate concentrations in dilute sulfuric acid solutions such as might be needed for the HRT during operation with D_2O in the blanket system, one run was made in which a solution containing 0.002 *m* H_2SO_4 and 0.0005 *m* $CuSO_4$ (30 ppm copper) was circulated in a stainless steel loop. The solution was maintained at 250°C for 200 hr and then at 300°C for 275 hr. Throughout the run the copper concentration of the solution remained constant and corrosion was insignificant in the velocity range of 10 to 90 fps.

Recently the Chemical Technology Division developed a solution for decontaminating stainless steel surfaces.[10] The decontaminating solution

[8] See ORNL CF-56-4-138 (to be issued) for details of heat treatments.

[9] J. C. Griess and H. C. Savage *et al.*, *HRP Quar. Prog. Rep. Oct. 31, 1955*, ORNL-2004, p 80.

[10] D. E. Ferguson, R. D. Baybarz, and R. E. Leuze, *HRP Quar. Prog. Rep. Jan. 31, 1956*, ORNL-2057, p 128.

consists of about 0.3 *m* $CrSO_4$ in 0.2 to 1.0 *m* H_2SO_4 and actually dissolves the ferric and chromic oxide scale. In cooperation with the Chemical Technology Division, four 100A loops were descaled. In each loop a solution containing approximately 0.3 *m* $CrSO_4$ and 0.5 *m* H_2SO_4 was circulated for about 3 hr at 80 to 85°C. In two loops two charges of solution were used; that is, at the end of the first 3-hr period the solution was replaced with a new one, which was circulated for an additional 3 hr.

Only in one case was defilming essentially complete and that was in one of the loops in which two charges of the descaling solution were used. In the other doubly charged loop run, scale removal was very incomplete, apparently because the chromous sulfate solution had been oxidized before use. In the other two loops scale removal was extensive but not complete. The solutions removed from these two loops had large amounts of suspended solids, and randomly located areas of the loop walls still were covered with tightly adherent scale. Analyses of the solutions showed that insufficient chromous sulfate was available to dissolve all the scale.

The efficiency of the utilization of chromous sulfate in dissolving the scale was about 50%, the remainder reducing hydrogen ions. The results indicate, however, that essentially all the scale could have been dissolved had sufficient $CrSO_4$ been available.

The corrosion rates of type 347 stainless steel specimens exposed to the defilming solution were as high as 1000 mpy in some cases. But since the exposure times were short, the extent of corrosion was no greater than a few tenths of a mil even in the worst cases. At low flow rates (approximately 15 fps) titanium and zirconium and their alloys were only slightly attacked, but at high flow rates the rate of attack was comparable to that observed on stainless steel. The attack at high flow rates was probably due to suspended particles impinging on the surface of the specimens with sufficient force to destroy the protective oxide films, thereby allowing the metal to corrode.

11.2 LABORATORY TESTS

J. L. English J. C. Griess

The susceptibility of type 347 stainless steel to stress corrosion cracking was demonstrated by a pipe U-bend spray test.[11] The test apparatus consisted of six U-bends of type 347 stainless steel welded pipe, four of which were fabricated from ½-in. sched-40 pipe and two from ⅜-in. sched-40 pipe. The U-bends were attached to common steam and condensate headers. Steam pressure at 60 psig (153°C) was maintained within the pipes, which were externally cooled by a continuous spray of tap water. During the test, which lasted for 10,790 hr, there were no obvious leaks in any of the pipes.

Considerable quantities of scale formed on the water-cooled surfaces of the pipes during the test. Chemical analyses of the scale showed that it contained 33.7% calcium, 3.7% magnesium, 2.2% sulfate, and 0.076% chloride (760 ppm). The remainder of the scale was probably carbonate and water.

After the scale was removed from the pipes, a liquid penetrant revealed the presence of numerous cracks randomly distributed over the entire surface of each head. Metallographic examination of several of these cracks showed that the cracking was transgranular and that at least some of the cracks had very nearly penetrated the pipe walls. In all probability the chloride ions in the water which concentrated in the scale were responsible for the observed cracking. These tests illustrate the sensitivity of austenitic stainless steel to stress corrosion cracking by water containing chloride ions.

In the last quarterly report[12] preliminary corrosion tests with Elgiloy, an alloy possibly suitable for use as a spring material in the liquid-level controller of the HRT, were described. Both vapor- and liquid-phase exposure to 0.04 *m* UO_2SO_4 containing 0.02 *m* H_2SO_4 and 0.005 *m* $CuSO_4$ at 300°C showed low general corrosion rates.

A continuation of these tests showed that Elgiloy, at least under the conditions of test, is susceptible to severe stress corrosion cracking. After a total testing time of about 1000 hr, specimens exposed to the liquid and to the vapor showed large cracks. The origin of the cracks appeared to be areas of highly localized residual stresses such as the sheared edges of the 30-mil-thick specimens and the numbers stamped on each specimen for identification purposes. Cracking was so

[11] E. L. Compere and J. L. English, *HRP Quar. Prog. Rep. July 31, 1954*, ORNL-1772, p 94.

[12] J. L. English and J. C. Griess, *HRP Quar. Prog. Jan. 31, 1956*, ORNL-2057, p 86.

severe on the specimen exposed to solution that a wedge-shaped portion had broken completely away from the remainder of the specimen. There was, however, no significant increase in the intensity of generalized corrosion attack on the specimen. The solution contained less than 2 ppm chlorine.

When a new supply of Elgiloy is available, further tests are planned for determining how heat treatment of the alloy influences its susceptibility to stress corrosion cracking.

Several high-strength titanium alloys were exposed to uranyl sulfate solutions of various concentrations in the temperature range 100 to 300°C. The alloys included in these tests were A110-AT (5% Al–2.5% Sn) and C130-AM (4% Al–4% Mn), both products of the Rem-Cru Titanium Corporation and MST 6Al-4V produced by Mallory-Sharon Titanium Corp. Under all conditions of test the observed corrosion behavior was excellent; thin, adherent, brilliantly colored films characterized the general appearance of the specimens. Stressed specimens showed no tendency toward cracking, and all specimens exhibited insignificant corrosion attack. The results obtained with titanium alloys were the same as those obtained with commercially pure titanium.

Further tests[13] with type 347 stainless steel coupled with titanium, Zircaloy-2, and gold showed that in 0.04 *m* UO_2SO_4 containing 0.02 *m* H_2SO_4 and 0.005 *m* $CuSO_4$ boiling at 100°C there is no detectable galvanic action. Uncoupled control specimens showed the same weight loss and the same appearance as did the coupled specimens. Previously reported results[14,15] indicated the absence of galvanic corrosion at 150, 200, and 250°C. Therefore under the conditions expected in the HRT no acceleration of corrosion would be expected by the joining of the above metals with type 347 stainless steel.

---

[13] *Ibid.*, p 87.

[14] J. C. Griess *et al.*, *Quarterly Report of the Solution Corrosion Group for the Period Ending Jan. 31, 1956*, ORNL CF-56-1-167, p 25.

[15] J. C. Griess, H. C. Savage, and F. J. Walter, *HRP Quar. Prog. Rep. July 31, 1954*, ORNL-1772, p 79.

12. SLURRY CORROSION

E. L. Compere
S. R. Buxton
G. E. Moore
R. M. Pierce[1]
H. C. Savage
S. A. Reed
R. M. Warner
D. B. Weaver[1]

12.1 PUMP LOOPS

Two tests,[2] runs CS-22W and CS-23, were made in the 100A pump loop CS during the quarter. Run CS-22W, a water run, was made in order to check over-all loop performance after modification of the condensate system used to provide purge water for the rotor cavity of the 100A pump. Run CS-23 was made with thorium oxide slurry charged to a concentration of 1200 g of thorium per kilogram of water. As in previous runs, a rapid drop in slurry concentration occurred. However, the concentration was increased gradually to 1000 g of thorium per kilogram of water when a newly developed slurry-addition system was employed. Both tests were made at 300°C with the addition of gaseous oxygen. Run CS-22W was terminated after 54 hr, while run CS-23 lasted for 312.6 hr.

In order to provide a larger and more reliable supply of condensate to purge the pump rotor cavity, and for other purposes, the loop condensate system was modified prior to run CS-22W to relieve the previously experienced gas binding in the condensate system. This was done by installing a 1-in. pipe instead of ¼-in. tubing between the pressurizer top and the condenser top. Thermal circulation of steam and oxygen thereby could occur via this and a lower return line because of the different densities of the heated steam-oxygen mixture in the pressurizer and the cooler oxygen-enriched gas in the condenser. A ¼-in. tubing connection from this 1-in. connecting pipe to the throat of a venturi in the bypass mixing line to the pressurizer provided an alternate, more positive means of relieving any gas binding of the condenser. Although it did not prove to be necessary on the CS loop, its operation was tested because of interest in connection with the use of a similar system on the in-pile slurry loop.

Run CS-22W was made in order to check out the performance of the above system. During the 54-hr test at 300°C with oxygenated water, condensation rates up to 7 liters/hr were obtained, and a flow of 4 to 6 liters/hr to the pump cavity was maintained. Operation of the condensate system was exceptionally steady. During a period in which the connection to the venturi was opened, thermocouples indicated a steady flow through the connecting line with continued steady operation of the condensate system at approximately the same condensation rate. Condenser capacity was estimated to be the limiting factor in these operations.

Before run CS-23, a newly developed slurry-addition device was connected to the system. It consisted of a flanged cone-bottomed slurry reservoir of 2.3-liter capacity, connected to the circulating pump suction line by means of ¼-in. tubing. Water from the condensate tank required to flush the slurry into the system entered through a tubing connection in the top flange; condensate flow was metered with a high-pressure rotameter and could be assisted, if required, by means of a pulsafeeder. By charging the reservoir with slurry and then flushing it into the system with condensate, thorium oxide could be added to the loop while operating at temperature and pressure and at the same time a corresponding volume (at room temperature) of water could be removed. Since the reservoir could then be drained to remove the water, it follows that it was possible for thorium oxide or water to be added to the loop or removed from it independently; thus the inventory and circulating concentration can be controlled to a degree not heretofore possible on this loop. Flow of condensate to the pump cavity passed through a branch circuit from the condensate tank and was separately metered and regulated.

During run CS-23 four additions of thorium oxide slurry were made by using this system. Operation was very satisfactory, and slurry transfer into the loop was more than 99.8% complete in each case. Numerous previous attempts to use a 1-gph Lapp pulsafeeder to charge slurry to a loop while it was at temperature and pressure had failed.

Three sample barrels, loaded with pin specimens, contained flow restrictors to give velocities of

[1]On loan from TVA.

[2]E. L. Compere, H. C. Savage *et al.*, *Dynamic Slurry Corrosion Studies*, ORNL CF-56-4-139 (to be issued).

10, 21, and 31 fps across the pins, with a total flow of 37 gpm. In addition, the bypass mixing line flow rate was originally 31 gpm and was reduced to 23 gpm at hour 265 of run CS-23.

For run CS-23 the loop was charged with 17.3 liters of a thorium oxide slurry from batch LO-2, containing 1200 g of thorium per kilogram of water. The thorium oxide had been prepared[3] at ORNL from specially pure thorium nitrate by oxalic acid precipitation followed by calcination at 800°C. Before the loop was charged, the slurry was passed while wet through a 200-mesh screen. The loop volume up to the bypass mixer line inlet in the pressurizer was 27.6 liters, and the wetted loop surface at temperature was 21,000 cm^2.

After startup, the loop was brought to 300°C. A sample indicated the concentration to be 612 g of thorium per kilogram of water, and four subsequent samples showed decreasing values between 500 and 444 g of thorium per kilogram of water. Between hours 149 and 220, three additions of slurry were made to the system, by means of the addition device, with the concentration increasing to an average level of 916 g of thorium per kilogram of water. A final addition, 24 hr before the shutdown at 312.6 hr, brought the concentration to 1008 g of thorium per kilogram of water.

Irregularities in the pump power demand, usually attributed to gassing, boiling, or cavitation in the pump, began at hour 120. Additions of water to the loop gave temporary relief. Increasing the oxygen overpressure to 350 psi did not help. The loop was shut down at hour 247 to check for leaks, but none were found. After 40 hr of down time, the pump was restarted. The slurry resuspended readily, as indicated by the return of pump power demand to the previous level and by chemical analysis of samples. The system was again shut down at hour 264, and the flow through the bypass mixing line was reduced from 31 to 23 gpm in an effort to reduce any entrainment of gas by the slurry between the pressurizer and the pump inlet. Circulation was restarted smoothly, and the loop was operated again at 300°C. The fluctuations in pump power demand were somewhat relieved.

A final addition of slurry was made at hour 288. At hour 294, increasing pump noise was noted, and the loop was shut down at hour 312.6 to avoid excessive damage to the pump.

Slurry was drained from the loop, and the system was examined. No caking or unusual accumulations of solids were found in the pressurizer or main circulating lines. Pasty solids (density 2.7) partially filled the annular channels of the sample barrels; similar deposits were found in capped tee arms serving as elbows.

Pump components suffered considerable wear. The front Graphitar bearing increased in inside diameter by 0.0485 in., and the rear by 0.0005 in. Titanium seal rings were badly worn. The front face of the impeller and especially the inlet hub were abraded and pitted, with the impeller weight loss being 29 g.

On the pin specimens exposed in run CS-23 the following corrosion rates (in mpy) were observed at 10, 21, and 31 fps, respectively: gold, 0.05, 0.07, 0.34; austenitic stainless steels, 3 to 4, 3 to 7, 8 to 11; titanium and titanium alloys, 3 to 7, 4, 10 to 13; platinum, 0.4, 0.6, 2; Zircaloy-2, 1, 1, 4. The corrosion rate for mild steel at 10 fps was 14 mpy and for tantalum at 21 fps was 0.7 mpy.

Generalized loop coorosion averaged 2.1 mpy based on stainless steel corrosion products found in the slurry. The corrosion rate appeared greatest at the beginning and after additions of fresh thorium oxide and appeared to diminish substantially in the course of 100 hr. This may be attributed to reduction in particle size of the slurry by pumping during this period, though evidence is not yet complete on this point. Attack rates for titanium appeared to parallel those for stainless steel, with slurry analyses for titanium accounting for three-fourths of the impeller weight loss.

A second slurry corrosion test facility, 100A pump loop BS, is currently being completed. This loop will permit a single main flow circuit to be used, in addition to the pressurizer mixing line, and will use straight-through sample barrels. A condensate system and a slurry-addition system similar to those developed for loop CS will be used. An all-titanium pump head will be used. These modifications are expected to result in less caking and plugging, more reliable pump operation, better slurry-concentration control, and a more precise knowledge of relative slurry velocity in the various sample barrels.

[3]E. L. Compere, H. C. Savage *et al.*, *Dynamic Slurry Corrosion Studies for Quarter Ending Jan. 31, 1956*, ORNL CF-56-1-168 (to be issued).

12.1.1 In-Pile Slurry Loop

Several short-term water runs were made in the experimental in-pile slurry loop to evaluate a succession of modifications to the loop pressurizer section and condensate system. A basic operational requirement of the present experimental in-pile slurry loop includes a condensate system capable of providing purge-water feed to the bearings of the 5-gpm pump. The condensate system is a scaled-down version of the system presently employed on the 100A pump loop CS described in this report. This system has been found to be satisfactory in slurry loop CS.

The loop contains several flanges so that the flow pattern of the system can be varied over a wide range. For example, all the flow or none of it could be directed through the top of the pressurizer. In addition, a venturi has been included in the $\frac{3}{8}$-in. line to the bottom section of the pressurizer. The suction side of the venturi can be used to pull the steam-gas mixture from the pressurizer through the condenser where the steam is condensed. The noncondensables are returned to the pressurizer via the venturi line. Such a device might simplify the design of a condensate system incorporated in an in-pile slurry loop by eliminating vent lines in addition to ensuring positive vapor flow conditions. The present system relies on thermal circulation of the steam-gas mixture.

The satisfactory operation of the above device was demonstrated by stable operation with water at 250°C, and 80 psi oxygen (room temperature), in runs of 2 to 6 hr duration. Condensate was regularly produced at 250°C by either thermal circulation or use of the venturi at rates of 1.5 liters/hr. A purge rate to the pump of 0.9 liter/hr was maintained.

As yet, operation of the modified loop with thorium oxide slurries has not been attempted. This is the next immediate objective, after which the loop geometry must be modified for installation in existing reactor facilities.

12.2 TOROIDS

Attack rates on type 347 stainless steel, titanium 75A, and Zircaloy-2 were obtained in toroids by circulating aqueous thorium oxide slurries of 1000 g of thorium per kilogram of water at 250°C with 100 psi oxygen pressure. A comparison was made previously[3] on the basis of the maximum calcination temperature of the oxide and the relative slurry velocity. The attack rates were shown to be independent of the calcination temperature, while the rates for the stainless steel and titanium indicated a linear to second-power dependence on the velocity.

The possible correlation[4] between ultimate size of the oxide particles as determined by gravitational sedimentation[5] and the attack rates has now been investigated. Degradation of the thorium oxide particles occurs during circulation to about the same extent as observed in loop tests.[6] The minimum size is apparently dependent on the oxide used, the 800°C calcined product from the Feed Materials Production Center at Fernald, Ohio, being degraded to an estimated average particle diameter of 0.1μ (83 wt % less than 0.7μ), while ORNL-produced batches D-17 and LO-1 showed a size between approximately 0.4- and 1.0-μ diameter.

However, at the present time uncertainties in the particle-size determination in the presence of large amounts of corrosion products and the suspected presence of magnetite, indicating an oxygen-depleted system, prevent an unambiguous correlation between attack rate and postrun particle size.

---

[4]G. E. Moore and E. L. Compere, *Dynamic Slurry Corrosion Studies, Quarter Ending April 30, 1956*, ORNL CF-56-4-139 (to be issued).

[5]G. W. Leddicotte and H. H. Miller, *Anal. Chem. Semiann. Prog. Rep. Oct. 20, 1954*, ORNL-1788, p 21.

[6]C. E. Schilling, *HRP Quar. Prog. Rep. Oct. 31, 1955*, ORNL-2004, p 179.

13. RADIATION CORROSION

G. H. Jenks

H. C. Savage

A. L. Bacarella
J. E. Baker
S. E. Bolt
R. J. Davis
H. O. Day
V. A. DeCarlo
H. A. Fisch
D. T. Jones
R. A. Lorenz
T. H. Mauney
J. R. McWherter
A. R. Olsen
J. A. Russell
M. D. Silverman
F. J. Walter
R. M. Warner
K. S. Warren
D. B. Weaver[1]
L. F. Woo
W. C. Yee

13.1 IN-PILE LOOPS

G. H. Jenks
H. C. Savage
J. E. Baker
S. E. Bolt
D. T. Jones
R. A. Lorenz
T. H. Mauney
J. R. McWherter
A. R. Olsen
J. A. Russell
F. J. Walter
R. M. Warner
D. B. Weaver[1]

13.1.1 Development and Construction

(a) General. – Construction of in-pile loop assemblies for operation in beam holes HB-2 and HB-4 at the LITR is continuing. With the accumulated experience in fabricating these loops and the standardization of component parts, the rate of construction of in-pile loops is more than adequate for the beam hole availability at the present time. This results partly from the longer period of operation of the last in-pile loop in beam hole HB-4 (approximately 2000 hr circulating time with loop L-2-12). In addition, the installation of an in-pile loop in beam hole HB-2 was delayed because of damage to the instrument panel in shipping, necessitating repair, replacement of some substandard valves in the auxiliary equipment chambers, and the relocation of the sampling table.

(b) HB-4 Loop Package. – In-pile loop L-4-13 was completed and tested during the past quarter and is now ready for installation in beam hole HB-4 at the LITR. The loop is made from type 347 stainless steel and is designed and tested for operation at temperatures and pressures up to 300°C and 2000 psia.

The type 347 stainless steel, tapered-channel, corrosion specimen holders in the core and in-line positions of loop L-4-13 contain corrosion coupons of type 309 SCb stainless steel, type 347 stainless steel, and crystal-bar zirconium. Impact specimens of zirconium with 20% niobium as an alloying element and of Zircaloy-3a are included in both the core and in-line positions. Two tensile specimens, one of Zircaloy-3a and one of titanium Ti-A40, are in the core position only. The loop will be installed in beam hole HB-4 as soon as necessary maintenance and repairs of auxiliary equipment are completed.

(c) HB-2 Loop Package. – Fabrication of an all-titanium in-pile loop,[2] L-2-14, was completed. The loop is designed for installation in beam hole HB-2 of the LITR and for operation at temperatures and pressures up to 300°C and 2000 psia. All welding was performed by the shielded-arc process with special jigs and/or trailers to ensure complete inert-gas coverage of all sections of metal heated by the welding process. The Metallurgical Group assisted in prescribing welding procedures and final evaluation of all welds for soundness. Figure 13.1 is a photograph of the completed loop.

An all-titanium, ORNL 5-gpm pump of the outboard-bearing design is employed in loop L-2-14. Bearings and journal bushings are of pure sintered aluminum oxide. A performance test of this pump was made in a test stand, and the results were compared with those for similar pumps made of type 347 stainless steel. No significant differences based on measurements of flow, head, and electrical power demand could be observed between the performance curves of the titanium and stainless steel pumps. The all-titanium loop assembly is now being installed in the mockup test facility at Y-12 for operational testing at design temperatures and pressures.

(d) ORR Loop. – Conceptual design studies of an in-pile corrosion loop facility for the ORR were initiated. The large facility on the north side of the ORR has been assigned to the Homogeneous

[1]On loan from TVA.

[2]G. H. Jenks *et al.*, *HRP Quar. Prog. Rep. Jan. 31, 1956*, ORNL-2057, p 91–92.

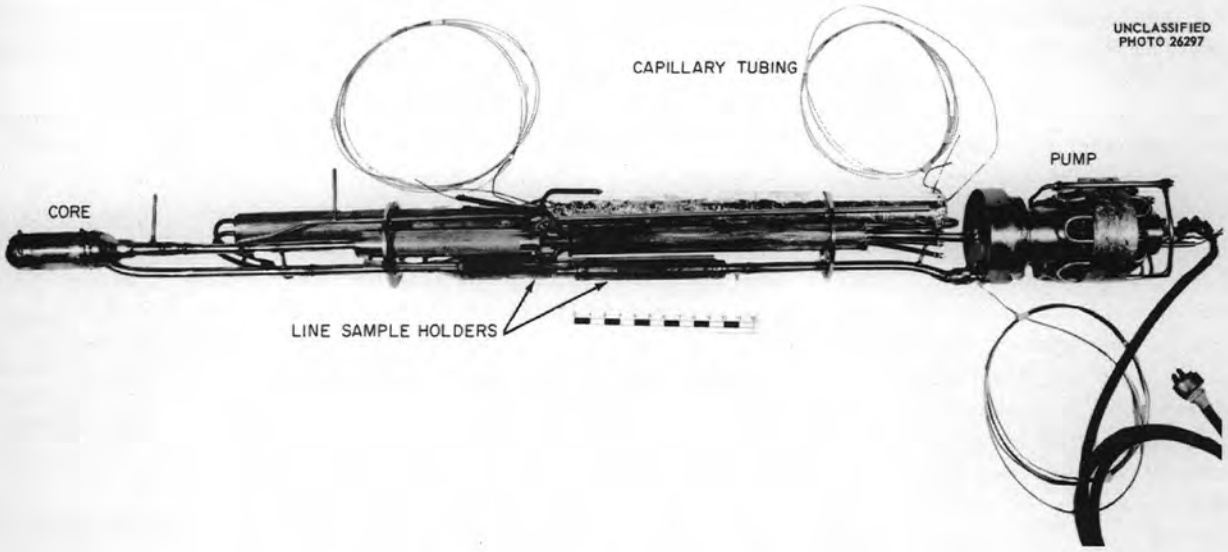

Fig. 13.1. Titanium In-Pile Loop L-2-14.

Reactor Project. In order to accommodate several experiments simultaneously, two 10-in. maximum and two 3-in. maximum diameter thimbles will be inserted in this facility. The loop, as planned, will operate in one of the 10-in.-dia holes.

In order to obtain a thermal flux as high as possible for the corrosion loop experiment, the space around the thimbles will be filled with a moderating material. This group has recommended heavy water for this purpose because of its desirable nuclear properties and because of the ease with which it may be adapted to any size of thimble. Beryllium, which would be more desirable from a maintenance standpoint, was considered, but it would make the facility less versatile and probably more expensive than would a heavy-water system.

The loop under consideration for the ORR is similar to the loops in use at the LITR and is being designed for operation at an average fission power density of 33 w/ml in a core volume of 300 ml. Calculations were made on the control of radiolytic gas and temperatures for the system, and proper control appears to be feasible with moderate modification of the present design.

Some anticipated characteristics of a loop in the ORR with a reactor fuel-element loading favorable to the north facility are as follows:

Solution Composition (*m*)	
UO_2SO_4	0.17
U^{235}	92.6 (%)
$CuSO_4$	0.1
H_2SO_4	0.04
Power Density (w/ml) in Loop Core (300 ml)	
Average	33
Maximum	~60
Temperatures (°C)	
Core inlet	275
Core outlet	282
Pressurizer	310
Hydrogen Partial Pressure (psi)	
Core	~130
Pressurizer	~6

13.1.2 In-Pile Loop Experiment L-4-11

Exposure of in-pile loop experiment L-4-11 in the LITR was completed. Disassembly and examination of the loop and loop specimens are in progress. Exceptionally low flow of solution through

the pressurizer was noted during almost the entire experiment. After the first 100 hr of circulation time with enriched solution, the flow dropped rapidly to about 20% of its initial value. At this point the reactor was shut down, a variable-frequency motor-generator set was installed from which the circulatory pump was operated for the balance of the experiment at 86 cps instead of at the normal 60-cycle line current, and attempts were made to unplug what was assumed to be a partially plugged pressurizer inlet or outlet line by varying the pressurizer and loop temperatures. After an additional 205 hr of circulation the loop was drained, given a standard pretreatment operation in a further attempt to clear the obstruction, charged with a fresh solution of enriched material, and again started up. Eight hundred hours later the flow to the pressurizer had dropped to about 12% of the original flow, and the experiment was terminated.

The two original enriched solutions charged to the loop and the makeup solution were approximately the same composition: UO_2SO_4, 0.17 *m*; $CuSO_4$, 0.031 *m*; H_2SO_4, 0.04 *m*. The first original solution also contained 504 ppm of nickel. The loop contained a variety of specimen materials, including sapphire, sintered aluminum oxide, Incoloy, crystal-bar zirconium, several stainless steel and titanium alloys, and a large group of Zircaloy-2 and Zircaloy-3 alloys.

The in-pile operation period with enriched solution was 1109 hr. The total circulation time was 344 hr for the first original solution and 786 hr for the second original solution for a total of 1130 hr. The energy output of the LITR during this time was 2175 Mwhr, and essentially all the power was liberated at the 3-Mw level.

13.1.3 In-Pile Loop Experiment L-4-12

Exposure of in-pile loop L-4-12 in the LITR was completed. Disassembly and examination of the loop have not yet begun. No major difficulties were encountered during operation of the loop, although it was necessary at one point to drain the solution from the loop to replace several valves which had become plugged in the sampling system. Operation continued after fresh solution had been charged to the experiment, until additional valve trouble made it advisable to terminate the experiment.

Unlike previous experiments, this one contained nontapered titanium coupon holders in both the core and in-line positions. Specimens were of stainless steel, Zircaloy-2, and titanium alloys. The loop solution was of the usual composition: UO_2SO_4, 0.17 *m*; H_2SO_4, 0.04 *m*; $CuSO_4$, 0.03 *m*. The in-pile operation period with enriched solution was 2019.6 hr. The energy output of the LITR during this time was 4385.5 Mwhr. For the initial 192 Mwhr, the reactor power was 1.5 Mw. Essentially all the subsequent energy was liberated at the 3-Mw level.

13.2 IN-PILE AUTOCLAVE TESTS

G. H. Jenks

R. J. Davis
H. O. Day
V. A. DeCarlo
H. A. Fisch
D. T. Jones
R. A. Lorenz
J. R. McWherter
A. R. Olsen
J. A. Russell
F. J. Walter
K. S. Warren
L. F. Woo

13.2.1 LITR Tests

The corrosion behavior of Zircaloy-2, titanium, and type 347 stainless steel in reactor-irradiated uranyl sulfate solutions was investigated further. One Zircaloy-2 experiment, Z-17, was completed, and another, Z-11, is in progress. Two experiments with stainless steel, H-95 and H-96, and one titanium experiment, T-2, were completed. In addition, a bomb from an early experiment,[3] Z-3, was opened and information obtained from the pins and solution irradiated in this bomb. Data for the experiments are presented in Table 13.1. As before, the values for irradiation time are based on the energy output of the LITR with 3 Mwhr of energy equivalent to 1 hr. The corrosion rate values are based on radiation time. A large proportion of the results shown have not been fully evaluated, and, where this is the case, the listed value is accompanied by an approximation sign. The plus-minus values which are listed are standard probable errors computed from the spread of the data.

The pin weight data for experiment Z-3 indicate that the high concentration of excess sulfuric acid markedly reduced the radiation corrosion of

[3] G. H. Jenks *et al.*, *HRP Quar. Prog. Rep. April 30, 1955*, ORNL-1895, p 119.

TABLE 13.1. LITR IN-PILE BOMB DATA

Bomb No.	LITR Beam Hole	Bomb Material	Solution Composition (m)			Enrichment (% U^{235})	Initial O_2 Pressure at 250°C, Approximate (psi)	Exposure Temperature (°C)	Fission Power Density (w/ml)	Irradiation Time (days)	Corrosion Rate For O_2 Data (mpy)	Over-all Corrosion Rate from Pins (mpy)
			UO_2SO_4	$CuSO_4$	H_2SO_4							
Z-3	HB-5	Zircaloy-2 (with three crystal-bar zirconium pins)	0.170	0.020	0.448	19.8	700	250	3.7	19.3	2.1 ± 0.1*	0.9 ± 0.1 Zircaloy-2 0.8 ± 0.2 crystal-bar zirconium
Z-11	HB-6	Zircaloy-2	0.172	0.010	0	93.2	550	250	~9	5.2	~8	Not available
			Plus 0.0054 m $KTcO_4$					280		2.1	~17	
								235		4.8	~6	
Z-17	HB-5	Zircaloy-2	0.169	0	0.040	6.0	500	250	~1.2	10.8	Variable	
										5.3**	0.4 → 1.9 → 1.5	
										4.3		
								280		6.9	~3.4	1.9
								250		4.5	~1.5	
H-95	HB-6	Type 347 stainless steel	0.042	0.049	0.039	93.2	550	250	~2.4	24.2	3.0 → 0.2	
								280		17.4	~0.3	0.7
										5.3**	?	
H-96	HB-6	Type 347 stainless steel	0.172	0.010	0	93.2	600	250	~9	25.2	Variable (see text)	2.8 ± 0.2
			Plus 0.0011 m $KTcO_4$									
T-2	HB-5	75-A titanium	0.172	0.040	0.040	93.2	750	250	~14	8.4	1.7	4.0 ± 0.1 (weight gain) 2.4 ± 0.3 (weight loss)

*This rate included an unknown amount of corrosion of steel capillary connections.
**At 1500 kw.

Zircaloy-2. It is known from other experiments[4] that the rate at the listed power density and in the absence of excess acid is about 4 mpy. The steel capillary connection was badly corroded in the experiment; oxygen consumed in this process probably accounts for the higher rate of attack indicated by the oxygen consumption data, since it was assumed in the calculations that oxygen had been consumed only in the oxidation of Zircaloy-2.

Experiment Z-11 was designed to test the effect of the TcO_4^- ion in solution on the radiation corrosion of Zircaloy-2. The oxygen data indicate that the additive has no effect on the corrosion. The indicated rates at 250 and 280°C are essentially those expected for a system containing no TcO_4^- but otherwise similar.

In all the previous Zircaloy-2 experiments the solutions contained added $CuSO_4$. In order to establish the effect of copper on the radiation corrosion of Zircaloy-2, experiment Z-17 was conducted without copper in the solution. As shown in Table 13.1, the enrichment was low and the fission power density was about 1 w/ml. At this low power density, the gamma-ray intensity in the exposure facility proved sufficient to effect the recombination of the majority of the radiolytic gas produced by fission recoils. The pressure of radiolytic gas during exposure both at 250 and 280°C reached a steady state of about 100 psi. For approximately 100 hr at the start of irradiation, the corrosion rate remained quite low. It then increased as shown in the table and remained fairly constant at a given temperature. The rate at 280°C was approximately double that at 250°C. The rate at 250°C is essentially the same as that determined for loop specimens exposed at the same power density but in solutions which contained 0.03 *m* $CuSO_4$. Hence, there is little indication that the presence or absence of cupric ion influences the radiation-induced corrosion.

The data for the stainless steel experiment H-95 are rather erratic. Within experimental error, little effect of temperature can be detected. The high rate listed in the table persisted for about 100 hr at the start of irradiation. It then decreased sharply to the low rate.

Experiment H-96 was designed as a test of the performance of stainless steel bomb systems containing no added acid, and, at the same time, of the effect of the TcO_4^- ion on the radiation-induced corrosion. The results were essentially the same as those obtained with an early bomb experiment,[5] H-51. The corrosion rate indicated by the oxygen increased from an initial value of about 0.6 mpy to a value of about 5.3 mpy after several days of irradiation. Upon continued exposure the rate slowly decreased to about 2.6 mpy. It should be pointed out that the composition of the solution was constantly changing during exposure, owing to the introduction of nickel and the loss of hydrogen ions. It is very probable that precipitation of uranium and copper took place fairly early in the test.

The earlier experiment, H-51, was similar to H-96 except that the solution contained no TcO_4^- and employed an oxygen pressure of about 250 psi. Also, the fission power density in H-51 was probably somewhat lower than in H-96. The results of the present experiment H-96 are regarded as evidence that the added H_2SO_4 was responsible for the improved corrosion behavior observed in the recent series of steel experiments and that the addition of TcO_4^- had no effect on the radiation-induced corrosion, at least in the absence of added acid.

The interpretation of the results of the titanium experiment, T-2, is not clear. The corrosion of the pins as indicated by weight gains before defilming is greater than that indicated by average weight losses after defilming. However, visual inspection indicated that, with the exception of one pin, some oxide remained on the pin surfaces after defilming. The weight loss and weight gain values for the pin which was the exception are in near agreement. Hence, it appears likely that the most nearly correct value for the over-all corrosion rate of the pins is that determined from the weight gains. However, this value is much greater than the over-all rate indicated by the oxygen data. This discrepancy is, at present, unsolved. It may be added that questions regarding the effect of power density and of temperature on the radiation-induced corrosion of titanium are also unresolved.

[4] G. H. Jenks *et al.*, *HRP Quar. Prog. Rep. Jan. 31, 1956*, ORNL-2057, p 97.

[5] C. H. Secoy *et al.*, *HRP Quar. Prog. Rep. July 31, 1954*, ORNL-1772, p 162.

13.2.2 MTR Tests

Exposure of experiment ORNL-15-5 in the MTR was completed. The autoclave and pin corrosion specimens for this experiment were of Zircaloy-2. The test solution was water-pressurized with about 400-psi oxygen. The experiment was installed in the HB-3 facility on January 16, 1956, and was operated during the subsequent cycle. During the operation the experiment was retracted for 138 hr, fully inserted for 104 hr, and partially inserted (70%) for 80 hr.

The corrosion during operation as indicated by the oxygen data is summarized in Table 13.2. Specimen weight data are not yet available. The indicated rate of 4 to 5 mpy for the fully inserted operation may be compared with a rate of about 11 mpy for a depleted UO_2SO_4 solution determined in the previous experiment,[6] ORNL-15-4. The power density and exposure temperature for the previous experiment and the present experiment were similar.

Data for both the activation of zirconium and the analysis of fission-product cesium are available from previous experiments[7,8] ORNL-15-1 and 15-2. The flux calculations from these data are not accurate, because there are two fluxes involved, one for the experiment when inserted and another when retracted. However, the data indicate that the values for the average flux and fission power density in the inserted position for these experiments were about two-thirds of those previously assumed. Hence, in experiment 15-2, for example, the fission power density in the exposed position was probably about 25 w/ml rather than the reported[8] 35 w/ml.

The titanium bomb that had been exposed in the MTR experiment[6] 15-3 was opened, and the titanium pin and pin holder and the platinum pin were examined. The average corrosion rate of the titanium specimen determined from the weight loss data and from the irradiation time was about 12 mpy. As reported previously, the oxygen data were erratic, but the maximum average corrosion rate indicated by the oxygen was about 7 mpy. It is estimated that during exposure the bomb wall temperatures were about 20°C lower than the pin temperatures; this difference in temperature may, in part, account for the difference between the oxygen data and the pin-weight data.

The weight loss determined for the platinum pin was 0.3 mg. This value is somewhat greater than the experimental error of the weighing and indicates that the platinum was attacked to a small extent.

[6] G. H. Jenks *et al.*, *HRP Quar. Prog. Rep. Jan. 31, 1956*, ORNL-2057, p 98.

[7] G. H. Jenks *et al.*, *HRP Quar. Prog. Rep. July 31, 1955*, ORNL-1943, p 130.

[8] G. H. Jenks *et al.*, *HRP Quar. Prog. Rep. Oct. 31, 1955*, ORNL-2004, p 152.

TABLE 13.2. CORROSION RATES INDICATED BY OXYGEN DATA, ORNL-15-5

Position	Estimated Power Density in Solution from Absorption of Fast Neutrons (w/ml)	Estimated Temperatures of Bomb Walls in Contact with Water (°C)	Corrosion Rate (mpy)
Fully inserted	4	295	4 to 5
Partially (70%) inserted	3	250	0.3
Retracted	0.4	280	1

14. METALLURGY

G. M. Adamson

R. G. Berggren
W. J. Fretague
W. J. Leonard
M. L. Picklesimer
G. B. Wadsworth
J. C. Wilson
J. K. White
C. H. Wodtke

14.1 PHYSICAL METALLURGY

M. L. Picklesimer G. B. Wadsworth

14.1.1 Effect of Hydrogen on Zirconium and Its Alloys

The metallographic procedure for the identification of hydrides in zirconium and its alloys[1] was considerably improved by use of alternate mechanical polishing on fine diamond paste wheels and electropolishing in a perchloric-acetic acid solution. This procedure neither pits the specimen nor leaves the hydride surface in too great relief for microscopic examination at high magnification. After being anodized, any hydride particle, large enough to be clearly resolved without oil immersion, can be identified by its golden-yellow color in contrast to the blue-to-purple color of the matrix material.

The following series of photomicrographs show the difference in distribution of the hydrides in Zircaloy-2 and in crystal-bar zirconium. All specimens were prepared by vacuum-annealing at 900°C for 24 hr, adding the desired amount of hydrogen at 900°C, homogeneizing at 900°C for 2 hr, and cooling at steps of 100°C every 30 min. Figure 14.1 is a bright-field micrograph from crystal-bar material containing 160 ppm of hydrogen. An examination of the same field under both bright field and polarized light shows that the hydrides, appearing as the white clumps, lie entirely within one alpha grain and do not occur in the grain boundaries. An examination of the entire specimen showed that, at most, there were no more hydride needles in the grain boundaries of the crystal-bar zirconium specimen than would occur for a random distribution of hydride needles throughout the specimen. Figure 14.2, a bright-field and a polarized-light photomicrograph of a crystal-bar specimen containing 500 ppm of hydrogen, confirms that the hydrides are within the grains.

The occurrence of the hydrides in the grain boundaries of Zircaloy-2 is shown in Figs. 14.3 and 14.4. An examination of Fig. 14.3 (Zircaloy-2 with 100 ppm H_2) and Fig. 14.4 (Zircaloy-2 with 350 ppm H_2) shows that even at these relatively high hydrogen levels the hydrides occur as films and plates in the grain boundaries and as clumps in the grain corners. Hydride needles have not been observed entirely within the alpha grains of Zircaloy-2 specimens that have been cooled relatively slowly from the heat-treating temperatures.

Crystal-bar zirconium specimens containing approximately 500 ppm of hydrogen were quenched from 900°C in oil and mercury. Figure 14.5 shows that the hydrides appear in the grains in a Widmanstätten pattern after an oil quench of a specimen containing 480 ppm of hydrogen. Figure 14.6 shows that the precipitation of hydride needles for the specimen containing 530 ppm of hydrogen and quenched in mercury was much less than that for the specimen shown in Fig. 14.5, indicating that a considerable quantity of hydrogen

Fig. 14.1. Microstructure of Crystal-Bar Zirconium with 160 ppm of Added Hydrogen. Bright field. 500X. Reduced 31%.

[1] M. L. Picklesimer and G. B. Wadsworth, *HRP Quar. Prog. Rep. Jan. 31, 1956*, ORNL-2057, p 101–104.

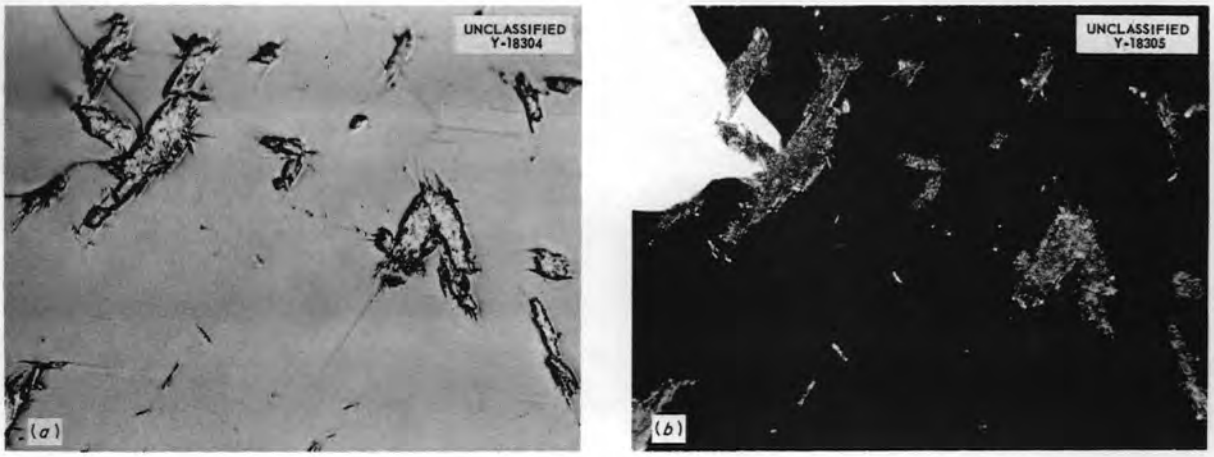

Fig. 14.2. Microstructure of Crystal-Bar Zirconium with 500 ppm of Added Hydrogen. (*a*) Bright field; (*b*) polarized light. 500X. Reduced 30.5%.

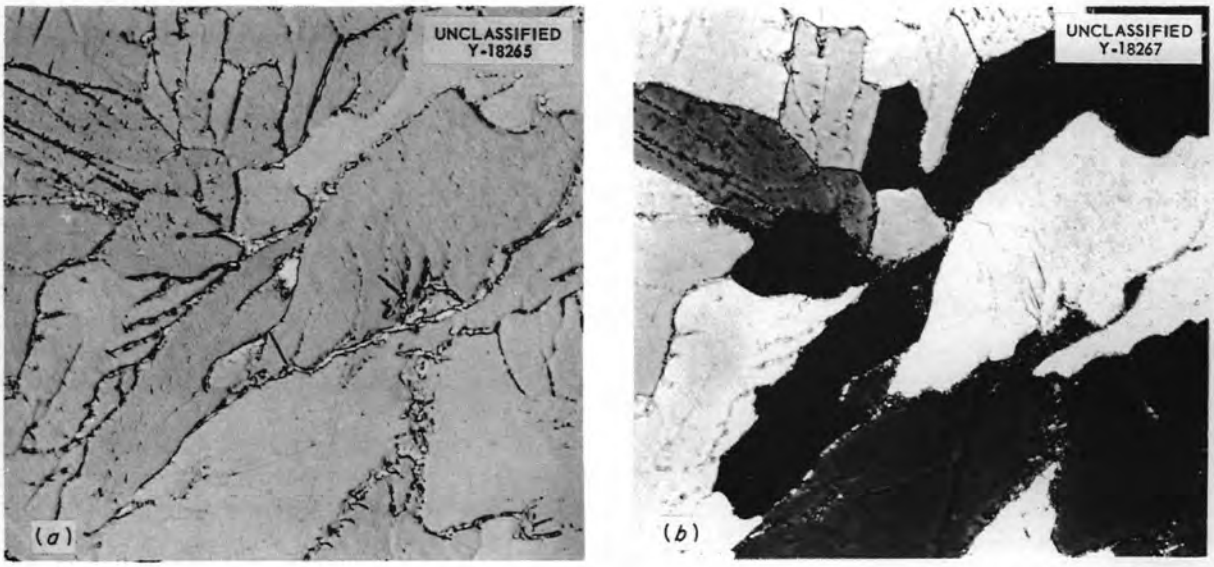

Fig. 14.3. Microstructure of Zircaloy-2 with 100 ppm of Added Hydrogen. (*a*) Bright field; (*b*) polarized light, 500X. Reduced 14%.

can be retained in a supersaturated solution by a fast cooling rate for the specimen. The maximum amount of hydrogen that can be retained on quenching will be determined by quenching specimens containing successively less and less hydrogen. These specimens will then be given various aging treatments to determine the rate of precipitation of hydrides from the supersaturated condition.

14.1.2 Zirconium Alloy Development

Alloys of the composition (wt %) 10, 15, and 20 Nb, 5 and 10 Mo, 5 Ta, 10 Nb + 5 Mo, 10 Nb + 5 Ta, 10 Nb + 5 Mo + 5 Ta, 15 Nb + 5 Mo, 10 Nb + 10 Mo, 10 Nb + 2 Fe, and 15 Nb + 2 Fe were arc-cast by using crystal-bar zirconium and high-purity alloying elements and were used to study the retention of the high-temperature beta phase to

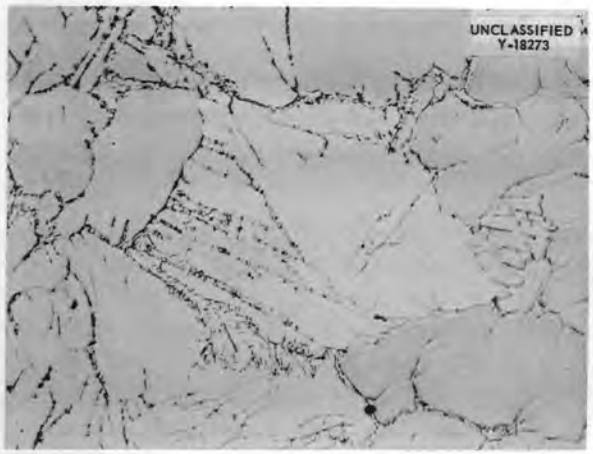

Fig. 14.4. Microstructure of Zircaloy-2 with 350 ppm of Added Hydrogen. Bright field. 500X. Reduced 31%.

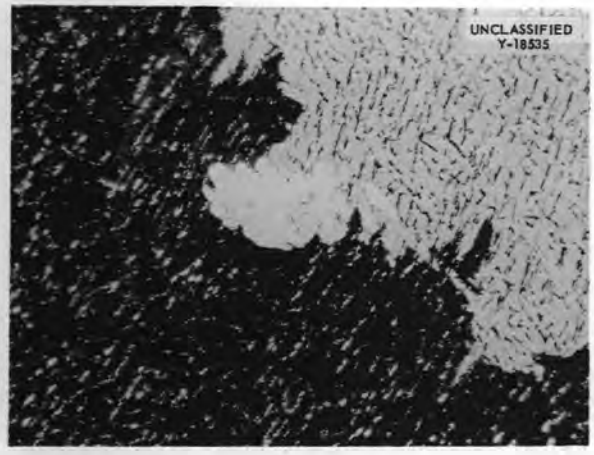

Fig. 14.5. Microstructure of Oil-quenched Crystal-Bar Zirconium Containing 480 ppm of Hydrogen. Polarized light. 500X. Reduced 31%.

room temperature by rapid cooling and the decomposition of the retained beta by subcritical heat treatments. All castings were held in evacuated quartz capsules for 2 hr at 850°C or higher and then water-quenched. The 10 wt % Mo casting was hot-rolled to a 0.100-in. strip at 700°C. An attempt was made to hot-roll the castings containing iron, but they fractured on the second pass. The remainder of the alloy castings were successfully cold-rolled to 0.100-in.-thick strips. Small specimens were cut from the strips and given a variety of heat treatments. Quenching from temperatures

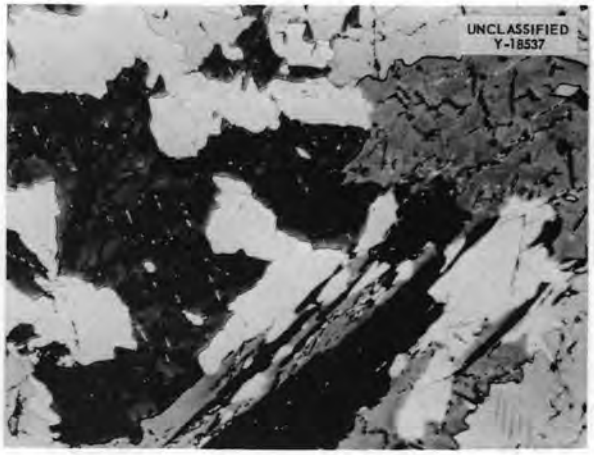

Fig. 14.6. Microstructure of Mercury-quenched Crystal-Bar Zirconium Containing 530 ppm of Hydrogen. Polarized light. 500X. Reduced 31%.

ranging from 700 to 1150°C into water did not result in the complete retention of the beta phase in any of the alloys, with the possible exception of the 10 wt % Mo alloy. All the alloys containing niobium showed a Widmanstätten precipitate consisting of very thin plates traversing the entire grain. The precipitate has not been identified as yet. X-ray-diffraction analyses showed only the high-temperature beta phase. Specimens of 15 and 20 wt % Nb were submitted to Battelle Memorial Institute for examination by glancing-electron diffraction. None of the specimens containing tantalum showed any retained beta phase. The 5 wt % Mo alloy showed a very fine irresolvable precipitate occurring generally throughout the specimen. The precipitate has not been identified. The 10 wt % Mo alloy has not yet been examined in detail. Only the cast structures were examined for the iron alloys, and their interpretation is questionable. Examination of all the alloys is continuing.

14.1.3 Structures of Zircaloy-2

Cathodic etching of Zircaloy-2 specimens confirmed the prior conclusion[1] that the precipitates and stringers observed in the as-fabricated materials are intermetallic compounds and not the pits or voids that had been postulated. The stringers show continuity with the matrix, as shown in the micrographs in Fig. 14.7.

Zircaloy-2 specimens were held at 1000°C for 30 min, water-quenched or air-cooled, cold-worked

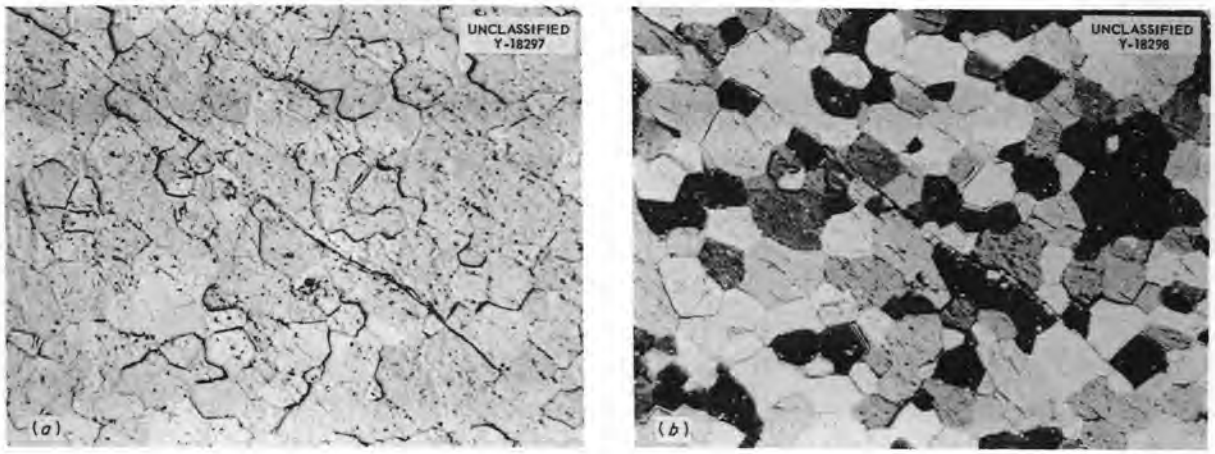

Fig. 14.7. Stringer in Zircaloy-2. (*a*) Bright field; (*b*) polarized light. Cathodic etch. 500X. Reduced 30%.

10, 15, or 20% reduction, and annealed at 800°C for 30 min. The specimens that were cold-worked 10% had a very fine grain structure in the center of the specimen. The thickness of the band with a fine-grained structure was increased and the grain size of the coarse-grained structure was decreased somewhat by cold-working 15%. A reduction of 20% was necessary to give a fine-grained structure throughout the thickness of the ¼-in. plate specimens used. The grain sizes for the air-cooled specimens were, in all cases, coarser than those for the water-quenched specimens by at least two ASTM grain size numbers.

Zircaloy-2 specimens that were cold-worked 20% after water-quenching and air-cooling from 1000°C and annealed at 800°C for 30 min were submitted for x-ray-diffraction determination of the preferred orientation of the material to determine whether there had been any changes from the highly preferred orientation of the starting material.[1]

14.2 MECHANICAL METALLURGY OF ZIRCONIUM ALLOYS

W. J. Fretague

14.2.1 Zircaloy-2

An experiment to determine the effect of aging of Zircaloy-2 at 250°C prior to impact testing was carried out.[2] Eight multiple-break subsize impact specimens were aged for varying lengths of time at 250°C. Table 14.1 lists the thermal history and the test results obtained. Figure 14.8 is a plot of the impact data obtained. The results obtained do not indicate any appreciable embrittlement from aging at 250°C. A second set of impact specimens is being aged for 1000 hr at 300, 350, 400, and 450°C prior to testing.

14.3 WELDING DEVELOPMENT

W. J. Leonard

14.3.1 Titanium Welding Development

Titanium welding in air of in-pile loop components and dynamic test loops continued on a production basis. Weld-test coupons made from similar sized pipe or shapes, by the same procedures, and tested by destructive tests in addition to metallographic examination indicated that titanium welds of good quality are being obtained in the actual production parts.

Successful welds were made in titanium pipe by using a modification of the consumable-insert procedure developed for stainless steel. It was found desirable to reduce the size of the wire from which the insert is machined from $\frac{5}{32}$ to a ⅛-in. diameter; the shape of the finished insert was also changed so that the stem of the mushroom would contain a higher percentage of the metal. During the actual welding, the torch is held at a 40-deg angle from the usual vertical position and one-third more current is used.

[2] W. J. Fretague, *Met. Semiann. Prog. Rep. Oct. 10, 1955*, ORNL-1988, p 95.

TABLE 14.1. IMPACT ENERGY vs TESTING TEMPERATURE DATA FOR AGED ZIRCALOY-2

Aging Time at 250°C (hr)	Specimen and Break No.	Testing Temperature (°C)	Impact Energy (in.-lb)
0	769-3	−100	8
500	773-3	−100	10
1085	770-3	−100	9
1585	774-3	−100	8
0	761-1	15	15
500	765-1	15	13
1085	762-1	15	12
1585	766-1	15	14
0	769-1	90	16
500	773-1	90	22
1085	770-1	90	20
1585	774-1	90	20
0	761-2	150	27
500	765-2	150	24
1085	762-2	150	27
1585	766-2	150	28
0	769-2	200	32
500	773-2	200	38
1085	770-2	200	34
1585	774-2	200	36
0	761-3	254	60*
500	765-3	254	60*
1085	762-3	254	60
1585	766-3	254	50

*Broke on rebound.

14.3.2 Welding of Titanium-lined Steel Pipes

Titanium-lined carbon steel pipe of approximately $\frac{3}{8}$-in. wall thickness, 3-in. nominal diameter, was welded by two methods. Neither yielded a completely satisfactory weld. The first method consisted in welding the root and first passes with titanium wire up to a level below the juncture of the carbon steel base metal and titanium base metal. The weld of titanium was sound. Carbon steel ribbon was then wrapped around the weld to give a wrapping of slightly over $\frac{1}{8}$-in. thickness to a level above the juncture line of the two base metals. The remaining groove was filled with carbon steel weld metal. The weld contained voids where complete fusion of the wrapped steel ribbon had not occurred. Cracks that extended into the base metal originated from these voids when sections cut from the pipe were subjected to a side bend test. This type of bend test is more severe than would be expected in use, but results of the test do indicate a weakness.

In the second method the first passes were again made with titanium weld metal; vanadium was, however, used as the transition material. Where the vanadium came in contact with the carbon steel base-metal wall, extensive cracking occurred. The vanadium weld metal did not cause cracking where it came in contact with titanium weld metal, Fig. 14.9. Carbon steel base metal, at the top in the photograph, caused extensive cracks on that

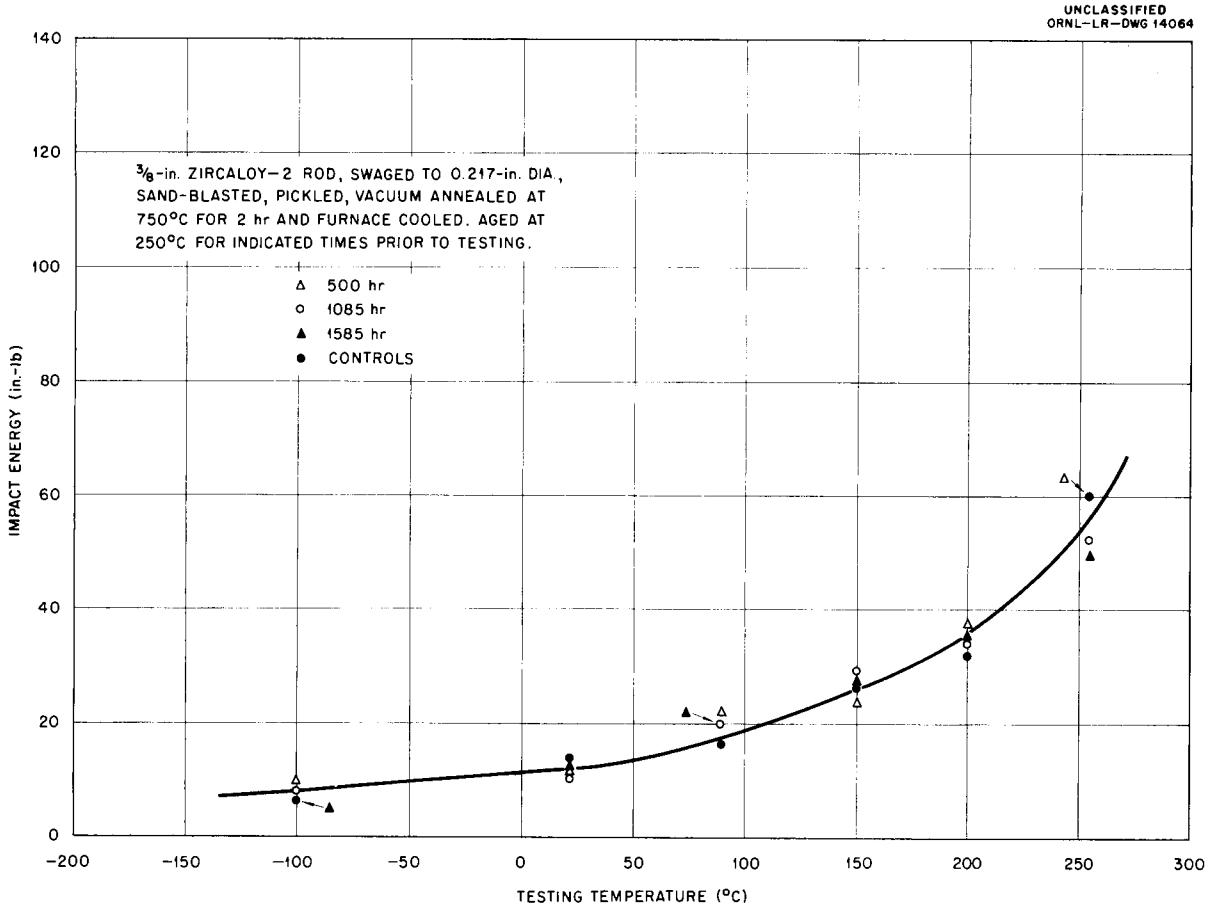

Fig. 14.8. Impact Energy vs Testing Temperature for Aged Zircaloy-2.

side of a vanadium weld bead, which is in the central area of the figure. The juncture of the vanadium weld bead with the titanium weld bead at the bottom of the figure caused no perceptible cracking. On completion of the vanadium layer, carbon steel weld metal was placed on the vanadium weld metal barrier. Extensive cracking occurred throughout the carbon steel weld bead. The joint was not filled any further, as this type of weld was not considered feasible. Microexamination of specimens revealed extensive cracking through the weld.

14.3.3 Inert-Gas-Shielded Arc Welding of Type 347 Stainless Steel

Satisfactory welds made according to HRP welding specifications were made in type 347 stainless steel, with argon, helium, and nitrogen used for protection on the root side of the welds.[3] Additional work was carried out on the use of nitrogen as a backup gas in the welding of type 347 stainless steel in a continued effort to take advantage of the low cost of nitrogen.

When K-25 water-pumped nitrogen (the grade that had been used in the previous study) was tested, satisfactory welds were made; however, considerable variation in quality was found among various gas cylinders. The welds varied in appearance from silver to a purple tinge. The specifications for this grade of nitrogen allow a maximum of 0.5% impurities with a –100°F dew point; all these impurities could be oxidizing gases. Similar series of tests were made with both liquid-pumped, high-purity dry nitrogen (99.8% minimum) and Linde

[3]W. J. Leonard, *HRP Quar. Prog. Rep. Oct. 31, 1955*, ORNL-2004, p 156.

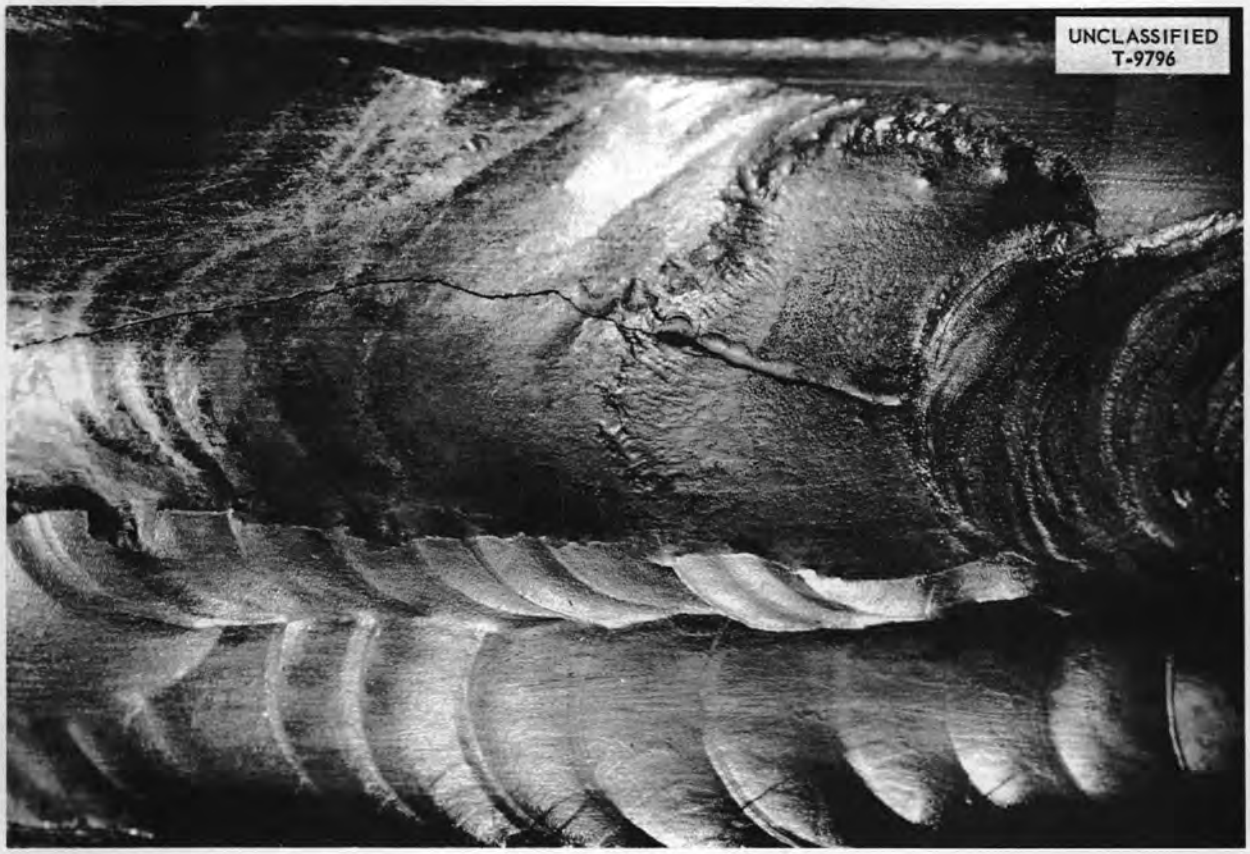

Fig. 14.9. Cracks in a Titanium, Vanadium, Steel Composite Weld.

TABLE 14.2. ANALYSES OF NITROGEN GAS

Type of Nitrogen	Impurities (ppm)				
	O_2	CO_2	H_2O	A	CH_4
Water-pumped	100	2	10	40	10
Liquid-pumped	20	1	3	72	
Linde high purity	<2	<2	7	<2	

high-purity dry nitrogen (99.9% minimum). In both cases welds that appeared to be excellent were made. With the first gas, the welds were equal to, or superior to, those obtained with helium, and those with the second were exceptionally clean. Analyses of the gas obtained from the three types of cylinders are tabulated in Table 14.2.

The mechanical tests and metallographic examination of these specimens were not completed; however, in the original work[3] no adverse effects were found when nitrogen was used for backup.

From these data, it appears that high-purity nitrogen can be used as a backup gas in stainless steel welding. A considerable saving in cost can be achieved by using the liquid-pumped nitrogen.

14.4 NONDESTRUCTIVE TESTING

J. K. White

14.4.1 Inspection of Pipe and Tubing

Of the several methods proposed for precision flaw detection in pipe, the pulse-echo ultrasonic one best suits our needs. Radiography is as easily interpreted but is slow and expensive. Eddy-current methods have a promising future but require considerable development to provide definitive flaw detection. Conventional ultrasonic contact scanning proved to be inadequate, as did several unconventional techniques. Contact could not be

maintained uniformly nor could Rayleigh waves[4] be suppressed satisfactorily. (Rayleigh waves may cause small surface flaws to obscure subsurface defects.)

A column-coupled, immersed technique was chosen. The Immerscope manufactured by Electro Circuits, Inc., gave a response sensitivity to small defects that was more than adequate. Indeed, one drawback to the method is its high sensitivity to shallow surface scratches. Either of two methods may be used to differentiate between shallow surface defects and more extensive flaws. The conventional A-scan oscilloscope trace may be selectively gated, or the B-scan oscilloscope presentation may be used. In the former, an alarm is triggered when a flaw indication greater than a set minimum travels through the gate. The gate is set at a point beyond the furthest travel of a purely surface indication. The sensitivity time control circuit provided on the Electro Circuits instrument serves as an aid in accentuating this difference in travel. In the B-scan presentation a rotated flaw appears as a diagonal line. The extent of the diagonal oscilloscope indication can be related directly to flaw depth within reasonable limits.

[4] J. W. S. Rayleigh, *Proc. London Math. Soc.* 17, 4–11 (1885).

14.4.2 Inspection of Reactor Components

A resonance type of ultrasonic thickness measurement technique was adapted to monitor the corrosion of the Zircaloy-2 HRT core vessel during reactor down time. Access to one particular spot on the outer side of the core vessel equator is gained through the inspection nozzle at the top of the blast shield. A folded positioner is lowered into the nozzle on a 20-ft tube and is extended by means of cables to spring-load a crystal transducer against the core vessel (Fig. 14.10). Original measurements were read out on the Branson Instruments, Inc., Audigage, but the length of coaxial cable necessary made it advisable to change the read-out instrument to the Branson Vidigage. A subsequent reading with the Vidigage indicates that, barring an error from residual

UNCLASSIFIED
PHOTO 17318

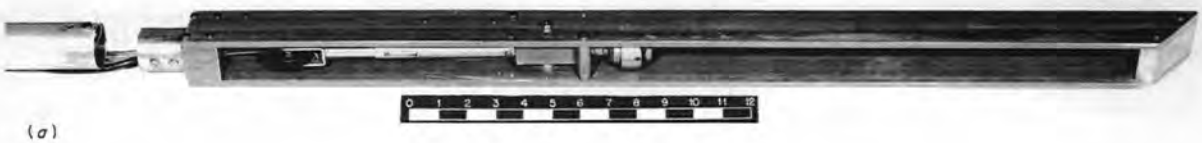

(*a*)

UNCLASSIFIED
PHOTO 17317

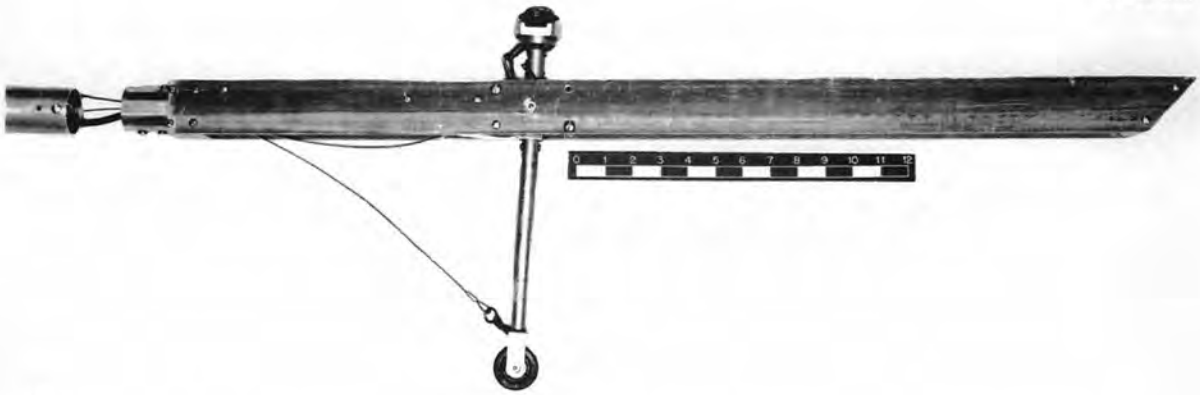

(*b*)

Fig. 14.10. Transducer and Holder for Measuring Core Tank Thickness. (*a*) Collapsed; (*b*) extended.

radiation effects on the crystal, the precision of the method should be on the order of 0.3%.

Three cast type 347 stainless steel P-14 pulsator housings from the pressure system of the injection pumps were examined after their failure in mockup service. Subsequently one of them was repaired, but it again failed in service. Ostensibly, all four failures were due to different causes, but there were certain points of similarity.

1. Without exception, the housings showed a nonhomogeneous macrostructure under radiography.

2. In most cases a number of stress raisers were present owing to a machining operation.

3. Certain gross defects – for example, a pipe defect completely through the vessel wall – indicated a lax inspection program on the part of the vendor.

As a result of these findings, four new P-9 pulsator housings from the reactor system were inspected. These all showed the same heterogeneous structure and all had stress-raising machine marks to a greater or less degree. One had several large blowholes, which were readily detected by radiography. A recommendation was made that these housings should be rejected and that an attempt should be made to obtain forgings rather than castings.

---

[5] R. G. Berggren and J. C. Wilson, *Solid State Semiann. Prog. Rep. Feb. 29, 1956*, ORNL-2051 (to be published).

14.5 EFFECTS OF RADIATION ON STRUCTURAL METALS AND ALLOYS

R. G. Berggren J. C. Wilson

14.5.1 Equipment and Facilities

A beam hole apparatus for irradiation of impact and tensile specimens is operating satisfactorily in the HB-3 facility of the MTR. Specimen temperatures in this experiment range from 55 to 180°F. Construction of an elevated-temperature apparatus for use in the MTR was started. Design of an apparatus for irradiation of titanium and zirconium alloy specimens at 575°F in the MTR is substantially complete. The design calculations will be checked in a mockup of the specimen chamber before final design is completed. An experiment for irradiation of tensile specimens in a lattice piece of the MTR in contact with the coolant water is being assembled. Specimens of ASTM-A212B steel, Carriloy T-1, and types 301 and 305 stainless steel have been irradiated at less than 200°F in the HB-3 facility of the LITR.

A number of improvements in the hot-cell apparatus are being developed which should result in increased speed and accuracy of such testing.

14.5.2 Nickel Steels

Notch-bar impact tests were conducted on an 8½% nickel steel irradiated in the LITR and MTR. Test results, reported in the Solid State Division semiannual report,[5] showed considerable decrease in impact-energy values. Further impact tests on other alloys are now in progress.

Part V

CHEMICAL ENGINEERING DEVELOPMENT

F. R. Bruce

15. THORIUM OXIDE SLURRY DEVELOPMENT

D. E. Ferguson J. P. McBride
V. D. Allred N. A. Krohn
A. R. Jones L. E. Morse
E. V. Jones C. E. Schilling
W. M. Woods

15.1 IRRADIATION STUDIES

A. R. Jones J. P. McBride
N. A. Krohn C. E. Schilling

Four aqueous slurries of 900°C calcined thorium-uranium oxide prepared by two different methods and containing 0.5 mole % (based on thorium) of 93% enriched uranium were irradiated in the LITR at 300°C in the dash-pot-stirred irradiation bomb. At a concentration of 1000 g of thorium per kilogram of H_2O, three of the slurries were too concentrated to be pumped for longer than a few hours, and the stirrer failed to operate after 9, 6, and 65 hr of stirring under irradiation. Out-of-pile control experiments behaved similarly. For the fourth experiment the slurry concentration was reduced to 500 g of thorium per kilogram of H_2O, and no stirring difficulty was experienced during the full 85 hr of irradiation.

The thorium-uranium oxide used in the experiments in which the stirring stopped after 9 and 6 hr had been prepared by wet-autoclaving overnight at 300°C a simple mixture of D-16 ThO_2 and $UO_3 \cdot H_2O$, drying the resulting mixed oxide, and recalcining it at 900°C. The mixed oxide used in the other two experiments had been prepared[1] from the thorium-uranous oxalates coprecipitated at 40°C and decomposed to the mixed oxide by a multistage calcination ending at 900°C.

All slurries were mixed before they were placed in the irradiation bombs, and the experimental setups were pretested at temperature before insertion into the reactor. Each slurry contained 1000 ppm of PdO as a catalyst for the recombination of radiolytic gases. An oxygen overpressure (250 to 300 psi at room temperature) was maintained during the experiments with the oxides prepared from the coprecipitated oxalates.

[1] A. R. Jones *et al.*, *HRP Quar. Prog. Rep. Jan. 31, 1956*, ORNL-2057, p 109–113.

15.1.1 Postirradiation Examination of Slurries

Three slurries of thorium-uranium oxide containing 0.5 mole % of natural uranium which had been irradiated[1] at 300°C in the LITR (LITR-11, 12, and 13) and two similar slurries which had been irradiated at 300°C in the ORNL Graphite Reactor (GR 9 and 10) were examined for possible irradiation damage. The irradiation times were 151, 68, and 172 hr for the LITR experiments and 318 and 313 hr for the Graphite Reactor irradiations. All slurries were visually unchanged and showed no change in average particle size or average crystallite size. No change in settled density was observed in the slurries irradiated in the Graphite Reactor. The slurries irradiated in the LITR showed settled-density increases of 8 to 16%. Since no material balances were obtained on the irradiated material, the settled-density data should be considered only as showing that no gross changes occurred in the slurry-settled densities as a result of the irradiations.

15.1.2 Radiographic Studies with the Dash-Pot Bomb

The behavior of thorium oxide slurries in the dash-pot-stirred slurry bomb from room temperature to 300°C is being investigated by means of x-ray photography. With 160-kv x rays and a current of 6 to 12 ma, the details of the bomb, the stirrer, and the slurry-water interfaces were sharply delineated in the photographs (see Fig. 15.1).

The initial studies were carried out with a slurry containing 500 g of thorium per kilogram of H_2O and prepared from D-16 thorium oxide recalcined at 900°C. The slurry appeared to be uniformly dispersed by the action of the stirrer from room temperature to 300°C. When the stirring was stopped at 100°C, the oxide settled down around the stirrer to form an apparently uniform settled bed (Fig. 15.1*a*); when the slurry settled at 200°C, marked structural formations appeared (Fig. 15.1*b*); when stirring was stopped at 300°C, the slurry

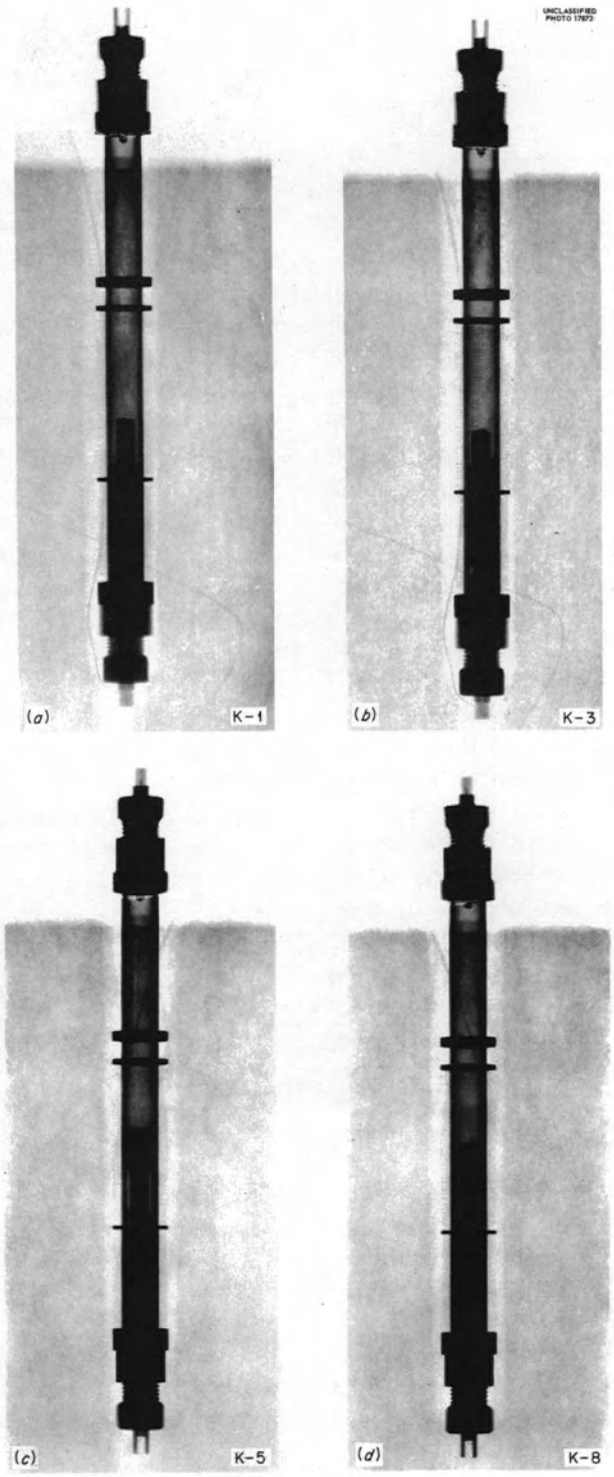

Fig. 15.1. X-Ray Photographs of a Thorium Oxide Slurry in the Dash-Pot-Stirred Irradiation Bomb. (*a*) After stirring and settling at 100°C; (*b*) after stirring and settling at 200°C; (*c*) after stirring and settling at 300°C; (*d*) after cooling to 110°C without stirring.

solids settled rapidly, forming a plug on top of the stirrer and a structure around it (Fig. 15.1*c*). Cooling to 110°C without stirring was not sufficient to break up this structure (Fig. 15.1*d*).

15.2 GAS RECOMBINATION STUDIES

L. E. Morse J. P. McBride

Out-of-pile investigation of the catalytic combination of stoichiometric hydrogen-oxygen mixtures in thorium-uranium oxide slurries containing molybdenum oxide catalyst continued with studies on the effect of catalyst concentrations from 0.05 to 0.20 *m*. With slurries containing 1000 g of thorium per kilogram of H_2O, all catalyst concentrations gave combination rates more than sufficient to maintain steady-state gas pressures at less than 2000 psi at 300°C in a TBR-type blanket.

The slurries were prepared by dispersing in water a mixture of 900°C recalcined D-16 thorium oxide, 0.5 mole % uranium trioxide monohydrate, and molybdenum oxide at the required concentration. The molybdenum oxide was prepared by heating ammonium paramolybdate at 430°C for 16 hr in a covered dish. The dry solids were mixed by tumbling them for 1 hr before dispersing in water. Prior to its use in a recombination experiment, the slurry was shaken for 3 hr at 280°C in the presence of an oxygen overpressure (250 to 300 psi at room temperature).

The slurries as prepared gave somewhat random combination rates, varying from 3 moles of hydrogen per hour per liter of slurry at 248°C and 500-psi hydrogen partial pressure for the 0.05 *m* MoO_3 concentration to 10 moles of hydrogen per hour per liter at 264°C and the same hydrogen pressure for the 0.20 *m* concentration, with a surprising minimum in reactivity occurring at 0.1 *m* concentration (see Table 15.1). Heating the slurries at 270 to 280°C under a hydrogen partial pressure greatly increased the combination activity for all catalyst concentrations, with the greatest relative increase occurring for the lowest concentration. After the hydrogen treatment, the slurry containing 0.05 *m* MoO_3 gave a combination rate, at 40°C and 500-psi hydrogen partial pressure, of 12 moles of hydrogen per hour per liter of slurry. This compares favorably with the combination rate obtained[2] with 0.01 *m* PdO catalyst of 3 moles of hydrogen per liter of slurry at 32°C and the same hydrogen partial pressure. In addition the molybdenum oxide catalyst appeared to be more resistant than the palladium catalyst to poisoning at room temperature. Reheating the slurries under an oxygen overpressure did not appear to affect the increase in activity brought about by the hydrogen treatment.

The results are summarized in Table 15.1 along with some data obtained previously[3] with a slurry of 660 g of thorium per kilogram of H_2O of pure oxide and an MoO_3 concentration of 0.1 *m*. An effort was made to obtain data at a temperature near 280°C, but in most cases the reaction rate at the lower temperatures was so rapid that all gas was consumed before this temperature could be attained.

The specific reaction rate constants, k_π, and the rates of hydrogen combination listed in Table 15.1 were obtained from the decrease in total gas pressure with time, first-order dependence (on hydrogen partial pressure) and perfect gas behavior being assumed. Experimental details and methods of analysis have been described previously.[4,5]

15.3 SLURRY VISCOSITY MEASUREMENTS

N. A. Krohn J. P. McBride
W. M. Woods

15.3.1 Slurry Viscosity Measurements in the Dash-Pot-Stirred Bomb

The relative viscosities of some thorium oxide and thorium-uranium oxide slurries were measured as a function of slurry concentration in the dash-pot-stirred slurry bomb by use of the method described previously.[1] In this method the operational characteristics of the bomb are calibrated for solutions of known viscosity, and the viscosity of a thorium oxide slurry being stirred in the bomb is determined by comparing the operational data with the calibration curves.

Table 15.2 lists the average viscosities observed for the various slurries at temperatures of 50 to 300°C. The viscosities of these slurries

[2] L. E. Morse and J. P. McBride, *HRP Quar. Prog. Rep. Oct. 31, 1955*, ORNL-2004, p 169–172.

[3] L. E. Morse and J. P. McBride, *HRP Quar. Prog. Rep. Jan. 31, 1956*, ORNL-2057, p 114.

[4] D. E. Ferguson *et al.*, *HRP Quar. Prog. Rep. Oct. 31, 1954*, ORNL-1813, p 143–144.

[5] H. F. McDuffie *et al.*, *Reactor Sci. Technol.* 4(2), 23 (1954), TID-2013.

TABLE 15.1. COMBINATION RATES OF STOICHIOMETRIC HYDROGEN AND OXYGEN MIXTURES IN THORIUM OXIDE SLURRIES CONTAINING MoO_3 CATALYST

Slurry: 900°C calcined ThO_2, 1000 g of Th per kilogram of H_2O; 0.5 mole % $UO_3 \cdot H_2O$; MoO_3; heated for 3 hr at 280°C under O_2 (250–300 psi at room temperature)

MoO_3 Concentration (m)	Conditions	Temperature (°C)	k_π (hr^{-1})	H_2 Combination Rate P_{H_2} = 500 psi (moles/hr/liter)
0.05	As prepared	248	7	3
	Heated for 1.5 hr under H_2 at 270–280°C[a]	40	11	12
0.10	As prepared	276	3	1
	Heated for 1.5 hr under H_2 at 270–280°C[a]	115	21	16
	Reheated reduced slurry for 2 hr under O_2 at 270–280°C[b]	206	67	31
0.15	As prepared	281	21	5
	Heated for 1.5 hr under H_2 at 270–280°C[a]	243	25	9
	Reheated reduced slurry for 2 hr under O_2 at 270–280°C[b]	253	19	6
0.20	As prepared	264	27	10
	Heated for 1.5 hr under H_2 at 270–280°C[a]	160	16	10
0.1[c]	As prepared	256	71	28
	Heated for 1.5 hr under H_2 at 270–280°C[a]	135	16	12
	Reheated reduced slurry for 2 hr under O_2 at 250°C[b]	204	49	26

[a]1000-psi H_2 at room temperature.
[b]500-psi O_2 at room temperature.
[c]In a slurry of 900°C oxide containing 660 g of thorium per kilogram of H_2O; see ref. 3.

as indicated by this method were found to be essentially independent of temperature.

A new technique is being used to make viscosity measurements in the dash-pot-stirred bomb. The stirrer is operated in such a manner that it always starts a stroke from its rest position in the bottom of the bomb and is dropped (by energizing the bottom coil) as soon as it attains its maximum rise as shown on the oscilloscope used in monitoring the stirring operation. Hence a situation is attained in which the time required for an object in a fluid medium to travel a fixed distance under a reproducible force function can be measured. In the present instance the rise time is equal to the product of the cycle time (reciprocal frequency) and the per cent of cycle time that the upper coil is energized.

Calibration curves of kinematic viscosity vs stirrer rise time were prepared from data obtained with the use of water and silicone oils of known viscosity. The curves are linear and yield viscosity values for slurries similar to those reported above and in the last quarterly report.[1]

15.3.2 Slurry Viscosity Measurements with the Ultraviscoson

Slurry viscosity measurements were made with the Ultraviscoson (Bendix Corporation, Model 621) with the view of adapting it for slurry viscosity measurements at high temperatures and pressures.

TABLE 15.2. RELATIVE VISCOSITIES OF SOME THORIUM AND THORIUM-URANIUM OXIDE SLURRIES

Slurry	Average Relative Viscosity (centistokes)				
	Slurry Concentration (g of Th per kg of D_2O)				
	250	500	750	1000	1250
D-16 thorium oxide (650°C)	3.9	4.8	7.1	12.6	27.4
900°C refired D-16 oxide	3.6	4.2	5.0	8.5	13.7
900°C fired D-16 oxide–0.5% UO_3[a]	3.5	3.8	5.1	6.8	11.0
900°C fired D-16 oxide–0.5% UO_3[a] (93.14% enriched uranium)	5.3	6.8		18.2	
900°C fired ThO_2–0.5% UO_3[b]	3.4	3.9	5.3	9.7	20.7
900°C refired D-16, pumped; X-28[c]	4.1	5.5	11.0	20.0	

[a]D-16 ThO_2–$UO_3 \cdot H_2O$ wet-autoclaved overnight at 300°C; fired at 900°C for 4 hr.
[b]Prepared from coprecipitated Th-U(IV) oxalates (see ref. 1) by multistage firing ending at 900°C.
[c]Pumped for 100 hr at 300°C at a concentration of 1000 g of thorium per kilogram of H_2O (see V. D. Allred, E. V. Jones, and J. P. McBride, *HRP Quar. Prog. Rep. Jan. 31, 1956*, ORNL-2057, p 115–121).

The viscosities of slurries of D-16 thorium oxide (650°C calcination) containing 217 to 1250 g of thorium per kilogram of H_2O were measured over the temperature range 25 to 90°C (see Fig. 15.2).

Up to thorium concentrations of 625 g per kilogram of H_2O, the slurry viscosities were essentially the same as those of water over the temperature range studied. Above this concentration the viscosities increased with increasing slurry concentration. At 25°C and a thorium concentration of 1250 g per kilogram of H_2O, the measured viscosity was 6 centipoises. The viscosities decreased with increasing temperature, the rate of decrease being greater for the higher slurry concentrations.

The viscosity values determined with the Ultraviscoson were much lower than those obtained for similar slurries with a Brookfield viscometer,[6] presumably because the Ultraviscoson measures viscosity at much higher shear stress.

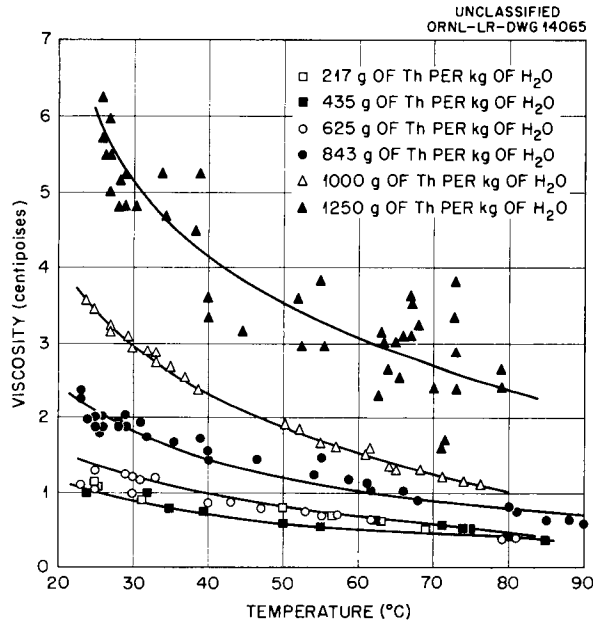

Fig. 15.2. Viscosity vs Temperature for Various Concentrations of D-16 ThO_2 Measured with the Ultraviscoson; Stainless Steel Probe, Rhodium Plated.

[6]C. E. Schilling, *HRP Quar. Prog. Rep. July 31, 1955*, ORNL-1943, p 194–196.

15.4 SLURRY CHARACTERIZATION AND PREPARATION STUDIES

V. D. Allred E. V. Jones
J. P. McBride

15.4.1 Settling Properties of Thorium Oxide Slurries

Previous reports[7-9] have indicated the desirability of a systematic study of the settling characteristics of thorium oxide slurries at the expected blanket operating temperatures. Such a study is of value not only for use in blanket design but also for the information which may be obtained on the effect of temperature on the flocculation and deflocculation characteristics of slurries, their redispersibility and settled-bed characteristics, and the effect of additives on slurry properties. Apparatus to carry out a study of the settling properties of slurries at elevated temperatures and pressures in a stainless steel container was constructed, and data are now being obtained on the settling properties of both pumped and unpumped slurries at temperatures up to 300°C.

In the equipment the settling slurry is continuously photographed by means of x radiography. Standard x-ray film is transported at a controlled speed past a vertical slot in a lead shield, behind which the slurry bomb and x-ray source are placed (Fig. 15.3). The bomb is heated in a block furnace containing a slot and is agitated by means of a pneumatic shaker. A typical radiograph of a settling slurry (oxide TO-10-900-24 at an initial concentration of 250 g of thorium per kilogram of H_2O and a temperature of 205°C) obtained with this device is shown in Fig. 15.4.

[7] V. D. Allred, E. V. Jones, and J. P. McBride, *HRP Quar. Prog. Rep. Jan. 31, 1956*, ORNL-2057, p 115–121.

[8] S. A. Reed, *HRP Quar. Prog. Rep. Jan. 31, 1955*, ORNL-1853, p 83–85.

[9] E. V. Jones, *HRP Quar. Prog. Rep. Oct. 31, 1955*, ORNL-2004, p 172–178.

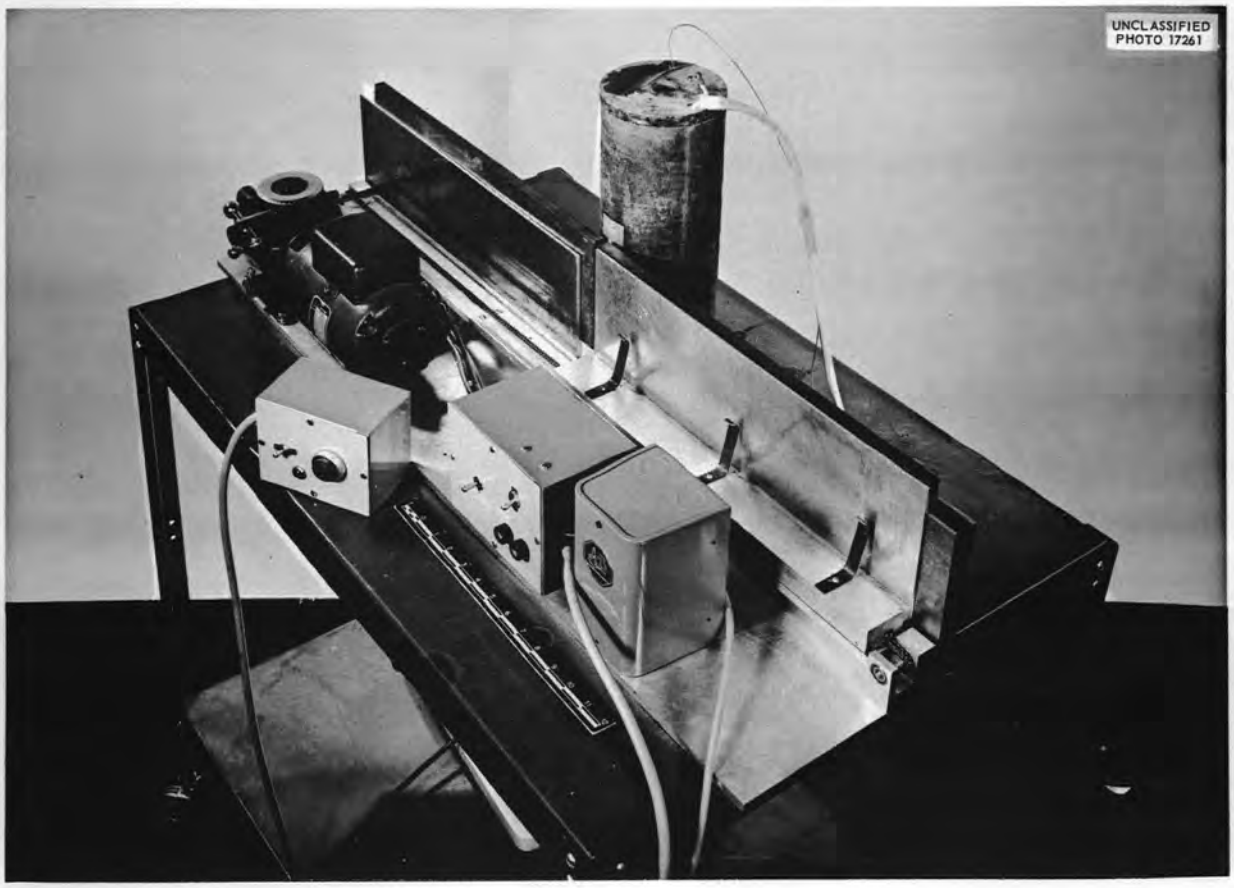

Fig. 15.3. Hindered-Settling Apparatus.

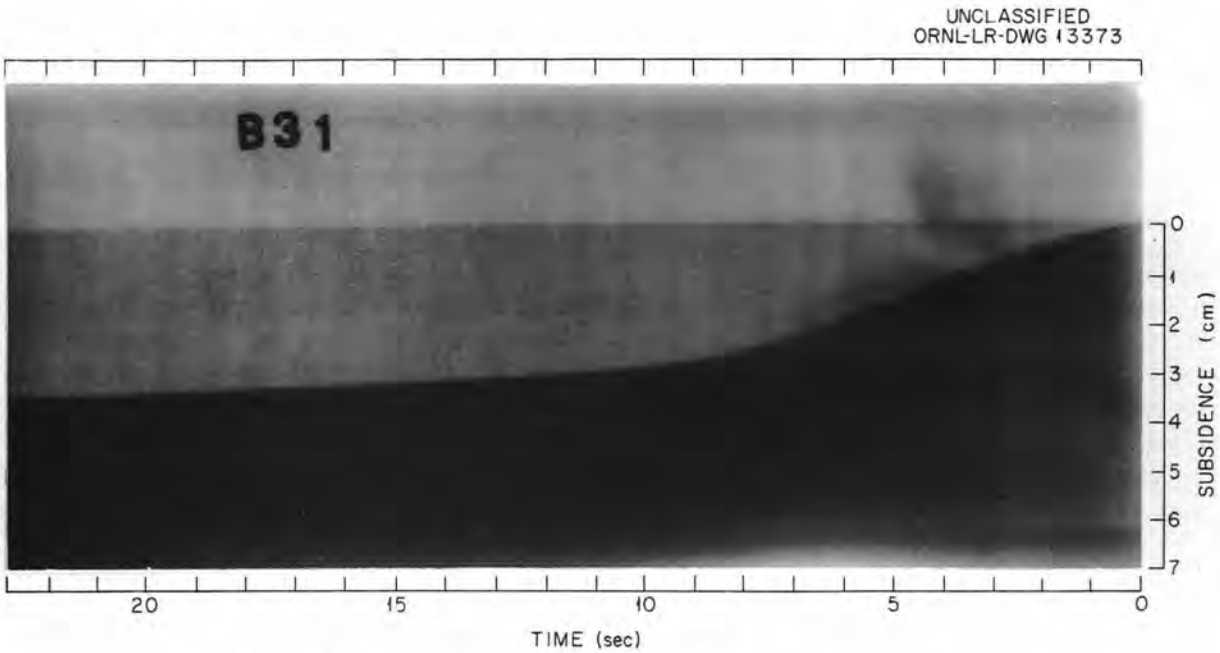

Fig. 15.4. Typical High-Temperature Hindered-Settling Curve.

Table 15.3 gives a summary of the initial settling-rate data obtained for a series of pumped oxides whose settling properties had previously been evaluated at temperatures up to 100°C in glass equipment.[7] The most important information obtained in these initial studies is that the pumped materials have critical concentrations[9] (i.e., the concentration at which a settling slurry enters compaction) of 500 to 700 g of thorium per liter. At a slurry concentration of 250 g of thorium per kilogram of H_2O, which is well below the critical concentration, the hindered-settling rate of oxide TO-10-900-24 increased markedly with increasing temperature from less than 0.2 cm/sec at 110°C to 0.66 cm/sec at 265°C.

From the hindered-settling data an apparent particle diameter corresponding to that obtained by the usual permeability technique was calculated by using an equation developed by DallaValle[7] (see Table 15.3). The fact that the particle diameter is constant with increasing temperature for a given slurry concentration indicates that the increase in the observed settling rate with temperature results primarily from a decrease in the viscosity of water with temperature rather than from a change in the flocculation characteristics of the slurry. The meaning of the decrease in the calculated particle size with an increase in the slurry concentration to 500 g of thorium per kilogram of H_2O is at present not understood, but it is probably associated with the fact that at this concentration the slurry is entering the compaction region.

15.4.2 Effect of Calcium Addition on Thorium Oxide

It has been shown that a densification of thoria ceramics can be attained by the addition of small amounts of calcium.[10] It was of interest therefore to determine whether or not thorium oxide for use in slurries could be made more dense by the addition of small amounts of calcium. It is conceivable that thoria particles so densified would be more resistant than the pure material to mechanical and chemical attrition. Results of preliminary experiments (Table 15.4 and Fig. 15.5) indicate that densification of slurry oxide can be obtained by calcium addition, and further study appears desirable.

The thorium-calcium oxide containing 1 mole % calcium for use in the study was prepared by coprecipitating the oxalates at 10°C and calcining for 24 hr at 400, 650, 800, 900, and 1000°C.

[10] J. R. Johnson and C. E. Curtis, *J. Am. Ceram. Soc.* 37, 611 (1954).

TABLE 15.3. HINDERED-SETTLING PROPERTIES OF SELECTED OXIDES

Oxide	Thorium Concentration (g per kg of H_2O)	Temperature (°C)	Hindered-Settling Rate[a] (cm/sec)	Calculated[b] Particle Size (microns)	Critical[a] Density (g of Th per kg of H_2O)	Settled Concentration (g of Th per kg of H_2O)	Remarks
TO-10-900-24[c] (pumped ~100 hr as V-8)	250	110	0.169	4.5	655		
	250	155	0.281	4.5	580		
	250	205	0.335	4.5	545		
	250	265	0.663	4.8	520	760	Settled at temperature for 90 min
	500	110	0.0061	1.2			
	500	158	0.0083	1.2			
	500	210	0.0116	1.2			
	500	265	0.0201	1.2		945	Settled at temperature for 90 min
	500					1345	Cooled to room temperature overnight; reheated to 265°C for 2 hr without stirring
D-16-900-24 (pumped ~100 hr as X-28)	250	265	0.650	4.9	545	735	Settled at temperature for 90 min
	250					1127	At 265°C for 3 hr at room temperature for 16 hr; reheated to 265°C for 2 hr without stirring
	500	196	0.055	2.5	660		
	500	265	0.136	3.3	665		
PO-10-900-24[c] (pumped ~100 hr as U-37)	250	100	0.154	4.5	470		
	250	150	0.325	4.8	460		
	250	200	0.462	4.8	420		
	250	265	0.560	4.6	460	615	Settled at temperature for 10 min
	500	97	0.0052	1.2			
	500	265				860	Settled at temperature for 90 min
	500					1040	Settled 2 hr at 265°C, then over weekend at room temperature; reheated to 265°C without stirring

[a]See ref. 9.

[b]$D_s \approx 4.15 \times 10^2 \left[\frac{U_0\mu}{\Delta\rho}\left(\frac{1-e}{e^3}\right)\right]^{1/2}$, (see ref. 7, p 120, where the constant "13" should be "130" and g_c is 980 cm/sec^2), where

D_s = apparent particle diameter, microns,

U_0 = hindered-settling rate, cm/sec,

$\Delta\rho$ = difference in densities of the oxide and the water, g/cm^3,

μ = viscosity, centipoises.

[c]See ref. 7.

Samples of the mixed oxide were taken for each calcination temperature and their properties determined.

Electron micrographs showed the mixed oxides to have the same characteristic cubical shape as the pure oxide has. The results of the sedimentation particle-size analysis were also very similar to those previously observed for the pure material.

Figure 15.5 shows the relation between the specific surface area and the crystallite size for similarly prepared pure oxide and mixed oxide. The product of surface area times crystallite size, πSD, shown in Table 15.4 has the same dimensions as specific volume (reciprocal density). As seen in Fig. 15.5, this value was decreased markedly for the mixed oxide, indicating that a densification occurred as a result of the 1700 ppm of calcium addition.

The settling data show that the slurry-settling rate was not markedly affected by the calcium

TABLE 15.4. SUMMARY OF CHARACTERISTIC PROPERTIES FOR ThO_2-CaO (1 mole % Ca)

Material*	Solid Characteristics				Suspension Properties						Remarks
	Crystallite Size (Å)	Specific Surface Area (m^2/g)	πSD ($\times 10^{-3}$)	Mean Particle Diameter (μ)	Hindered-Settling Rate** (cm/sec) at 27°C	50°C	75°C	98°C	Settled Concentration (g of Th per kg of H_2O)	pH of Supernatant	
TC-10-400-24	50	31.4	1.6								
TC-10-650-24	136	18.4	2.5								
TC-10-800-24	269	9.2	2.5								
TC-10-900-24	425	6.0	2.5	1.0	0.0234	0.0312	0.0315	0.0554	1340	10.3	
TC-10-1000-24	745	4.7	3.5	1.1	0.0167	0.0240	0.0324	0.0428	1315	10.1	
TO-10-900-24	550	6.3	3.5	1.3	0.0604		0.0330	0.0468	1090	9.8	Pure oxide
TC-10-900-24 autoclaved at 800°C for 22 hr					0.0103				1510	9.6	Ca^{++} in supernatant <50 μg/ml (less than 6% of total)
TC-10-1000-24 autoclaved at 300°C for 22 hr					0.0214				1390	9.4	Ca^{++} in supernatant <20 μg/ ml (less than 2.3% of total in suspension

*The first number in the series indicates the oxalate precipitation temperature (in °C); the second number, the final firing temperature (in °C); and the last number the firing time (in hours) at temperature.

**At a concentration of 500 g of thorium per kilogram of H_2O.

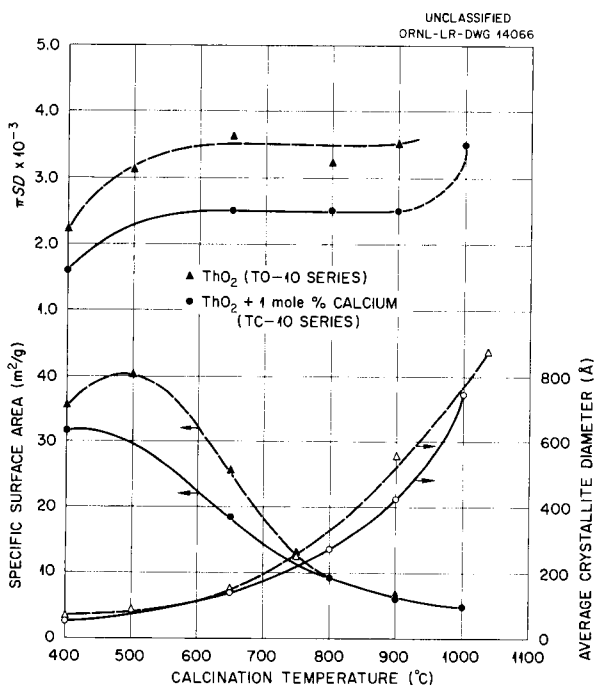

Fig. 15.5. Effect of Calcium Addition on Properties of Thorium Oxide.

addition. This is consistent with the results of the particle-size analysis. In addition the settled concentration of the mixed oxide increased; this higher concentration is compatible with the apparent densification of the oxide particles.

Autoclaving at 300°C an aqueous slurry of the mixed oxide containing a thorium concentration of 500 g per kilogram of H_2O resulted in the dissolution of a maximum of 6% of the total calcium contained in the solid and did not impair the handling properties of the suspension.

15.5 SOL STABILITY STUDIES[11]

Sols with ThO_2/NO_3^- mole ratios as high as 6.3/1 have been obtained by dialysis of thorium nitrate solutions adjusted to pH 3.6 with ammonium hydroxide. No extended stability tests have yet been made. One sol, fluid at the boiling point of water, was charged to a bomb and held at 300°C for seven days. It was charged as a paste at room temperature with a ThO_2 concentration of 529 g per kilogram of H_2O. The bomb leaked and the recovered thoria had the appearance of a dried

[11]Work done at Houdry Process Corporation.

gel. The solid redispersed immediately in water to an opalescent sol, which had a concentration of approximately 40 g per kilogram of H_2O and showed no signs of sedimentation on standing for two weeks.

Studies of the production of thoria sols by the use of anion exchange indicated that the limited capacity of the beds and the difficulty in controlling precipitation in the beds make them undesirable for use in making concentrated sols. However, it is possible that anion exchange may be useful in replacing the initial ion with other stabilizing ions in sols produced by other means.

15.6 ThO_2 DISSOLUTION[12]

Thorium oxide dissolving tests have established minimum acid concentrations of 0.03 *M* HF and 2.0 *M* final free HNO_3 as being required for producing 1.5 *M* thorium solution from simulated blanket solids calcined at 800°C. It was found that these concentrations resulted in complete solution of a charge of solids in less than 4 hr at reflux conditions but that decreasing the excess HNO_3 to 1.0 *M* or decreasing the HF to 0.02 *M* each failed to give complete solution after 6 hr. The rate was accelerated by increasing the HNO_3 concentration to 4 *M* excess (with 0.04 *M* HF), giving a dissolving time of 30 min. Further increases in acid concentrations were attended by rapid attack of the stainless steel reaction vessel. Dissolving rates of the solids were not significantly decreased by the addition of UO_2SO_4 and corrosion products in the proportions which would result from drying equal volumes of spent core solution and blanket slurry at 300°C. Tests with such a mixture indicated that 0.04 *M* HF and 2.0 *M* free HNO_3 gave complete solution in 4 hr.

[12]Work done at Vitro Laboratories.

16. FUEL PROCESSING

D. E. Ferguson E. O. Nurmi
R. W. Horton R. A. McNees S. Petersen

16.1 FISSION-PRODUCT CHEMISTRY

16.1.1 Iodine Chemistry

The valence-state distribution of iodine in uranyl sulfate solutions at 250°C was affected by the composition of the gas phase above the solution. With 0.02 *m* UO_2SO_4–0.005 *m* H_2SO_4 solutions at 250°C and under an initial oxygen pressure of 200 psi at room temperature, the free/combined iodine ratio was 9/1. Addition of 15-psi hydrogen to 200-psi oxygen (room temperature) increased the ratio at 250°C to 12/1. When 50-psi hydrogen and only 100-psi oxygen was used, the ratio dropped to 8/1. The experimental data were considerably more scattered with mixtures of hydrogen and oxygen than with oxygen alone.

Ruthenium sharply decreased the free/combined iodine ratio at 250°C from 9/1 to 0.1/1. This effect was noticed when ruthenium was initially present in solution or in the film on the surfaces of the stainless steel equipment used for the experiment. In the latter case complete defilming of the equipment was necessary before the original ratio (9/1) could be obtained even without adding ruthenium. The effect of ruthenium could be partially offset by the presence of either hydrogen or stainless steel, which suggests that a higher valence state of ruthenium was responsible for the effects noticed. Transfer of iodine at 250°C from uranyl sulfate solutions to silver in the vapor phase was also inhibited by the presence of ruthenium in the solution.

Experimental evidence was obtained which indicates that the reaction between silver and iodine is not an irreversible reaction at 250°C. Transfer of iodine from silver to solution through the gas phase was observed, and exchange of iodine between silver and solution was practically complete at 250°C in a few hours.

16.1.2 Iodine-Removal Development Studies[1]

Final fabrication steps and pressure testing of the 1000-psi ejector loop were completed, and preliminary runs were made with water and nitrogen overpressure at 270°C. Liquid and gas flows through the ejector were estimated from orifice meter measurements (corrected for loop temperature and pressure) as 0.69 gpm and 0.0235 lb/min, respectively. A batch scrubber with provision for periodic sampling was installed in the gas loop to take up iodine from the strip gas.

The characteristics of gas and liquid flow through the ejector were observed in a preliminary run at room temperature and atmospheric pressure. The jet was unstable when the gas inlet was not throttled; this resulted in a fluctuating suction pressure and inefficient gas pumping. Some fluctuation of gas pressure was observed at 270°C, but a complete study of the flow characteristics at high temperature has not yet been made.

Bench-scale experiments demonstrating the use of neutral water and dilute Ag_2SO_4 solutions to scrub iodine from a gas stream were concluded. In one test iodine vapor was absorbed with water, and the reaction was followed by periodic sampling of the batch scrubber and effluent gas streams. The scrubber functioned with approximately 98% efficiency until an iodine concentration of 0.0076 g/liter was reached in the scrub liquid, at which time the efficiency decreased noticeably.

Silver ion in the scrubber solution greatly extended the capacity and efficiency of the unit by precipitating dissolved iodine immediately as AgI. An absorber using dilute Ag_2SO_4 functioned with virtually 100% efficiency until all the silver ion was precipitated. The use of silver solution in a reactor system would, of course, require elaborate precautions against possible entrainment in the gas being recycled to the fuel stripper. In a static experiment all iodine charged to a bomb containing 0.1 *M* NaOH at 260°C was found in the liquid phase as IO_3^- ion. Solutions of NaOH are thus attractive as scrubbing agents for an iodine-bearing strip gas under the same limitations as for Ag_2SO_4, offering high decontamination factors but requiring effective isolation from the fuel system.

As an adjunct to the preparation of a conceptual flowsheet for vapor-phase iodine processing of a

[1]Work done at Vitro Laboratories, KLX-10026 (to be issued).

full-scale reactor, as well as to provide a basis for understanding the behavior of iodine in the HRT, additional measurements of vapor-liquid and valence distribution coefficients are being made to substantiate data previously reported.[2] In tests to date the equilibrium distribution coefficient (mole fraction of I_2 in vapor to mole fraction of I_2 in liquid) in fuel solution at pH 2.1 has been found consistently in the range 6 to 12. No significant variation with temperature in the range 260 to 330°C or with oxygen overpressure was observed. The tendency of elemental iodine to partition in favor of the liquid phase in neutral-water solution is significantly greater, yielding gas-to-liquid distribution constants in the range 0.2 to 0.5.

The valence state of iodine in uranyl sulfate solution shows little dependence on temperature and is approximately 7 to 1 in favor of the elemental form at 260 to 330°C; increased oxygen pressure appears to favor the elemental state. In runs in which no oxygen overpressure was added to the vessel, some iodine (initially charged as iodide ion) remained in the −1 state. The ratio of elemental to ionic forms of iodine was in the range of 1.0/1 to 2.2/1 in neutral-water solutions and in simulated fuel (pH 2.1) at low temperatures or low oxygen pressures. Ratios as high as 9.2/1 were obtained in fuel solution at 310°C and 570-psi oxygen.

16.1.3 Selenium

Selenium dissolved in simulated reactor fuel to the extent of 50 to 250 mg per kilogram of H_2O. With as much as 250 mg of selenium per kilogram of H_2O present in 0.02 *m* UO_2SO_4–0.005 *m* H_2SO_4 solutions heated at 300°C in quartz tubes, there was always a precipitate. Precipitates were larger for Se(IV) than for Se(VI). Under the same conditions there was no precipitate if only 50 mg of selenium per kilogram of H_2O was present.

16.1.4 Antimony

Similar experiments with antimony indicated a maximum solubility of less than 500 mg of antimony per kilogram of H_2O. Tracer experiments showed that at 275°C the amount of antimony remaining in solution was only 20 ± 5 mg of antimony per kilogram of H_2O.

16.1.5 Niobium

Hydrous niobium oxide suspended in simulated fuel solution gave no indication of dissolving at 300°C. However, at 250 to 300°C there was a slow transition from a gelatinous to a crystalline solid. Upon cooling, the crystalline material slowly reverted to an amorphous form.

16.1.6 Technetium

Technetium in the heptavalent state was very soluble; in the tetravalent state it was only slightly soluble. At 275°C, with a hydrogen atmosphere over the solution, Tc(VII) was reduced and TcO_2 precipitated, leaving in solution only 12 mg of technetium per kilogram of H_2O. The uranium also precipitated. When TcO_2 was suspended in simulated fuel solution at 250°C, it did not dissolve when the atmosphere above the solution was 20% oxygen. However, at 250°C with greater than 90% oxygen, it dissolved rapidly to give a solution containing 9.7 g of technetium per kilogram of H_2O.

16.1.7 Rhenium

In comparing rhenium with technetium it was found that Re(VII) was not reduced and precipitated under the conditions that resulted in precipitation of TcO_2. Uranium did not precipitate under a hydrogen atmosphere in the presence of Re(VII) as it did when Tc(VII) was present.

16.2 REACTOR SOLIDS DISSOLUTION

In further studies on the dissolution of reactor-formed solids, such dissolution being necessary to avoid the necessity of handling radioactive solids and to obtain a representative sample, 10.8 *M* H_2SO_4 was a satisfactory solvent.

Following operation of the hydroclones in the HRT Chemical Plant, the solids accumulated in the underflow pot will be resuspended in fuel solution and a sample taken. Since the reliability of sampling a slurry under these conditions is doubtful, complete dissolution of the collected solids is desirable to obtain a representative sample. The composition of the solids dissolved ranged from practically pure simulated fission-product solids to solids consisting of 90% corrosion products. The solids had been subjected to treatment ranging from no heating to drying at 300°C. Aging, for seven days at 300°C in fuel

[2] H. F. Reichard *et al.*, *Homogeneous Reactor Fuel Reprocessing, Quarterly Progress Report, July 1–September 30, 1955, Job 1087*, KLX-10012 (Nov. 15, 1955).

solution, of mixtures simulating those expected from reactor and chemical plant operation did not decrease the effectiveness of this acid. Solids taken from loops at Y-12 after hundreds of hours of operation were also satisfactorily dissolved.

The rate of dissolution was high unless the dried solids had been fired above 300°C. With a ratio of 30 ml of acid to 100 mg of solid, the reaction was essentially complete after 30 min at 165 to 170°C. Thirty milliliters of this acid dissolved, when used in three successive 10-ml portions, 1 g of simulated solids which contained 90% Zircaloy-2 corrosion products and which had been aged for one week at 300°C. A 0.4 *M* chromous sulfate–1.0 *M* sulfuric acid treatment of this material gave only 6% dissolution when 100 mg of solids was treated with 30 ml of reagent.

Dilute nitric acid was more effective than concentrated acid for leaching the uranium contained in such solids. For typical simulated reactor solids containing 0.2% uranium, 3 *M* HNO_3 dissolved 25% of the uranium but less than 5% of the gross solids present. The addition of $(NH_4)_2Ce(NO_3)_6$ to 2.3 *M* HNO_3 increased the leaching action of the acid and, after 20 hr of refluxing, dissolved 60 to 70% of the uranium while dissolving only 15% of the solids. Two molar H_2SO_4 with $Ce(HSO_4)_4$ gave approximately the same results, but chromous sulfate leached almost none of the uranium from the solids.

17. PLUTONIUM-PRODUCER BLANKET PROCESSING

D. E. Ferguson
J. M. Chilton
P. A. Haas
E. O. Nurmi
S. S. Kirslis
R. E. Leuze

The study of plutonium chemistry included adsorption of plutonium on metals, plutonium solubility in UO_2SO_4-Li_2SO_4 solutions, and in-pile experiments. A titanium-lined hydroclone and a pump were tested on loop T-1. A facility for housing loops used in testing plutonium-producer blanket processing is being designed.

17.1 ADSORPTION OF PLUTONIUM ON METALS

Experimental determination of plutonium adsorption on titanium, Zircaloy-2, and type 347 stainless steel as a function of time and plutonium concentration under simulated reactor conditions was only partially successful. There was considerable variation in results under apparently identical experimental conditions. This variation was probably the result of a difference in the amount and nature of the oxide film on the metal adsorption coupons even though they were machined from the same stock and were handled in the same manner. The least deviation was obtained for titanium; the deviations for Zircaloy-2 and type 347 stainless steel were great enough to mask, partially or even completely, the adsorption dependence on a plutonium concentration and exposure time (Fig. 17.1).

The amount of plutonium adsorbed increased with increasing time and increasing plutonium concentration. These data and similar data at other plutonium concentrations up to 3 mg per kilogram of H_2O and other times up to 160 hr can be approximately expressed by the equation

$$(1) \qquad A(\mathrm{Ti}) = 0.01\, C^{2/3} t^{1/2} ,$$

where A(Ti) is plutonium adsorption on titanium in $\mu g/cm^2$, C is the dissolved plutonium concentration in mg/kg of H_2O, and t is the exposure time in hours. This equation is useful only in determining the order of magnitude of plutonium adsorption. In a total of 104 experiments, the observed values differed from calculated values by a factor of more than 4 in 15% of the cases and by a factor of more than 2 in 25% of the cases.

Plutonium adsorption was greater on Zircaloy-2 than on titanium under the same conditions. Plutonium adsorption on Zircaloy-2 increased with time in about the same manner as on titanium. These data indicate that plutonium adsorption does not increase uniformly with plutonium concentration; however, this is probably a result of masking due to differences in oxide film on the metal. By assuming the same form of equation as for titanium, the adsorption of plutonium on Zircaloy-2 may be expressed approximately by

$$(2) \qquad A(\mathrm{Zr\text{-}2}) = 0.03\, C^{2/3} t^{1/2} .$$

The units are the same as in Eq. 1. In a total of 86 experiments, the values differed from calculated values by a factor of more than 4 in 25% of the cases and by a factor of more than 2 in 35% of the cases.

Results of experiments on plutonium adsorption on type 347 stainless steel indicated that the amount of plutonium adsorbed is proportional to the exposure time instead of to the square root of the exposure time.

The experiments were made with different plutonium concentrations, low enough to prevent

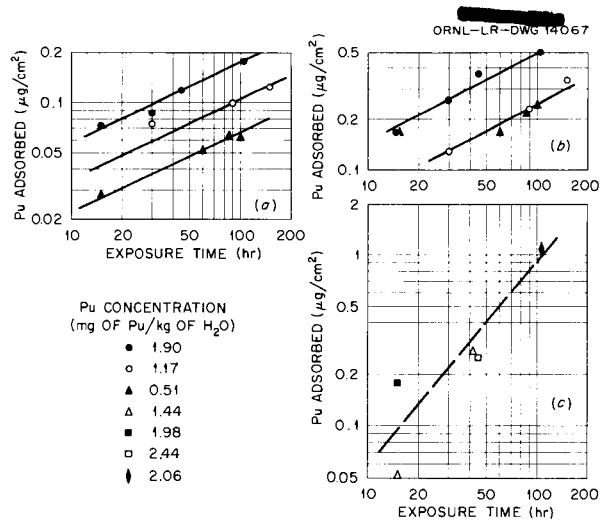

Fig. 17.1. Plutonium Adsorption from 1.4 *m* UO_2SO_4 on (*a*) Titanium, (*b*) Zircaloy-2, (*c*) Type 347 Stainless Steel.

PuO_2 precipitation, and for different exposure times. All other conditions were held constant. The metal samples were heated to 250°C in 1.4 *m* UO_2SO_4 contained in a pyrex-lined autoclave under 90-psi oxygen and 180-psi hydrogen pressure. All coupons of each metal were machined from the same stock in an effort to eliminate metal differences.

The importance of the oxide film on the metals was evidenced by the fact that titanium pretreated in 1.4 *m* UO_2SO_4 at 250°C under air for 16 hr adsorbed 20 times as much plutonium as did the untreated titanium. Zircaloy-2 pretreated in this manner adsorbed 7 times as much plutonium as did the untreated Zircaloy-2. Titanium and Zircaloy-2 pretreated similarly under 90-psi oxygen and 180-psi hydrogen adsorbed about the same amount of plutonium as the untreated metal did. These adsorption tests were made in 1.4 *m* UO_2SO_4 containing 1.3 mg of plutonium per kilogram of H_2O. The solution was heated to 250°C in a pyrex-lined autoclave under 190-psi hydrogen and 95-psi oxygen.

These results indicate that the surface condition of the metal is a major variable. To understand plutonium adsorption and to estimate the amount of plutonium adsorbed in an operating reactor, the nature of the oxide film must be understood.

17.2 SOLUBILITY OF PLUTONIUM IN URANYL SULFATE–LITHIUM SULFATE SOLUTIONS

Results of plutonium solubility measurements in 4.0 *m* UO_2SO_4–4.0 *m* Li_2SO_4 at 250°C varied considerably. The solubility of Pu(IV) was quite low and varied from 8 to 20 mg per kilogram of H_2O. When a solution containing 4.0 *m* UO_2SO_4–4.0 *m* Li_2SO_4 and 4.7 g of plutonium per kilogram of H_2O was heated under 200-psi oxygen at 250°C for 24 hr, part of the plutonium was oxidized to Pu(VI); the total plutonium remaining in solution was 40 to 50 mg per kilogram of H_2O. Under these conditions, but with 0.1 *m* chromium added, there was more oxidation to Pu(VI), and the total plutonium in solution was 130 and 220 mg per kilogram of H_2O in duplicate tests. When acid was added to the solution, the solubility of Pu(IV) was increased. For a solution containing 0.1 *m* chromium and 0.05 *m* H_2SO_4, the soluble plutonium was 350 mg per kilogram of H_2O, and, when the acid was increased to 0.1 *m*, the plutonium solubility was 520 mg per kilogram of H_2O. Since these results were obtained in single scouting experiments, they do not necessarily represent exact solubilities. However, they do indicate that it is difficult to keep enough plutonium in solution for a single-region plutonium burner reactor.

17.3 IN-PILE CHEMISTRY OF PLUTONIUM AND NEPTUNIUM

The results of an experiment in which 1.43 *m* UO_2SO_4 (natural uranium) containing 0.010 *m* $CuSO_4$ was irradiated in the LITR at 250°C are in doubt because of handling and analytical difficulties. After 10 days of irradiation, less than 1% of the plutonium and less than 2% of the neptunium were found as a loose precipitate. Most of the plutonium and about half the neptunium were found on the titanium bomb walls. The rest of the neptunium and plutonium remained in solution. Preliminary indications are that about 15 mg of plutonium per kilogram of H_2O remained in solution. This is 5 times the solubility measured in out-of-pile experiments.

The experimental difficulties were primarily due to inadequate facilities for handling highly radioactive materials and to the formation of peroxide during a 30-hr decay period when the solution was at room temperature. The inadequate facilities made it impossible to thoroughly wash the bomb walls. It is possible that some of the plutonium and neptunium reported found on the bomb walls was held there in a fairly loose UO_4 precipitate. For plutonium and neptunium analyses the interference of certain short-lived fission products was not anticipated. As a result the initial analytical results were incorrect, and all calculations were based on analyses run after most of the neptunium had decayed. This resulted in considerable error, since results were corrected back to the time of bomb removal from the reactor. In the near future adequate shielded facilities will be available.

17.4 PROCESS TESTING LOOPS

17.4.1 Equipment Tests

Test loop T-1 has operated for 700 hr at over 250°C with 1.4 *m* UO_2SO_4–0.3 *m* H_2SO_4. About 650 hr of this time was at 255 to 260°C. Inspection at the end of 350 hr showed no attack on the all-titanium hydroclone or on other titanium

components. The type 347 stainless steel at the back of the pump scroll case showed severe attack and was the source of 3.4 g of nickel in the loop solution (Fig. 17.2). Despite this corrosion, operation of the pump was trouble-free throughout the 700 hr, with 600 hr of this time at 74 to 90 cps. There were no detectable changes in the pump bearing or rotor dimensions after 400 hr of operation. This pump is the original 2000-psi ORNL canned-rotor design with a single graphite bearing, and is mounted in a vertical position with the head end downward.

Components are being fabricated for loop P-1, which is designed for dynamic out-of-pile studies of plutonium behavior under HRT blanket conditions. A major problem is supplying hydrogen and oxygen to represent these gases as normally present in a blanket from radiolytic decomposition of water. Present data indicate that an addition of 1 ft^3 (STP) of hydrogen and 0.5 ft^3 (STP) of oxygen per shift will give a cycle of 150 to 50 psi oxygen overpressure and 300 to 100 psi hydrogen overpressure. The UO_2SO_4 solution will catalyze the recombination of the gases at this rate even though no copper catalyst is used.

A prototype pressurizer is being fabricated to permit tests of the danger of detonation of the oxygen and hydrogen gas in the pressurizer. A spark or a resistance heater will be used to initiate the reaction. The proposed loop pressurizer is designed to promote thorough contacting of the vapor by the entering liquid stream and thus avoid segregation of the explosive gas mixture. A blast shield is designed to contain the metal fragments

PHOTO-17271

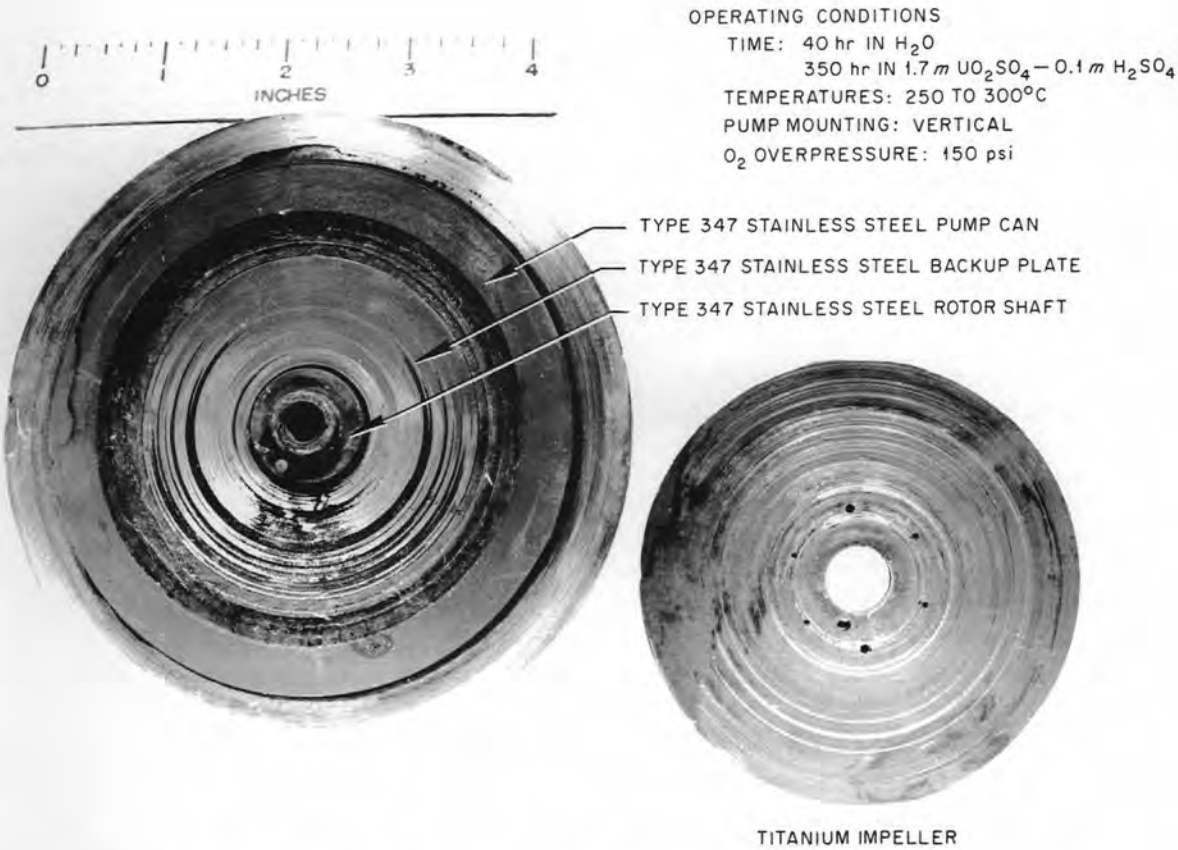

Fig. 17.2. ORNL 2000-psi Canned-Rotor-Pump Components After Use on Loop T-1.

from a pressurizer failure and prevent their rupturing the outer loop can.

Prototypes of loop components are being tested, where necessary, to establish design parameters. Flow restrictors to give a 100-ft pressure drop at 100 gpm were tested and found to give the design value. The over-all coefficient for air cooling of the loop is being determined in a test heat exchanger.

17.4.2 Plutonium-Producer Blanket Processing Loop Facility

A facility for housing all future plutonium-producer blanket processing loops is being designed for the basement area in Building 4501. This facility will contain radioactive material in case of a major loop failure and includes separate ventilation and off-gas systems. Construction drawings are being prepared by the ORNL Engineering Division, and much of the equipment has been requisitioned.

18. EQUIPMENT DECONTAMINATION

D. E. Ferguson

R. E. Leuze R. D. Baybarz

The object of the homogeneous reactor equipment-decontamination program is to develop methods for removing fission products and plutonium deposited on metal surfaces in the reactor or chemical plant. Strong reducing agents such as chromous sulfate, titanous chloride, stannous chloride, and nascent hydrogen were previously reported[1] to be effective for removing the oxide film deposited on stainless steel by contact with uranyl sulfate solutions at 250°C. Chromous sulfate in dilute sulfuric acid is considered the most promising reagent for decontaminating homogeneous reactor and process equipment. It removes the oxide scale from titanium, stainless steel, and Zircaloy; it dissolves these oxide scales, with the exception of ZrO_2; it dissolves adsorbed plutonium and fission products; and it contains no materials that would interfere with reactor operation if not completely removed from the system.

18.1 OXIDE SCALE REMOVAL

The effectiveness of chromous sulfate solutions was shown by satisfactorily removing large amounts of corrosion oxides from type 347 stainless steel test loops that had been operated for several years with UO_2SO_4 solutions at temperatures above 250°C. After the loops had been treated for 4 hr with 0.4 *M* $CrSO_4$–0.5 *M* H_2SO_4 at 85°C, essentially all the oxide was removed and the metal surfaces were clean. Some of the oxide was removed as a fine suspension. Complete dissolution was not obtained because of either insufficient chromous ion or insufficient acid, since all solids were dissolved when treated with a fresh solution. Corrosion rates during descaling of the loop were several hundred mils per year compared with about 10 mpy determined in a number of static corrosion tests. The reason for this difference is not known; however, such corrosion rates are not serious since only 4 hr is required for complete descaling. (For additional data concerning loop descaling, refer to Sec. 11.1.2.)

In laboratory tests with metal coupons, oxide film removal in a reasonable time required that the solution be at least 0.2 *M* in H_2SO_4. The oxide removal rate increased markedly with increasing H_2SO_4 concentration up to 0.5 *M* H_2SO_4. At higher concentrations the rate of oxide removal was slightly greater, but corrosion of the base metal also increased.

At 23°C a solution containing 0.4 *M* $CrSO_4$–1.0 *M* H_2SO_4 converted the oxide film on type 347 stainless steel to a loosely held oxide in 2 hr and completely dissolved the film in 12 hr. At 87°C the oxide film was completely dissolved in 2 hr. Temperatures above 100°C cannot be used, since the chromous ion at such temperatures is oxidized by water to release hydrogen.

18.2 DECONTAMINATION

A 3-in. length of ½-in.-IPS stainless steel pipe from an in-pile loop (see Sec. 13.1.2) was decontaminated from 25 r/hr to 0.9 r/hr by contacting it with 0.4 *M* $CrSO_4$–0.5 *M* H_2SO_4 at 85°C for 2 hr. Essentially all the remaining activity was from neutron-induced activity in the stainless steel. About 80% of the gamma activity removed by the chromous sulfate solution was zirconium and niobium; the rest was primarily ruthenium and cesium. A small amount of white ZrO_2, which probably came from Zircaloy-2 corrosion samples, did not dissolve in the chromous sulfate solution.

Contaminated type 347 stainless steel coupons were decontaminated from 750 to 1000 mr/hr to 4 mr/hr, and 97 to 99.7% of the plutonium was removed, by treating them with 0.4 *M* $CrSO_4$–0.5 *M* H_2SO_4 for 2 hr at 23°C. The oxide film was converted to a loosely held oxide, which was washed away with a stream of water. The same reagent at 85°C completely dissolved the oxide film in 2 hr and reduced the activity from 500 to 800 mr/hr to 35 mr/hr. More than 99.9% of the plutonium was removed, and in some cases plutonium decontamination factors were as high as 10^5. Apparently some of the active material was dissolved and replated on the base metal, since a 10% NaOH–2.5% sodium tartrate–2.5% H_2O_2 solution rapidly reduced the 35 mr/hr to 2 to 3 mr/hr.

[1] D. E. Ferguson, R. D. Baybarz, and R. E. Leuze, *HRP Quar. Prog. Rep. Jan. 31, 1956*, ORNL-2057, p 128.

Contaminated titanium and Zircaloy-2 coupons were decontaminated from 120 to 130 mr/hr to 3 mr/hr by a 2-hr contact with 0.4 *M* $CrSO_4$–1.0 *M* H_2SO_4 at 87°C. Ninety-eight per cent of the adsorbed plutonium was removed.

The coupons were contaminated for use in the tests by a 100-hr contact at 250°C with 1.7 *m* UO_2SO_4 solution containing mixed fission products and 90 mg of plutonium per kilogram of H_2O. The atmosphere over the solution was 350-psi oxygen.

Part VI

SUPPORTING CHEMICAL RESEARCH

E. H. Taylor

19. AQUEOUS SYSTEMS AT ELEVATED TEMPERATURES

C. H. Secoy

F. E. Clark F. J. Loprest
J. S. Gill W. L. Marshall
R. Slusher

19.1 CONCENTRATED SALT SOLUTIONS FOR REACTOR FUEL MEDIA OR HEAT EXCHANGER FLUIDS

F. J. Loprest W. L. Marshall C. H. Secoy

It has been suggested that aqueous salt solutions might be of interest as heat transfer agents for use in nuclear reactors. Presumably, by dissolving a salt in water, the vapor pressure of water could be lowered sufficiently so that power removal operations could be carried out at higher temperatures and still not exceed a particular maximum pressure limitation. The higher operating temperature would result in greater thermodynamic efficiency, provided that other properties of the water-salt system were favorable or, if unfavorable, were offset by the higher available temperature.

It is perhaps possible that concentrated aqueous salt solutions could be adapted for use in homogeneous reactors utilizing either solutions or slurries. For example, soluble uranium salts could be dissolved in a high-concentration aqueous salt solution to produce a final solution of low vapor pressure. Such a system might also alleviate the problem of hydrolytic precipitation in very dilute uranyl salt solutions. As another alternative, concentrated aqueous salt solutions could well provide stable media for the suspension of insoluble UO_3 or ThO_2 to form slurries capable of fueling a reactor.

There is a good possibility that aqueous-salt heat-transfer systems will be radiation- and thermally stable as contrasted to the radiation and thermal decomposition of organic liquids, that is, diphenyl and others, at high temperature. In comparison with fused salt systems, which are solids at room temperature, aqueous salt solutions can be selected which are liquid from 25°C to temperatures above 400°C. In addition an appreciable concentration of moderator is present as hydrogen or deuterium constituents of water, thus providing suitable conditions for thermal reactors.

The purpose of this investigation was to select and explore several aqueous salt systems with respect to vapor-pressure lowering. The following factors were considered in their selection: The salt selected must show a sufficiently high solubility in water throughout the high temperature range to achieve the desired vapor-pressure lowering. It is desirable, but not necessary, that the water-salt system be liquid at room temperature. The salt must have sufficient thermal and radiation stability in water for satisfactory use, and the nuclide components of the salt must have low-neutron-absorption cross sections and must not produce highly radioactive daughter nuclides. In addition, the usual properties of heat exchanger fluids, such as viscosity, heat capacity, thermal conductivity, and density, must be considered.

With these factors in mind, several aqueous salt systems were selected for vapor-pressure measurements. These systems were (1) 3.8 m Li_2SO_4 plus 3.8 m UO_2SO_4 (combined solution), (2) Li_2SO_4 (saturated), (3) $MgSO_4$ (saturated), (4) 50.0 wt % $LiNO_3$, and (5) several $Ca(NO_3)_2$ solutions.

The experimental data were obtained by direct measurement of vapor pressure with the use, in most of the runs, of a precision Heise pressure gage. Data for the systems of interest are comparatively shown in Tables 19.1 and 19.2 and in Fig. 19.1. Experimental data were obtained at every 2 to 5°C interval; however, in Fig. 19.1 and in the tables, only the data at approximately 10°C intervals are given. The actual vapor pressure can be obtained by multiplying the ratio, p/p_0, where p is the experimental pressure of the solution and p_0 is the saturated steam pressure, by the vapor pressure of saturated steam at the particular temperature.

The data indicate no large changes of p/p_0 as a function of temperature, at least up to 400°C. It is not certain at this time whether the small changes of p/p_0 with temperature for each particular curve are significant or whether they are due to inaccuracies arising from experimental techniques. The solution concentrations are those at room temperature and do not represent the true concentration at the high temperature. The high-temperature concentrations, however, should not

TABLE 19.1. VAPOR-PRESSURE DATA FOR SEVERAL SALT–WATER SYSTEMS

50.0 wt % $LiNO_3$ (14.5 *m* or 0.207 mole fraction)		3.8 *m* Li_2SO_4 3.8 *m* UO_2SO_4		$LiSO_4$ (sat.)		$MgSO_4$ (sat.)	
t(°C)	p/p_0*	t(°C)	p/p_0	t(°C)	p/p_0	t(°C)	p/p_0
214	0.407	220	0.71	240	0.97	225	0.92
220	0.407	225	0.70	245	0.90	235	0.92
225	0.405	230	0.73	248	0.88	245	0.91
230	0.402	240	0.72	250	0.91	256	0.98
234	0.401	245	0.73	252	0.94	260	0.96
238	0.399	250	0.74	260	0.95	262	0.97
243	0.399	255	0.75	265	0.96	267	0.95
250	0.399	260	0.75	270	0.97	275	0.94
254	0.405	270	0.78	275	0.98	281	0.96
259	0.403	275	0.79				
270	0.407	280	0.81				
275	0.406	285	0.81				
280	0.408						

*p_0 = pressure of saturated steam (Osborne and Myers, U. S. Bureau of Standards); p = experimental pressure of the solution.

differ from the room temperature value by more than several per cent at the highest temperature.

In Fig. 19.2, p/p_0 measured at 350°C is plotted as a function of the mole fraction of $Ca(NO_3)_2$. A mole fraction of 0.2 corresponds to the stable solid hydrate, $Ca(NO_3)_2 \cdot 4H_2O$, at room temperature. This solid melts at 42.7°C to form a liquid which is apparently stable to above 400°C. A slight orange-red vapor-phase coloration is observable in sealed silica tubes in the temperature range 450 to 500°C, thus indicating some decomposition of the nitrate to nitrogen oxides. Lithium nitrate–water solutions apparently are as stable as $Ca(NO_3)_2 \cdot H_2O$. A 50.0 wt % $LiNO_3$ solution is liquid from room temperature to above 400°C.

Figure 19.3 indicates the possible increase in operating temperature for $Ca(NO_3)_2 \cdot 4H_2O$ liquid over that of pure water at a particular temperature and pressure. For example, for a pressure of 2398 psi, $Ca(NO_3)_2 \cdot 4H_2O$ liquid could be used at 412°C, 72°C above the temperature at which water has the same vapor pressure. Since the line in Fig. 19.3 is essentially straight, it can be represented by the equation, $\Delta t = 0.1875t + 7.00$.

In conclusion, favorable vapor-pressure lowering could be achieved by using concentrated aqueous salt solutions, which might indicate possible advantages to be attained over pure water, organic, and fused-salt heat-transfer agents. It would remain to be seen how the other heat transfer factors and the radiation stability would compare with the other liquid media after the differences in allowable operating temperatures and in the other factors were considered.

19.2 A STUDY OF DILUTE SOLUTIONS IN THE SYSTEM UO_2SO_4-$CuSO_4$-$NiSO_4$-H_2SO_4-H_2O

F. E. Clark C. H. Secoy
J. S. Gill R. Slusher

The purpose of the study on the system UO_2SO_4-$CuSO_4$-$NiSO_4$-H_2SO_4-H_2O was to ascertain the maximum temperature at which solutions of specified compositions could be held without the appearance of a nonhomogeneity. A nonhomogeneity might

TABLE 19.2. VAPOR PRESSURES OF $Ca(NO_3)_2$–H_2O SOLUTIONS

Concentration of $Ca(NO_3)_2$ (wt %)											
69.5 (13.8 *m* or 0.20 mole fraction)		61.6 (9.80 *m* or 0.15 mole fraction)		50.3 (6.17 *m* or 0.10 mole fraction)		37.7 (4.50 *m* or 0.075 mole fraction)		32.4 (2.92 *m* or 0.05 mole fraction)		Pure Water	
t(°C)	p/p_0	t(°C)	p/p_0	t(°C)	p/p_0	t(°C)	p/p_0	t(°C)	p/p_0	t(°C)	p/p_0
200	0.413	200	0.622	201	0.622	204	0.898	200	0.942	200	1.000
212	0.417	211	0.603			217	0.888	212	0.930	210	1.014
222	0.432	222	0.571	212	0.656	228	0.869	222	0.943	225	1.000
234	0.411	234	0.569			239	0.832	230	0.953	235	1.004
250	0.407	246	0.575	222	0.657	247	0.848	238	0.959	245	1.007
264	0.420	250	0.575	228	0.665	257	0.838	246	0.968	250	1.009
278	0.421	258	0.589	238	0.672	271	0.838	250	0.967	260	1.013
297	0.435	266	0.593	245	0.679	283	0.819	258	0.974	270	1.006
313	0.436	274	0.600	250	0.679	292	0.810	266	0.973	280	1.010
322	0.437	282	0.604	260	0.687	313	0.810	278	0.972	290	1.002
330	0.434	290	0.608	273	0.695	319	0.804	286	0.963	300	1.005
336	0.434	298	0.609	280	0.706	334	0.802	294	0.961	310	1.008
340	0.434	306	0.607	290	0.701	340	0.806	300	0.951	320	1.002
347	0.433	314	0.606	300	0.699	354	0.790	308	0.948	330	1.007
350	0.434	322	0.602	310	0.699	360	0.783	318	0.935	345	0.999
355	0.428	330	0.600	321	0.696	370	0.783	324	0.927	350	1.002
360	0.425	338	0.577	330	0.691			332	0.922	360	1.006
365	0.428	348	0.573	340	0.692			340	0.911	370	1.012
370	0.426	358	0.542	350	0.686			348	0.901	374	1.018
		368	0.545	360	0.683			356	0.891		
		370	0.544	370	0.678			365	0.883		
		380	0.54*	380	0.67*			372	0.879		
		388	0.54*	390	0.68*			380	0.88*		
				400	0.67*			390	0.88*		
								400	0.88*		

*Using extrapolated values for p_0.

involve the formation of a second liquid phase or the formation of one or more solid phases. The composition variables were limited to selected values for each of the components in the range of HRT interests. The nominal values chosen were:

	Molality
UO_2SO_4	0.04
$CuSO_4$	0, 0.005, 0.01, 0.02, 0.03, 0.04
$NiSO_4$	0, 0.01, 0.02, 0.03, 0.04
H_2SO_4	0.01, 0.02, 0.03

Ninety stock solutions representing all combinations of these values were prepared. The analysis of these solutions has not been completed, but in all completed cases the analytical values agree with the nominal concentrations within a few per cent.

The method of determining the phase transition points consisted in sealing samples of the solution in 1-mm quartz tubing and observing the solution with a 6X telemicroscope while the tube was being heated in an aluminum block furnace. Agitation was obtained by intermittent vibration of the tube with a Burgess Vibro-Tool.

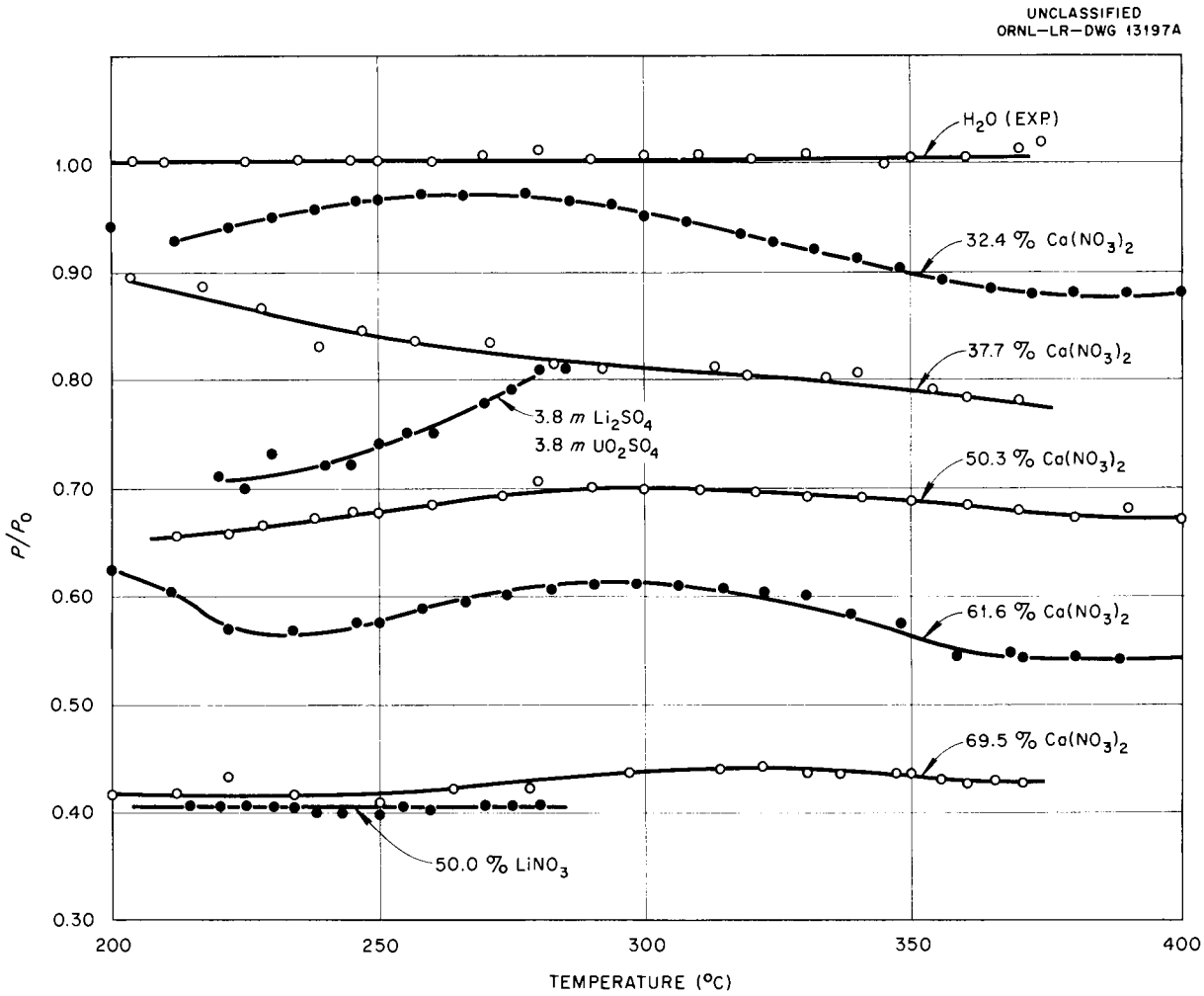

Fig. 19.1. Vapor Pressures of Several Aqueous Salt Solutions.

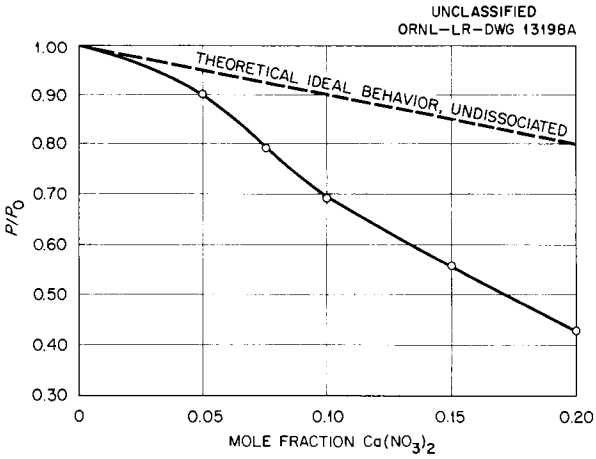

Fig. 19.2. Vapor Pressures of $Ca(NO_3)_2$ Solutions at 350°C.

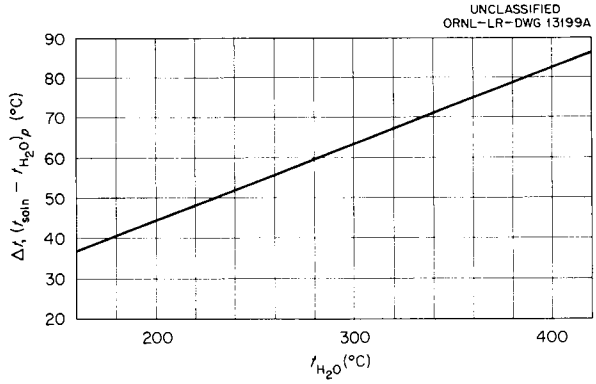

Fig. 19.3. Comparison of $(t_{soln} - t_{H_2O})$ at Constant Pressure.

Early in the work some indication of attack on the quartz was observed after 30 min of heating. Therefore all tubes were arbitrarily limited to not more than 15 min in the hot furnace. For each solution a series of tubes was employed, the first being used to determine the approximate temperature of transition and succeeding tubes to fix the temperature more accurately and to verify the observation by duplication. The short duration of the equilibration and the rather limited stirring obtainable introduce doubt as to whether equilibrium was really established. This fact, as well as uncertainty as to the amount of corrosion of the quartz, makes the data presented in Table 19.3 of qualitative value. Further doubt as to the validity of the temperatures as given arises from the fact that, even though the phase transitions in all cases were sharp and reversible, the amount of material involved is very small. The initial appearance of the solids was usually very difficult to detect, and redissolving of the crystals upon lowering the temperature was usually too slow for the arbitrarily imposed time limit.

No effort has been made to identify any of the solid phases. In Table 19.3 they have been placed in one of two groups designated "YS" (yellow solid) and "GS" (green solid), respectively. All species in the YS-group probably contain uranium, and members of the GS-group may contain uranium. Two of the solutions, Nos. 4501 and 4502, yielded a finely divided red solid upon quenching from temperatures above about 250°C. The red solid could not be obtained without the quench, and it slowly redissolved. It appears to be the same as a red solid obtained in earlier work as an equilibrium phase in solutions of lower excess acid concentration, which was tentatively identified as a copper uranate. Other possible solid phases which have previously been identified include the following:

$NiO \cdot 2.5UO_3 \cdot SO_3 \cdot xH_2O$	Yellow
$NiO \cdot 4UO_3 \cdot 2SO_3 \cdot yH_2O$	Orange-yellow
$3CuO \cdot SO_3 \cdot 2H_2O$	Green
$4CuO \cdot SO_3 \cdot 3H_2O$	Green
$CuO \cdot 2UO_3 \cdot 2SO_3 \cdot 7H_2O$	Dark green

Several general conclusions appear to be valid from an inspection of the data. At low copper or nickel concentrations the initial phase separation is the appearance of the second liquid phase. Increasing either the copper sulfate concentration or the nickel sulfate concentration lowers the temperature of phase separation slightly. Increasing the acid concentration elevates the temperature, being more effective in the absence of copper and nickel than in their presence. At higher nickel or copper concentrations a solid phase appears at temperatures lower than two-liquid-phase phenomena, and, as either of these ion concentrations increase further, the temperature of precipitation drops rapidly. Increasing the excess acid alleviates this effect somewhat. The data indicate that operation of the HRT at the maximum design temperature (300°C) with the proposed solution composition will result in precipitation of uranium if the nickel concentration is allowed to rise to more than about 0.02 *m*. It is assumed that there will be 0.02 *m* excess acid (50% based on the uranium) plus enough acid to equal the nickel concentration. Conditions in parts of the pressurizer appear to be in an even more doubtful state.

TABLE 19.3. OBSERVED TEMPERATURES OF THE APPEARANCE OF NONHOMOGENEITY IN THE SYSTEM UO_2SO_4-$CuSO_4$-$NiSO_4$-H_2SO_4-H_2O

Solution No.	$CuSO_4$ (m)	$NiSO_4$ (m)	New Phase*	Temperature (°C)
		0.04 m UO_2SO_4; 0.01 m H_2SO_4		
4001	None	None	2 LP	335
4011	None	0.01	2 LP	325
4021	None	0.02	YS	295
4031	None	0.03	YS	<288
4041	None	0.04	YS	247
4501	0.005	None	2 LP**	318
4511	0.005	0.01	2 LP	323
4521	0.005	0.02	YS	287
4531	0.005	0.03	YS	265
4541	0.005	0.04	YS	231
4101	0.01	None	2 LP	318
4111	0.01	0.01	2 LP	317
4121	0.01	0.02	YS	280
4131	0.01	0.03	YS	<273
4201	0.02	None	2 LP	316
4211	0.02	0.01	2 LP	313
4221	0.02	0.02	YS + GS	277
4231	0.02	0.03	GS	255
4301	0.03	None	2 LP	308
4311	0.03	0.01	GS	255
4321	0.03	0.02	GS	238
4331	0.03	0.03	GS	220
4401	0.04	None	GS	256
4411	0.04	0.01	GS	226
4421	0.04	0.02	GS	215
4431	0.04	0.03	GS	208
		0.04 m UO_2SO_4; 0.02 m H_2SO_4		
4002	None	None	2 LP	345
4012	None	0.01	2 LP	328
4022	None	0.02	2 LP	313
4032	None	0.03	YS	279
4042	None	0.04	YS	268
4502	0.005	None	2 LP**	327
4512	0.005	0.01	2 LP	323
4522	0.005	0.02	2 LP	316
4532	0.005	0.03	YS	291
4102	0.01	None	2 LP	330
4112	0.01	0.01	2 LP	332
4122	0.01	0.02	2 LP	315
4132	0.01	0.03	YS	272

TABLE 19.3. (continued)

Solution No.	$CuSO_4$ (m)	$NiSO_4$ (m)	New Phase*	Temperature (°C)
4202	0.02	None	2 LP	322
4212	0.02	0.01	2 LP	323
4222	0.02	0.02	2 LP	314
4232	0.02	0.03	2 LP	315
4302	0.03	None	2 LP	320
4312	0.03	0.01	2 LP	314
4322	0.03	0.02	YS	311
4332	0.03	0.03	YS	283
4402	0.04	None	2 LP	324
4412	0.04	0.01	YS	260
4422	0.04	0.02	GS	313
4432	0.04	0.03	GS	241
		0.04 m UO_2SO_4; 0.03 m H_2SO_4		
4003	None	None	2 LP	352
4013	None	0.01	2 LP	333
4023	None	0.02	2 LP	322
4033	None	0.03	YS	311
4043	None	0.04	YS	291
4503	0.005	None	2 LP	332
4513	0.005	0.01	2 LP	335
4523	0.005	0.02	2 LP	323
4533	0.005	0.03	2 LP + YS	335
4103	0.01	None	2 LP	335
4113	0.01	0.01	2 LP	334
4123	0.01	0.02	2 LP	323
4133	0.01	0.03	YS	290
4203	0.02	None	2 LP	328
4213	0.02	0.01	2 LP	328
4223	0.02	0.02	2 LP	323
4233	0.02	0.03	2 LP	323
4303	0.03	None	2 LP	326
4313	0.03	0.01	2 LP	324
4323	0.03	0.02	2 LP	328
4333	0.03	0.03	2 LP	320
4403	0.04	None	2 LP	328
4413	0.04	0.01	2 LP	325
4423	0.04	0.02	2 LP	331
4433	0.04	0.03	YS	299

*2 LP indicates appearance of second liquid phase; YS indicates appearance of white, yellowish-white, or orange-yellow solid; GS indicates appearance of green or bluish-green solid.

**Produced finely divided red solid upon quenching.

20. RADIATION STUDIES OF THORIUM NITRATE SOLUTIONS

J. W. Boyle H. A. Mahlman

Three of the principal decomposition products obtained from irradiated thorium nitrate solutions are hydrogen, oxygen, and nitrogen; 100-ev yields[1] of these gases have been reported previously for various types of radiation. Of considerable importance to the thorium nitrate blanket program is the back reaction between nitrogen and the other decomposition gases. Since the nitrogen in a breeder blanket will have to be N^{15}, any molecular nitrogen produced by radiation decomposition will have to be collected and converted to nitrate for reinsertion into the blanket if a steady-state nitrogen pressure is not attained at operating temperatures and pressures.

The solution used for studying the extent of the back reaction between nitrogen and the other gases was 7 *m* in $Th(NO_3)_4 \cdot 2HNO_3$ and 0.06 *m* in enriched $UO_2(NO_3)_2$. Thermal decomposition of this solution to yield gaseous products was quite pronounced at elevated temperatures. This thermal decomposition at elevated temperatures was reversible when the solution was cooled. Equilibrium between the gaseous decomposition products and the solution was attained almost instantaneously at temperatures above 140°C and more slowly as the temperature was lowered. The vapor pressure, which gives a measure of the thermal decomposition, was determined over the temperature range 140 to 290°C. A logarithmic plot[2] of the vapor pressure of the solution, P_{Th}, against the vapor pressure of pure water, P_{H_2O}, at the same temperature gave a straight line:

$$\log P_{Th} = 1.049 \log P_{H_2O} + 0.071 \ .$$

Two type 347 stainless steel, platinum-lined autoclaves containing the above solution were irradiated in hole 11 of the Graphite Reactor and showed that there was little back reaction involving nitrogen in the temperature range 140 to 240°C. The pressure of permanent gas increased linearly with dose in each of the experiments. During the second experiment the temperature was increased once to 290°C, at which temperature a leak was suspected. The temperature was immediately lowered below 200°C, and the pressure again increased linearly for four more days; then the experiment was terminated.

Three similar autoclaves were heated out-of-pile, and all three leaked when the temperature was raised above 275°C. The leak at the high temperature was apparently caused by the low thermal expansion of platinum, which was used in sealing the tubing to the type 347 stainless steel autoclave. The difference in the thermal expansion coefficients of platinum and type 347 stainless steel produced a net loosening of the closure as the temperature was increased. When a suitable autoclave has been prepared the reaction at 290°C will be investigated.

The composition of the gas collected at the end of the autoclave experiments and of the residual gas after the hydrogen was burned off is compared in Table 20.1 with the composition of the gas from a typical silica ampoule experiment.

[1] J. W. Boyle and H. A. Mahlman, *HRP Quar. Prog. Rep. Jan. 31, 1955*, ORNL-1853, p 201.

[2] D. F. Othmer, *Ind. Eng. Chem.* 32, 841–856 (1940).

TABLE 20.1. COMPARISON OF COMPOSITION OF GASES IN AUTOCLAVE AND IN AMPOULE

Constituent	Composition of Gas Collected (%)		Composition of Residual Gas	
	Autoclave	Ampoule	Autoclave	Ampoule
O_2	68.3	44.2	68.8	67.6
N_2	29.5	8.6	29.9	27.0
H_2	0.8	45.5		
N_2O	0.8	0.8	0.8	2.5
CO_2	0.5	0.9	0.5	2.8

The platinum lining catalytically recombined most of the hydrogen with oxygen in the autoclave experiments so that only a trace of hydrogen was present at the end of the experiment.[3] The autoclave and ampoule experiments agreed fairly well when the hydrogen and corresponding amount of oxygen were removed from the sample. This is shown by the last two columns in Table 20.1.

The material balance found in the ampoule studies is satisfactory if the following decomposition reactions are assumed:

(1) H_2 production: $H_2O \rightsquigarrow H_2 + \frac{1}{2}O_2$

(2) N_2 production: $2HNO_3 \rightsquigarrow H_2O + N_2 + 2\frac{1}{2}O_2$

(3) N_2O production: $2HNO_3 \rightsquigarrow H_2O + N_2O + 2O_2$

(4) CO_2 production: $(CH_2)_x + x1\frac{1}{2}O_2 \rightsquigarrow xH_2O + xCO_2$

Oxygen is produced in reactions 1, 2, and 3 and is consumed in reaction 4. A material balance was also obtained in the autoclave experiment assuming that a small amount of air (3.2%) contaminated the sample. The method used to collect the gas sample would allow a small amount of air to mix with the sample before the analysis was made.

[3] J. W. Boyle and H. A. Mahlman, *Chem. Semiann. Prog. Rep. Dec. 20, 1955*, ORNL-2046, p 70.

21. CAPTURE CROSS SECTION OF U^{236}

J. O. Blomeke[1] J. Halperin R. W. Stoughton

A measurement was made of the effective capture cross section of U^{236} in highly irradiated MTR fuel elements. This was done by analyzing the Np^{237} formed from the U^{235} by the following series of reactions:

$$(1)\quad U^{235} \xrightarrow{(n,\gamma)} U^{236} \xrightarrow{(n,\gamma)} U^{237} \xrightarrow[6.7\ d]{\beta^-} Np^{237} \xrightarrow{(n,\gamma)}$$

$$U^{235} \xrightarrow{(n,f)}$$

Eleven fuel elements and shim rods which had been exposed to integrated flux-times ranging from about 8×10^{20} to 2×10^{21} neutrons/cm^2 were processed[2,3] in the ORNL Pilot Plant (Operation Neptex) to recover the Np^{237} that had been produced. Seven of the fuel elements were individually dissolved and sampled for analysis. The remaining four were dissolved together and analyzed as one batch. A measure of the flux-time was obtained by a mass analysis of the uranium in each sample.[4] The measured U^{236}/U^{235} ratio together with the cross section of U^{235} and U^{236} (see Table 21.1) permitted a calculation of an integrated flux-time for the irradiation. The effective capture cross sections of U^{236} could then be computed from radiochemical analyses of the Np^{237} in each

[1]Chemical Technology Division.

[2]E. Shank, personal communication.

[3]F. T. Howard and W. H. Sullivan, *Oak Ridge National Laboratory Status and Progress Report January 1956*, ORNL-2044 (Feb. 7, 1956).

[4]The mass analyses were carried out by L. O. Gilpatrick, J. Sites, J. R. Walton, and C. R. Baldock.

TABLE 21.1. YIELDS OF U^{236} AND Np^{237} AND DERIVED EFFECTIVE CROSS SECTION OF U^{236}

Sample No.	Initial U^{235} Content (g)	Final U^{235} Content (g)		U^{236}/U^{235} (exp)	ϕt ($\times 10^{-20}$)	Np^{237}/U^{235}, $\times 10^3$ (exp)	$\sigma(U^{236})_{eff}$* (barns)
		Calculated	Experimental				
AFA-100	169	95.7	84.5	0.1177	8.35	1.90	36
MD-100	169	66.0	74.6	0.239	13.8	5.40	30
MD-200	168	45.7	49.7	0.403	19.1	10.7	24
MD-300	131	57.0	62.2	0.1976	12.2	5.0	38
MD-400	109	45.6	48.9	0.213	12.8	5.85	39
MD-500	169	73.0	74.5	0.201	12.3	3.62	27
MD-600	131	50.4	52.3	0.273	14.0	6.68	36
MD-700	131	52.9	59.5	0.226	13.3	6.30	38
MD-800**	479	155	158	0.318	16.6	9.54	32

*Based upon $\sigma_c(U^{235})_{eff} = 106$ barns, $\sigma_a(U^{235})_{eff} = 685$ barns, $\sigma_a(Np^{237})_{eff} = 170$ barns.

**Consists of composite of four fuel elements.

sample of dissolved fuel. The pertinent equations for this calculation are as follows:

$$(2) \qquad \frac{U^{236}}{U^{235}} = \frac{\sigma_c(U^{235})}{\sigma(U^{236}) - \sigma_a(U^{235})} \left\{ 1 - e^{+[\sigma_a(U^{235}) - \sigma(U^{236})]\phi t} \right\} ,$$

$$(3) \qquad \frac{Np^{237}}{U^{235}} = \sigma(U^{236})\, \sigma_c(U^{235}) \left\{ \frac{1}{[\sigma(Np^{237}) - \sigma_a(U^{235})][\sigma(U^{236})\, \sigma_a(U^{235})]} + \right.$$

$$\left. + \frac{e^{[\sigma_a(U^{235}) - \sigma(U^{236})]\phi t}}{[\sigma(Np^{237}) - \sigma(U^{236})][\sigma_a(U^{235}) - \sigma(U^{236})]} + \frac{e^{[\sigma_a(U^{235}) - \sigma(Np^{237})]\phi t}}{[\sigma(U^{236}) - \sigma(Np^{237})][\sigma_a(U^{235}) - \sigma(Np^{237})]} \right\} .$$

The data and results obtained in these experiments are summarized in Table 21.1. The accuracy of the U^{236}/U^{235} ratio on which the flux-time is based is probably within 2%. However, the error in the uranium analyses plus the uncertainties in the total solution volume are in the range of 10 to 15%. An estimated chemical yield of 85% was applied to the Np^{237} analyses, and the uncertainty in that analysis is also estimated as ±10%. The values of $\sigma(U^{236})_{eff}$ for each run are tabulated in the last column of Table 21.1. There is internal evidence suggesting faulty analyses in sample MD-200. An average of the effective capture cross sections of U^{236} (excluding MD-200) for these irradiations is $\sigma(U^{236})_{eff} = 34 \pm 6$ barns.

This value may be compared with the thermal value of 6 barns reported by Pomerance[5] and an effective reactor cross section of 24 ± 7 barns reported by Auclair[6] and co-workers for the Saclay reactor. It is thus apparent that U^{236} (analogous to U^{238}) has a very large resonance integral compared with its thermal cross section. In the core of a reactor where the ratio of resonance to thermal flux is highest, U^{236} absorbs neutrons of resonance energies predominantly.

J. A. Harvey and V. E. Pilcher[7] have measured the resonance parameters of U^{236} with the BNL fast chopper. Their data yield a resonance integral of

$$\int_{0.4} \sigma(U^{236}) d(\ln E) = 312 \text{ barns} .$$

This latter value of the resonance integral is consistent with the high effective cross section of U^{236} shown in Table 21.1. Since the resonance effect is large, an observed effective cross section of U^{236} will be very sensitive to both the particular reactor and the exact position in which the sample is irradiated. This would appear to account for the difference in effective cross sections reported by Auclair and co-workers and the value reported here.

[5] D. J. Hughes and J. A. Harvey, *Neutron Cross Sections*, BNL-325 (July 1, 1955).

[6] J. M. Auclair *et al.*, *Compt. rend.* 241, 392 (1955).

[7] V. E. Pilcher, D. J. Hughes, and J. A. Harvey, "Neutron Resonance Parameters of U^{234} and U^{236}," *Bull. Am. Phys. Soc.* 1, Series II, 187 (1956).

22. PROTACTINIUM CHEMISTRY

B. Weaver F. M. Scheitlin

22.1 EXTRACTION OF PROTACTINIUM

A study of the extraction of tracer protactinium by kerosene solutions of di(2-ethylhexyl)phosphoric acid was continued. The addition of 2% (wt/vol %) 2-ethyl hexanol to 0.1 *M* di(2-ethylhexyl)phosphoric acid in kerosene was observed to increase the distribution coefficient of tracer protactinium between this solvent and 0.1 *M* HNO_3 from 32 to 154.

It is probable that observed distribution coefficients and differences between them in HNO_3 systems are only apparent. The above coefficients were obtained from a solution that was two months old. When the freshly extracted organic phases were re-equilibrated with HNO_3 solutions, widely varying coefficients were found. Results are shown in Table 22.1. It appears that tracer protactinium in HNO_3 exists in more than one state, one of which is highly extractable under the experimental conditions. The experiment has not been carried far enough to determine whether there is an equilibrium between two states with a definite rate of transformation. This behavior is parallel to that previously observed[1] in tributyl phosphate–nitric acid systems, where the distribution coefficients were very small.

Protactinium was easily stripped from the organic solvent by a 10% aqueous solution of $(NH_4)_2CO_3$. The ammonium salt of D2EHP is soluble in kerosene.

TABLE 22.1. DISTRIBUTION COEFFICIENTS FOR PROTACTINIUM INTO 0.1 *M* D2EHP + 2% 2EH

Molarity of HNO_3	Extract No.	*D* (org/aq)
0.1	1	154
0.1	2	7×10^3
0.5	1	114
0.5	2	1840
0.5	3	$>3 \times 10^5$

22.2 EXTRACTION OF THORIUM AND RARE EARTHS

Since thorium also extracts into 0.1 *M* D2EHP–kerosene–2% 2EH, an attempt was made to find conditions which would reduce its extractability. The extraction of yttrium, as a representative of the rare earths, was also studied. These experiments were done on a macro scale. Some results are shown in Table 22.2.

22.3 BEHAVIOR OF PROTACTINIUM TOWARD HYDROXYLAMINE

Tracer protactinium and thorium were carried with iron precipitated by NH_2OH. Uranium is held in solution by complexing under the same conditions.

[1] S. S. Brandt and A. T. Gresky, *Progress Report: Laboratory Development of the Thorex Process*, ORNL-1367, p 88–89 (Dec. 17, 1952).

TABLE 22.2. DISTRIBUTION COEFFICIENTS FOR THORIUM AND YTTRIUM INTO ORGANIC SOLVENTS

Aqueous Phase	Organic Phase	Phase Ratio	*D* (org/aq)
0.5 *M* HNO_3–0.0366 *M* Th	0.1 *M* D2EHP (2% 2EH)–kerosene	1	$>10^3$
2.0 *M* HNO_3–0.0366 *M* Th	0.1 *M* D2EHP (2% 2EH)–kerosene	1	27
0.5 *M* HNO_3–0.02 *M* Y	0.1 *M* D2EHP (2% 2EH)–kerosene	1	0.17
4.0 *M* HNO_3–0.02 *M* Y	0.1 *M* D2EHP (2% 2EH)–kerosene	1	0
0.5 *M* HNO_3–0.0366 *M* Th	*DIBC in kerosene (1:1)	1	0
0.5 *M* HNO_3–0.0366 *M* Th	0.1 *M* D2EHP + 2% DIBC in kerosene	1	$>10^3$
0.5 *M* HNO_3–0.0366 *M* Th	0.1 *M* D2EHP + 10% 2EH in kerosene	2	$>10^3$

*DIBC = Diisobutyl carbinol.

22.4 CARRIER PRECIPITATION OF PROTACTINIUM

Tracer protactinium was carried to the extent of greater than 99% by $FePO_4$ from a chloride solution. Conditions were as follows: 0.006 *M* Fe, 0.3 *M* H_3PO_4, ~2 *M* NaCl, and 1.5 *M* NH_4Cl at pH 1.5. The $FePO_4$ is readily soluble in acids, but the extraction coefficient of protactinium into diisobutyl carbinol from 6 *M* HCl containing $FePO_4$ is only 0.33. The iron extracts approximately as well.